Investigation on the fine tuning of different performance parameters of High Temperature Superconductors

DOCTOR OF PHILOSOPHY

ASHOK K.B.

Register No. D-TKM18JAN011

Department of Mechanical Engineering

TKM College of Engineering, Kollam

APJ ABDUL KALAM TECHNOLOGICAL UNIVERSITY

Thiruvananthapuram

2023

Investigation on the fine tuning of different performance parameters of High Temperature Superconductors

Submitted in partial fulfillment of the
requirements of the degree of

DOCTOR OF PHILOSOPHY

ASHOK K.B.

Register No. D-TKM18JAN011

Supervisors:

Dr. Rijo Jacob Thomas
&
Dr. Jose Prakash M

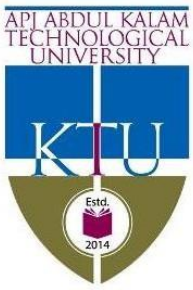

Department of Mechanical Engineering

TKM College of Engineering, Kollam

APJ ABDUL KALAM TECHNOLOGICAL UNIVERSITY

Thiruvananthapuram

2023

DECLARATION

I declare that this written submission represents my ideas in my own words and where others' ideas or words have been included, I have adequately cited and referenced the original sources. I also declare that I have adhered to all principles of academic honesty and integrity and have not misrepresented or fabricated or falsified any idea/data/fact/source in my submission. I understand that any violation of the above will be cause for disciplinary action by the University and can also evoke penal action from the sources which have thus not been properly cited or from whom proper permissions have not been taken when needed.

ASHOK K.B.

Register No: D-TKM18JAN011

Date: 22/08/2023

CERTIFICATE

It is certified that the work contained in the thesis titled **"Investigation on the fine tuning of different performance parameters of High Temperature Superconductors"** by Ashok K.B.," has been carried out under our supervision and that this work has not been submitted elsewhere for a degree.

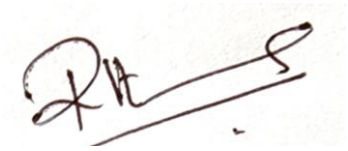

Dr. Rijo Jacob Thomas
(Research Supervisor)
Assistant Professor
Department of Mechanical Engineering
TKM College of Engineering
Kollam, Kerala

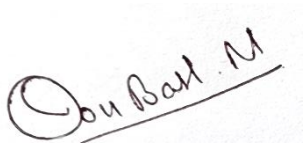

Dr. Jose Prakash M
(Research Co-supervisor)
Retired Professor
Department of Mechanical Engineering
TKM College of Engineering
Kollam, Kerala

Date: 22/08/2023

Place: Kollam, Kerala

Acknowledgements

I consider myself really fortunate and pleased to be a part of such demanding study, with the equally powerful titled **"Investigation and fine tuning of different performance characteristics of High Temperature Superconductors**." All praise to the All Mighty, without Whom this opportunity and its successful fulfilment would not have been conceivable.

I would like to thank my supervisors, Dr. Rijo Jacob Thomas, Assistant Professor, Department of Mechanical Engineering, TKM College of Engineering, Kollam and Prof. Jose Prakash M, former Professor and Head, Department of Mechanical Engineering, TKM College of Engineering, for their guidance and assistance throughout the project research. Dr. Rijo has helped me grasp the subject and provided me with confidence, encouragement, guidance, and support from the beginning to the end. Prof. Jose Prakash M constantly provided me with intelligent guidance and creative criticism, and he remained patient and interested in my thesis until it was successfully completed. The friendliness of my supervisors was crucial in bringing this research to a logical conclusion. I must emphasise that working under their supervision was a fantastic learning experience, and the entire training provided has and will continue to influence my future life.

Dr. Arend Nijhuis, EMS group, University of Twente, has my heartfelt gratitude for his collaboration and gracious support throughout the research. I would gratefully acknowledge the help provided by the EMS group in carrying out the simulation studies using COMSOL Multiphysics. I would like to express my sincere gratitude to the external DC members, Prof. Tide PS, Professor, CUSAT School of Engineering and Dr. Deepak Kumar Agarwal, senior ISRO scientist, LPSC, for their cooperation and timely suggestions. I am also grateful to internal DC members Dr. Shafi KA and Dr. Sajid Mohammed Professors of the Department of Mechanical Engineering at TKMCE for their insightful recommendations and contributions.

I am grateful to all of the other Professors of the Department of Mechanical Engineering, TKM College of Engineering, especially Dr. Abdul Rasheed (former HOD) Dr. Dileep P. N. (present HOD), Dr. Krishnakumar TS, Dr. Leena R, and Dr. Sheeba A, for their helpful recommendations and support on numerous occasions. I would like to express my

heartfelt gratefulness to Prof. Dr. T. A. Shahul Hameed, the Principal of TKM College of Engineering, Kollam, Kerala.

I would like to express my gratitude to the Management of the College, TKM college Engineering for providing me with all the required resources and assistance in carrying out this job. I would like to thank all the faculty and staff members of TKM College of Engineering who have supported me; even a little help made a big difference. I am grateful to the AICTE for financial support with the National Doctoral Fellowship (NDF) for the full term. This work would not have been feasible without the use of COMSOL Multiphysics®software, Veusz, Mendeley, Grammarly, Quilbot, and websites such as Google, Wikipedia, ScienceDirect, IOP, and IEEE, as their resources allowed me to conduct a thorough literature review.

Throughout my time at TKM College of Engineering, I was surrounded by a welcoming and upbeat group of fellow Scholars. Mr. Binet Monachan and Mr. Ashwin Vijay, my lab partner and roommate with whom I spent practically all of my time, deserve special thanks. We worked together day and night, and I learned a lot from and because of them. Mr. Anadhu Krishnan, Mr. Shajan S, Mr. Sigikumar, Mr. Renjish Vijay, Mr. Aravid, Mr. Manu, Mr. Abhishek, Mr. Asif, Mr. Lijin, and all my co-researchers at TKMCE have made my time at TKMCE more fun. I am appreciative for the assistance provided by the technical staff, particularly Mr. Muneer, Remi N. M. and Mr. Rajeesh.

I'd would like to thank dear Sujithra, my loving, supportive, understanding, and encouraging wife, and her loving family for their understanding and for allowing me to remain married to the gruelling and demanding research.

I am also grateful to my sister, Dr. Prathibha Balan, for her affection and motherly guidance, as well as Mr. Praphul Pradeep, my brother-in-law.

I must conclude this indebtedness by thanking everyone who contributed to the successful completion of this thesis and apologising for not noting their names during this academic journey.

Last but not least, I would like to express my heartfelt gratitude to my parents, 'Achan' (Mr. Balan K) and 'Amma,' (Mrs. Leela K) whose unwavering support has been selfless and unwavering, and without whom I would never have been able to begin on or achieve such goals in my life.

Abstract

Nuclear fusion can be considered as a viable source of energy in the future when considering the high depletion rate of conventional energy sources and the increase in energy demands. Superconducting magnets being an integral part of any nuclear fusion reactor, wires and cables that can carry a huge amount of current without any loss and with minimum cost are to be developed. The high-temperature superconductors (HTS) are considered to be cost-effective when compared to low-temperature superconductors (LTS). However, the development of HTS-based wires or cables requires much research, mostly because majority of them are brittle. The second-generation HTS of the rare-earth barium copper oxide (REBCO) family are potentially promising because of their large current density and low hysteresis losses. However, being brittle in nature, they must be first transformed into tapes before being converted into superconducting cables and wires for use. REBCO conductors also have many desirable properties required for various applications, such as strength, flexibility, and strain tolerance for winding, and current densities at high to very high magnetic fields even at liquid nitrogen temperatures (77 K). However, they can degrade and lose their superconducting property unless they are kept within certain limits (known as critical limits) in terms of temperature, current density, magnetic field, and structural strain. It is necessary to determine these critical limits for any given type, geometry and size of superconductor when they are subjected to mechanical forces/stresses. HTS tapes and cables being expensive, the experimental investigations for determining these critical limits are costly and also challenging. This is mainly due to their brittle nature, high current density, and cryogenic operating temperatures. Therefore, the use of simulation studies employing FEM software is found to be a viable option. This study, using simulation, attempts to understand the degradation of the REBCO tapes under different mechanical loading (tensile, bending, torsion, cyclic and winding loads) and also by varying the geometric parameters of the tape. The geometry parameters considered are the thickness of the constituting layers (mainly those made of Hastelloy and copper), width of the tape, winding angle, central core diameter, etc. Parametric studies carried out by varying the type and magnitude of the forces applied on them will help to identify the relative involvement of each geometric parameter on performance of the superconducting tape. The model for the simulation studies has been developed using COMSOL Multiphysics and have been compared with the

experimental and simulation studies reported in the literature. The results are obtained under tension, bending, torsion winding loads and also under the fatigue type of loading.

The results obtained reveal that Hastelloy and copper thicknesses have a significant influence on the development of intrinsic strain under tensile and bending loads; but found to be not much significant in the case of torsional load. The tape width is found to be the most crucial parameter in case of torsional loads. By decreasing the tape width, the critical limits can be pushed further, giving more flexibility for the manufacturers to accommodate combined tensile and torsional loads. Decreasing the tape width by 75 %, increased the maximum allowable angle of twist by 326 %. The winding study of simple superconducting CORC cable revealed that 45^{o} is the best angle for winding, and also found that, the intrinsic strain in the REBCO layer is increased with the decrease in the central core diameter. The fatigue loading studies showed that the bending load is the most severe one of the three types of loading. Also, it is found that, upon fatigue type loading, the Hastelloy layer fails first, followed by the bottom copper layer, the silver layer, and then the top copper layer for the given tape configuration and loading conditions.

It is found that the role of each tape parameter is different depending on the type of load applied. Under the tensile type of load, the thickness of the Hastelloy and copper layers is more significant than other tape parameters. Whereas, under bending, the thickness of the Hastelloy layer has more important role. Under the torsional load, the width of the tape is the most determining parameter. The thickness of the Hastelloy and copper layers is significant in the case of fatigue type of loading for tension, bending and torsion.

The various results obtained are expected to help the manufacturers and researchers to develop better HTS REBCO tapes and cables when they are subjected to tension, bending, torsion, cyclic and winding loads as well as under fatigue type of loading.

Table of Contents

List of Figures

List of Tables

Abbreviations, Nomenclature and Notations

Abbreviations

BSCCO	Bismuth-Strontium-Calcium-Copper-Oxide
CCRC	Coated Conductor Rutherford Cable
CeO_2	Cerium oxide
CORC	Conductor on Round Core cable
DyBCO	Dysprosium-Barium-Copper-Oxide
FEA	Finite Element Analysis
FUS	Fatigue Usage Factor
HTS	High-Temperature Superconductor
IBAD	Ion Beam Assisted Deposition
ISD	Inclined Substrate Deposition
ITER	International Thermonuclear Experimental Reactor
LTS	Low-Temperature Superconductor
MgB_2	Magnesium-diboride
MgO	Magnesium oxide
MOCVD	Metal-Organic Chemical Vapour Deposition
Nb_3Sn	Niobium-Tin
NbTi	Niobium-Titanium
PLD	Pulsed Laser Deposition
RABITS	Rolling Assisted Biaxially Textured Substrate Method
RACC	Roebel Assembled Coated Conductor cables
REBCO	Rare-Earth-Barium-Copper-Oxide
RSCCCT	Round Strands Composed of Coated Conductor Tapes cable
TSTC	Twisted Stacked-Tape Cable
YBCO	Yttrium-Barium-Copper-Oxide

Nomenclature

T_c	Critical Temperature (K),
j_c	Critical current density (A/mm^2)
B_c	Critical magnetic field (T)
B_{Ex}	External magnetic field (T)
B_{Int}	Internal magnetic field (T)
T	Temperature (K)
V_{fc}, V_{fh}	Volume fractions of copper and Hastelloy
n	Transformation factor
I	Moment of inertia (kg.m^2)
d	Distance between the neutral axis and the centroid of material (mm)
I_c	Critical current (A)
f	Stress factor (MPa)
k	Normal sensitivity coefficient
E	Young's modulus (GPa)
P	First Piola-Kirchhoff stress (MPa)
F	Deformation gradient tensor
S	Second Piola-Kirchhoff stress (MPa)

Notations

σ	Stress tensor (MPa)
ε	Strain tensor
ρ	Density (kg/ m^3)
ε_{th}	Thermal strain
$a(\alpha)$	Strain sensitivity of critical current
σ_a	stress amplitude (N/m^2)
σ_{max}	Maximum stress (MPa)
σ_{min}	Minimum stress (MPa)

v	Poisson ratio
ε_{eng}	Engineering strain
α	Coefficient of thermal expansion (K^{-1})

Chapter 1

Introduction

1.1. Introduction

One of the major concerns of the world today is the depletion of energy sources and the increasing energy demand. Natural resources of energy are scarce now in the universe, as they form naturally taking thousands of years. The rate of replenishing these stockpiles and the rate of depletion are not comparable. The energy outlook report from the International Energy Agency (IEA) reveals that global energy demand has increased by 4.6 % in the last year [1]. Coal, gas, oil, nuclear energy, traditional biomass, other renewable energy are the major energy resources in India, and their contribution is depicted in Figure 1.1.

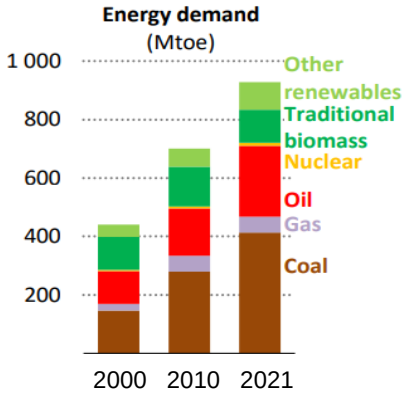

Figure 1.1: India's energy demand in different years [1]

Energy demand in 2022 has nearly doubled from that was in 2000. The percentage utilisation of renewable energy sources has been increasing in the last decades, but it is not enough to fulfil all the energy requirements of the world. Non-renewable energy sources like oil, gas, and coal are widely used today but are highly polluting. As fossil fuels are becoming scarce and with the rising of the global energy demand, the debate over tomorrow's energy sources resurfaces. Nuclear fusion is projected as the most viable solution for meeting future energy demands considering the scaleup factor and dependability. Nuclear energy is cost-effective and does not contribute to the greenhouse effect. In this perspective, nuclear fusion appears to be a perfect option for achieving sustainability, availability, and reliability in future energy utilization.

The nuclear fusion energy potential is enormous: just 100 kg of deuterium combined with 300 kg of tritium may generate 1000 MWe in a year, which is equal to 175 tonnes of natural uranium, 1.8 million tonnes of oil, or 2.6 million tonnes of coal [2]. Deuterium is abundant in seawater and lithium reserves/ mined (from which tritium is produced) is available for more than a thousand years [2]. Technology must progress significantly to utilise this powerful and long-lasting energy. The thermal energy of plasma produced by fusion of atom (generally hydrogen isotopes) is extracted to produce fusion energy. Plasma confinement is difficult because no substance on earth can withstand more than 100 million degrees Celsius temperatures that is required for the ionization. One of the potential solutions to the problem is to confine the charged plasma under a strong magnetic field. The conventional electromagnet cannot be used to produce a high magnetic field due to the heating losses and restriction of the size of the system. Superconductors must be employed to reduce conductor size and heating losses.

The promising energy project, International Thermonuclear Experimental Reactor (ITER) is developing in Saint-Paul-lès-Durance, France. India is one of 35 countries working together to construct the largest tokamak in the world. The magnetic fusion device aims to establish the possibility of large-scale fusion on the surface of the earth by using the same mechanism that powers the Sun and the stars. The superconducting fusion experiments are getting closer to the point where the nuclear fusion reaction will gain energy. The ITER, currently the largest fusion experiment, will be used to accomplish this. To produce the required magnetic fields, ITER uses the LTS elements niobium-titanium (NbTi) and niobium-tin (Nb_3Sn). ITER's magnets are kept superconducting by cooling them with liquid helium (He).

Liquid or gaseous helium is used to cool LTS. Future fusion magnets may use coated conductors (CC) or tapes made of rare-earth-barium-copper-oxide (Rare-Earth$_1$Ba$_2$Cu$_3$O$_{7-x}$ or REBCO) tapes, which are second-generation high-temperature superconductors (HTS). These materials outperform LTS materials at very high background magnetic fields in terms of their mechanical characteristics and current densities. In addition, liquid nitrogen can be used to cool HTS to operating temperatures at 77 K as opposed to liquid helium at 4 K. As a result, the design of the cryostat, electrical cold testing, and cooling equipment and systems for the magnets can all be simplified. Helium may also be avoided as a cooling liquid because it is in scarce supply on earth.

However, most of the HTS materials identified are brittle and therefore making wire/ cable etc., are challenging. Consequently, special configuration and cable production methods are adopted for producing HTS wires/ cables. However, it must be ensured that HTS materials are not damaged/'degraded' (lose its superconducting property) in their production and application stages. Therefore, the strain developed in the REBCO (HTS material) during the production and application stages has to be within the allowable limits. Hence, it is required to find the allowable limits for the various combination of the geometrical and operational parameters.

1.2. Superconductivity

Heike Kamerlingh Onnes discovered superconductivity in 1911 at the University of Leiden, the Netherlands [3, 4]. He found that the resistance of Mercury suddenly drops to zero when it is cooled to liquid helium temperatures (< 4.2 K) as depicted in Figure 1.2. He was awarded the Nobel Prize in 1913 for this ground-breaking discovery. However, he was unable to describe the physics involved. Since then, many people have attempted to formulate many hypotheses. Unfortunately, superconductivity currently lacks a solid explanation for the visible and hidden characteristics of this beautiful phenomenon. Researchers took a long time to come up with a reasonable explanation.

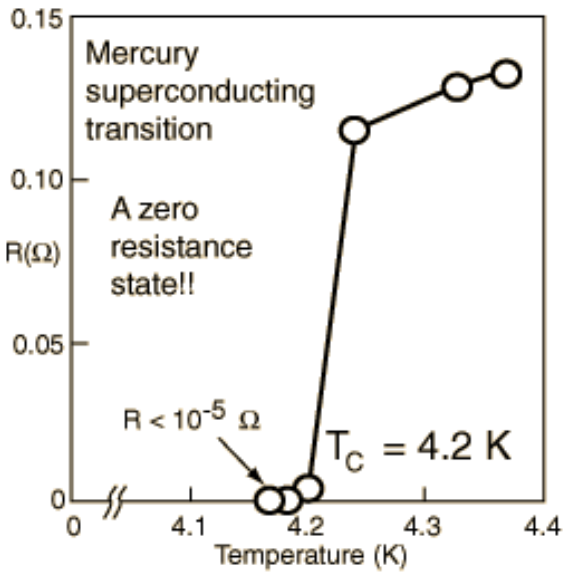

Figure 1.2: Schematic of the discovery of superconductivity.

Walther Meissner and Robert Ochsenfeld discovered the Meissner effect [5-8] in 1933, which stated another defining characteristic of superconductivity: the expulsion of magnetic flux when superconducting material is exposed to an external magnetic field. Based on classical electrodynamics, the London theory was the first to explain superconductivity successfully. This macroscopic theory was put forward by London Brothers in 1935 [9, 10]. It successfully explains the Meissner effect, but it is valid only for homogeneous materials. The **Ginzburg-Landau theory** [11] can be considered as an extension of the previous model proposed in 1950. It explains superconductivity with the help of a single wave function. This is based on Landau's theory of second-order phase transitions of free energy in superconductors. It is stated that a macroscopic quantum effect causes the superconducting phenomenon and also valid for non-homogeneous

materials. However, it provided new insights into superconductivity in terms of coherence length and penetration depth.

John Bardeen, John Robert Schrieffer, and Leon Cooper suggested the microscopic BCS theory in 1957 [10, 12] and they were awarded Nobel Prize in 1972. It explained the superconductivity of conventional superconductors, but the theory fails to explain the characteristics of most of the type II superconductors [10, 12]. BCS theory explained superconductivity by using electrons with opposite spins forming cooper pairs of the same energy state, resulting in a negative cloud that distorts the lattice structure and creates a zero resistance Path. The fundamental tenet of the BCS theory is that two electrons in a superconductor have the ability to link together forming a Cooper pair (bonded pair formed when two electrons come into attractive contact with one another). The nominal positions of the positive ions are deformed because of the attraction of an electron that travels through the lattice. The displaced ions draw the second electron from the Cooper pair. Note that this second electron can only be attracted to the lattice distortion if it approaches before the ions have returned to their equilibrium positions. This results in a weak, delayed force of attraction between the two electrons. Thus, distorted lattice structure gives a channel with zero resistance.

1.2.1 Critical parameters

Critical parameters define the conditions under which a superconductor keeps its superconducting properties. The critical parameters are temperature (T_c), current density (j_c) and the magnetic field (B_c). If any of these is beyond its critical limit, the superconductor loses its superconductivity. The critical parameters are interdependent as depicted in Figure 1.3. For instance, the critical limit of temperature changes with the values of magnetic field and current density.

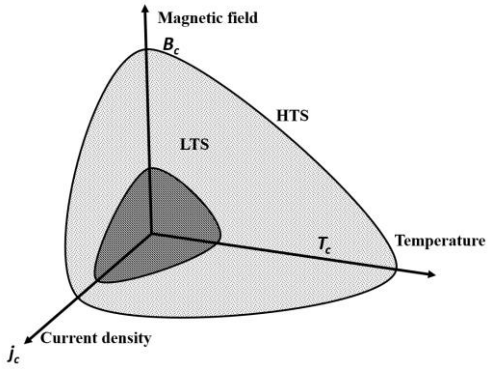

Figure 1.3: Critical parameters

Similarly, if the magnetic field is increased, its critical current density is also decreased proportionally.

Critical temperature means the temperature at which electrical resistance becomes zero. Below this range, it behaves as superconductor. The change from the normal to superconducting states is abrupt. Critical current density and critical magnetic field can also be defined similarly. If the critical limit is crossed, it suddenly changes from a superconducting to a normal state. The value of the critical magnetic field mainly depends on the temperature and material. The temperature-dependent critical magnetic field has been reported in the literature [13, 14].

$$B_c\,(T) = B_0\,(0K).\,(1 - (\frac{T}{T_c})^2) \tag{1.1}$$

The magnetic field is created in two ways either by the current passing through the superconductor and the magnetic field applied externally (background field). This demonstrates that current in the superconductor reduces the background field at which the transition between the superconducting state and the normal state occurs. So the critical current density and the external magnetic field are dependent and reported by different researchers [13, 15].

$$j_c = \frac{\alpha_B}{B_{Ext}+B_0} \tag{1.2}$$

Where 'α_B' and 'B_0' are constants and dependent on the material of the superconductor. 'B_0' is in the order of milli tesla and 'B_{Ext}' in the order of several tesla. So critical current density is inversely proportional to the external magnetic field.

In the case of superconductors, the electrical resistance is zero and there is no electrical field along the conductor. When transition occurs from a superconducting state to normal conducting state, the electrical field 'E' appears. Figure 1.4 shows the gradual transition from the superconducting state to a normal state, but in the case of the ideal superconductor, this transition is sudden. So ideal superconductor cannot be used for technical applications.

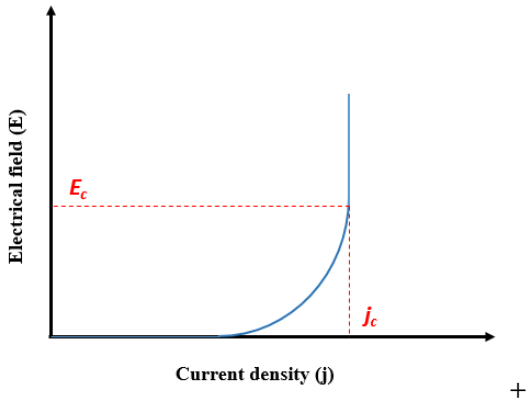

Figure 1.4: Electrical field and current density relation for technical superconductors [16]

The electrical field and current density correlation is expressed with the help of the power-law of superconductors and mentioned below in equation 1.3 [13, 17].

$$E = E_c . (\frac{j}{j_c})^n \quad (1.3)$$

Where *'E_c'* and 'j_c'are the critical electrical field and critical current density respectively. The electric field is the criterion for finding the critical current because the transition from the superconducting state to the normal state is a sudden process. For LTS (NbTi and Nb_3Sn) the critical electric fields are set to 0.1 Vcm^{-1} according to international standards [13]. '*Ec*' is taken as 1 Vcm^{-1} for the first-generation HTS, $Bi_2Sr_2Ca_2Cu_3O_y$ (BSCCO) tapes [13]. However, the 'E_c' of REBCO tapes are yet to be standardized. However, researchers are adopting 'E_c' of 0.1 V cm^{-1} as low threshold is crucial for magnetic applications. In addition to all these parameters, the physical strain also leads to the degradation of the superconductors [17, 18].

1.2.2 Type I and type II superconductors

Superconductivity is destroyed by high magnetic fields and restores to the normal conducting state. Type I and II superconductors can be distinguished based on the nature of this transition. Figure 1.5 depicts the internal magnetic field strength, 'B_{Int}' as a function of the applied external magnetic field, 'B_{Ext}'. Region 1, 2, and 3 represent the Meissner phase 1, Shubnikov phase and normal conducting phase respectively. The internal field is found to be zero (as predicted by the Meissner effect) until a critical magnetic field, 'B_{c1}' is reached, and then an abrupt transition to the normal state has occurred. This causes the applied field to penetrate inside the superconductor. Type I

superconductors are those that exhibit this sudden transition to the normal state above a critical magnetic field one depicted in Figure 1.5a.

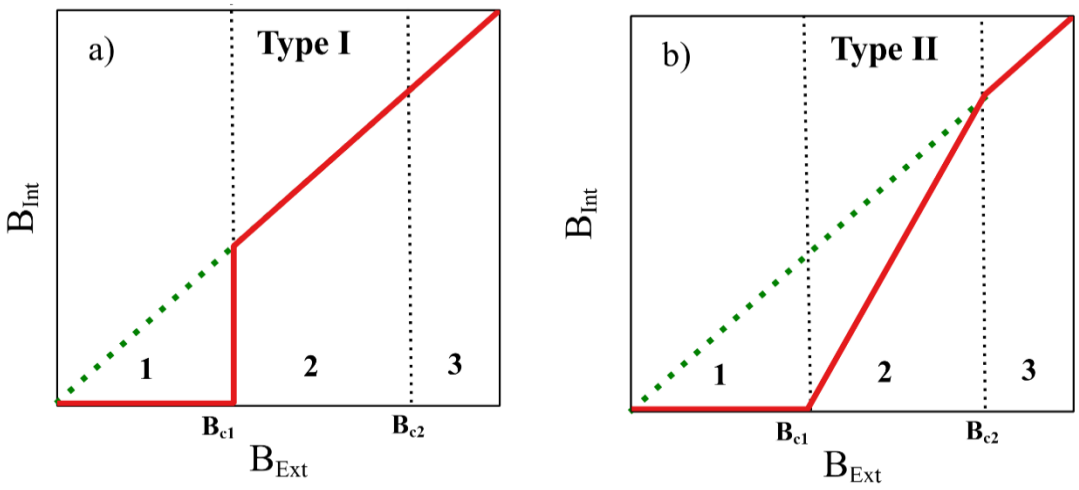

Figure 1.5: a) Type I superconductor behaviour b) Type II superconductor behaviour

Meanwhile, Type II superconductors, respond to a magnetic field differently, as illustrated in Figure 1.5b. 'B_{c1}' and 'B_{c2}' are the critical magnetic field one and two. The applied field starts to permeate the superconductor's interior at 'B_{c1}'. At this moment, the superconductivity is preserved. On the second region, with considerably higher critical field, '*Bc2'*, the superconductivity vanishes. The Meissner effect is incomplete for applied fields between B_{c1} and 'B_{c2}' known as the Shubnikov phase, allowing the superconductor to withstand very high magnetic fields.

A second phase transition occurs at considerably higher magnetic fields. The Shubnikov phase breaks down at the upper critical magnetic field '$B_{c2'}$, and the alloy returns to its normal conducting state. The change from the Meissner to the Shubnikov phase takes place at very low magnetic fields of just a few milli tesla. The second transition happens at fields of several tesla or higher. Because 'B_{c2}' is substantially larger than 'B_{c1}', only type II superconductors are viable for technical power applications including magnets, rotating machines, transformers, fault current limiters, and power cables.

1.3. Applications of superconductors

Nuclear fusion is regarded as the most promising source of energy in the future. The process of nuclear fusion happens when two light nuclei fuse to generate a heavier nucleus, releasing a tremendous quantity of energy. In the nuclear fusion reaction, Deuterium and Tritium should be heated to millions of degrees Celsius, in which atoms combine to form a heavier nucleus and release energy. However, no material on the earth can resist such a high level of energy. Plasma confinement with high magnetic fields is one possible approach and superconductors can create such strong magnetic fields. As if now, the ITER is the world's largest fusion experiment that employs LTS magnets made of NbTi and Nb_3Sn to produce suitably high magnetic fields.

For the current world, the most valuable thing is time. Superconducting maglev trains will make a huge impact on transportation and save time. Powerful electromagnets made of superconductors have been used to build levitating trains. The train can levitate while traveling ahead because conventional electromagnets on a guideway beneath it repel (or attract) the superconducting electromagnets. The maglev train has several advantages, including no friction between the rail and the train, minimal power consumption, and quiet operation. One of the first commercial operations of the maglev train is reported in 2006 from Xangai and the Pudong airport (30 km), China. Various countries, including Japan, the United States, Australia, and China, are actively developing superconducting maglev trains that can travel at speeds of over 600 km/h.

The development of a large, steady magnetic field for use in medical imaging is the most significant and widely used commercial application of superconductivity. A medical imaging technology named MRI scanning provides two-dimensional images of any anomalies, cancerous regions, or other bodily parts. The efficiency of scanning technology can be increased by using superconducting magnets instead of normal electromagnets. Another application in the superconductivity is the power grid and fault current limiter. Current can be transported without any resistance with higher transport capability. Some of the global superconducting project details are mentioned in Table 1.1 [19, 20].

Table 1.1: Superconducting global projects for power transmission [19, 20]

Year	***Local***	***Length [m]***	***Capacity***
2008	*USA (long Island)*	*600*	*574 (138kV AC, 2.4kA)*
2011	*China*	*360*	*13(1.3kV DC, 10kA)*
2013	*Korea (Icheon)*	*100*	*154(154kV AC, 10kA*
2014	*Germany*	*1000*	*40 (10kV AC, 3.75kA)*
2014	*Japan (Ishikari)*	*2000*	*100 (710kV DC, 5kA)*
2014	*Korea (Jeju)*	*500*	*500 (80kV DC)*
2014	*USA (Westchester)*	*170*	*96(13.8kV AC, 5kA*
2015	*Russia(st.petersburgo)*	*2500*	*50 (20kV DC, 2.5kA)*
2015	*Korea (Jeju)*	*1000*	*154(154kVAC,3.75kA)*
2015	*Japan(Yokohama)*	*250*	*200(66kV AC,5kA)*
2017	*Netherlands(Amsterdam)*	*6000*	*250 (50kV AC)*

The magnetic field of superconducting quantum interference devices (SQUID) is extremely sensitive. Even the magnetic field of the brain can be sensed using SQUID (10^{-13} Tesla). It can be utilised to perform non-invasive brain diagnostics. Nuclear Magnetic Resonance (NMR) is a powerful spectroscopic technique that is widely used in fundamental and applied research in different areas, including biology, materials science, medicine, and physics. Another important application of superconductivity is in the magnetic energy storage **(**Superconducting Magnetic Energy Storage, SMES). By using powerful superconducting magnets, the capacity and the efficiency of the system can be increased.

Superconductivity is used in the transformer, generator, and motors in order to improve their efficiency. The application of this technology in electric power starts in the early 1960s with the use of LTS. Europeans (ABB and Alstom), Japanese (KEPC), and Americans (Westinghouse) conducted extensive research (USA) with these electrical power appliances with LTS [20]. However, the cost of the cooling system requirement is high for the LTS based system. After the discovery of the HTS in 1986, scientific progress in these electrical applications has accelerated. HTS electrical system have several advantages, including higher efficiency, the ability to run above-rated power without compromising life, being smaller, lighter, and quieter. In addition to this, the losses in an electrical generator associated with rotor windings and armature bar, can be eliminated.

So, HTS superconductors have opened new insights into the technology and its applications. There are numerous other applications for superconductivity, all of which improves the system efficiency and performance. It will enable significant energy and financial savings.

1.4. Superconducting materials for technical applications

Superconducting materials used frequently for technical applications includes two LTS type materials and four HTS type materials. LTS materials are NbTi and Nb_3Sn and HTS materials include $Bi_2Sr_2Ca_1Cu_2O_y$ (BSCCO 2212) as round wires and $Bi_2Sr_2Ca_2Cu_3O_y$ (BSCCO 2223) as tape or bulk material and rare-earth barium copper oxide (Rare-earth$_1$Ba$_2$Cu$_3$O$_{7-x}$ or REBCO as bulk or tape material), and Magnesium-diboride (MgB_2). The critical temperature of each material is given in Table 1.2. There is no clear boundary temperature to differentiate between LTS and HTS superconductors. However, researchers use 30 K or liquid nitrogen boiling point temperature (77K) to differentiate between HTS and LTS.

Table 1.2: Critical temperature of technical superconductors

Material	***Critical temperature (K)***
NbTi (LTS)	*9.5*
Nb_3Sn (LTS)	*18.3*
MgB2 (HTS)	*39*
REBCO (HTS)	*92-95*
BSCCO2212 (HTS)	*95*
BSCCO2223 (HTS)	*107*

NbTi superconductors are mainly used for medium magnetic field application which includes magneto-resonance-imaging (MRI) devices, accelerator magnets or some fusion magnets [13, 15]. The Nb_3Sn compound is utilised to produce a magnetic field of 15-20 T [13, 15]. The MgB_2 compound is mostly used in satellite wire, low to medium magnetic field applications. BSCCO2223 is mostly utilised as a power cable and current leads in medium-field applications. BSCCO2212 and REBCO materials are required if the magnetic field required is more than 20 T [13, 21].

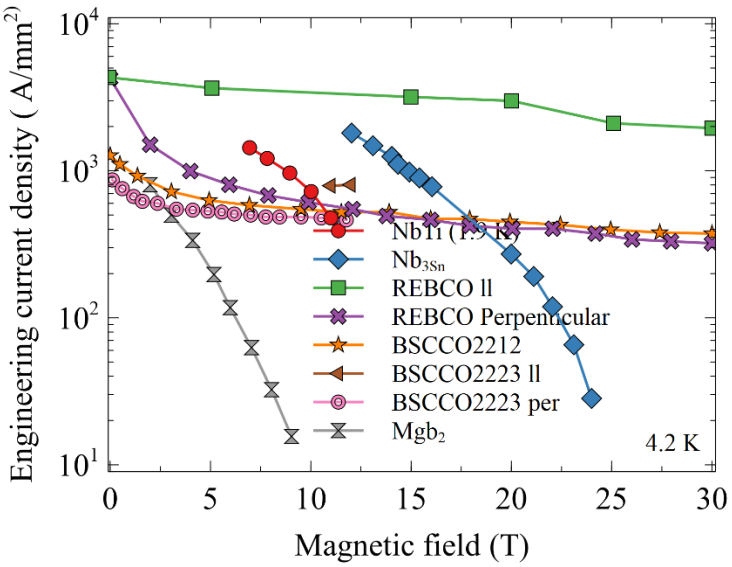

Figure 1.6: Variation of engineering current density with change in magnetic field [13]

Variation of engineering current density with changes in the magnetic field is depicted in Figure 1.6. It may be noted that the magnetic field is increased with decreasing the engineering current density for all the technical superconductors. Please note that this graph is plotted at 4.2 K for all the materials except for NbTi kept at 1.9 K. It is also observed that when the magnetic field is perpendicular to the material, then there is a sudden decrease in the engineering current density. REBCO and BSCCO2212 material shows stable engineering current density with an increase in the magnetic field. So, it can be used for high magnetic field applications. A comparison of these superconducting materials is given in Table 1.3 based on different aspects. Even though making REBCO superconductors is difficult, it has outstanding mechanical properties and can produce powerful magnets. REBCO material is a potential candidate for the 'DEMO' programme and other nuclear fusion initiatives that is expected to provide stable and continuous electricity.

Table 1.3: Comparison of technical superconductors

	NbTi	***Nb_3Sn***	***REBCO***	***BSCCO2212***	***BSCCO2223***
Magnetic field	*Medium field*	*High field*	*Very high field*	*Low field*	*Very high field*
Mechanical properties	*Very good(ductile)*	*Bad (Brittle)*	*Very good*	*Depending upon lamination*	*Bad*
Strain dependence on critical current	*Low*	*High*	*Low*	*Medium*	*Medium*
Cost of raw material	*Low*	*Low*	*Low*	*High*	*High*
Producing	*Simple*	*Medium*	*very complex*	*Medium*	*Complex*
Availability	*Very good*	*Very good*	*Medium*	*Bad*	*Bad*

REBCO, high-temperature superconductors are perovskite crystalline chemical compounds [22, 23]. And it is available in bulk crystal form and coated conductor form. Comparing coated conductors (CC) to bulk crystals, bulk crystals have a lower critical current density. As a result, bulk crystals are primarily used in magnetic bearings [24] and maglev trains [25]. Fusion magnets are not made from bulk crystals. Coated conductors, on the other hand, are the future candidate for fusion magnets. The alignment of the grain boundaries and saturation of oxygen with copper is very important to determine the superconducting properties of the REBCO material. REBCO acts as a superconductor when the copper is partially saturated with oxygen ($x < 0.55$, orthorhombic) and as an insulator when the oxygen concentration is low ($0.55 \leq x \leq 1$, tetragonal structure) [23].

1.5. Cabling configurations

Converting superconducting materials into wires and cables are challenging especially when they are brittle in nature as in the case of HTS. Many times, the superconducting materials are coated on a substrate and then the substrate is reinforced with other layers for turning it into wires and cables Some of the popular ones are presented here.

1.5.1. Roebel Assembled Coated Conductor (RACC) cables

The method of forming a group of insulated flat copper conductors into a rectangular rod for the use in large electrical machines was proposed by Ludwig Roebel in 1912 [26]. The Karlsruhe Institute of Technology (KIT) and Industrial Research Limited are the principal developers of RACC cables [27-29] made of REBCO tapes. RACC cables are made up of meander-shaped coated conductor tapes constructed using the Roebel process, resulting in rectangular cables with the same width as their constituent REBCO tapes. The number of tapes in the RACC cable is dependent on the thickness of the cable as well as its twist pitch as depicted in Figure 1.7. A part of the tape is wasted when REBCO tape is punched in a meander shape.

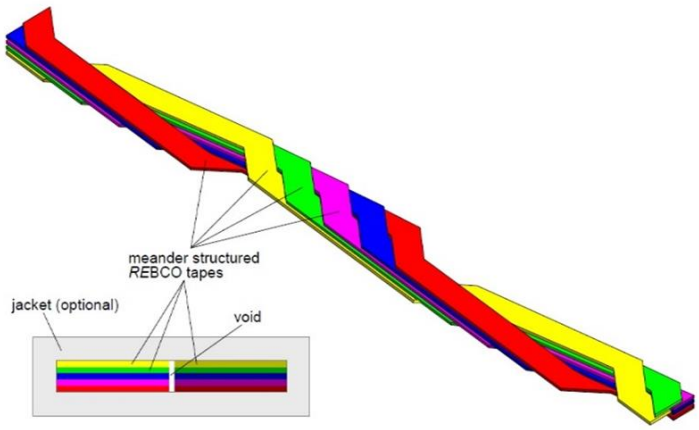

Figure 1.7: Schematic of Roebel Assembled Coated Conductor with 5 tapes [30]

RACC cables are having anisotropic mechanical properties and the manufacturing of the cable is complex. However, the degradation of the cable due to its manufacturing process is low. It is having “U-shape” or “stair” type contacting method. It shows the complete transposition of the current. Scaling to fusion currents is not possible for RACC cables. For electrical stabilization, copper tapes are added. It is having poor mechanical properties. Voids must be filled to prevent movement & distribute loads.

1.5.2. Coated Conductor Rutherford Cable (CCRC)

The Rutherford winding process is used to wrap many RACC cables around a former, resulting in Coated Conductor Rutherford Cable (CCRCs). The RACC sub cables are held in place by the grooves in the former. RACC wires are bent in and out of plane around a structural former in this way.

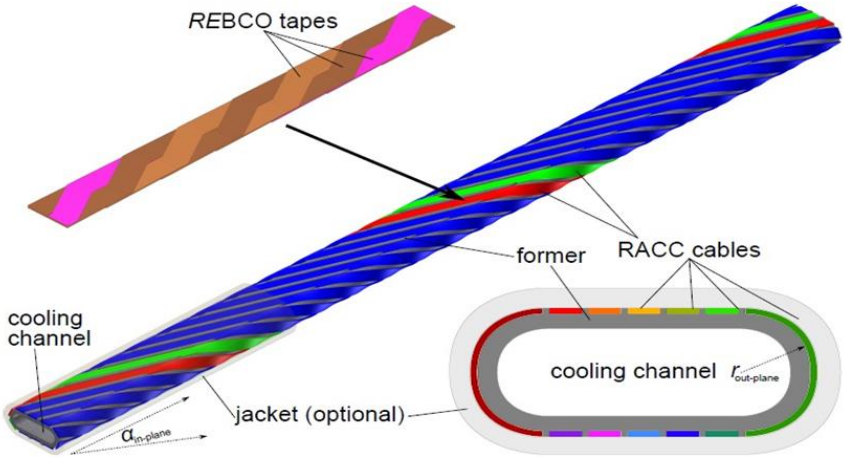

Figure 1.8: Schematic drawing of CCRC cables with cables wound over a former of structural material [13, 31]

Mechanical stability of the entire cable and cooling channels is also provided by the former as depicted in Figure 1.8. For added mechanical stability, CCRCs can be outfitted with a structural material jacket. Rutherford cabling method completely transposes the strands. The strands' superconductor tapes and RACC's sub cables are also completely transposed. CCRCs can be scaled up to extremely high currents by increasing the number of RACC sub cables and REBCO tapes per sub cable. Small RACC sub cables are used as strands in the CCRC concept. RACC contacting methods can therefore be employed in CCRCs, but on a lesser scale and multiple times for each CCRC. The "stair" or "double stair" designs are viable options since they use fewer REBCO tapes per RACC sub cable. To homogenize the contact resistance between the RACC sub cables, symmetric arrangements with similar copper cross-sectional areas and distances are required.

In conclusion, CCRC cables are having two cable stages and their manufacturing is very complex. It is having "U-shape" or "stair" type contacting method. It is having complete transposition. Scaling to fusion currents is possible for CCRC cables but a high cross-section area is necessary. For electrical stabilisation, copper tapes or former can be used.

1.5.3. Twisted Stacked-Tape Cable (TSTC)

M. Takayasu *et al*. proposed Twisted Stacked-Tape Cable (TSTC) in 2011 and it is represented in Figure 1.9. It offers a high current density as well as a scalable cabling system that may be used for a large-scale magnet. The Massachusetts Institute of Technology's Plasma Science and Fusion Center is working on the TSTC concept [32, 33].

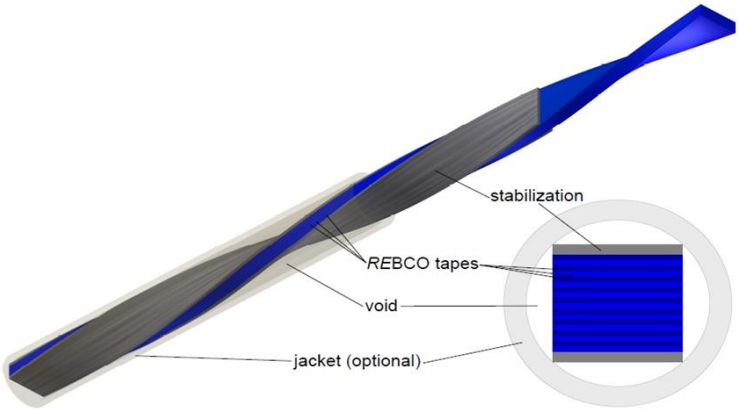

Figure 1.9: Schematic of a single Twisted Stacked-Tape cable (TSTC) [13]

Several REBCO tapes are stacked and twisted to form Twisted Stacked-Tape Cables. The top and bottom of the REBCO tape stack can be covered with 1 mm thick copper tapes of the same width. Additional electrical and mechanical stability is provided by the copper tapes. The twisted stack is placed within a structural material tube (sheath). All spaces between the TSTC and the sheath must be filled to restrict the tapes from moving and to minimise stress concentrations. Glue, resin or solder are the suitable filling materials. A single TSTC stack can only hold a certain number of tapes and the ideal stack thickness is equal to the tape width. For instance, stack sizes of roughly 40 Superpower^{TM} type tapes are required to attain 4 mm width. Several TSTCs must be combined to improve the current carrying capacity. The TSTC stacks can be sub-cables of a larger cable, similar to the RACC cables in the CCRC concept. To stabilise the cable, several TSTC stacks can be placed into the grooves of a former made of structural or stabilising material. Multi-stack TSTCs can also be provided with structural material jackets for further mechanical stabilisation.

In radial directions, TSTCs are isotropic due to their round geometry. As a result, only two types of mechanical loads must be considered: (1) longitudinal mechanical loads and (2) radial mechanical loads [13, 34]. Magnet conductors experience hoop stresses that are parallel to the cable. Because REBCO tapes are arranged nearly straight in the TSTC concept, the mechanical performance of TSTCs is found in a parallel direction by the average mechanical properties of the former and the tapes. The TSTC concept is an excellent alternative for applications with considerable mechanical loads in the parallel direction, like high-field magnets.

1.5.4. Round Strands Composed of Coated Conductor Tapes (RSCCCT) cable

In 2012, D. Uglietti et al. proposed the RSCCCT cable concept. There are two stages of cabling in this HTS cable concept. Stacks of REBCO tapes are soldered between two semi-circular copper profiles during the first cabling stage. The resultant conductor is almost round, as shown in Figure 1.10, because each REBCO stack contains a few tapes. The superconducting tapes are partially transposed as a result of their twisting.

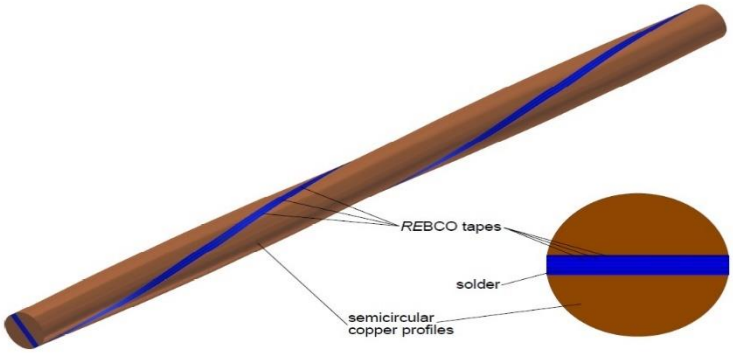

Figure 1.10: Scheme of first cabling stage of RSCCCT with REBCO tapes soldered between two semi-circular copper profiles [13].

The initial phase resembles the TSTC idea. However, the second stage of cabling is distinct. In the RSCCCT cable design, the first stage of cabling's roughly circular conductors is stranded. It completely transposes the strands. As the REBCO tapes are only partially transposed during the first stage of twisting, the overall transposition of this idea remains incomplete when the cable's self-field is considered. Considering only magnetic background fields, the second stage's transposition meets the criteria for complete overall transposition. Due to the strong background fields of fusion magnets, the magnetic self-field of each conductor can be neglected. The contracting method used for RSCCCT and TSTC is the same, BSCCO-REBCO connectors help to make the

contact. As a conductor in fusion magnets, the large copper fraction of RSCCCT cables is advantageous for electrical stabilisation.

1.5.5. Conductor on Round Core (CORC) cable

The cable concept has been proposed and developed by D.C. van der Laan et al. in 2009 [35, 36]. The central core and REBCO tape are the key parts of a CORC cable. A centre former is wound with REBCO tapes to form the CORC cable.

Tapes are wrapped around the conductor on a round core cable. A copper rod or a copper power cable is used as a former in most CORC cables. The former contributes to both electrical and mechanical stabilisation. The cable's forced flow cooling can also be accomplished using a hollow former. Figure 1.11 depicts a CORC cable with multiple layers and how the winding orientation between each layer has been reversed. The tapes are wound in opposite directions around a former and the inner layer stays close to the centre while the outer layer stays away from the centre. The transposition of the CORC cable is partial.

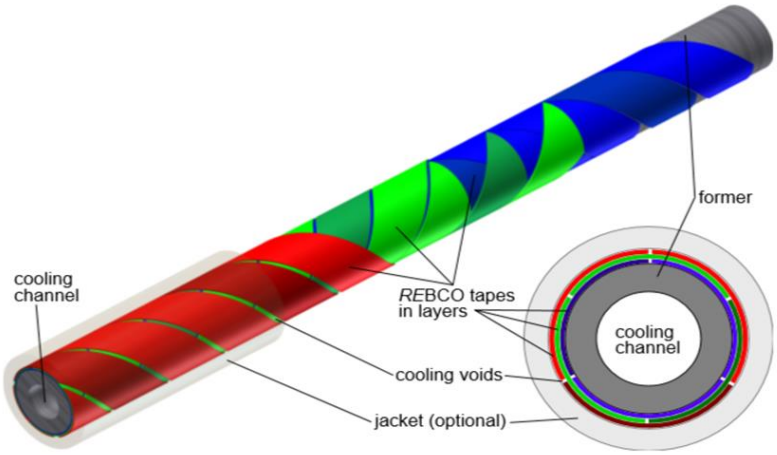

Figure 1.11: Schematic drawing of CORC cable wound on round former with reversed winding direction for each layer [13].

The round geometry of CORC cable makes it isotropic in the radial direction. The cable's longitudinal and radial mechanical loads are considered the most important. All crystal unit cells c-axis (001) is perpendicular to the tape surface in the tapes. The a (100) and b (010) axes are in the tape plane, parallel to or perpendicular to the tape direction. The orientations of the a- and b-axes may vary from grain to grain. If the mechanical load is applied along the tape, it operates on the a-axis in certain grains. In contrast, the b-axis is strained in other grains. When the tape is wound at 45 degrees around the core, it has some advantages since it works equally on the a-and b-axes of all grains. As a result, there

is the lowest amount of strain [37]. Therefore, CORC cables are thus excellent for mechanical loads that are both longitudinal and radial.

1.6. Comparison of different cabling configuration

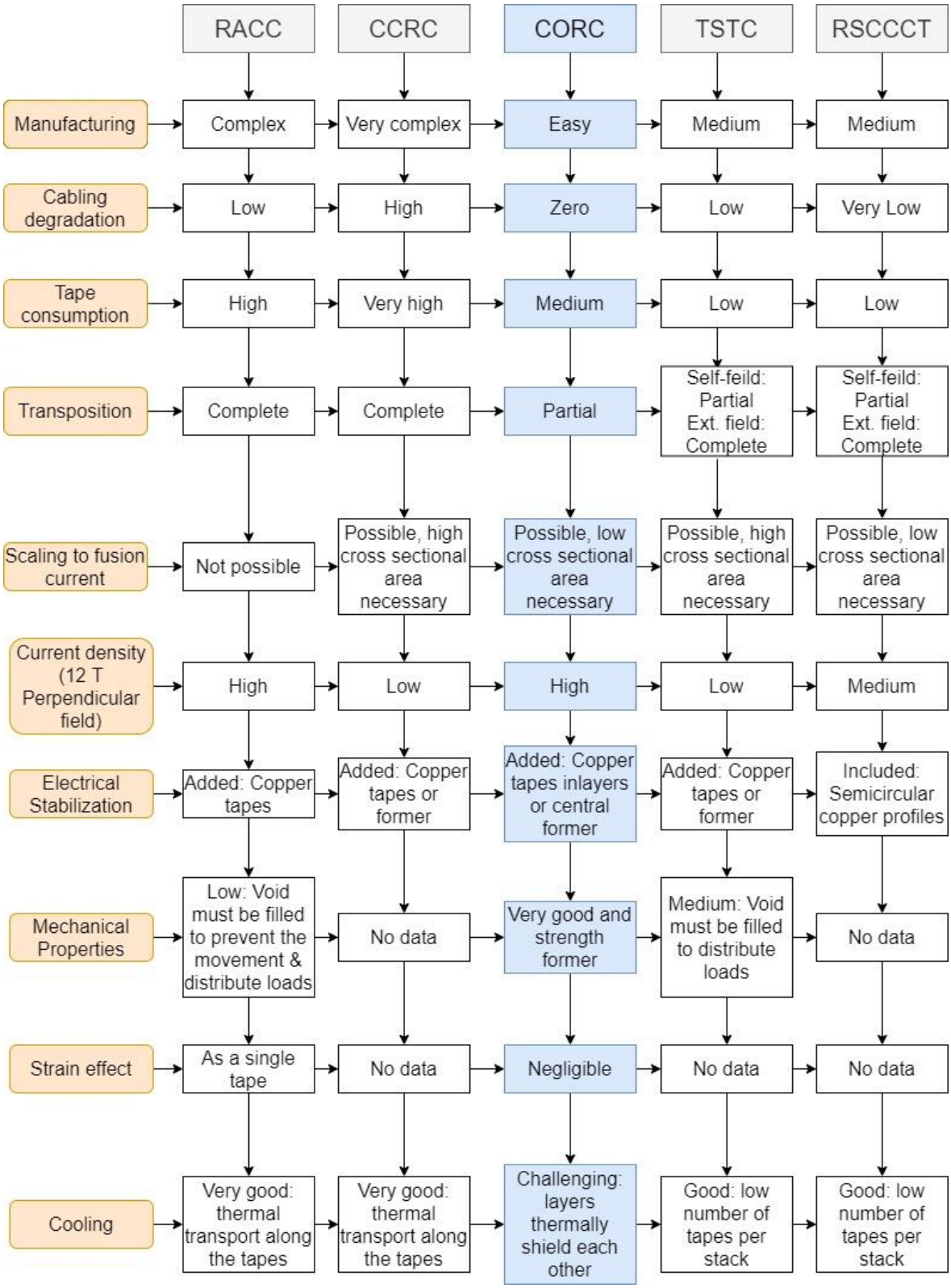

Figure 1.12: Comparison of different cabling configurations

After conducting a review of various superconductor cables, it has been found that CORC cables are the most promising one for REBCO type materials. The use of CORC cables for future superconducting advancements are expected in terms of ease of manufacturing, cabling degradation, mechanical characteristics, and electrical stability. CORC cable cooling is a bit challenging, therefore various research works are underway to address it.

1.7 Quenching and related issues

When the critical limit of the superconductor is exceeded, quenching may occur. Also, when the magnetic field, current density, temperature, and physical strain exceed a particular limit, and it can cause quenching and eventual degradation. Quenching of the superconducting magnet is one of the major concerns that occurred in the superconductors mainly due to the development of small amounts of heat and eventually spread and damage the whole system. Large Hadron Collider (LHC), a particle accelerator at CERN in Geneva, is the largest and maybe most complex piece of scientific equipment ever created. Due to the accelerator's reliance on the reliable operation of around 10,000 superconducting magnets containing approximately 15,000 MJ of magnetic energy. This was cooled by 130 tonnes of helium at temperatures of 1.9 and 4.2 K. After 10 days from the first operation of LHC in 2008, September 10, a short circuit (induced by the mechanical displacement) resulted in an accident that burned a hole in a container holding liquid helium [13]. The explosion that followed left the machine inoperable until 2009 July. If the $\frac{I}{I_c}$ is greater than 0.8, then the minimum quench energy is in the order of 10μJ. So, the operation of superconducting magnets, precise design of geometrical parameters, insulation, coil winding, coil curing, and coil assembly is required for smooth and safe operation.

This research work focuses on how the physical strain influences the degradation of REBCO tape and CORC cable. Therefore, a complete literature survey on various cases where physical strain may developed in the superconductor including tensile, bending, twisting, fatigue, and their combined effects are presented.

Chapter 2

Literature Review

2.1 Introduction

The role superconductors can play in meeting the huge energy demands of the future is significant. The HTS type of superconducting materials is expected to have the potential to improve efficiency and reduce the cost. The process of converting brittle HTS materials to wires and cables through different cabling concepts are available.

2.1.1 Significance of High-Temperature Superconductors

Georg Bednorz and K. Alex Müller discovered HTS in 1986. In 1987, they received the Nobel Prize in Physics for "their significant advance in the discovery of superconductivity in ceramic materials. The use of HTS materials in fusion machines significantly increases the efficiency, as reported by W.H. Fietz et al. in 2011 [21]. HTS achieves greater thermal stability to guard against the magnet system's failure and reduce

the nuclear radiation shield's thickness. It has also been documented that, compared to their counterparts, HTS have maintained a high critical current density at increasing temperatures and magnetic fields. The amount of fusion power in a fusion tokamak system is proportional to the fourth power magnetic field [2]. Using HTS material in coils and current leads would be promising approach for future fusion reactors. If the coils could run at temperatures above 65 K, this would significantly benefit in reducing the operating cost. It might be possible to reduce the size of the machine and simplify the cryostat by avoiding the radiation shield of the coils. Additionally, using less power for refrigeration reduces both investment and maintenance costs.

Significant progress has been made in the capacity of HTS to carry a high current under a high magnetic field by improving their flux pinning capabilities through inserting nano-scale defects [1]. The scientific community is interested in REBCO compounds to attain the fields in the span of 30-50 T in superconducting magnets [2, 3]. D C van der Laan compared HTS and LTS based on the development of magnetic field capability and the cooling medium employed [38]. In liquid helium, LTS are restricted to magnetic fields of 20–22 T [38]. Due to their exceptionally high upper critical magnetic field, HTS are the only materials that can be used to generate magnetic fields larger than 22 T [38]. According to the Japanese national project, HTS cables are capable of achieving a considerable power capacity and low-loss power transmission [39]. Fujikura Ltd. developed a 66 kV-5 kArms HTS power cable utilising high critical current REBCO tapes. They successfully developed a 20 m-long 66 kV-5 kArms HTS power line with less than 2 W/m AC loss [39].

2.1.2 Configuration of High-Temperature Superconductor tapes

The basic configuration of superpower® REBCO (Rare Earth Barium Copper Oxide) 2G (second generation) HTS wire is shown in Figure 2.1. The superconducting REBCO tape comprises different layers such as copper stabiliser, silver over layer, REBCO, substrate, and buffer stack.

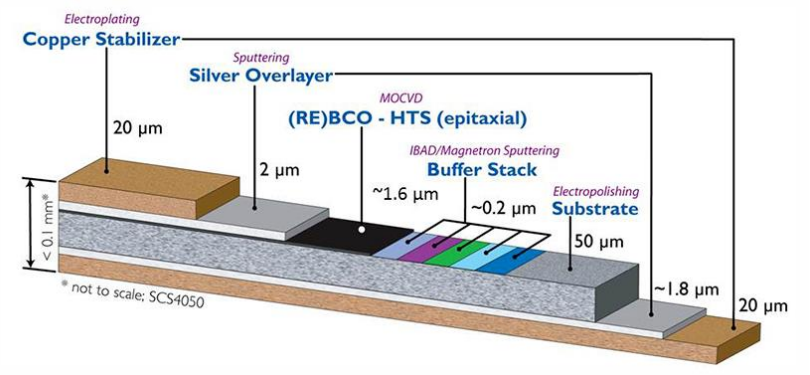

Figure 2.1: Configuration of SuperPower® 2G HTS Tape SCS4050 [40].

The substrate is usually made with Hastelloy (C276), Stainless steel, lanthanum aluminate ($LaAlO_3$), Nikkel and silver [41]. Buffer layers are the combination of different ceramic oxides such as magnesium oxide (MgO), Cerium oxide (CeO_2) and Yttria-stabilised Zirconium materials [41]. The materials electrical and mechanical properties depend on the 41properties of the constituting layers and the crystal lattice alignment [42, 43]. The Inclined Substrate Deposition (ISD), Ion Beam Assisted Deposition (IBAD), Rolling Assisted Biaxially Textured Substrate Method (RABITS), Pulsed Laser Deposition (PLD), Electron Beam Co-Evaporation, Metal-Organic Chemical Vapour Deposition (MOCVD) are some of the processing techniques utilised for substrate, buffer layer, and REBCO [42, 44, 45, 46, 47, 48, 49].

2.1.3 Development of strain in High-Temperature Superconducting tapes

The different types of mechanical loads are acting on the superconducting tapes during their operation and manufacturing stages. One of the major forces during its operation manufacturing stages is the magnetic Lorentz force. Thermal force is due to repeated heating and cooling down. Fatigue loads are developed in mobile systems and also in rotating members in addition to the fatigue load due to Lorentz force. Mechanical forces acting on the REBCO tapes and cables during the manufacturing phase. Residual strain is another force that developed during the production time of the tape. Different mechanical loads act on them are tension, bending, torsion and transverse load [50]. The individual loads as well as the combined effect of each load should be maintained below the critical limit so as to ensure smooth and safe operation of the superconductors. Stress induced is highly dependent on the material's intrinsic properties, such as its yield strength and Young's modulus. On the other hand, the strain values are not varying much with changes in material properties. Therefore, the strain values are most frequently used in

the calculations for determining the dimensions of HTS tapes [50]. Figure 2.2 represents how the strain values are distributed in the tape with different loading such as tension, bending and torsion [50]. The distribution of the strain based on the type of load is reported [50]. It is important to understand the degradation of the superconductor under these loads and also the critical limits beyond which they degrade.

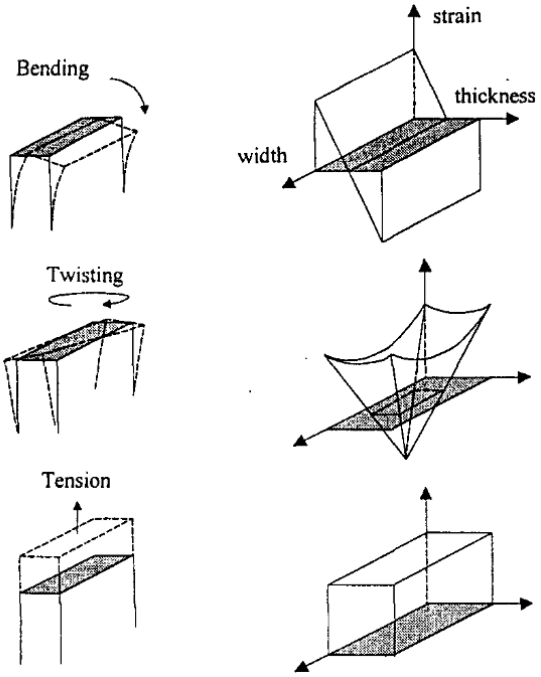

Figure 2.2: Strain distribution for three different modes of loading [50].

A detailed literature review is carried out for each loading, such as tension, bending and twisting and winding. The studies reported on the fatigue failure in the REBCO tape under different mechanical loads are also presented in the subsequent sections.

2.2 Effect of tensile loading on High- Temperature Superconducting tapes.

Tension is one of the straightforward forms of mechanical load; however, may lead to the degradation of the tape and eventual quenching. Superconductors can be fractured by tensile loads from the exterior. Non-homogeneities or sharp notches between grains can raise local stress levels, leading to the start of cracks [50]. Low grain connection can also contribute to the start of cracks at lower stress levels. The uniaxial strain influence on the critical current of the superconductors can be explained in terms of compressive pre-strain, irreversible strain and elastic strain sensitivity of the upper critical field and peak pinning force [51]. The pre-compressive strain mainly developed due to the difference in the thermal expansion coefficient of the layer when subjected to cooling down from its production temperature to operating temperature. After the

production process, the residual strain is developed in the REBCO tape and is compressive in nature. This compressive component decreases during the tensile loading and eventually comes to a strain-free state [52]. The force-free state is evaluated from the mechanical properties of about 0.17 % and 0.26 % at 298 K and 77 K respectively [52]. The strain at which the residual strain on the superconducting tape becomes zero is referred to as force-free strain [53]. There are reports that this strain-free state occurs for YBCO compounds with 0.18-0.42 % strain depending on the geometrical configuration and the manufacturing methods [54]. The maximum value of critical current is observed at the strain-free state.

The residual strain developed in the REBCO layer is dependent on the processing technique. Residual strain in the REBCO layer is compared when it is prepared by a different process such as DC sputtering and pulsed laser deposition (PLD). These results show residual strain values as 54 MPa and 282 MPa respectively [55]. The residual strain in the REBCO layer and other constituting layers is affected by the temperature of the substrate, in addition to the processing technique. The following equation can be used to represent the residual stress in the material [55, 56].

$$\sigma_{res} = \sigma_{in} + \sigma_{th} + \sigma_{ex} \tag{2.1}$$

Where σ_{res} is the total residual stress in the material and σ_{in} is the intrinsic stress developed during the deposition process. It is due to various defects and lattice mismatches between the layers. σ_{th} is the thermal stress developed due to the cooling after deposition, and σ_{ex} is the stress developed due to the external force.

The residual stress/strain in the REBCO layer is usually measured by the X-ray diffraction ($\sin^2\Psi$ method) method, and the coordinate system for X-ray diffraction is shown in Figure 2.3 [41, 55].

$$\frac{\Delta d}{d} = \frac{d_{\Psi} - d_T}{d_T} = \sigma_{\emptyset} \frac{(1+V_c)}{E_c} \sin^2\Psi \tag{2.2}$$

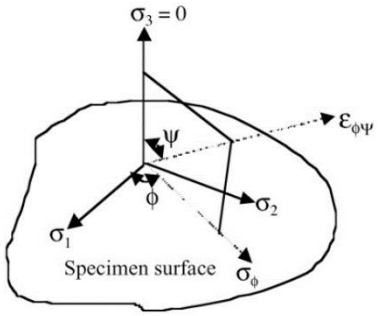

Figure 2.3: Coordinate system for X-ray diffraction

where dψ and dT represent the measured lattice spacings of the film at angles ψ and 0◦ to σ_3, and E and v represent the film's elastic moduli and Poisson ratio, respectively.

DYBCO did not show any peak critical current in the tensile region under tensile loading. However, compressive strain is applied to the DyBCO layer by bending, showing the peak critical current in the superconducting layer [52, 57]. Like DyBCO, the SmBCO compound is also in the tensile strain state; the critical current decreased monotonically with the applied tensile strain [57]. It is also reported that when the tensile load is applied to the superconducting tape, the change in the mechanical properties is divided into three stages, Elastic, micro yielding, and macro yielding [53, 57]. Hastelloy and copper behave plastically in the micro yielding phase, while the YBCO layer remains in the elastic region [52, 58]. The mechanical characteristics tested at 77 K demonstrated that the annealed Hastelloy C-276 substrate material at 963 K exhibited discontinuous yielding, thermal stability, and inertness to the buffer layer [57]. It may be because of the low carbon and silicon composition, which prevents carbide precipitation at grain boundaries.

The mechanical properties of the substrate material are critical for determining the allowed strain limit in coated conductors, and the strain value at quenching is not influenced by the buffer layer or superconducting materials [57]. However, the critical current value recovered even after the applied strain reached 0.30 % for CeO2/YSZ buffered tape and less than 0.22 % for MgO buffered tape [59]. The use of metallic stabilisers additionally increases the reversible limit of the coated conductor [54]. The reversible limit of a Stainless steel-reinforced YBCO-coated conductor is double that of a non-stabilised conductor [54]. The critical current (*Ic*) degrading behaviour of YBCO-coated conductors manufactured using the RABiTS-PLD process may be separated into two stages. Stage I: When the strain was released, the YBCO film behaved elastically, and Ic recovered. Stage II: Ic degradation is caused by cracking in the YBCO film due to plastic deformation of the substrate or the stabilising layer [54]. The stress-strain

correlation for commercial REBCO coated conductors from five different industrial manufacturers, including Bruker HTS, Fujikura, SuNAM, SuperOx, and SuperPower, was examined at 77 K (self-field) and 4.2 K (19 T) [60]. These tapes have different electro-mechanical and mechanical properties due to the manufacturers' use of various materials and deposition techniques. The irreversible strain limit varied from 0.45 % to 0.72 % [60]. It is also reported that the young's modulus of all the tapes does not vary with temperature, but a 10 % higher yield strength is found at a lower temperature (4.2K). This implies that temperature also has a significant impact on the degradation of the tape [60]. The irreversibility limit of REBCO tape from different manufacturers are also reported. The irreversible limit varies from the different manufacturers in the range of 0.25 to 0.6 % applied strain [15]. The tape's stress-strain characteristics depend on the size and properties of the substrate material [15]. The majority of the tape performs well under applied compressive strain. The irreversible limit is also dependent on the temperature and the Superpower® 2G SCS4050 tape shows a higher irreversible limit at 4.2 K than 77K [1].

The performance of tape under torsion, tensile, and transverse loading was investigated by K Ilin *et al*. in 2015 [17]. The effect of thickness of copper stabiliser layers and the non-uniformity of the tape surface profile on the critical force was also confirmed. Systematic measurements were performed on a single REBCO tape, and the tape's response to axial tension, torsion, and transverse stress was calculated. An experimental study and detailed finite element modelling of the 3D stress-strain state in a single REBCO tape under various loads starting from the initial tape processing phase, during production and up to the operating stage were discussed in the paper. The models account for temperature dependence and elastic-plastic properties of the tape materials. The critical strain in the REBCO layer is about 0.7 % (Corresponding to 0.45 % of intrinsic axial strain) as given in Figure 2.4 [17, 52].

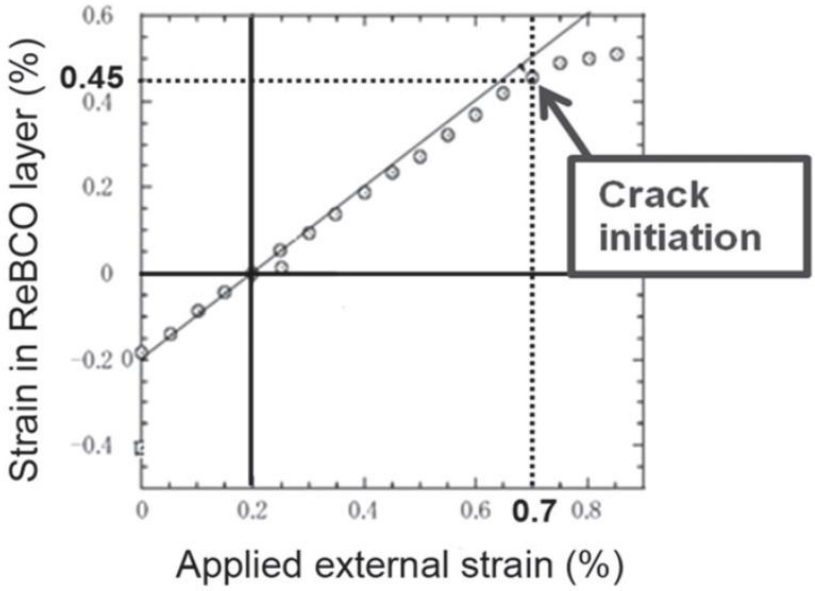

Figure 2.4: Crack initiation in the REBCO layer under tensile loading [17, 52]

The copper layer improves the fracture toughness of the tape and delays crack formation. The value of the irreversible limit increased from 0.4 % to 0.5% when YBCO-coated conductors were electroplated with copper [61]. 11 % decrease in the critical current density is observed at 77 K. However, when the temperature is reduced to 4 K, the drop in the critical current density is reduced to 3.5% [61]. The paper also reported the influence of the magnetic field on the irreversible limit. The magnetic field is increased from 0.5 T to 3 T; the sensitivity of critical current density to strain decreases. However, after 3 T to 16 T, an increase in the sensitivity of critical current density to strain is observed [61].

The reversibility of critical current with strain is evaluated for thin and thick YBCO-coated conductors at 77 K and 4 K and a varying magnetic field from 0 T to 16 T [61]. The reversible effect is dependent on temperature and magnetic field. The effect of strain appears to decrease with reducing the temperature [61]. The strain influence on critical current at different magnetic fields is determined at the YBCO layer, and it is discovered that strain sensitivity increases with temperature, and the magnetic field effect on critical current is more prominent at higher temperatures [62].

2.3 Effect of bending on high-temperature superconducting tapes

The bending load is acted on the superconducting tape during the manufacturing stage of superconducting cables/wires and magnets and also in the application stage due to the effect of Lorentz force. It is reported to be the most critical one, out of the different mechanical loads.

The reversible degradation of HTS was first reported in 2003 [63]. MOD-RABiTS sample shows that the 40 % critical current reversible reduction is observed when subjected to 0.95% compressive strain. Under applied tensile strain, the critical current first increases slightly for YBCO, then further tensile strain critical current reversibly decreases, and finally, irreversible degradation occurs [63]. The power-law expression best describes the strain dependence of critical current density in self-field for YBCO manufactured by different production methods [63].

$$\frac{J_c(\epsilon)}{J_c(\epsilon_0)} = 1 - a|\epsilon_0|^{2.2\pm0.02} \tag{2.3}$$

Where 'a' is the strain sensitivity parameter, 'ϵ' and 'ϵ_0' are intrinsic strain and intrinsic strain at maximum critical current density, respectively.

In 1999, a winding study related to BSCCO material found that 48 % of critical current degradation happens when the bending diameter changes from 11.5 cm to 5 cm (10μv criterion was used) [64]. The critical bending diameter is considered as 5 cm because after that there is a sudden decrease in the critical current was observed [64]. A new design of bending of BSCCO tape was reported in 2004, which facilitates the measurement of bending strains to single BSCCO tapes without any tape manipulation or handling throughout the experiment [65]. It helps to avoid the continuous heating and cooldown problems during the investigation. Also, they use the calps to attach the fixture, which helps prevent the soldering issues and overheating problems that damage the tape. The paper also reported that the filament structure, sheath composition, and filling factor substantially influence the strain limit where filament cracks happen [65]. The behaviour-critical current degradation of BSCCO under bending loading is gradual and consistent, which is different from tensile loading behaviour [66]. Simultaneous initiation of crack and growth was observed for BSCCO compound up to the irreversible limit, and after the irreversible limit, this growth is different for different sections. Literature provides simple equations for calculating the bending strain for hard and easy bending [66-68]. The

bending load is applied in thickness and width direction in the case of easy and hard bending, respectively.

$$\epsilon = \frac{W}{2r+W} \times 100 \quad \text{(Hard bending)} \tag{2.4}$$

$$\epsilon = \frac{t}{2r+t} \times 100 \quad \text{(Easy bending)} \tag{2.5}$$

Where '*w*' and '*t*' are the width and thickness of the tape, respectively.

The pictorial representation of strain distribution of easy and hard bending is provided below [68].

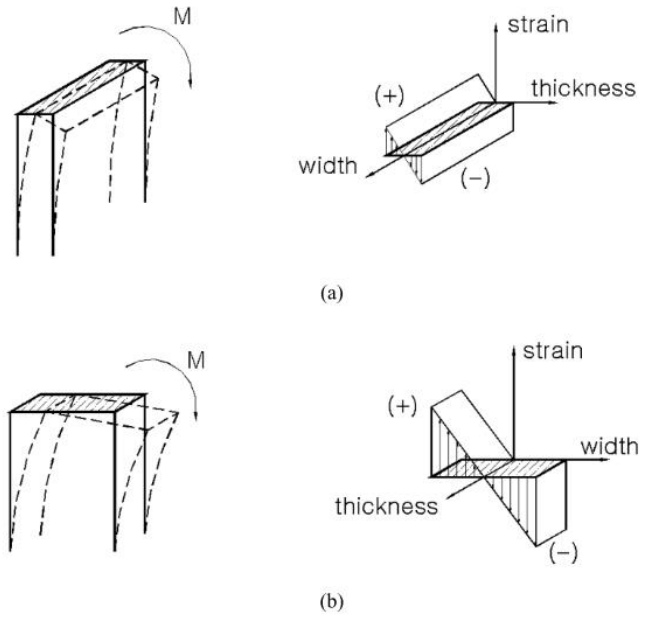

Figure 2.5: Strain distribution under a) easy bending and b) hard bending [68]

The easy bending of YBCO tape is reported with 4.3 mm width and 0.19 mm thickness; 95% of critical current retention was observed in the strain limit of 0.35-0.45 % of bending strain [69]. On the other hand, in the case of hard bending, no significant degradation of critical current was found upto 0.6 % of bending strain. However, it is found that winding a single pancake coil with a diameter of up to almost 12 mm is feasible at 0.65 % bending strain for the YBCO tape in simple bending [69].

The experimental investigation under bending for second generation REBCO tape and strand is reported [70]. The strand has a round cross-section consisting of 4 sub-strands, each composed of 18 REBCO tape. The sub-strands are arranged so that 1 and 3 sub-strands undergo in-plane bending (hard bending), and the other two undergo out-of-

plane bending (easy bending). The literature found the minimum bending radii for each case. The minimum bending radii for the strand is 352 mm, and for the tape under in-plane and out-of-plane bending is 229 and 5.8 mm, respectively [70].

The out-of-plane bending characteristics of REBCO tape are discussed in the literature [71]. The easy (90^o) and hard (0^o) bending is considered the two ends of out-of-plane bending. In out-of-plane bending, the angle is maintained between 0^o and 90^o. The critical bending radius for 2.5 mm tape at different angles is given below in Table 2.1 [71].

Table 2.1: Critical bending radii and bending strain for out-of-plane bending [71]

Bending angle	***Critical bending diameter (mm)***	***Critical bending strain***
0^o	*420*	*0.595%*
15^o	*408*	*0.595%*
30^o	*408*	*0.538%*
45^o	*260*	*0.695%*
60^o	*200*	*0.649%*
75^o	*70*	*1.002%*

When the bending angle increases from hard to easy bending, the critical bending diameter decreases and the tape's ability to withstand the strain increases.

In 2005, the critical current dependence on bending strain was investigated to use YBCO material in the solenoid and pancake-type magnets [72] They chose different configurations of the YBCO tape with Hastelloy, buffer layer, YBCO and silver cap layer. The heat cycle test was carried out ten times by applying tensile strains of around 0%, 0.30%, and 0.50% and found any degradation in all three samples [72].

The pre-compression strain of a typical A15 (e.g., Nb_3Sn) structure compound is in the range of 0.2 % to 0.4 % and also shows good elastic strain sensitivities. Unlike A15 superconductors, B1 and C15 crystal structure superconductors have no appreciable elastic strain dependence on critical current density [51]. The 5 % reversible reduction in critical current for YBCO was reported in the literature when the bending radii comes to 0.25-0.28 m [73]. The YBCO layer's thickness does not depend on the critical current density under in-plane bending [73]. The sensitivity of the critical current density of the

YBCO-coated conductor on in-plane bending depends on the axial strain and the width of the tape [73]. The effective width of the tape is slightly smaller (slitting edge damage) than the physical width, which might be why the width is dependent on critical current density.

When the REBCO tape is subjected to a bending load, the position of the neutral axis is crucial. The distance between the REBCO layer and the neutral axis is a critical parameter determining the amount of strain developed in the REBCO layer. Suppose the REBCO layer is above the neutral axis, tensile strain is induced in the REBCO layer. On the other hand, the compressive strain is produced (when positioned below the neutral axis). To understand the influence of bending strain on the REBCO tape, copper is electroplated only on the top side of the REBCO tape, and a bending load is applied to the REBCO tape [74]. The study found that the location of the neutral axis is fixed in the elastic regime and positioned between the silver REBCO interface. The copper layer would reach its elastic limit and be unable to carry the additional stress or strain when the bending diameter is reduced (bending strain increased). As a result, the neutral axis moves in the direction of Hastelloy to achieve the desired balance of stresses between the tensile and compressive sides. At a smaller diameter, the strain eventually rises to the point where the Hastelloy begins to yield under tension. Once the substrate reaches its yield point in compression, the neutral axis position shifts back towards the REBCO layer to balance the stress balance [74].

Electroplating the copper stabiliser to one side of the REBCO tape is one of the best approaches to reduce the compressive strain induced in the REBCO layer during the bending due to the shift of the neutral axis close to the REBCO layer. Soumen Kar et al. in 2017, carried out the bending study by wounding the 2 mm REBCO tape over the central core, whose diameter varied from 12.5 mm to 0.51 mm [75]. It is found that 22 μm substrate with 20 μm and 30 μm copper electroplated only on one side shows no significant critical current degradation at 0.81 mm and 1.1 mm bending diameter, respectively [75]. Also reported that the 50 μm substrate sample degraded faster than the 22 μm sample [75]. It is concluded that using a thinner substrate and one-side copper plated REBCO tape can improve the critical current reversible limit [75]. The position of the neutral axial is calculated from the internal stress balance, and zero bending strain is developed at the neutral axis. So, the position of the neutral axis is important. Placing the neutral axis at the REBCO layer will help improve the tape's performance under bending.

The equation for placing the neutral axis at the REBCO layer with substrate, silver overlayer and solder is reported in the literature is given below [76],

$$E_o t_o^2 + 2\, E_o\, t_l\, t_o + E_l t_l^2 - E_s t_s^2 = 0 \tag{2.6}$$

Where *'t*' and '*E*' stand for the layer thickness and Young's modulus, respectively, and '*s*', '*o*', and '*l*' represent the substrate, silver overlayer, and solder (copper layer), respectively.

The bending study was carried out by taking four different samples from Shanghai **Superconductor Technology (SST) and Suzhou Advanced Materials Research Institute (SAMRI)** (Two samples from each) [77]. They also found the critical bending radii for each case and determined the cause for critical current degradation with the help of chemical etching and ESEM (environmental scanning electron microscope). The transverse cracks are developed during the bending that blocks the longitudinal current path and leads to the tape's degradation [77]. The critical bending radii for SST236 (50 μm substrate thickness and 85 μm stabiliser) and SST380 (50 μm substrate thickness and 160 μm stabiliser) are 6-7 and 4-5 range, respectively [77]. However, the critical bending radii of the SAMRI sample (61 μm substrate thickness and, 180 and 316 μm stabiliser) are around 4 mm. This shows the better bending tolerance of REBCO tape from SAMRI. One major difference between these samples is that STT conductors used PLD technique, and SAMRI conductors adopted the MOCVD technique.

The critical current characteristics in the length direction under winding are analysed through non-contact, continuous critical current measurement using Mcorder equipment was reported in 2019 [78]. The bent diameter was calculated by winding the YBCO tape over a 4.5 mm central core in two different ways. The first one is the YBCO layer facing outside, and the second one, the YBCO layer, faces inside. It is found that the YBCO layer facing inside is the best option because the smallest safe bending diameter for the YBCO face inside and outside is greater than 14 mm and less than 4.5 mm, respectively [78]. The paper also fitted the normalised critical current data to a sigmoid-like function when the tape faces outside during the winding.

$$I_{c\_normal} = \frac{1}{1+e^{-\alpha*(d-\beta)}} \tag{2.7}$$

Where '*d', 'α',* and *'β'* are the bending diameter, the transferring region's gradient (1742 m^{-1}), and the transferring region's central point ($9.8e^{-3}$ m), respectively. From the above function, it was reported that at bending radii of 9.8 mm and 4.5 mm, respectively, 50% and 1% of the critical current is retained, while 97.5 % of the critical current is maintained at a bending diameter of 14 mm [78]. In another study, the thicknesses of the silver cap varied from 10 µm to 30 µm in steps of 10 µm, keeping the Hastelloy thickness constant at 100 µm. The results show that when using thicker silver cap layers, there is an improvement in the first degradation point of the YBCO superconductor [22].

After bending the wires to various diameters between 10 and 3.5 cm, Jeremy D. Weiss *et al*. performed current measurements on tapes taken from CORC cable of 2 and 3 mm width [79]. Although it was bent to a diameter of 3.5 cm, these thin wires are incredibly flexible and hold close to 90 % of their initial critical current. An engineering current density of 233 A/mm^2 at 4.2 K and 10 T was seen in a small 5-turn solenoid built and tested as a function of the applied magnetic field [79].

Recent studies show that reversible degradation is observed when the tape is subjected to compressive bending, and irreversible degradation or damage is observed during tensile bending. Depending on the position of the neutral axis and that of the REBCO layer, the intrinsic strain in the REBCO layer can be compressive or tensile in nature [67] Therefore, it has to be make sure that the REBCO layer is in the compressive side of the tape during the bending process. The thickness of the substrate significantly influences strain development. Using a substrate with a smaller thickness can minimise the overall area of the REBCO tape, which is a simple and appealing strategy. Reducing the overall thickness of the wire is an efficient approach to raise the critical current density. Using this thinner substrate instead of the typical 50 µm thick substrate and with the same critical current will helps to increase the critical current density by 30% to 45% [80]. A dramatic improvement in the critical current density and bend tolerance was reported in the literature with the ultra-thin substrate with copper stabiliser [80].

The findings from the bending load investigations since 1999 on different HTS materials is consolidated in Table 2.2.

Table 2.2: Important findings under the bending load scenario

Year	***Compound***	***Hastelloy thickness (µm)***	***Strain / Bending radius***	***Findings***	***Reference***
1999	*BSCCO*	*-*	*Bending radius reduces from 11.5 cm to 5 cm*	*48 % reversible critical current reduction*	*[64]*
2003	*BSCCO*	*-*	*1 % of bending strain*	*Gradual and consistent critical current degradation is observed.*	*[66]*
2005	*YBCO*	*100*	*Compressive bending strain up to 0.6 %*	*No degradation*	*[72]*
2005	*YBCO*	*100*	*Tensile bending strain up to 0.5 %*	*No degradation*	*[72]*
2007	*YBCO*	*75*	*0.95 % of compressive strain*	*40 % reversible critical current reduction*	*[63]*
2008	*YBCO*	*50*	*0.25- 0.28 m of bending radii*	*5 % critical current reduction*	*[73]*
2012	*YBCO*	*80*	*0.35-0.45 % of bending strain*	*95 % critical current retention*	*[69]*
2016	*REBCO*	*0.11 mm total thickness*	*Bending radius = 5.8 mm (In-plane- bending)*	*95 % critical current retention*	*[70]*
2016	*REBCO*	*0.11 mm total thickness*	*Bending radius = 229 mm (out-of-plane-bending)*	*95 % critical current retention*	*[70]*

2017	*REBCO*	*22*	*Bending radius = 0.81mm*	*No significant critical current degradation*	*[75]*
		50	*Bending radius = 3.19 mm*	*40 % critical current reduction*	*[75]*
2017	*REBCO*	*30*	*3.5 mm*	*10 % critical current reduction*	*[79]*
2019	*YBCO*	*50*	*4.5 mm*	*1 % critical current retention (YBCO facing outside)*	*[78]*
2022	*REBCO*	*50*	*Bending radius = 6-7 (80 stabiliser thickness) and 4-5 (160 stabiliser thickness)*	*95 % critical current retention*	*[77]*
2022	*REBCO*	*60*	*Bending radius = 4 mm*	*95 % critical current retention*	*[77]*

It may be observed from Table 2.2, the Hastelloy thickness has profound influence on the degradation of the superconductor and also the strain induced in REBCO tape. Therefore, Hastelloy thickness is considered as an important parameter in the design stage of the REBCO tape.

2.4 Effect of torsional loading on high temperature superconducting tapes

The torsional strain could not be avoided during the winding process, and the studies on the strain dependence on critical current degradation is limited in the open literature. Less than 10 % of critical current degradation is observed for the BSCCO compound when the twist angle reaches 60^{o} where the torsional strain is 5.5 % [64]. The impact of torsional strain on the degradation of the HTS material is less than bending and tensile loading.

When subjected to torsion, the critical degradation of the BSCCO compound is gradual when the torsion angle exceeds 150^o [66]. Similar to BSCCO compound, gradual degradation is also reported for YBCO coated conductors under torsion [81]. This is recognised by the consistent degradation of the critical current along the tape's longitudinal direction at each subsection. In this study, the torsional angle is varied from 0 to 450^o in steps of 30^o. The strain dependence on critical current is separated into three regions. In 0 to 180^o of the angle of rotation, no notable degradation was observed. But in the second region, the angle of rotation between 180^o -390^o, gradual degradation of critical current is reported. In the third region, between 390^o-450^o, there is a rapid degradation of critical current was reported [81]. The paper also reported that 95 % of critical current retention corresponded to 80 mm twist pitch [81]. Another study reported in the literature found that the critical current of YBCO tape remains unchanged up to 120 degrees. Beyond that a sudden change in the critical current occurred [82]. But in the case of BSCCO tape, critical current degrades above 150 degrees. But the direct comparison of YBCO and BSCCO tape is not possible in this case because 4.1 mm wide YBCO tape and 10 mm wide BSCCO tape were chosen for the study [82]. Tape width is a significant parameter that affects the degradation of the tape. The torsional strain effect of YBCO and BSCCO compounds on critical current degradation was well described and available in the literature [83]. By twisting the tape up to a 200 mm twist-pitch, the critical currents of the 4 mm wide YBCO tape were unaffected, but the critical currents decreased very sharply below the 130 mm twist-pitch [33, 83]. But in the case of 3 mm width, BSCCO tapes show 2 % of critical degradation at 200 mm twist pitch, then sharply decreased with increasing the twist pitch. In the literature it is also reported that this critical current in the BSCCO tape is irreversible, whereas 2G YBCO tapes are pretty strong against mechanical twists and no permanent degradation is observed when the twisting force was removed [83]. The axial longitudinal strain in the superconducting tape is analytically provided as follows [83].

$$\varepsilon_x = \frac{1}{2}\left(\frac{\gamma_{max}}{t}\right)^2\left(x^2 - \frac{w^2}{12}\right) \tag{2.8}$$

$$\varepsilon_{max} = \frac{w^2\theta^2}{12} \tag{2.9}$$

$$\varepsilon_{max} = \frac{-w^2\theta^2}{24} \tag{2.10}$$

Where maximum shear strain $'\gamma_{max}' = '\theta t'$, 't', 'w', and $'\theta'$ are the thickness, width and twist per unit length of the tape. The maximum strain value occurs at the tape's far end, and the minimum value occurs at the tape centre.

Torsional studies have been reported in the literature by different manufacturers of HTS conductors. Two samples were each taken from Shanghai Superconductor Technology (SST) and Suzhou Advanced Materials Research Institute (SAMRI). The critical twist pitch corresponding to each loading situation is given in the Table 2.3 [77].

Table 2.3: Critical twist pitch from different manufacturers [77]

Manufacturer	***Hastelloy thickness (µm)***	***Stabiliser thickness (µm)***	***Width (mm)***	***Critical twist pitch (mm)***
SST	*50*	*85*	*4*	*90.2*
SST	*50*	*160*	*4*	*255.9*
SAMRI	*61*	*180*	*4*	*86.4*
SAMRI	*61*	*316*	*4*	*82.3*

The REBCO tape manufactured by SAMRI (MOCVD technique used) shows more uniformity and stability under torsional loading as it is evident from the table. MOCVD method help to provide better tape compared to the PLD technique ones. The literature also illustrates that critical current degradation, mainly due to the oblique cracks caused by torsion and the cracks are developed from side to centre [77]. The twist pitch is calculated using the following equation;

$$Twist\ pitch = \frac{L}{\theta/_{360^o}} \tag{2.11}$$

Where 'L' is the length of the sample and $'\theta'$ is the torsional angle. The pure torsional and combined tensile and torsional load on REBCO tape from three different manufacturers is reported in the literature [84]. It is found that all three samples start to degrade steeply when the twist pitch is below 80 mm. For this case, the tape width slightly varies from 4.1 to 4.42 [84].

Under combined tension and torsion, 10 % reversible degradation in the REBCO tape is observed when the twist pitch is 200 mm, and the maximum tensile stress is 700 MPa [84]. A fixed axial tensile strain on the tape of 0.3 % approaches the critical value

of 0.45 % at a 183° twist angle, where the highest strain is found near the edge of the ReBCO layer [17]. In 2009 studies on the critical current degradation of YBCO tape under torsion and tension reported the results by classifying them into three different regions [85]. In the first region, up to 26^o/cm, a negligible effect of applied torsion on critical current is found. In the second region, a linear relationship between the applied torsion and critical current degradation is observed (26^o/cm- 47^o/cm). In the final region a sudden drop in the critical current is observed above 47^o/cm. In 2013, Luisa Chiesa developed a probe that simultaneously measures both torsional torque and critical current [86]. In his experiment, the torsional load applied on the YBCO tape from different manufacturers such as AMSC and Super-power. It is found that rapid degradation of critical current is observed for both tapes when the angle of twist reached below 70 mm [86]. The paper also reported that twisted stacked tape cable with AMSC tape is harder than that of Superpower tapes.

A study in 2013 has developed an analytical expression of critical current dependence on twist pitch for YBCO and BSCCO (2223) compounds [87]. The paper reported that 95 % critical current retention was observed when the twist pitch reached a value of 114 mm and 80-90 mm, respectively, for YBCO and BSCCO [87]. The paper also discussed the sensitivity of twists at different temperatures and found that at lower temperatures sensitivity of twists is slightly lower compared to high temperatures. The findings related to the torsional studies are consolidated in Table 2.4.

Table 2.4: Consolidated findings of different HTS materials under the torsional load scenario

Year	***Compound***	***Tape width (mm)***	***Torsional load***	***Findings***	***Reference***
1999	*BSCCO*	*-*	*60^o*	*< 10 % critical current degradation*	*[64]*
2003	*BSCCO*	*2.95-3.7*	*< 150^o*	*Gradual degradation of critical current is observed.*	*[66]*

2003	*YBCO*	*4.15-4.42*	*<70 mm twist pitch*	*Rapid degradation of critical current is observed.*	*[86]*
2007	*YBCO*	*4.1*	*120^o*	*The critical current remains unchanged up to 120^o angle of rotation*	*[82]*
2007	*BSCCO*	*10*	*150^o*	*Critical current degrades above 150^o.*	*[82]*
2007	*YBCO*	*4.3*	*114 mm twist pitch*	*95 % critical current retention*	*[81]*
2009	*YBCO*	*4.1*	*26^o/ cm*	*Negligible effect on applied torsion*	*[85]*
2009	*YBCO*	*4.1*	*26^o/ cm- 47^o/ cm*	*A linear relationship between applied torsion and critical current*	*[85]*
2009	*YBCO*	*4.1*	*Above 47^o/ cm*	*Sudden drop in critical current*	*[85]*
2010	*YBCO*	*4*	*200 mm twist pitch*	*Critical current unaffected*	*[83]*
2010	*YBCO*	*4*	*130 mm > twist pitch*	*Critical current degrades very sharply*	*[83]*
2010	*BSCCO*	*3*	*200 mm twist pitch*	*2 % critical current degradation is observed*	*[83]*
2013	*YBCO*	*4.1-4.4*	*114 mm twist pitch*	*5 % critical current degradation*	*[87]*
2013	*BSCCO*	*4.5*	*80-90 mm twist pitch*	*5 % critical current degradation*	*[87]*
2015	*REBCO*	*4.1-4.42*	*80 mm > twist pitch*	*Critical current sharply decreases*	*[84]*

2015	*REBCO*	*4.1-4.42*	*200 mm twist pitch + 700 MPa*	*10 % critical current degradation*	*[84]*
2015	*REBCO*	*4 mm*	*183^o angle of rotation + 0.3 % tensile strain*	*0.45 intrinsic strain criterion is observed*	*[17]*
2022	*REBCO*	*4 mm*	*> 4.3^o/ mm*	*Reversible degradation*	*[88]*
2022	*REBCO*	*4 mm*	*< 4.3^o/ mm*	*Rapid and irreversible degradation*	*[88]*

It may be observed from the table that, different high-temperature superconductor behaves differently and tape width also influence the degradation of the HTS tape. Therefore, Tape width can be considered as a crucial parameter for the further study under torsion.

2.5 Effect of winding on high temperature superconducting tapes

The critical current degradation caused by the winding process of the Bi-2223 compound was investigated and reported in 1999 [16]. In the winding process, the critical current degradation in the wire mainly comes from tensile, bending and torsional strain [16]. A winding study on a simple superconducting CORC cable conducted found that winding angle, core diameter and tape width are crucial parameters that influence the development of strain in the tape [36]. It is found that, during the winding, the outer layer of the tape is in the tensile state, and the inner layers are in the compressive state. For this reason, the REBCO layer is placed below the neutral axis to get more flexibility for the manufacturers. However, the study did not consider individual properties of each layer in their model. Instead, a homogenisation approach was taken by weighing Young's modulus of the copper, substrate, and superconducting layers based on the volume fraction of each material [36].

D C van der Laan investigated the electro-mechanical characteristics of conductors coated with YBa2Cu3O7 under high axial compressive strain in 2009 [35]. The critical current is up to 2% strain and exhibits no irreversible damage [35]. With the

help of the results reported here, a new technique for creating $YBa_2Cu_3O_7$ coated conductor cabling for use in low ac-loss and high-field magnet applications has been developed. Coated conductors are wrapped around a former that has a relatively small diameter. Full conductor transposition is possible with this idea, along with high cable critical currents, low inductance, and a reasonably high engineering current density. A record critical current of 5021 A was measured in 2013 at 4.2 K and 19 T using CORC cable [38]. This number corresponds to an engineering current density of 114 A/mm^2 in a cable with an outer diameter of 7.5 mm [38]. This is the greatest current density till recorded for a superconducting wire under such powerful magnetic fields. A current density of at least 300 A /mm^2 and a cable-bending diameter as small as 40 mm were measured in 2015, which had previously been impossible with superconducting tapes produced on substrates that were 50 µm thick [89]. Compared to earlier cables wound by hand, a specialised cable machine made higher-quality cables with superior tape retention performance. With a reduction in cable diameter from 7.5 mm to 6.0 mm, the thinner substrate (38 µm) indicated an almost two-fold increase in engineering current density from 114 A /mm^2 to 216.8 A /mm^2 at 4.2 K and 20 T [89]. This indicates that winding tension and Hastelloy's thickness significantly impact the CORC cable's performance.

The greatest performance of any CORC® cable to date was measured in 2016. The measured cable critical current of 7030 A at 4.2 K in a background field of 17 T equals a current density of 344 A /mm^2 [90]. They were able to extrapolate the cable performance to 20 T using the magnetic field dependence, and they predicted a critical current of 5654 A and a current density of 309 A /mm^2 [90]. The findings unequivocally demonstrate that significant strides are being achieved toward removing the current density barrier to the use of CORC® cables in the upcoming accelerator magnets. SuperPower Inc. in 2020 developed REBCO tapes made on a 25 µm thick Hastelloy® substrate. The highest current density was ever recorded in a CORC® conductor, with a critical current as high as 6231 A (12 T, 4.2 K), with an engineering current density of 678 A/mm^2 extrapolates to over 450 A/mm^2 at 20 T [91]. The improvement in the engineering current density from the last few years for the CORC cable is given in Table 2.5. From the table, it is clear that substrate thickness and core diameter significantly influence the engineering current density and a considerable improvement in the engineering current density from 2013 to 2020.

Table 2.5: Improvement of engineering current density in CORC cable in the past years

Year	***Diameter (mm)***	***Substrate thickness (µm)***	***Engineering current density at 4.2 K and 20 T (A/mm^2)***
2013	*7.5*	*50*	*114*
2015	*6*	*38*	*216.8*
2016	*5.1*	*30*	*309*
2020	*3.1-3.42*	*25*	*450*

A FE simulation of the 3D SSS in a CORC® wire under bending strain was performed in 2018 [92]. The critical intrinsic tensile strain value of 0.45 % is used to determine the point at which a tape's performance starts to degrade permanently. A parametric analysis including dependent variables was conducted to pursue further the optimisation of CORC cables and wires for various applications. The flexibility and engineering current density increase with a smaller core diameter, but tape with a thinner Hastelloy layer is needed [92]. CORC cable is able to pass 40 % of critical current at 123 K for one minute without any degradation [93]. This was an interesting finding that showed the high degree of stability in the CORC cable.

Using the result from the bending experiment, Soumen Kar et al. selected the central core diameter as 0.81 (using ETP grade copper) and the tape configuration with 22 µm Hastelloy, 20 µm copper (electroplated on a single side), 2 µm silver cap and 1 µm REBCO material [75]. They performed the winding by hand up to six layers by varying the twist pitch from 2.8 (first layer) to 4.4 (sixth layer). Bending experiments were conducted using this sample and found that when the bend diameter is reduced to 6 cm, there is no appreciable critical current degradation. The critical current begins to degrade at 5 cm bending diameter and experienced the highest degradation of 17% at 3 cm bend diameter [75].

A cable wrapped from GdBa2Cu3O7-coated conductors with an outer diameter of 7.5 mm and a critical current of around 2800 A at 76 K and self-field was described in 2011 [94]. The smaller size and flexibility of the cable make it suited for Navy and Air Force power transmission'. This enables the electric power transmission superconducting wire lines with smaller diameters. They are also suitable for high-field magnet applications due to their ability to increase the engineering current density while maintaining flexibility. The advantages of a ready-to-use shape offer CORC wires an

appealing option for applications requiring high current densities and high-field magnets with small bending diameters between 4.2 and 77 K [79].

The strain sensitivity on the critical current in the REBCO coated conductors during the winding for 50 mm, 75 mm, and 100 mm mandrel diameter was reported in the literature [67]. The mandrel diameter and pitch-to-width ratio are significant parameters determining the degradation point. The critical current starts to degrade at 2, 2.5, and 4 pitch-to-width ratios, corresponding to 50 mm, 75mm, and 100 mm mandrel diameter [67]. In CORC cable, REBCO tape is wound helically; hence, only a portion of total axial tensile strain is experienced during tensile loading. As a result, the tensile load-bearing capacity of the CORC cable is increased ten times that of the REBCO tape [95]. The irreversible strain limit for CORC cable or wire is about -1.2 % when the tape is wound into the CORC cable configuration [95]. Usually, the core of the CORC cable is chosen with high yield strength like hardened copper, stainless steel, beryllium-copper etc. [95]. The torsional strain in the REBCO layer is more prominent at smaller winding angles [95]. The literature concludes that the CORC cable is one of the best superconducting cable configurations for future applications like superconducting magnet, military, power grid etc.

2.6 Effect of Fatigue type of mechanical loads on high-temperature superconducting tapes

The cumulative influence of fatigue type of loading may cause the HTS superconducting materials to fail due to the repeated application of stress. This stress can be of different types like thermal, mechanical etc.

The cyclic thermal load is caused by the cooldown of superconductor using a cryogen or cryo refrigerator and its heating up when not in operation. Another source is alternating current applications, in which the stress caused by the Lorentz force that varies periodically at the same frequency as that of the current. The next source is the rotational (centrifugal) stress, which arises in applications requiring rotating equipment such as motors and generators. Also, random loads in any mobile system which is less predictable can also causes fatigue failure [61].

A high cycle fatigue test on DyBaCuO bulk superconductor is reported in the literature [96] at room temperature. The stress ratio and the frequency chosen for their experiment are 0.1 and 20 Hz, respectively. The specimens fail about $2x\ 10^4$ cycles when

the applied cyclic tensile load exceeds 60 MPa. The threshold stress intensity of this superconductor is reported to be in the range of 0.93 to 1.33 MPa/$\sqrt{m}$.

Many researchers are reported that the crack propagation initiated at the edges of the sample and propagated towards the centre [97-99]. Wei Chen *et al*. conducted a detailed experimental investigation on fatigue and found that stress ratio, amplitude, and external magnetic field are the parameter that influence the irreversible limit. The critical current value of YBCO tape is inversely proportional to the external magnetic field. According to the study, the amplitude has a bigger impact than the maximum stress value. It is reported that under fatigue loading with a stress ratio of 0.7 and a maximum stress value of 600 MPa, the critical current degradation does not happen below 10^4 cycles. The critical current of YBCO tape drops when the number of fatigue cycles reaches $3x10^4$ [100].

Studies have been conducted to find out the effect of fatigue, on the superconducting BSCCO2223 compound. One study found that there is no significant critical current degradation when the strain is kept between -0.2 % and 0.2 % for up to 5000 cycles [101]. Another study reported that for reinforced BSCCO2223 tape conductor, the maximum fatigue tolerable c-axis tensile stress for up to 10^5 cycles is approximately 24 MPa [74]. The fatigue strength of the multifilamentary BSCCO2223 material can be improved by sheath alloyed with Ag, Mn, etc [102]. The fatigue strength of the steel foiled reinforced BSCCO2223 superconducting tape was higher than that of the Mn sheath alloyed one [103].

Sugano *et al*. described two different mechanisms for fatigue damage. The first is caused by fatigue fracture of the Hastelloy substrate, and the second by fatigue fracture of the silver stabiliser layer. In the first case, there is insignificant critical current degradation; whereas, there is only a slight decrease in the critical current degradation in the second case [104]. Also, it is found that, most of the stress is carried in the Hastelloy (substrate) material. The fatigue and yield strength of superconductor can be dependent on the temperature. The yield strength of the SmBCO reported is 411 MPa to 573 MPa respectively at room temperature and 77K [105]. The fatigue life of the SmBCO compound is specified as $5x10^4$ to 10^6 cycles, and the fatigue strength as 401 MPa and 487 MPa, respectively, corresponding to stress ratios of 0.1 and 0.05 [105].

A high cycle uniaxial fatigue test is carried out on GdBCO CC tapes of 4 mm and 12 mm widths [106]. The 4 mm width shows a lesser fatigue limit than the 12 mm width one due to the slit edge effect in the 4 mm wide tape. Also reported that, regardless of the tape width, the characteristic strength of the tape at 77 K is in the following order.

Yield strength > Irreversible stress limit > Mechanical fatigue limit > Electrical fatigue limit.

The transverse cycle fatigue studies on HTS are limited in the open literature. Ekin *et al*. conducted the transverse fatigue study on the YBCO superconductor and reported that the critical current degraded by about 2 % after 2000 cycles of transverse load and amplitude of 122 MPa [107]. Static and dynamic fatigue study on REBCO tape through-thickness is reported in the literature [108]. In the case of normal longitudinal fatigue analysis, metal fatigue is dominant because the superconducting ceramic layer is parallel to a metal substrate and a copper stabiliser. However, in the case of fatigue through the thickness, the metals and superconducting ceramic layers are in series. Therefore, the ceramic superconducting layer controls the fatigue strength and the crack in the REBCO layer due to the Subcritical Crack Growth (SCG) [108]. The paper also reported that the fatigue crack strength does not reduce when used at low temperatures [108].

The fatigue behaviour of the GdBCO with stainless-steel substrate is studied under cyclic tensile loading manufactured by SuNAM. The results obtained are compared with the previous result of those manufactured by Superpower, reported in the literature [98, 99]. The critical current degradation after 1, 10, 10^2,10^3,10^4 and 10^5 cycles is noted corresponding to the strain level of 0.35%, 0.45% and 0.50%. Critical current degradation is initially noticed for strains of 0.35 % and 0.45 % after 10^4 cycles, whereas for strains at 0.50 % level, critical current decreases after 10^3 cycles [98]. SEM image of GdBCO compound after fatigue analysis revealed that there are two major reason for the degradation of the superconducting tape [98]. One is micro-cracks initiated at the conductor edge and propagated inward. The second is due to the delamination of the superconducting layer. So bonding between the layers is a very important parameter. This needs to be checked and improved during the manufacturing process itself.

The fatigue crack growth rate and fatigue life in the interface between the different layers of the superconducting REBCO tape is calculated using Displacement-Energy Model (DEM) [109]. The results show that critical fatigue growth rate in the tape is 2.54

pm/cycle coreesponding to 3.9 x 10^5 cycles [109] for which the applied stress range is 0.35-0.46 % and 0.002-0.007 stress ratio.

The fatigue test under tensile loading was reported in the literature for YBCO tape without copper stabiliser and one side copper stabiliser (with thickness of Hastelloy 100 µm and copper stabiliser as 100 µm). It is found that the mechanism of fatigue fracture starts from the Hastelloy layer. Also, it is reported that adding the copper stabiliser layer increases the fatigue strength of YBCO tape by 19 % for a 0.5 stress ratio [110]. The fatigue analysis is conducted for YBCO tape with one side copper stabiliser layer at a maximum load of 1720 N and a stress ratio of 0.5 and found that no degradation is observed up to 10^6 cycles. Then extract copper from the REBCO tape and carry out the tensile analysis. It has been noted that the copper layer's yield strength has increased and reached saturation after 10^5 cycles [110].

The long-term reliability studies of GdBCO tape are reported in the literature [111]. The static fatigue analysis was carryout in a U-shaped bend section (100 mm, 75 mm and 50 mm bent diameters) to find the fatigue limit. At 100 mm bending diameter, 5 % critical current degradation criteria are crossed at 50 and 40 hours under 0.88 and 0.9 times of irreversible limit (when subjected to uniaxial tension test = 650 MPa) [111]. However, at a 75 mm bending radius, 5 % critical current degradation criteria are crossed at 22 and 2 hours under 0.88 and 0.9 times of irreversible limit [111]. The paper also defined the electrical fatigue limit based on time elapsed (100 hours) and 95 % critical current retention criteria. The electrical fatigue limit was found to be 0.63, 0.83, and 0.86 times of irreversible limit corresponding to 50, 75, and 100 mm bending diameters, respectively [111].

The high cycle fatigue test for Single Tape Wider Co-wind (STWC) was reported in the literature. The study revealed that at pressures of nearly 100 MPa, a coil with REBCO tape wider than its co-wind, exhibited a 5% permanent critical current reduction [112]. The impact of cyclic transverse load on round HTS strands from two different manufacturers at 77 K was reported [113]. According to reports, SuperOx strand does not lose fatigue properties for cyclic loads of 20 MPa and 30 MPa, but at 40 MPa, strand performance began to decline after 800 cycles (with a 5% degradation). In comparison, the SuperPower sample with the non-annealed copper profiles has shown to have very

stable performance for the load amplitudes up to 40 MPa: strand's critical current was almost unaffected after 1000 load cycles [113].

The fatigue analysis of REBCO tape when subjected to repeated bending load and torsional load is limited in the open literature. In 2009, critical current degradation due to repeated bending load was reported for a 10 mm width and 100 μm Hastelloy thick tape [114]. The repeated bending load varied from a lower limit of 0.1 % strain to an upper limit of 0.91 %, 0.93 %, and 0.94 % strain. It is found that when the upper limit is 0.93 % and 0.94 %, the critical current degraded suddenly after 10^4 cycles. However, when the upper limit is 0.91 %, the sudden decrease in the critical current is visible after $2x10^4$ cycles [114].

Tomokazu Matake in 1977 reported that the fatigue cracks are initiated in the slip band and it appeared in the direction of maximum shearing stress [115]. The fatigue crack is caused by the repetition of slip in the crystal and its propagation is caused by normal tensile stress. This Matake criterion coincides with the empirical equation suggested by Gough for the brittle material [115].

2.7 Technological Gaps

A detailed literature survey on the superconducting tapes/ cables under different mechanical loads such as thermal, tensile, bending, twisting, and fatigue loads is carried out. Some of the major research gaps are identified.

Limited studies on the estimation of degradation in HTS superconducting cables under mechanical, thermal, and fatigue loading conditions are observed in the open literature. In addition, the determination of the extent of degradation in HTS tapes under different mechanical loading and its role on layer thicknesses and width are not explored in detail, since superconducting CORC cables/wires are in the developing stage. Studies on the influence of the winding of REBCO are limited and not available for a wide range of geometrical parameters. Another critical factor that leads to the degradation of the superconducting tape/ cable is the fatigue type of loading. HTS are more susceptible to fatigue due to repetitive thermal and electro-mechanical loads. However, the influence of fatigue loading on the performance of HTS REBCO tapes cannot be fully understood from the current open literature.

Therefore, the objective of the study is formulated based on the technological gaps identified. The literature have also helped in finding the methodology to be adopted in

achieving each objective. Some of the fundamental theories related to the selected methodology/ approaches are also discussed in the subsequent chapters.

Chapter 3

Objectives and Methodology

3.1 Objectives of the thesis

The overall objective of the work is to simulate and experimentally validate the degradation in superconducting REBCO tapes of various geometric sizes under different loading conditions. The specific objectives for accomplishing the overall objective are as follows.

- Estimate the amount of strain developed in HTS REBCO tapes of different sizes and layer thicknesses under **tensile loading** conditions.
- Determine the extent of degradation in HTS tapes under **bending** and its role on layer thicknesses and width.
- Find out the combined effect of **torsion and tension** loads on the performance of HTS tapes under various tape dimensions.

- Evaluate the influence of the **winding** process of REBCO tapes on CORC cable configuration under various geometrical parameters.
- Carry out studies to bring out the role of **fatigue** loading on HTS tapes of varying layer thicknesses and width.

The specific objectives target the performance variation of HTS REBCO tape when subjected to different loading conditions. At first, the tape will be subjected to tensile load. The geometrical parameters of the tape will also varied to find the critical loading condition under tension. Afterwards, the degradation of the tape when subjected to bending and twisting loads are investigated for different geometrical configurations. The fourth stage, the effect of winding on a single layer superconducting CORC cable is carried out. Effect of critical central core diameter, best winding angle, layer thicknesses and tape width are investigated. The final stage deals with fatigue analysis of superconducting REBCO tape under repeated cyclic tensile, bending and torsional loads. Each specific objective will be accomplished so that the overall objective of the degradation in REBCO superconducting tapes under various geometry and mechanical loading conditions are achieved.

3.2 Methodology

The methodology for accomplishing each specific objective and thereby the overall objective is schematically depicted using a flow chart 3.1.

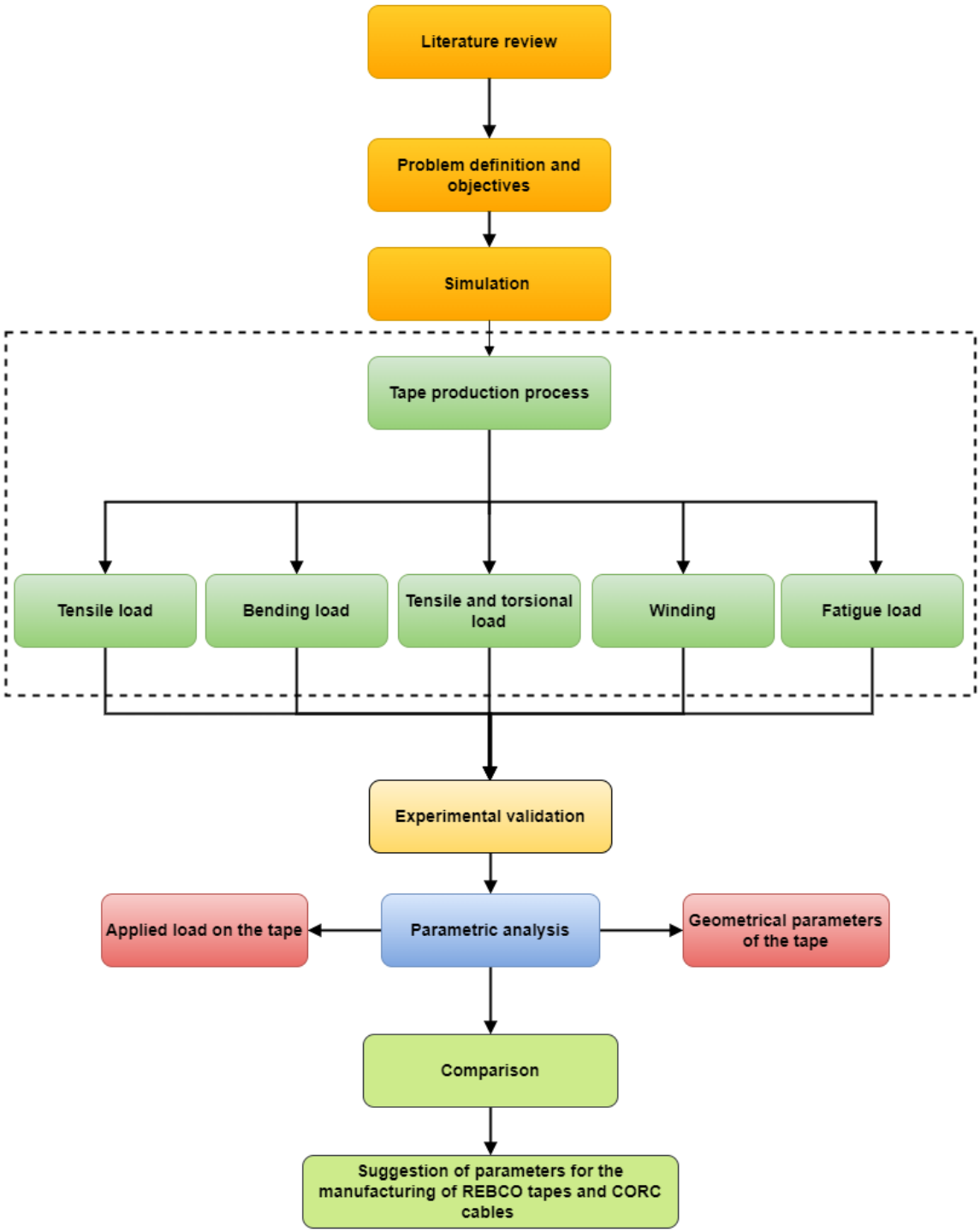

Figure 3.1: Methodology adopted to accomplish the objectives

According to the methodology, the investigations start with a detailed literature review to recognize the challenges and the gap areas that need to be concentrated. This will give rise to the problem definition and the formulation of the objectives. In order to accomplish each of the objectives, simulation-based analyses are chosen. The HTS tape is modelled right from its production phase. The REBCO tape production process consists of two steps. In the first step, REBCO film is deposited on the substrate using the MOCVD method. MOCVD is conducted at 1020 K, and then it is cooled to 333K. At 333 K, copper electroplating is performed to create the copper stabilising layers, and then it is cooled down to room temperature. During the production stage, the cooldown from 1023 K to 77K residual strain induced in the tape. It may be noted that this residual strain value is critical in the case of superconductors. After that, the tape is subjected to various mechanical loads. The mechanical loads include tension, bending, and combined tension and torsion load. In addition to this, winding simulation is also carried out, which includes the combined effect of tension, torsion, and bending loads. Afterwards, the tape is subjected to fatigue loads. The fatigue failure is significant because the HTS tapes are subjected to fatigue loadings while in operation in terms of repeated thermal cycles, periodic electromagnetic force, etc. along with the repeated structural loads. This will adversely impact the performance of superconductors and result in the degradation of superconducting wires and cables in magnets and power systems.

The simulation results obtained will be compared with the experimental results available in the open literature. Once the simulation results are in good agreement with the experimental ones, parametric analyses are carried out under different loading and geometrical conditions of the tape. The mechanical loads are varied within a practical range as understood from the literature. The geometrical parameters considered are the thickness of Hastelloy, copper layers, tape width, winding angle, and core diameter. After completing the parametric analysis, the result obtained out of different parametric studies are compared and consolidated. The critical parameters for manufacturing REBCO tape and CORC cables are thus determined.

3.3 Finite element analysis

Finite element analysis is the process of solving the physical phenomenon using the numerical technique. The detailed step involved FEA analysis is depicted in Figure 3.2. Engineers utilise FEA software to reduce the number of physical prototypes and experiments and optimise components throughout the design phase to build better products faster and save money.

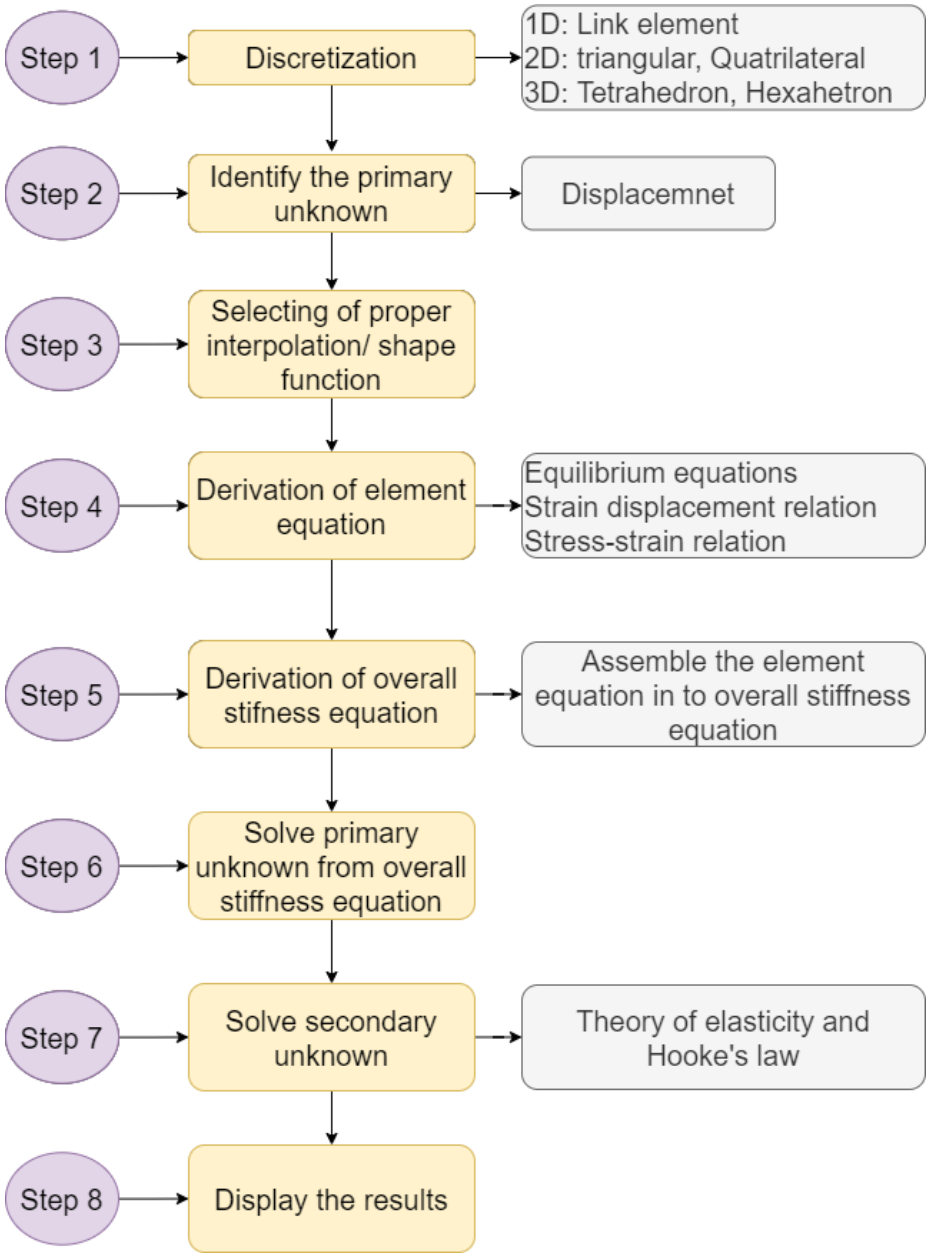

Figure 3.2: Different steps involved in the Finite Element Analysis (FEA)

The discretisation of the geometry is the first step in the finite element method to break down the geometry into smaller elements. In one-dimensional geometry, the link element is employed, in two-dimensional geometry, triangle or quadrilateral elements are used, and in three-dimensional geometry, tetrahedron or hexahedron elements are primarily used. Identify the primary unknown and apply the boundary condition after discretisation. The primary unknown in structural problems is displacement. The most crucial step is to choose the interpolation or shape function. Based on the element type, simple linear, quadratic, cubic, and others, the interpolation functions are selected. The next step is to derive and apply the element-equation to each element. Equilibrium equations, strain displacement relations, and stress-strain relations are the governing equations in structural problems. In the fifth step, the element equations are combined to form an overall equation (Overall stiffness matrix). In the sixth step, use the numerical techniques like the Gauss elimination etc. to solve the overall equation and thereby determine the primary unknown (displacement). The seventh step implements the theory of elasticity and Hooke's law to calculate secondary unknowns such as strain and stress. In the final step, the results are displayed and interpreted.

3.4 FEA Software

Modelling has a vital role in engineering and design. Simulation modelling is the act of creating and analysing a mathematical replica of a physical model to determine under what situations and in what ways a part might fail, how efficient it is, the maximum load it can withstand, method to improve its performance etc. A mathematical model helps to save money and production time. Complex problems can be simulated with the help of simulation software without producing any prototypes. One of the most appealing aspects of simulation analysis is parameter analysis; any parameter can be modified easily and quickly.

3.4.1 COMSOL Multiphysics

The COMSOL Multiphysics general-purpose FEA software platform is based on cutting-edge numerical techniques. It offers a number of physical interfaces and tools for applications in the electrical, mechanical, and chemical fields. The attractive feature of this software is that it provides to couple different physics phenomena.

Regardless of the application, COMSOL Desktop is a strong integrated platform built for cross-disciplinary product development with a fixed workflow. The model tree in the model builder provides the model's complete structure, including geometry, mesh, and physics settings, boundary conditions, studies, solver, post-processing, and visualisation. COMSOL Multiphysics is not good enough to draw complicated geometry, so it offers Live Link connections to well-developed CAD packages like Solid Works, CATIA, Pro/ENGINEER, Revit, AutoCAD, Inventor, Solid Edge, etc. Also, it offers a good programming environment by live link connection with MATLAB.

Material properties, boundary conditions, source or sink terms etc., can be defined with the help of user-defined equations. Material properties also can be imported in .txt, .xlsx, .dat format as a function. It will automatically do extrapolation and interpolation without any additional computation. Loads, parameters etc. can be changed step by step with the help of auxiliary sweep and parameter sweep.

Results can be exported to text files in the .txt, .dat, and .csv formats. WithLiveLink™ *for* Excel®, results can be exported to the Microsoft® Excel® .xlsx format.

3.4.2 Hooke's Law

Hooke's law states that the stress is directly proportional to strain when a material is loaded within the elastic limit [116] . The Hooke's law of linear elasticity is usually written as,

$$\sigma_{ij} = C_{ijkl}\,\varepsilon_{kl} \tag{3.1}$$

Where 'σ' and 'ε' are the stress and strain tensor of second-order, while the constitutive tensor C is a fourth-order tensor.

3.4.3 Analysis of deformation

For structural analysis of tiny and finite deformations, COMSOL Multiphysics uses a comprehensive Lagrangian model. This demonstrates that the calculated stress and deformation state are always related to the configuration of the material relative to its present position in space. Therefore, spatially varying material properties can be evaluated just once for the initial material configuration, and do not change when the solid

deforms and rotates [117]. During deformation, the particle follows the path provided by [117],

$$\boldsymbol{x} = \boldsymbol{x}(\boldsymbol{X},t) \tag{3.2}$$

$$\boldsymbol{x} = \boldsymbol{X} + u(\boldsymbol{X},t) \tag{3.3}$$

Where x, X represents the spatial and material coordinates, and u is the displacement. The displacement is a function of the material coordinates (X, Y, Z) but not the spatial coordinates directly (x, y, z). As a result, derivatives can only be computed with respect to the material coordinates. The coordinate mapping is pictorially represented in Figure 3.3 [117].

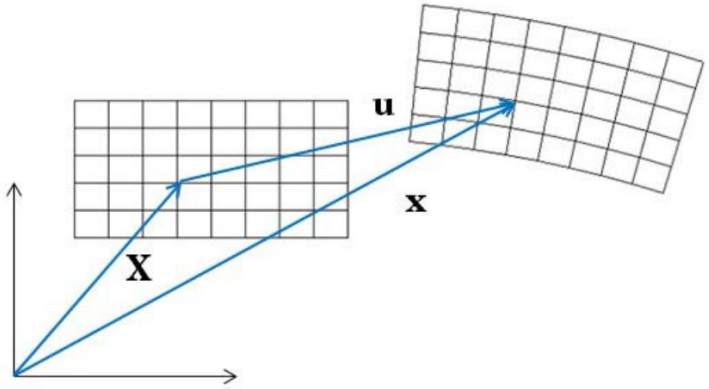

Figure 3.3: Pictorial representation of the spatial and material coordinate mapping

The gradient operator is represented with respect to material coordinate is represented as,

$$\nabla = \nabla_x = \left[\frac{\partial}{\partial X}, \frac{\partial}{\partial Y}, \frac{\partial}{\partial Z}\right] \tag{3.4}$$

So the gradient of displacement is always provided with respect to material coordinate in COMSOL Multiphysics [117],

$$\nabla u = \begin{bmatrix} \frac{\partial u}{\partial X} & \frac{\partial u}{\partial Y} & \frac{\partial u}{\partial Z} \\ \frac{\partial v}{\partial X} & \frac{\partial v}{\partial Y} & \frac{\partial v}{\partial Z} \\ \frac{\partial w}{\partial X} & \frac{\partial w}{\partial Y} & \frac{\partial w}{\partial Z} \end{bmatrix} \tag{3.5}$$

Using the deformation gradient tensor F, the mapping from an infinitesimal line element, dX, to the equivalent deformed line element, dx, is illustrated. Deformation gradient '*F*' completely represents the local straining and rotation of the material. It is a two-point

tensor (double vector) that transforms into a vector for each of its indexes. The reference and current configurations are involved in *F*.

$$dx = \frac{\partial x}{\partial X} dX = F dX \tag{3.6}$$

The deformation of the material also leads to the change in the density, and it is represented in equation 3.7[117].

$$\frac{dV}{dV_o} = \frac{\rho_o}{\rho} = \det(F) = J \tag{3.7}$$

Where 'ρ_o' and 'ρ' represent the initial and current density after the deformation, the volumetric change with respect to the initial state is represented by the determinants of the deformation gradient tensor F. Determinants of deformation gradient are always positive, and it is less than one for compression and more than one for expansion. In the case of pure rigid body and incompressible materials, J = 1.

In general, mass-density is considered constant in the material formulation in COMSOL Multiphysics because it is formulated for fixed material particles. So one of the assumptions used here is temperature-independent mass density, and change in the volume with temperature is incorporated with the help of thermal expansion coefficient data.

3.4.4 Deformation calculation

The deformation gradient tensor '*F'* combines the material and spatial coordinates, and is asymmetric. A singular value decomposition can be used to calculate the amount of stretch or rotation that a unit volume material has experienced. Right polar decomposition is applied on the deformation gradient,

$$F = RU \tag{3.8}$$

Where U is the right stretch tensor in the material frame and *R* is the proper orthogonal tensor (det(F) =1 and $R^{-1}=R^{T}$). The rotation tensor *R* describes the rigid rotation, and the symmetric tensor U provides all information about the material's deformation. The eigenvalues of U tensor λ_1, λ_2, and λ_3 are the principal stretch.

$$\lambda = \frac{\boldsymbol{L}}{\boldsymbol{L_o}} = 1 + \varepsilon_{eng} \tag{3.9}$$

Where L_o, L are the initial and current length, respectively, and ε_{eng} is the engineering strain. λ_1, λ_2, and λ_3 are acted along the three mutually perpendicular directions. In the case of nonlinear analysis, the Green-Lagrange strain tensor is usually used to represent the strain in COMSOL Multiphysics software [117].

$$\text{Green-Lagrange strain } '\varepsilon' = \frac{1}{2}(C-I) = \frac{1}{2}(FF^T-I) \tag{3.10}$$

Where C is the right Cauchy-Green deformation tensor ($FF^T=U^2$) [117]. The Green-Lagrange strain tensor is represented by using displacement component, and the cartesian coordinate is,

$$\varepsilon_{ij} = \frac{1}{2}\left(\frac{\partial u_i}{\partial X_j} + \frac{\partial u_j}{\partial X_i} + \frac{\partial u_k}{\partial X_i}\frac{\partial u_k}{\partial X_j}\right) \tag{3.11}$$

Please note that "ε' denote the Green-Lagrange strain in nonlinear analysis and engineering strain in the linear analysis.

3.4.5 Engineering strain

The strain is used to define the state of strain at a point. In the case of small-displacement and rotation, normal and shear strain components are represented below,

$$\varepsilon_x = \frac{\partial u}{\partial x} \tag{3.12}$$

$$\varepsilon_y = \frac{\partial v}{\partial y} \tag{3.13}$$

$$\varepsilon_x = \frac{\partial w}{\partial z} \tag{3.14}$$

$$\varepsilon_{xy} = \frac{\gamma_{xy}}{2} = \frac{1}{2}\left(\frac{\partial u}{\partial y} + \frac{\partial v}{\partial x}\right) \tag{3.15}$$

$$\varepsilon_{yz} = \frac{\gamma_{yz}}{2} = \frac{1}{2}\left(\frac{\partial v}{\partial z} + \frac{\partial w}{\partial y}\right) \tag{3.16}$$

$$\varepsilon_{xz} = \frac{\gamma_{xz}}{2} = \frac{1}{2}\left(\frac{\partial u}{\partial z} + \frac{\partial w}{\partial x}\right) \tag{3.17}$$

$$\varepsilon = \begin{bmatrix} \varepsilon_x & \varepsilon_{xy} & \varepsilon_{xz} \\ \varepsilon_{xy} & \varepsilon_y & \varepsilon_{yz} \\ \varepsilon_{xz} & \varepsilon_{yz} & \varepsilon_z \end{bmatrix} \tag{3.18}$$

3.4.6 Strain contribution due to inelastic strain

Total strain developed is the combination of elastic strain and inelastic strain. Inelastic strain, which includes, Initial strain (ε_0), External strain (ε_{ex}), Thermal strain (ε_{th}), Hygroscopic strain(ε_{hs}), Plastic strain (ε_p), Creep strain, (ε_{cr}), and Viscoplastic strain (ε_{vp}). So total strain can be represented as

$$\varepsilon = \varepsilon_e + \varepsilon_{inel} \tag{3.19}$$

$$\varepsilon_{inel} = \varepsilon_0 + \varepsilon_{ex} + \varepsilon_{th} + \varepsilon_{hs} + \varepsilon_p + \varepsilon_{cr} + \varepsilon_{vp} \tag{3.20}$$

The thermal strain mentioned in equation 3.19 can be computed using the following expression,

$$\varepsilon_{th} = \alpha\,(T - T_{ref}) \tag{3.21}$$

Where 'α' is the coefficient of thermal expansion (CTE) and T, T_{ref} are the current and strain-free reference temperatures.

Total deformation gradient F can be represented as follows,

$$F = F_{el}\,F_{inel} \tag{3.22}$$

The deformation gradient tensor is also mapped from material frame to spatial frame. However, in this case, three frames are involved. The F_{inel} tensor is mapped from the material frame to the intermediate frame, and the F_{el} tensor is mapped from the intermediate frame to the spatial frame. F_{el} also can be computed using the inverse of F_{inel} in equation 3.20,

$$F_{el} = F\,F_{inel}^{-1} \tag{3.23}$$

The elastic right Cauchy-Green deformation tensor can be computed using F_{el} and then find the elastic Green-Lagrange strain tensor.

$$C = F_{el}^{T}\,F_{el} \tag{3.24}$$

$$\varepsilon_{el} = \frac{1}{2}(C_{el} - I) \tag{3.25}$$

The different inelastic processes (thermal expansion, plasticity etc.) are applied subsequently to calculate the total inelastic deformation tensor F_{inel}.

$$F_{inel} = F_1F_2F_3F_4 \ldots \tag{3.26}$$

Plastic strains are primarily expressed as the plastic deformation gradient tensor, F_{pl}, in cases with high plasticity. From the plastic deformation gradient tensor, the plastic Green-Lagrange strain tensor is computed as,

$$\varepsilon_{pl} = \frac{1}{2}(F_{pl}{}^{T} F_{pl} - I) \tag{3.27}$$

3.4.7 Different types of stress

There are several kinds of stress tensors that are frequently used in COMSOL Multiphysics, including Cauchy stress 'σ', First Piola-Kirchhoff stress 'P', Second Piola-Kirchhoff stress 'S' etc. Cauchy stress is defined as a force per deformed area in fixed spatial directions and is symmetrical. First, the Piola-Kirchhoff stress is a two-point unsymmetric tensor, with the force in the spatial frame and the area in the orthogonal (material) frame. The force and area of the second Piola-Kirchhoff stress, which is a symmetric tensor, are both in the material frame. The stress should be considered as the second Piola-Kirchhoff stress in geometrically nonlinear analysis. The stress represented as,

$$S = F^{-1}P \tag{3.28}$$

$$\sigma = J^{-1}PF^{T} = J^{-1}FSF^{T} \tag{3.29}$$

The distinction between all the three stress measures vanishes and converges to a single value in the case of linear analysis.

3.4.8 Equation of motion

The expression "P" = "FS" can be used to calculate the first Piola-Kirchhoff stress "P" from the second Piola-Kirchhoff stress. The equation of motion is expressed as follows, where nominal stress is another name for the first Piola-Kirchhoff stress [117].

$$\rho_o \frac{\partial^2 \boldsymbol{u}}{\partial t^2} = F_V - \nabla_X . P \tag{3.30}$$

Where 'F_V' and 'ρ_o' are the volume force vector and the density corresponding to the initial undeformed state. The volume force vector 'F_V' contains components in the real configuration but is expressed in terms of the undeformed volume. The tensor divergence operator is calculated with regard to the material frame's coordinates. The equation 3.30 can be represented in vector and tensor component form,

$$\rho_o \frac{\partial^2 u_x}{\partial t^2} = F_{Vx} - \left(\frac{\partial P_{xX}}{\partial X} + \frac{\partial P_{xY}}{\partial Y} + \frac{\partial P_{xZ}}{\partial Z}\right) \tag{3.31}$$

$$\rho_o \frac{\partial^2 u_y}{\partial t^2} = F_{Vy} - \left(\frac{\partial P_{yX}}{\partial X} + \frac{\partial P_{yY}}{\partial Y} + \frac{\partial P_{yZ}}{\partial Z}\right) \tag{3.32}$$

$$\rho_o \frac{\partial^2 u_z}{\partial t^2} = F_{Vz} - \left(\frac{\partial P_{zX}}{\partial X} + \frac{\partial P_{zY}}{\partial Y} + \frac{\partial P_{zZ}}{\partial Z}\right) \tag{3.33}$$

Equation 3.29 can be used to determine the Cauchy stress. True stress is a symmetric tensor that correlates forces in the current configuration (spatial frame) to areas in the current configuration. The following form can be used to express equation 3.30 in terms of Cauchy stress,

$$\rho \frac{\partial^2 u}{\partial t^2} = f_V - \nabla_x . \sigma \tag{3.34}$$

Where 'f_V' and 'ρ' are the volume force vector and density corresponding to the actual deformed state. In this case, the volume force vector components are in the spatial frame with respect to the deformed volume. The divergence operator is computed with respect to the spatial coordinates.

Above mentioned approaches and theories are used in the COMSOL Multiphysics to develop the simulation models.

3.5 The organization of the thesis

The thesis is divided into ten chapters, and the chapter-wise split up is given as follows:

Chapter 1. Introduction: This chapter introduces the area of research, emphasizing the significance, applications, and challenges in the field of research.

Chapter 2. Literature Review: Extensive literature survey has been done on various superconducting wires/ tapes of HTS tape and also on the different mechanical loads

applied on them like tensile, thermal, bending, twisting, winding and fatigue. The research gaps identified to find out the overall and specific objective of the work.

Chapter 3. Methodology: This chapter discusses the objectives of the research study. And also, the methodology followed to accomplish the objectives.

Chapter 4. Effect of residual strain and tensile load on the degradation of REBCO superconducting tape: This chapter discusses how residual strain affects tape degradation under tensile loading. In the first stage, the residual strain is calculated analytically and numerically, and the results are compared. The degradation of the tape under tensile loading is evaluated in the latter stage, and critical parameters for the degradation of tape are suggested.

Chapter 5. Effect of bending load on the degradation of REBCO superconducting tape: This chapter discusses the impact of bending loading on the degradation of superconducting REBCO tape. The initial phase of this chapter deals with the analytical calculation of bending strain using the Flexure formula. In the later stage, degradation of REBCO tape under bending load is evaluated numerically with and without using plastic strain. In the final phase, critical current degradation of the REBCO tape is calculated using the power law and the numerical simulation results.

Chapter 6. Effect of twisting and combined tensile and twisting loads on the degradation of REBCO superconducting tape: Twisting load, which is another crucial load that leads to the degradation of superconducting REBCO tape is studied in detail. The initial stage of this chapter evaluates the effect of twisting on the degradation of tape. In the later stage, critical current degradation is calculated using the empirical relation reported in the literature.

Chapter 7. Effect of winding on the degradation of REBCO superconducting tape: This chapter deals with the winding of simple superconducting CORC cable and then evaluates critical winding parameters. Parameters considered for this study are core diameter, winding angle, tape width, Hastelloy and copper thickness. The final stage, critical current degradation of the REBCO tape, is evaluated using the empirical correlation reported in the literature.

Chapter 8: Effect of fatigue loads on the degradation of REBCO superconducting tape: This chapter evaluates the ability of REBCO tape to withstand repeated cyclic loads for different geometrical configurations when subjected to tensile, bending, and twisting forces. The results obtained for the three types of repeated loads are compared to each other. The maximum allowable repeated tensile, bending, and twisting loads values for different copper and Hastelloy thicknesses are also presented.

Chapter 9: Conclusions: This chapter consolidates the important findings from each chapter and discusses the significance of each load on the degradation of the REBCO tape.

Chapter 4

Effect of residual strain and tensile load on the degradation of REBCO superconducting tape

Different mechanical loads causes strain to be induced in the REBCO layer, which leads to the eventual degradation of the tape. One of the most important factors to consider while analyzing the degradation of REBCO tape is the induced-strain in the tape. The residual strain developed in the tape also contributes towards the development of induced-strain in the REBO tape. The degradation of the REBCO tape under various loading conditions is further investigated in the following chapters.

4.1. Introduction

The second-generation HTS like the REBCO are brittle in nature. They must first be transformed into tapes before being converted into superconducting cables & wires for use in various applications. The superconducting REBCO material is deposited/ coated

on a substrate layer for making tapes. Different types of deposition techniques are used to convert REBCO material into tapes. MOCVD is used to deposit REBCO material into the substrate. The MOCVD method shows superior properties, grain orientation, and cost-effectiveness compared to other types of techniques. During the MOCVD process, the materials are subjected to temperatures up to 1020 K; later, when used as superconducting cables/ wires, they are cooled to liquid nitrogen temperature as low as 77 K. Due to this wide range of temperature variations, residual strain is developed in the tape. These residual strains significantly impact the operation and reliability. The effects of residual strain on the structural properties of the superconducting layer are studied. In addition, it is essential to understand how changes in the different geometrical parameters of the tape influences the residual strain.

Understanding and regulating residual stress can help to define the occurrence of peak critical current values in REBCO tapes. This, in turn, aids in designing and customising these tapes to meet the specific requirements of many applications [118]. This residual strain is formed mainly due to the difference in the thermal expansion coefficient between the constituting layers in the REBCO tape [118, 119]. Tensile load is the simplest form of the load that acts on the tape during the manufacturing stage and application phase of the superconducting cable. In this study, initially the residual strain developed is calculated and then the effect of tensile loading is studied by applying the tensile load on the tape. The pictorial representation of the REBCO tape is shown in Figure 4.1.

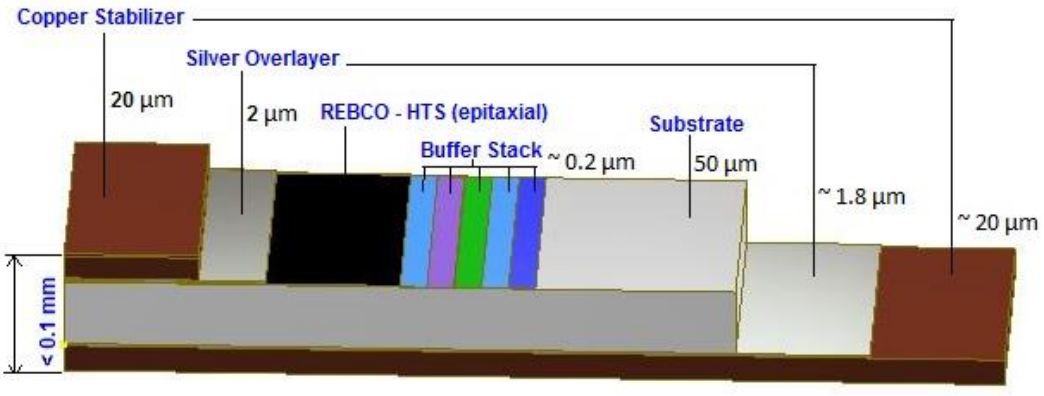

Figure 4.1: Pictorial representation of the constituent layer of REBCO tape [120].

A superconducting layer is grown over buffer layers coated on a Hastelloy substrate (Hastelloy, stainless steel or nickel alloys). Buffer layers avoid diffusion

between substrate and REBCO layer and allow homogeneous growth by compensating lattice mismatch. RABITS, ABAD (Alternating Beam Assisted Deposition) or IBAD is used to provide good alignment of grains for longer tapes [119]. A good texture decreases the angle between grain boundaries, which is necessary for higher performance. Copper is electroplated around the tape for additional electrical, mechanical and chemical stability. Copper thickness is important because it grows as the induced residual strain in the REBCO layer increases, hence increasing the irreversible axial strain limit [52, 121]. The thickness of the REBCO layer depends upon the manufacturing method used. All matrix materials' thermal and mechanical properties are essential in determining the relative strain developed in each layer due to differences in thermal expansion coefficients. The whole physical process of production of a REBCO-type tape is modelled.

4.2. Modelling

The modelling of the tape production process, including its cooldown, is divided into two steps. In the initial state, REBCO tape is deposited on the substrate (Hastelloy C276) using MOCVD process. This is the most crucial step in the actual situation because the quality of this operation impacts the tape's overall transport properties. The pictorial representation of the tape production process is shown in Figure 4.2.

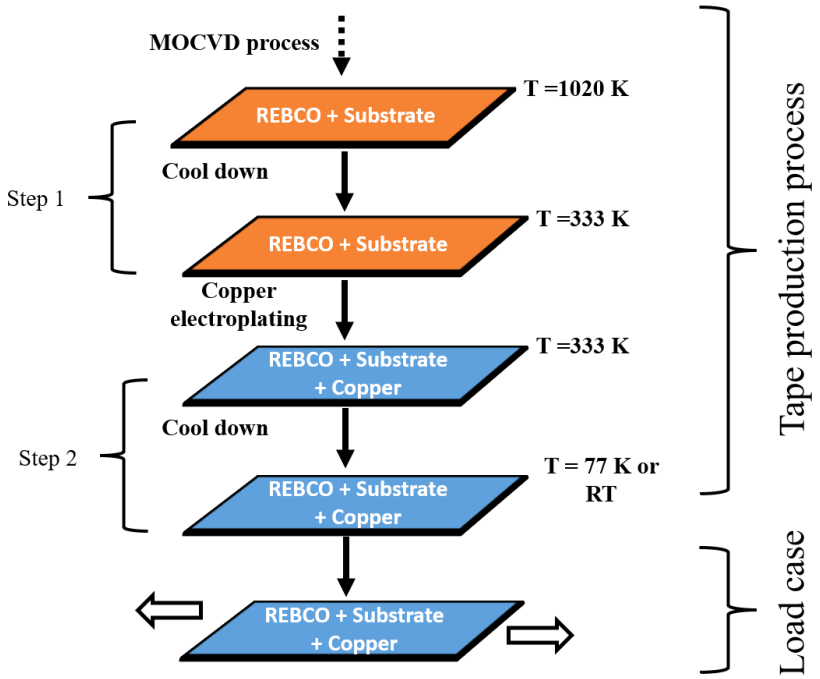

Figure 4.2: Pictorial representation of the production process and loading phase of REBCO tape.

After the deposition of REBCO into the substrate, it is cooled down to 333 K. The remaining layers of the tape including the copper layers are electroplated. Then, the second step is to cool down the tape to room or operating temperature (liquid nitrogen temperature) to evaluate the residual strain developed in the REBCO layer. In the final stage, the tensile load is applied to find the critical degradation point of the tape. The superconducting tape considered in this study is the REBCO type designated as SCS4050 [121], where the numbers 40 and 50 represent the thickness of copper and Hastelloy layers in micrometres, respectively. The cross-section of the tape showing different layers is depicted. The tensile load is applied to the REBCO tape to calculate the critical limit. The geometry of the tape considered for the analysis is 4 mm width, and 10 mm length with a thickness of 0.091 mm, as shown in Figure 4.3.

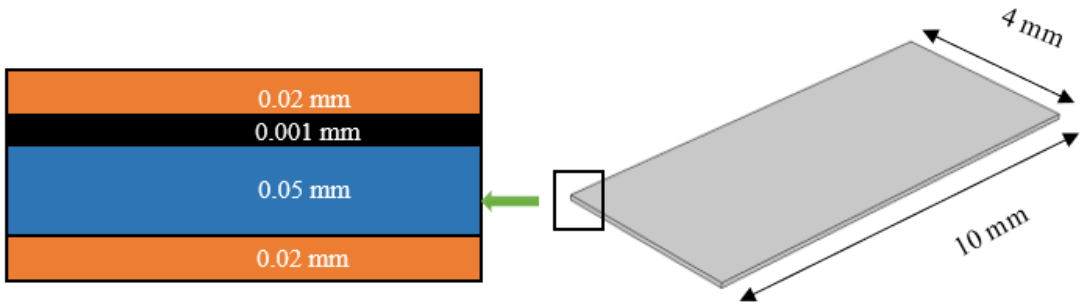

Figure 4.3: Geometric representation of REBCO tape selected and its layers.

Only REBCO, Hastelloy and copper are considered for the modelling of the tape and neglect the buffer layer and silver overlayer throughout analysis. Because stress contribution due to these layers are negligible due to it small thicknesses. Similar assumptions are also taken by other researchers [17]. The assumptions considered for the modelling are,

- Poisson's ratio, thermal expansion coefficients of all materials, and other material properties of REBCO are independent of temperature.
- Linear temperature-dependent properties of Hastelloy and Copper are used.
- Stress contribution from buffer and silver cap layers is considered negligible due to their very low thickness
- REBCO is elastic under the whole range of applied load

In the final part, a geometrically parametric study is conducted by varying the thickness and width of the REBCO tape. The effects of residual strain and tensile load on the REBCO layer are found. For each case, the critical limit under the residual strain and tensile loading conditions in the superconducting REBCO layer of tape is determined.

4.2.1. Meshing and boundary conditions

A mesh-independent study is conducted to identify the optimal mesh for the model. The optimal mesh identified and used for this analysis is 14 elements along the width, 36 elements along the length and 4 elements along the thickness of the REBCO tape. The approach used is the Birth and death method [122]. Adding a passive copper layer is the first step of modelling. This passive copper layer deforms freely without providing any stress during the initial cool down (Step 1). This is accomplished by providing a very low Young's modulus' value to the copper layers in the first step. Copper is electroplated on the deformed geometry before the second step of the modelling (cooling down from 333 K to RT/ 77 K). In the second step, the actual properties are provided to all the layers to obtain the residual stress/ strain.

4.2.2. Material properties

Material properties selected for the modelling are given the Table 4.1. The plastic properties of Hastelloy and copper are considered and plotted in Figure 4.4. REBCO is considered elastic under the whole range of applied load.

Table 4.1: Material properties of Hastelloy, copper and REBCO [17]

	Hastelloy		***Copper***		***REBCO***
	293.15 [K]	*77 [K]*	*293.15 [K]*	*77 [K]*	
Young's Modulus (GPa)	*223*	*228*	*80*	*98*	*157*
Yield stress (MPa)	*891*	*1141*	*120*	*146*	*.....*
Poissons ratio	*0.307*	*0.307*	*0.34*	*0.34*	*0.3*
Thermal expansion coefficient	1.34×10^{-5}	1.34×10^{-5}	1.37×10^{-5}	1.37×10^{-5}	1.1×10^{-5}

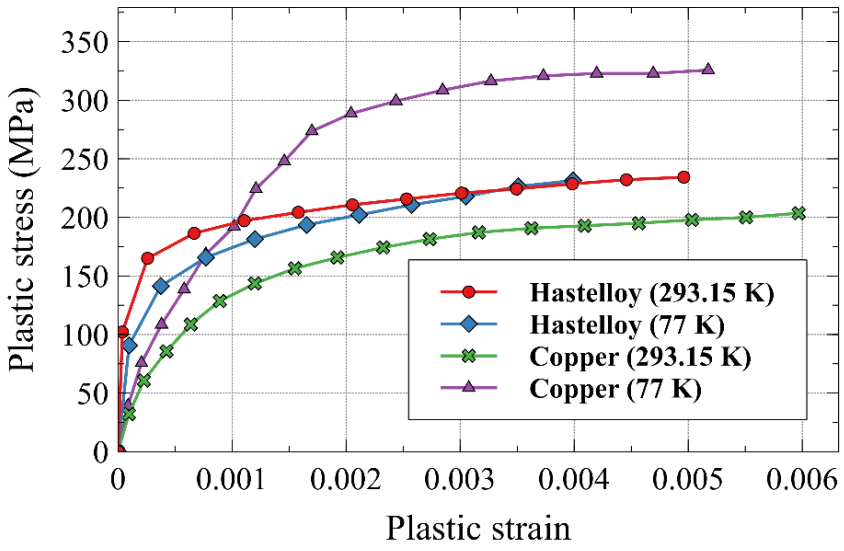

Figure 4.4: Plastic properties of Hastelloy and copper [17].

Both the plastic properties and elastic properties are directly taken from the literature [17].

4.2.3. Analytical Approach for Residual Strain Calculation

The residual strain developed during the production process of the REBCO tape can be calculated using the analytical equation 4.1 [52].

$$\frac{((\alpha_h-\alpha_r)*V_{fh}*E_h*\Delta T_1+(\alpha_c-\alpha_r)*V_{fc}*E_c*\Delta T_2)}{V_{fh}*E_h*\Delta T_1+V_{fc}*E_c*\Delta T_2}*\Delta T_1 \quad (4.1)$$

Where α_h, α_r, α_c are the thermal expansion coefficients of the Hastelloy, REBCO layer and that of the copper layer, respectively. V_{fc}, V_{fh} are the volume fractions of copper and Hastelloy, respectively. E_h, and E_c are Young's modulus of Hastelloy and copper. ΔT_1= (293.15 K (or 77K) - MOCVD temperature) and ΔT_2= (293.15 (or 77K) - copper electroplating temperature). And the MOCVD temperature is 1020 K, and the electroplating temperature for copper is 333 K.

4.2.4. Validation

Table 4.2 depicts the numerical simulation model is successfully validated by comparing with experimental and simulation results published in the literature [17]. Both results show good agreement, and a maximum deviation of 3 % is observed between the present simulation result and the result published by K llin et al. [17]. Analytical evaluations are also carried out to verify the residual compressive strain generated at the

end of the manufacturing process. The residual strain in the REBCO layer is compressive due to the difference in the thermal expansion coefficient of constituting layers.

Table 4.2: Comparison of present study and previous studies

Parameter	***Experimental Data literature [17]***	***FEM Literature [17]***	***FEM (Present study)***	***Analytical (Present study)***
Residual strain in REBCO layer at RT (%)	*-0.20*	*-0.17*	*-0.17*	*-0.17*
Residual strain in REBCO layer at 77 K (%)	-	*-0.237*	*-0.242*	*-0.245*

The intrinsic axial strain in the REBCO layer should not exceed 0.45 % to prevent degradation of the superconducting wire. The strain developed in the REBCO layer is calculated in these conditions to determine the threshold criterion for irreversible critical current degradation. C. Zhou et al. [123] evaluated the performance of SuperPower® REBCO tape in a critical current-strain testing rig. The results of their experimental work are compared with this simulation results. The intrinsic strain versus applied strain in the REBCO tape under tensile loading at liquid nitrogen temperature is depicted in Figure 4.5.

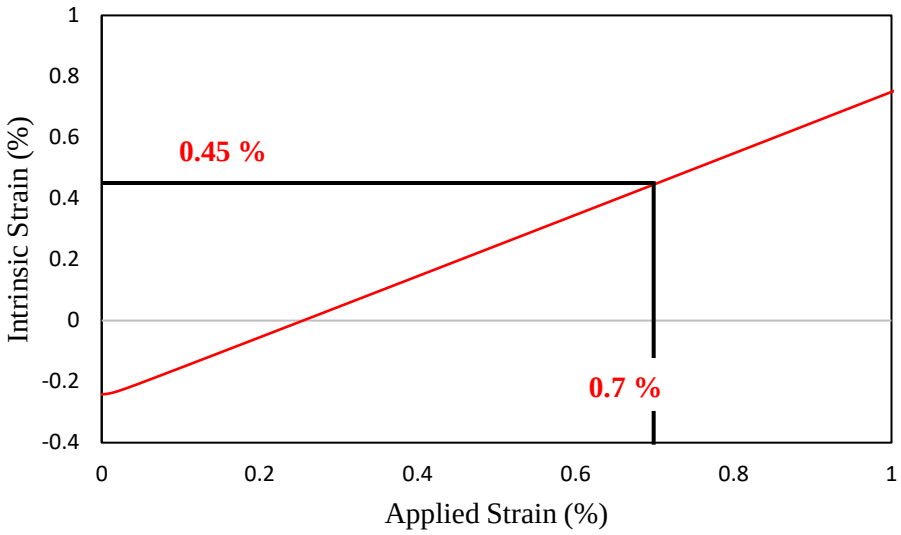

Figure 4.5: Intrinsic strain vs applied strain in the REBCO layer at room temperature.

It may be noted that after the production process there is 0.242 % residual strain is developed in the tape. So, when the applied strain is 0 %, the intrinsic axial strain in the REBCO layer is -0.242 %. It is also noted that there is a linear relationship between the applied strain and the intrinsic axial strain. To achieve a strain-free state, need to apply around 0.25 % of applied strain. Researchers will be benefited by understanding the strain-free state of the REBCO tape corresponding to different geometrical configurations.

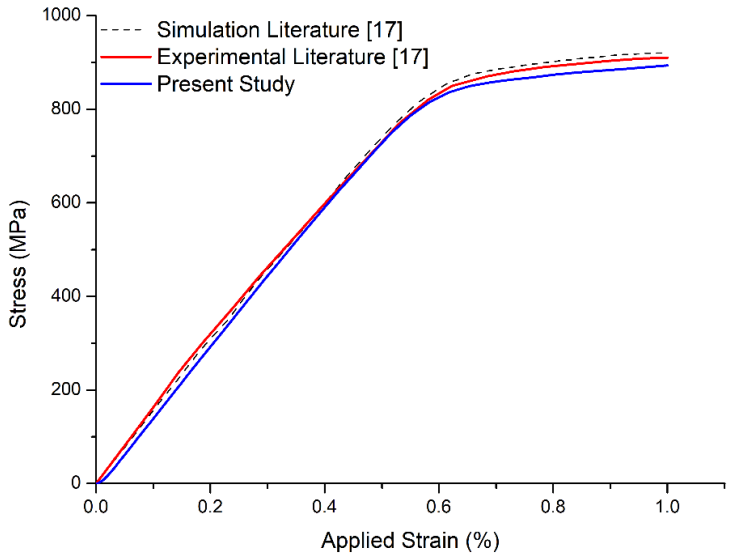

Figure 4.6: Stress vs percentage of applied strain in the REBCO tape at room temperature.

Figure 4.6 depicts the applied strain versus stress in the REBCO tape under tensile loading at room temperature. Both experimental and simulation findings illustrate good agreement, with a maximum deviation of 1.8 % between the two. It may be noted that when the intrinsic tensile strain reaches 0.45 %, causing REBCO tape degradation, the stress developed in the REBCO tape is 861 MPa and the applied strain is 0.7 %. This simulation model is used to carry out the parametric studies mentioned in the subsequent sections.

4.3. Results and discussion

The effect of each geometrical parameter on the development of residual strain is examined in this section by numerical simulation and analytical calculations. The parameters considered for this analysis are Hastelloy thickness, copper thickness and tape width.

4.3.1. Residual strain computed analytically at room temperature and 77 K

Figure 4.7 depicts the variation of residual strain with changes in Hastelloy thickness calculated analytically at room temperature. It may be noted that as the Hastelloy thickness decreases, the compressive residual strain in the REBCO layer increases.

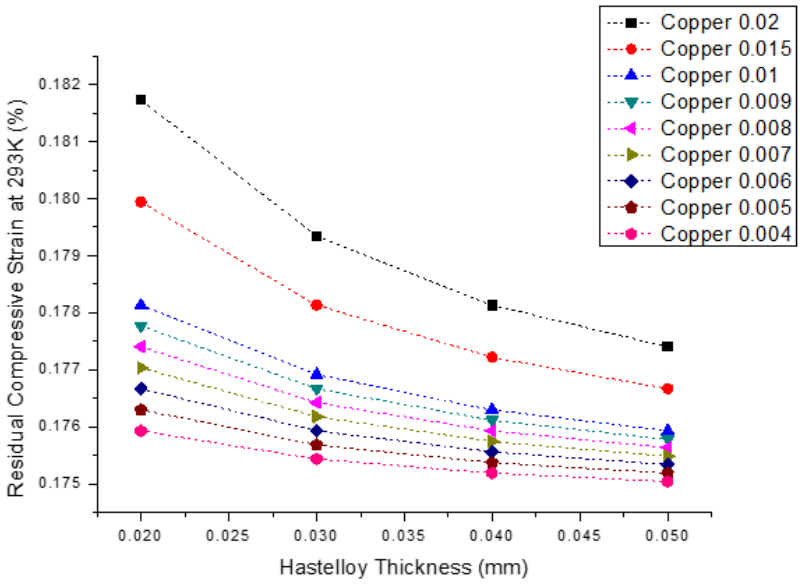

Figure 4.7: Residual compressive strain at room temperature calculated analytically

When reducing the thickness of the copper from 0.02 mm to 0.004 mm, the value of the residual compressive strain at room temperature approaches a constant value with

changes in Hastelloy thickness for any particular copper thickness. For instance, when the Hastelloy thickness varied from 0.05 mm to 0.02 mm for a particular copper thickness of 0.02 mm, the residual compressive strain increased by 2.44 %. Similarly, When the copper thickness is varied from 0.02 mm to 0.004 mm, the residual compressive strain induced in the REBCO layer decreases. Compressive strain decreases by 1.33 % when the copper thickness is reduced from 0.02 mm to 0.004 mm at a Hastelloy thickness of 0.05 mm (maximum). The decrease for the exact change in copper thickness is 3.3 % if the thickness of the Hastelloy is minimum (0.02 mm). Please note that tape width kept a constant of 4 mm. It may also be observed that the graph becomes steeper at a smaller Hastelloy thickness.

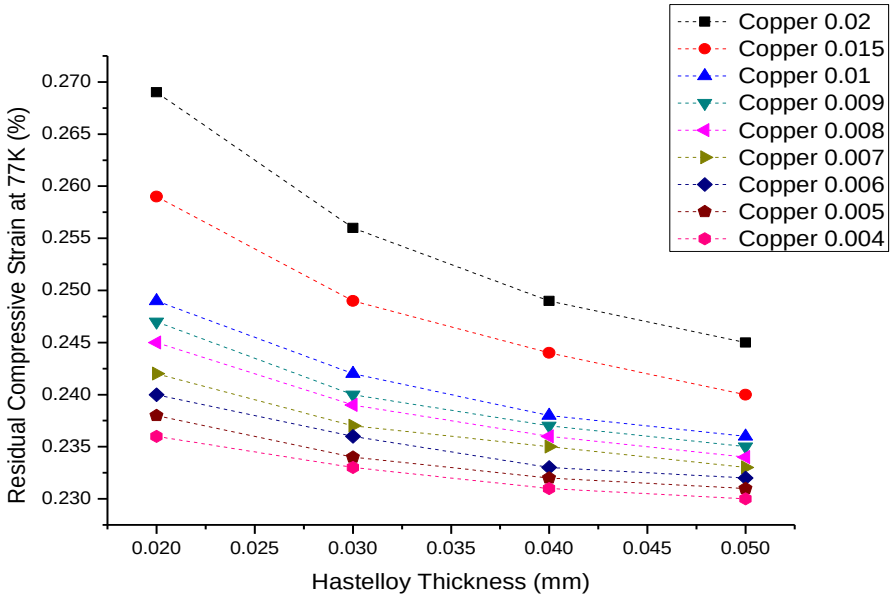

Figure 4.8: Residual compressive strain at 77 K calculated analytically

Figure 4.8 shows the variation of residual compressive strain with changes in Hastelloy thickness of different copper thicknesses at 77 K. More residual strain is developed at 77 K compared to room temperature. Similar to the previous case (room temperature), the residual compressive strain increases with a reduction in Hastelloy thickness. For instance, when the copper thickness is reduced from 0.02 mm to 0.004 mm, the residual compressive strain at 0.05 mm and 0.02 mm Hastelloy thicknesses drop by 5.7 % and 12.3 %, respectively. The reason for the variation of residual strain with changes in Hastelloy and copper thicknesses is further investigated.

When the tape cools down to liquid nitrogen/ room temperature, copper undergoes more compressive strain and also tries to pull the REBCO and Hastelloy to the

compressive side because copper has a high value of thermal expansion coefficient. At the same time, REBCO and Hastelloy pull back the copper to the tensile side, as shown in Figure 4.9. It may be noted that the thermal expansion coefficient of REBCO, Hastelloy and Copper are 1.1×10^{-5}, 1.34×10^{-5} and 1.77×10^{-5}, respectively.

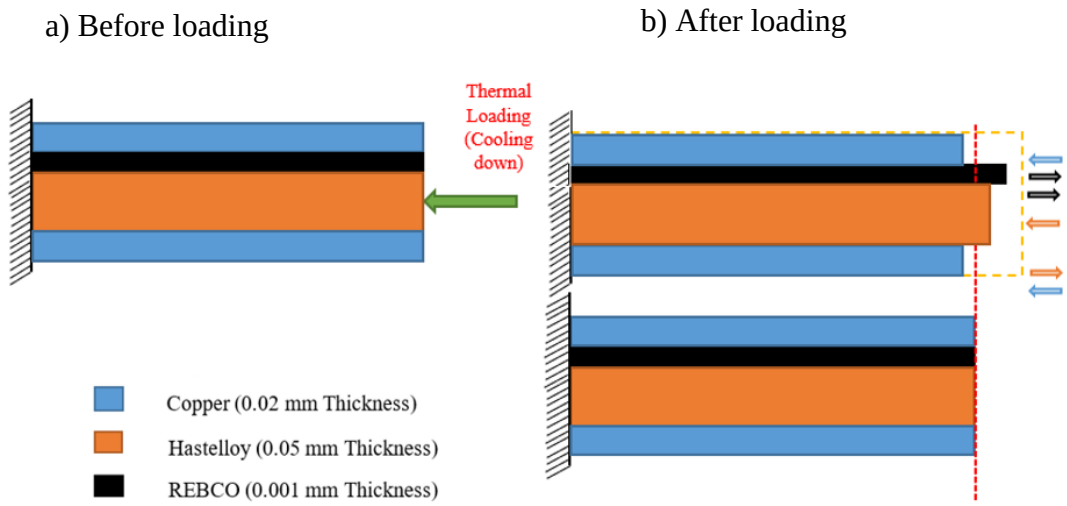

Figure 4.9: Schematic diagram of thermal loading: a) Before loading b) After loading (no bonding between the layers) c) After loading (actual situation)

Each layer's volume fraction influences the development of the pulling load between the layers. Considering the effect between the REBCO and Hastelloy layers, Hastelloy tries to pull the REBCO layer to the compressive side, and the REBCO layer tries to pull the Hastelloy to the tensile side. After the production process, the combined effect of each layer's pulling force significantly influences the development of the final residual strain.

4.3.2. Residual strain computed by numerical simulation at 77 K.

The variation of residuals strain with changes in Hastelloy thickness corresponding to different copper thicknesses is illustrated in Figure 4.10. Similar to analytical calculation, it may be noted from the figure that Hastelloy thickness decreases with increasing the residual compressive strain developed in the REBCO layer except for 0.004 mm and 0.005 mm copper thicknesses.

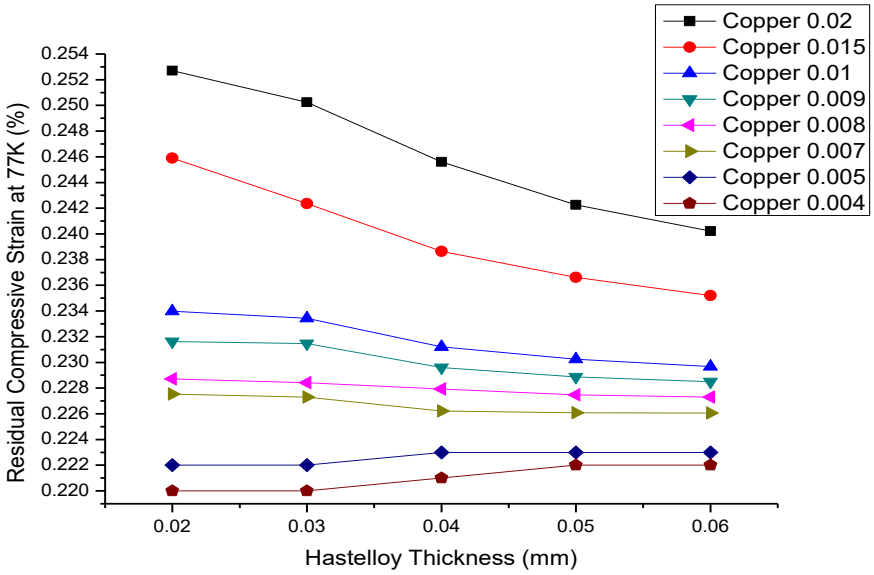

Figure 4.10: Residual compressive strain at 77 K at different copper and Hastelloy by simulation

The residual compressive strain increases by 5.19 % at a copper thickness of 0.02 mm and 4 mm wide tape when the Hastelloy thickness is reduced from 0.06 mm to 0.02 mm. The residual compressive strain is reduced by 7.5 % and 13 % when lowering the copper thickness from 0.02 mm to 0.004 mm at 0.06 mm and 0.02 mm Hastelloy thickness. The observed trend is the same as the trend obtained in the analytical calculations. It is also observed that if the Hastelloy thickness is reduced by 60 % at a copper thickness of 0.02mm, the residual compressive strain at 77 K increases in simulation by 4.31 %, but the percentage increase is 9.79 % by analytical calculation.

4.3.3. Comparison of analytical result with the numerical simulation result at 77 K

Figure 4.11 depicts the comparison of residual strain calculated by analytical calculation, and the percentage deviation between the two sets of values is plotted for different Hastelloy and copper thicknesses.

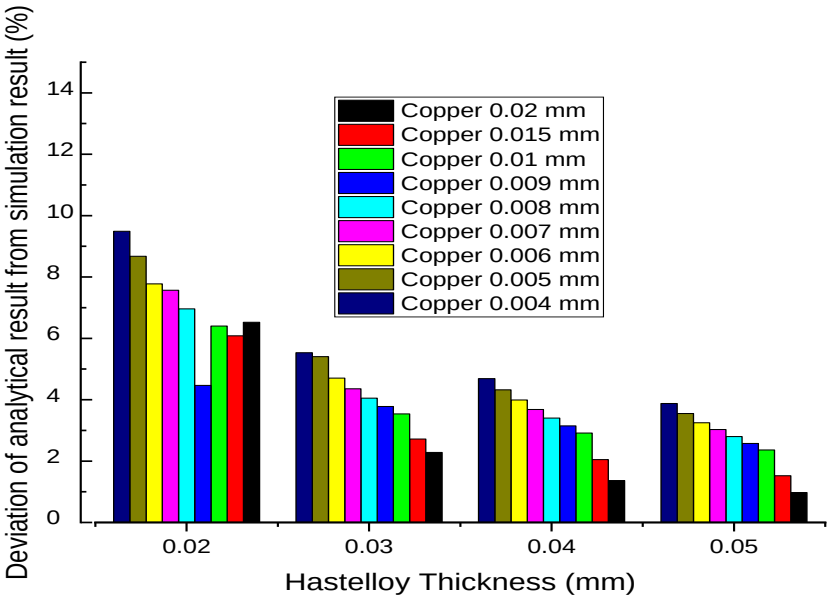

Figure 4.11: Simulation result deviation from the analytical value of residual strain at different copper thickness

The results obtained from the analytical calculations and simulation are in good agreement. It may be noted that the percentage deviation between the numerical simulation and the analytical computation increases when the copper and Hastelloy thickness decreases. The maximum deviation observed is 9.5% for 0.02 Hastelloy and 0.004 mm copper thickness. It is also observed that the analytical equation is not accurate in predicting the residual compressive strain behaviour for small tape thickness. If the tape thickness is less than 2.9μm, then an alternative equation is required to predict residual compressive strain behaviour.

4.3.4. Residual strain with changes in the tape width

Variation of residual strain with variation in tape width and copper thickness at 77 K is demarcated in Figure 4.12. It may be noted that the residual compressive strain is nearly the same for all three tape widths, with a maximum deviation of 1%.

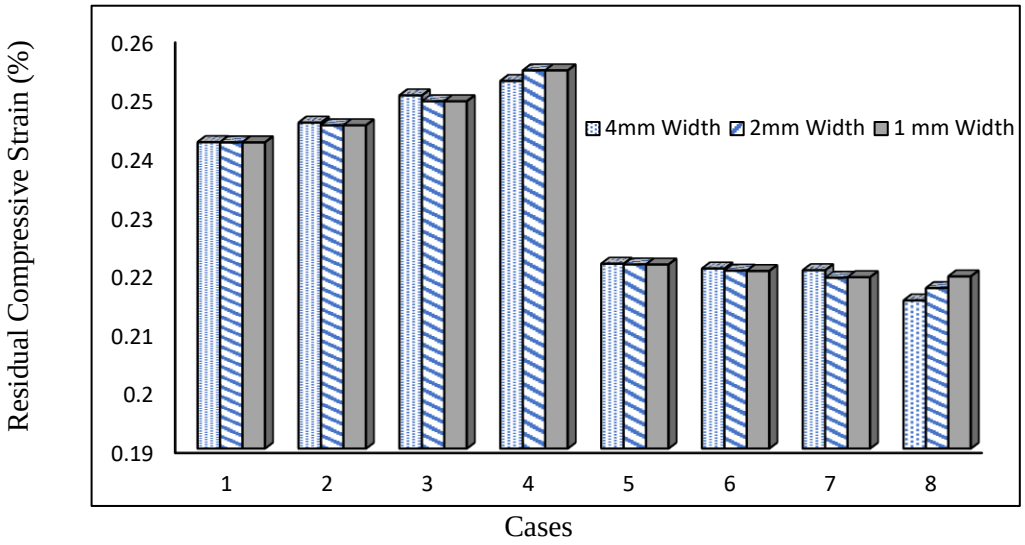

Figure 4.12: Residual compressive strain at 77 K by simulation at different tape width (where case 1-4: copper thickness=0.02 mm and Hastelloy thickness decreases from 0.05mm to 0.02mm in the step of 0.01mm ; Case 5-8 : copper thickness= 0.01mm and Hastelloy thickness decreases from 0.05mm to 0.02mm in the step of 0.01mm).

The variation of residual strain with tape width is found to be not significant because the volume fraction of the tape does not change with changes in tape width.

4.3.5. Effect of Hastelloy thickness in the development of intrinsic stress in the REBCO layer

Figures 4.13, 4.14, and 4.15 show the relationship between the application of force, the development of stress, and the development of the intrinsic REBCO strain. REBCO strain varies linearly in all three cases with the applied force up to a given value, then a sudden increase in REBCO strain is observed to a slight rise in applied force under tensile loading. The thick horizontal and vertical line is marked in the Figures to mention the critical limit corresponding to the 0.45 % intrinsic axial strain in the REBCO layer.

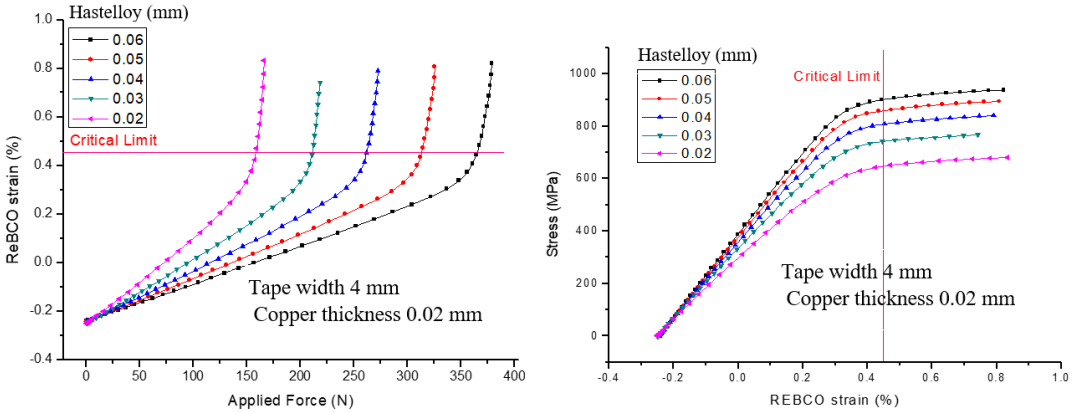

Figure 4.13: a) REBCO strain VS applied force b) Stress VS REBCO strain at varying Hastelloy thickness for 0.02 mm copper thickness

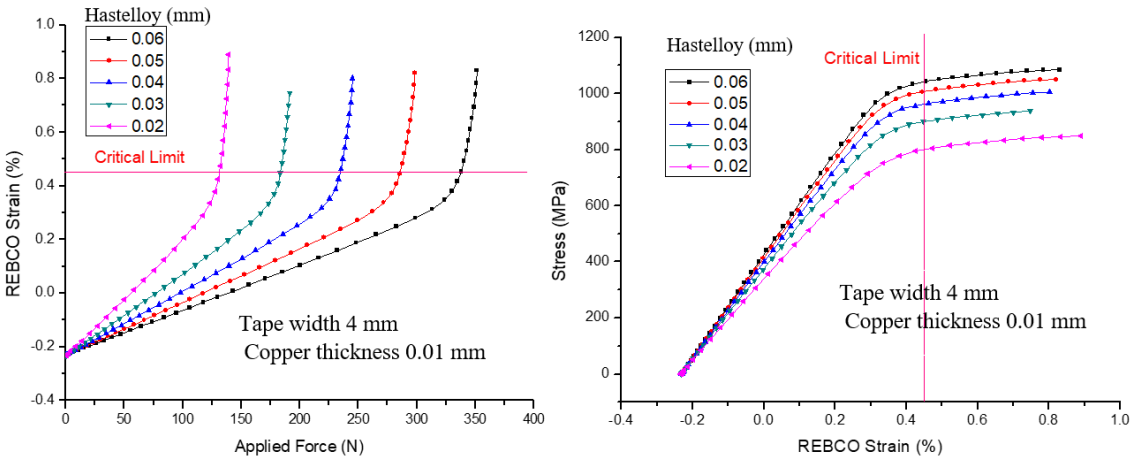

Figure 4.14: a) REBCO strain VS applied force b) Stress VS REBCO at varying Hastelloy thickness for 0.01 mm copper thickness

The thickness of copper also influences the force that can be applied and the stress that develops. It may be noted that the force which can be applied without causing degradation to the tape, the critical limit decreases with a decrease in Hastelloy thickness. Beyond the critical limit, the increase in the REBCO strain is almost vertical with the increase in the applied force. Therefore, it is imperative that this type of REBCO tape must be operated well below the critical limit to ensure that there is no degradation. A similar relationship can be noted between the stress developed and the thickness of the Hastelloy.

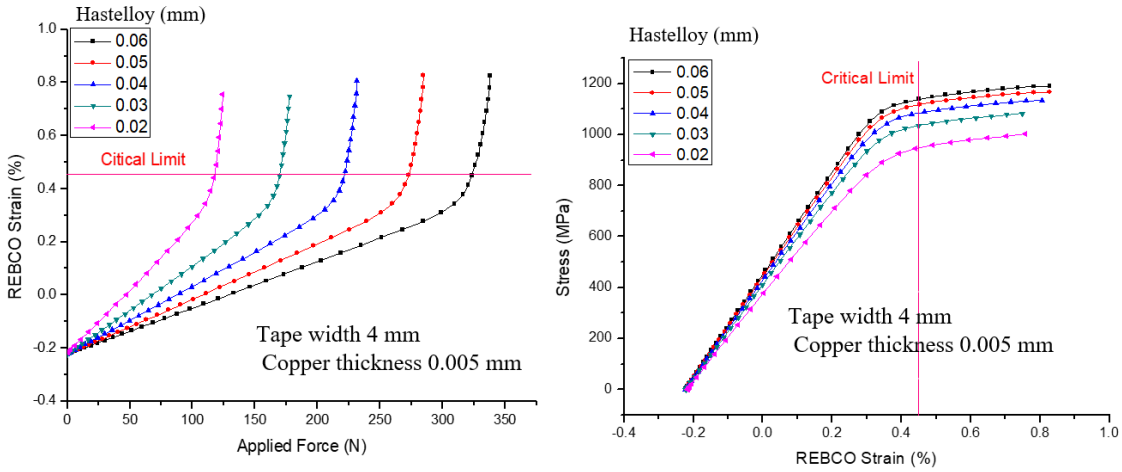

Figure 4.15: a) REBCO strain VS applied force b) Stress VS REBCO strain at varying Hastelloy thickness for 0.005 mm copper thickness

It is also evident that there is a complete upward shift for the REBCO VS stress strain graph, with decreased copper thickness and a complete leftward shift for the force applied VS REBCO strain. It implies that the stress developed increases with a decrease in copper thickness but the force that can be applied decreases. This is due to the reduction in cross-sectional area due to reduced thickness of the copper layers.

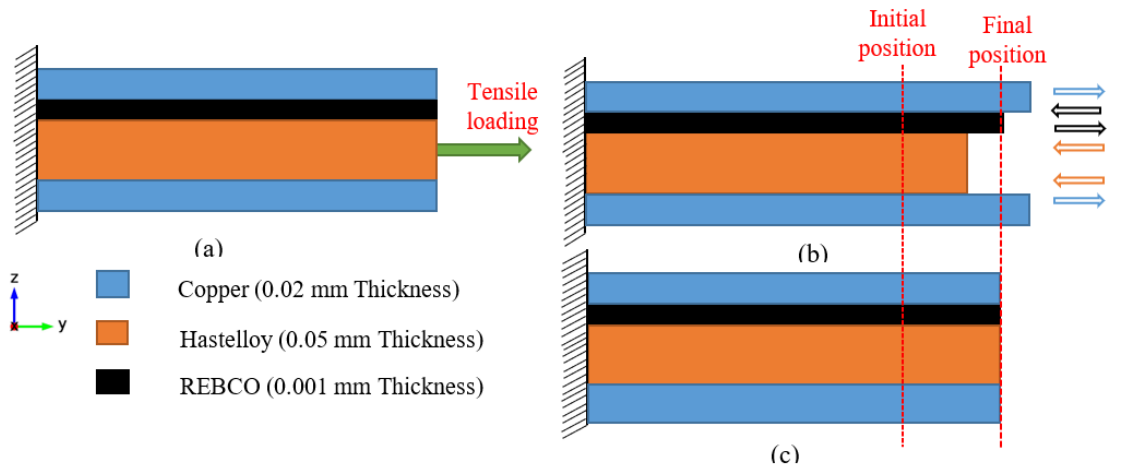

Figure 4.16: Schematic diagram of tensile loading a) Before loading b) After loading (no bonding between the layers) c) After loading (actual situation)

Variation in the Hastelloy and copper thickness with changes in the critical limit may be due to the variation of the volume fraction of material. It is very similar to the thermal loading explained in the Figure 4.9. But, Young's modulus of the constituent

material depends on the final position of the tape. The material with lowest Young's modulus value elongates more and vice-versa. Copper and REBCO try to pull the Hastelloy to the tensile side and Hastelloy try to pull back to the compressive side, as shown in figure 4.16. The combined effect of each layer's pulling force has a crucial impact on the development of the final strain at the end of the tensile load.

4.3.6. Effect of tape width in the development of intrinsic stress and strain in the REBCO layer

Figures 4.17 depict the applied force variation with changes in intrinsic axial strain in the REBCO layer. It may be noted that intrinsic axial strain increases with increasing the applied force up to a particular value, then there is a slight increase in the force that leads to a sudden increase in the intrinsic axial strain.

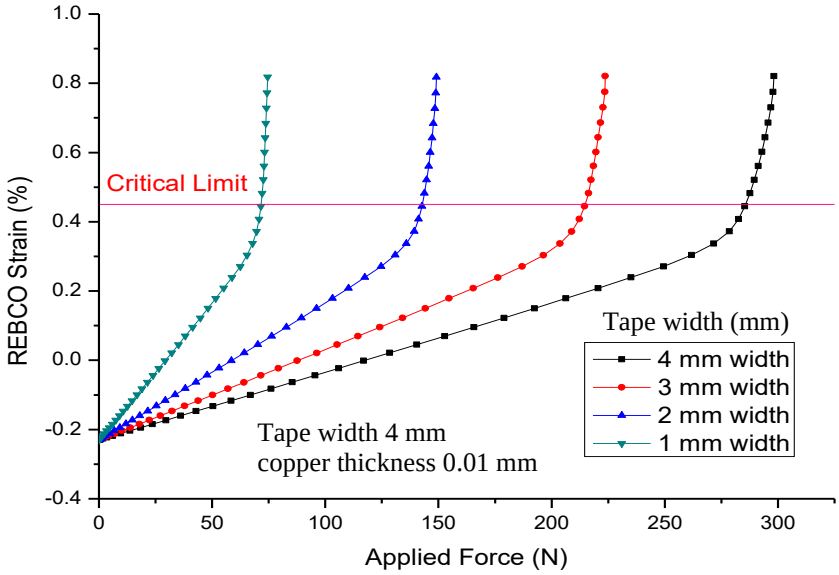

Figure 4.17: Variation of Applied force with changes in intrinsic axial strain in the REBCO layer

It is also observed that, as the width of the tape decreases, the force which can withstand without degradation decreases. For instance, the tape width decreases by 1/4th (from 4 mm to 1 mm), the critical force that it can withstand is reduced by 75 %.

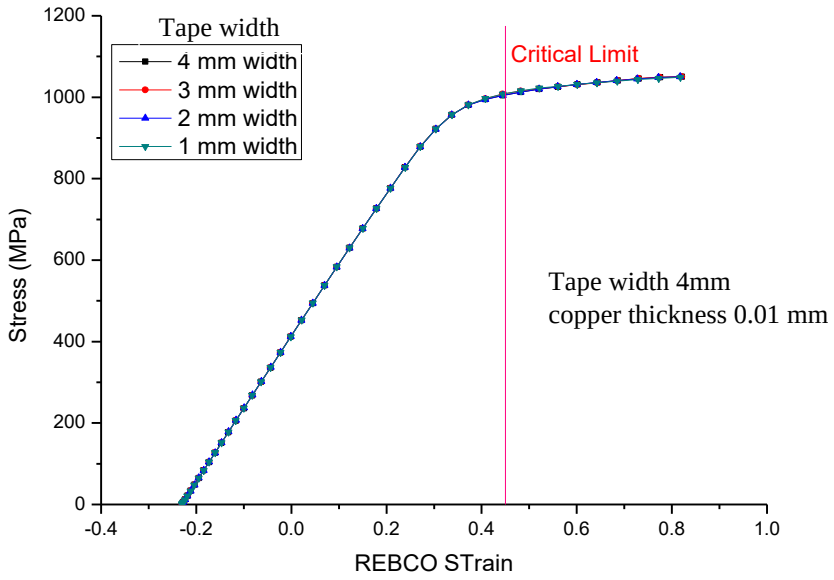

Figure 4.18: Relationship between stress and intrinsic axial strain in the REBCO layer.

Figure 4.18 shows the relationship between the developed stress and the intrinsic axial strain at different tape widths. The graph shows that tape width does not influence the stress developed as they are all overlapped; however, the force applied in the REBCO layer corresponds to the intrinsic axial strain changes.

4.3.7. Comparison of critical limits in the REBCO tape

The critical force at different copper thicknesses from figures 4.13, 4.14 and 4.15 at different Hastelloy thicknesses is consolidated and plotted in figure 4.19. It may be noted that with an increase in Hastelloy and copper thickness, the critical force that can withstand without any degradation increases. It is also observed that the relationship between the critical force and the Hastelloy thickness is linear. When the thickness of the copper layers are decreases by 75%, the critical force decreases by 12 % and 25 % respectively at 0.06 mm and 0.02 mm thickness of Hastelloy. When decreasing the Hastelloy thickness from 0.06 mm to 0.02 mm (about 66 %), the critical force decreased by almost 66 %.

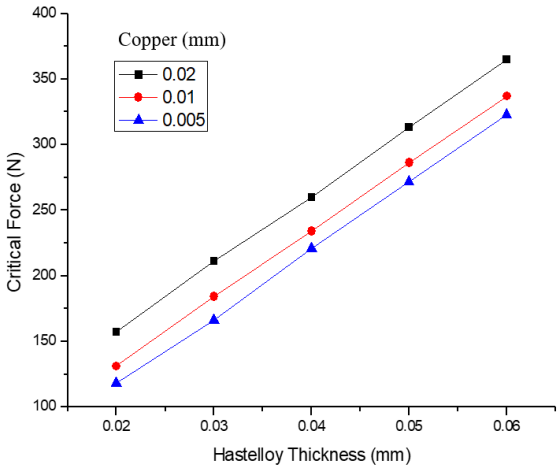

Figure 4.19: Hastelloy thickness VS Critical force at different copper thickness

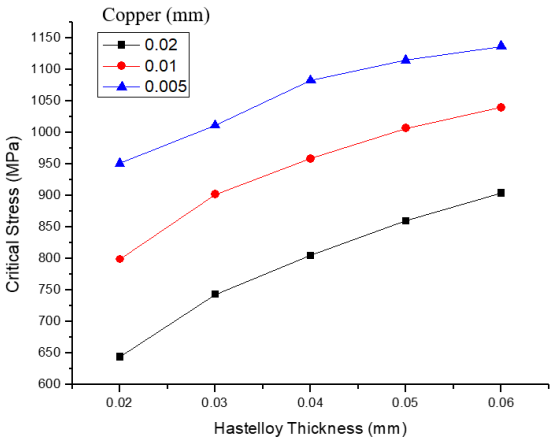

Figure 4.20: Hastelloy thickness VS Critical Stress at different copper thickness

Variation of critical stress with varying Hastelloy thickness at different copper thicknesses is shown in Figure 4.20. The critical stress developed also follows the same trend; with an increase in Hastelloy thickness, the critical stress of the REBCO tape increases. It is also found that as the copper thickness decreases by 75 % the critical stress decreases by 21 % and 32 % respectively at 0.06 Hastelloy thickness 0.02 mm Hastelloy thickness.

From all the above graphs, it may be inferred that tape thickness significantly influences the development of intrinsic axial strain in the REBCO layer under tensile loading. When the thickness of the tape is reduced, the critical current density increases, but the critical force limit of the tape decreases. Thus, the dimensions of the tape can be chosen based on the application and the load.

4.4. Summary

The effect of residual strain on the occurrence of peak critical current and its impact on tape degradation under tensile loading is investigated. The residual strain is calculated both analytically and numerically. The effect of Hastelloy thickness on residual strain is also investigated, and it is found that residual strain increases as Hastelloy thickness decreases. Tensile loading studies are performed for various Hastelloy, copper, and tape width configurations and the corresponding critical force values are determined. The important results may be summarised as follows,

- Residual strain is induced in the REBCO tape because of the wide temperature changes to which the tape is subjected during its manufacturing and application stages. The residual strain induced when bringing down the tape from 1020 K to liquid nitrogen temperature is 30 % more than the induced residual strain when cooling down the tape from 1020K to room temperature.
- The quantity of residual strain-induced is about 50 % of the tensile degradation limit of the tape in terms of the absolute value.
- However, since this residual strain is compressive in nature, it helps to withstand more loads when subjected to tensile loads.
- The residual strain-induced changes with variation layer thicknesses. With the decrease in the thickness of the substrate layer (Hastelloy), the residual strain-induced will increase. A 66 % decrease in the Hastelloy layer resulted in about a 5 % increase in residual strain.
- Similarly, with the decrease in the reinforcement layers (copper), the residual strain-induced decreases. An 80 % decrease in the thickness of copper layers has resulted in about an 8% decrease in the compressive residual strain.
- Decreasing the width of the tape was found to have no effect on the induced residual strain.
- The REBCO tapes are degraded beyond certain loads when subjected to tensile loading. These critical limits change with variation in geometrical parameters like layer thicknesses and width of the tape. The force corresponding to critical limit is termed as the critical force that the tape can withstand without getting degraded.
- This critical force decreases almost linearly with decrease in Hastelloy thickness; thereby reducing the quantity of tensile load the tape can withstand. Decreasing the Hastelloy thickness by 66 %, decreases the critical force by almost 66 %. However, decreasing the copper thickness by 75 %, decrease the critical force only by 13 %.
- This critical force decreases almost linearly with decrease in the width of the tape. Decreasing the tape width by 75 %, decreases the critical force that it can withstand by 75 %.

Therefore, it is understood that the residual strain induced in REBCO tapes are significant and cannot be neglected while performing modelling studies on such superconducting

tapes. Therefore, residual strain induced in the tape not neglected and considered for the rest of the study.

Chapter 5

Effect of bending load on the degradation of REBCO superconducting tape

5.1. Introduction

The effect of thermal and tensile loading and their eventual degradation limits are studied in the previous chapter, it is required to understand the effects of other types of mechanical loads on the REBCO tape. Another important type of mechanical load that a HTS tape is subjected to is the bending load. The REBCO tapes are subjected to bending load during the manufacturing of wires, cables, superconducting magnets etc. It is very important to determine the mechanical strength of the superconductor and its degradation limits under bending. The superconductor's degradation limits depend not only on the bending radii; but also on the geometrical parameters such as the thickness of Hastelloy, copper layers.

While changing the parameters, the effect of bending on strain development in the REBCO layer is determined. For each bending radii, the variations in the induced strain are determined. When varying the thickness of substrate and reinforcement layers, the role of the position of the neutral axis while bending is thoroughly investigated. The results of both analytical and simulation methods are compared. This analysis is carried out in stages. In the initial phase, the strain in the REBCO layer is calculated analytically using the Flexure formula. The residual strain developed during the production process of the tape and plastic property of the Hastelloy and copper is neglected in this calculation. However, in the later stage, the residual strain and plastic properties are taken into consideration. Finally, critical current retention is determined using the power law.

5.2. Analytical approach for determining the induced strain in the REBCO layer

A pictorial representation of the REBCO tape subjected to bending load is shown in figure 5.1. Kindly note that the REBCO tape considered here is an approximated model of the actual one shown in Figure 4.1. The buffer and silver cap layers are not considered from the mechanical point of view as the stress contribution from these two layers is negligible owing to their very low thickness [17].

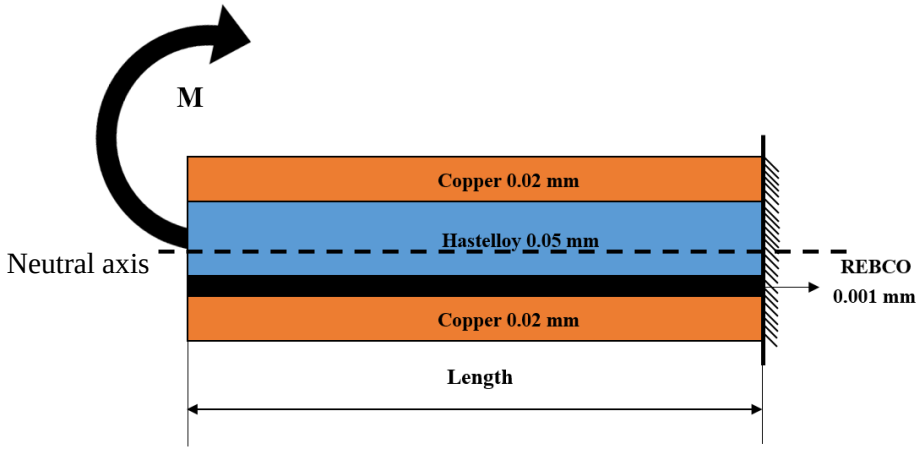

Figure 5.1: Cross-sectional view of a REBCO tape subjected to the bending load

To obtain smaller bending radii, the tape strip utilized in this investigation has a length of 5 mm. Bending is done along the length of the tape, as shown in the diagram. The bending moment on one end of the tape is '*M*,' while the other end is fixed, causing the tape to bend. Using the Flexure formula and assuming the tape as a beam, the maximum stress developed in the REBCO layer is computed. The Flexure formula is created for a tape of homogeneous material. Therefore, it cannot be used to calculate the normal stress in a composite beam directly. However, a method transformed section approach is developed

for converting the cross-section of a composite beam into one comprised of a single material [116]. After completing this transformation, the Flexure formula can be used to calculate the stress. When a bending moment is applied to a tape, like the homogeneous tape, the overall cross-section area of the tape remains unchanged after bending. Normal stress rises linearly from zero at the neutral axis to a maximum in the farthest location from the neutral axis. In this analysis, the Hastelloy and REBCO layers are converted to copper using the transformed sectional approach. The new width of Hastelloy can be calculated by considering a small element in Hastelloy with a width *dz* and thickness *dy* (as illustrated in Figure 5.2), where the force *dF* acts on the tape's area *dA= dzdy*.

$$dF = \sigma dA = (E_h \varepsilon) dzdy \tag{5.1}$$

'σ' is the normal stress acting on the elemental area '*dA*'. E_h, E_c and E_r are Young's modulus of Hastelloy, copper and REBCO, respectively. After applying the transformed section method, all the materials are converted to as equivalent homogeneous material (in this case copper). So, the width of the corresponding element is assumed as *ndz*.

$$dF' = \sigma' dA' = (E_c \varepsilon) ndzdy \tag{5.2}$$

Both the force terms in equations 5.1 and 5.2 are equated, such that they produce the same moment about the neutral axis.

$$(E_h \varepsilon) dzdy = (E_c \varepsilon) ndzdy \tag{5.3}$$

$$n = \frac{E_h}{E_c} \tag{5.4}$$

The transformation factor is the dimensionless number '*n*'. It specifies that the original tape's cross-section with width '*W*' must be stretched to a new width '$W_2 = nW$'. The normal stress distribution throughout the changed cross-section will be linear once the tape has been transformed into a single-layer material. The altered area's neutral axis (centroid) and moment of inertia are easily computed. The stress at each point of the transformed one can be calculated using the flexure formula in the normal manner.

$$\frac{M}{I}=\frac{6}{Y}=\frac{E}{R} \tag{5.5}$$

The stress in the transformed tape will be equivalent to the stress in the actual tape. However, the changed material's stress must be doubled by the transformation factor (*n*). Because the area of the converted material, "$dA' = ndzdy$", is n times the area of the original material, "$dA' = dzdy$,"

$$dF = \sigma dA = \sigma' dA' \tag{5.6}$$

$$\sigma dzdy = \sigma' ndzdy \tag{5.7}$$

$$\sigma = n\sigma' \tag{5.8}$$

The same method is used to convert the REBCO layer into an equivalent copper layer of different widths, corresponding to the difference in their Young's moduli. The Flexure formula is used to determine the normal stress values after the whole tape is converted to equivalent copper material.

5.2.1. Determination of the neutral axis for the analytical studies

As mentioned in the previous section, to calculate the position of the neutral axis and the strain developed in the REBCO layer, Hastelloy and REBCO layers are converted to equivalent copper based on the modular ratio. The modular ratio for REBCO and Hastelloy are denoted respectively as $'m'$ and $'n'$.

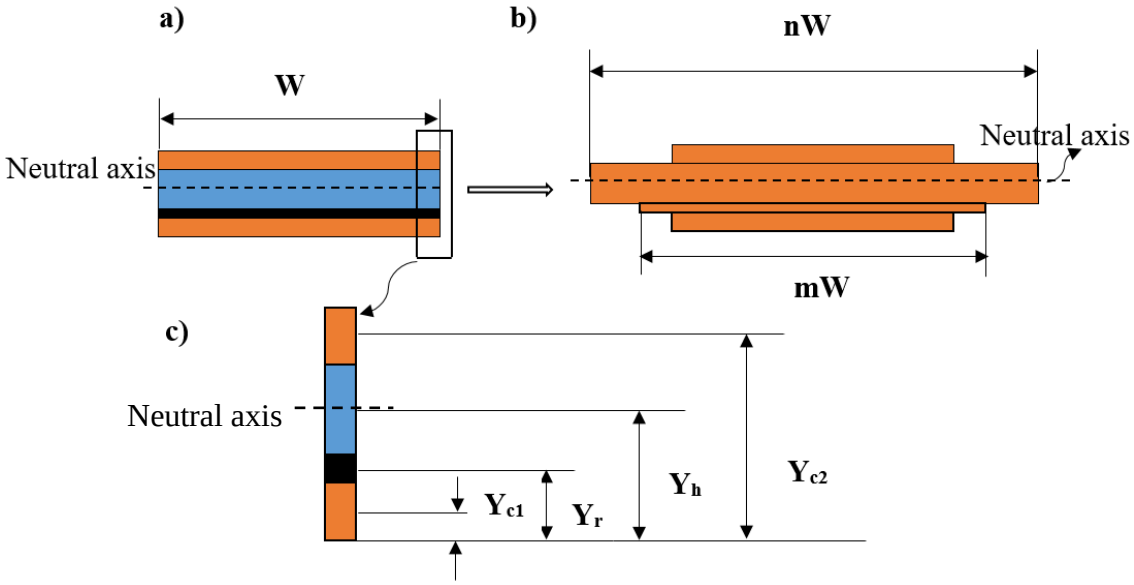

Figure 5.2: Transformation of (a) the composite REBCO tape (b) into single material of copper and the (c) enlarged view of REBCO tape. [Y_{c1},Y_r,Y_h,Y_{c2} are the distance between bottom side of the tape to the centroid of bottom copper layer, REBCO layer, Hastelloy layer and top copper layer respectively]

Therefore, the length of the REBCO layer is increased by '*m*' times, and that of Hastelloy is increased by '*n*' times and depicted in Figure 5.2.

$$m = \frac{E_r}{E_c} \tag{5.9}$$

$$n = \frac{E_h}{E_c} \tag{5.10}$$

Where E_r, E_c and E_h are Young's modulus of REBCO, copper and Hastelloy, respectively. The neutral axis of the transformed geometry and original untransformed geometry is the same because the thickness of the REBCO tape is maintained at the same value. Y_{c1}, Y_r, Y_h, Y_{c2} are the distance between the bottom side of the tape to the centroid of each material. The calculation of the neutral axis is described in Table 5.1. Where A_c, A_r, and A_h are the cross-sectional areas of copper, REBCO, and Hastelloy, respectively.

Table 5.1: Parameters for finding the position of the neutral axis

Material	***Area (A)***	***Y***	***AY***
Copper 1	A_c	Y_{c1}	$A_c\ Y_{c1}$
REBCO	A_r	Y_r	$A_r Y_r$
Hastelloy	A_h	Y_h	$A_h Y_h$
Copper 2	A_c	Y_{c2}	$A_c\ Y_{c2}$

$$\text{Neutral axis} = \frac{A_c Y_{c1} + A_r Y_r + A_h Y_h + A_c Y_{c2}}{A_c + A_r + A_h + A_c} \quad [116, 124] \tag{5.11}$$

The following equation can be used to calculate the moment of inertia [116],

$$I = \sum \left(\left(\frac{bh^3}{12} \right) + Ad^2 \right) \quad (5.12)$$

Where '*d*' is the distance between the neutral axis and the centroid of material sections. *h*, *b* and *A* are respectively the thickness, new width and area of each layer. The parallel axis theorem is used to find out the moment of inertia of each material. Finally, all these moments of inertia can be added to find out the total moment of inertia. Then the Flexure formula is used to find out the stress induced in the REBCO layer.

5.3. Numerical modelling of REBCO tape

5.3.1. Mesh, boundary conditions and properties

The bending of REBCO tape is simulated using 5 mm length, 4 mm width, and 0.091 mm thickness REBCO tape. The meshed geometry of the REBCO tape is depicted in Figure 5.3.

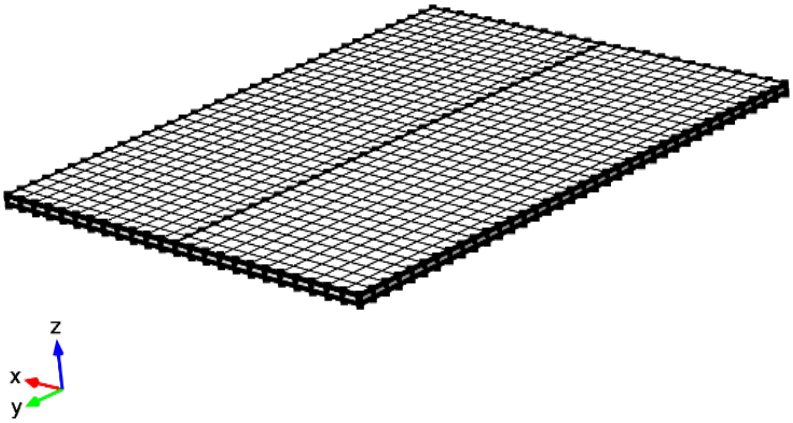

Figure 5.3: Meshed geometry of REBCO tape subjected to bending load

Copper, REBCO, and Hastelloy have a thickness of 0.02, 0.001, and 0.05 mm, respectively. The boundary condition is set up so that one side of the tape is stationary. The other is rotated 270^o about the x-axis using a rigid connector with the centre of rotation (0, 0, (0.091/2)). Properties of different layer materials such as copper, Hastelloy, REBCO are already provided in chapter 4 in Table 4.1.

5.3.2. Mesh independent study

Figure 5.4 shows a mesh-independent investigation that is carried out by varying the mesh. The optimal mesh is selected based on the accuracy and time required for the analysis.

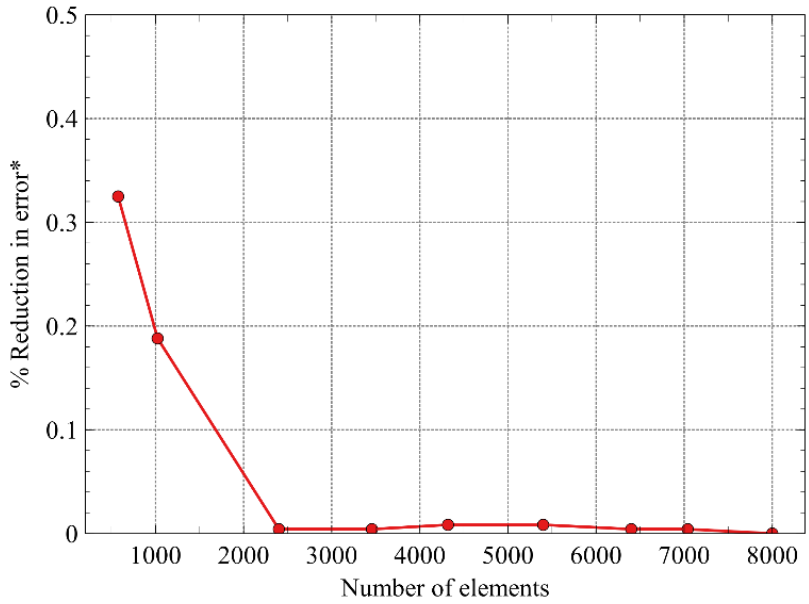

Figure 5.4: Effect of increase in the number of elements on percentage reduction in error

$$^{*}\text{Percentage reduction in error} = \frac{(Averege\ intrinsic\ strain)_{Previous} - (Averege\ intrinsic\ strain)_{Current}}{(Averege\ intrinsic\ strain)_{Previous}} \quad (5.13)$$

For this bending analysis, 36 elements along the width and 24 elements the along length direction gives the optimum mesh. Along the thickness direction, 4 elements are taken, each material having one element.

5.4. Results and discussion

The analytical method approximates the composite layers to a single material layer, the effect of bending on the superconducting material (REBCO) is to be calculated in terms of intrinsic axial strain. The Flexure formula is used in the analytical approach to calculate the maximum stress developed in the REBCO layer. The effects of change in the thickness of the substrate (made of Hastelloy) and the stabiliser material (of copper) on the superconducting REBCO layer are determined using parametric studies. Each results obtained are presented.

5.4.1. Effect of thickness of Hastelloy on the induced strain in the REBCO layer

The effect of varying the thickness of the substrate layer made of Hastelloy is studied and is plotted in figure 5.5. It may be noted that varying the thickness of the substrate changes the distance between the neutral axis and the bottom side of the REBCO layer. This, in turn, may influence the strain induced in the REBCO layer. These values are also plotted.

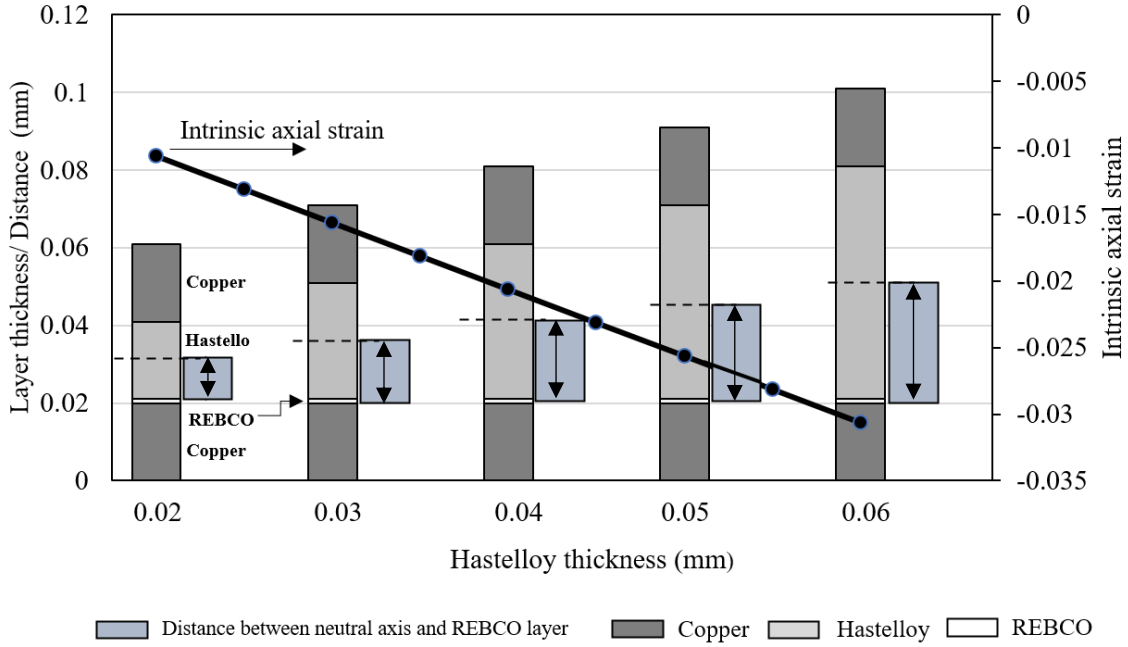

Figure 5.5: Effect of thickness of Hastelloy layer on the induced strain in the REBCO for 1 mm bending radius and 0.02 mm copper thickness

The intrinsic axial compressive strain increases as the thickness of Hastelloy increases. The resulting stress is compressive because the REBCO layer lies below the neutral axis upon bending. The figure also depicts how the distance between the neutral axis and the bottom side of the REBCO layer (boxes with arrow marked inside) is increased linearly when increasing the thickness of Hastelloy. Correspondingly it can be observed that the intrinsic axial strain in the REBCO layer is increased linearly.

5.4.2. Effect of thickness of copper on the induced strain in the REBCO layer

In superconducting HTS tapes, the copper stabiliser is utilised as a reinforcement sandwich layer to protect and electrically stabilise the other layers, such as the superconducting material and its substrate. One of the most commonly used copper stabilisers are of 0.02 mm thick. The effect of changing the copper thickness on the intrinsic strain created in the REBCO layer due to bending is investigated in this section.

It should be noted that the copper layers are provided as sandwich, with the top and bottom copper layers protecting all the other layers in between. The distance between the neutral axis and the bottom side of the REBCO layer does not change when the thickness of these copper layers is varied symmetrically on both sides. This is depicted in Figure 5.6.

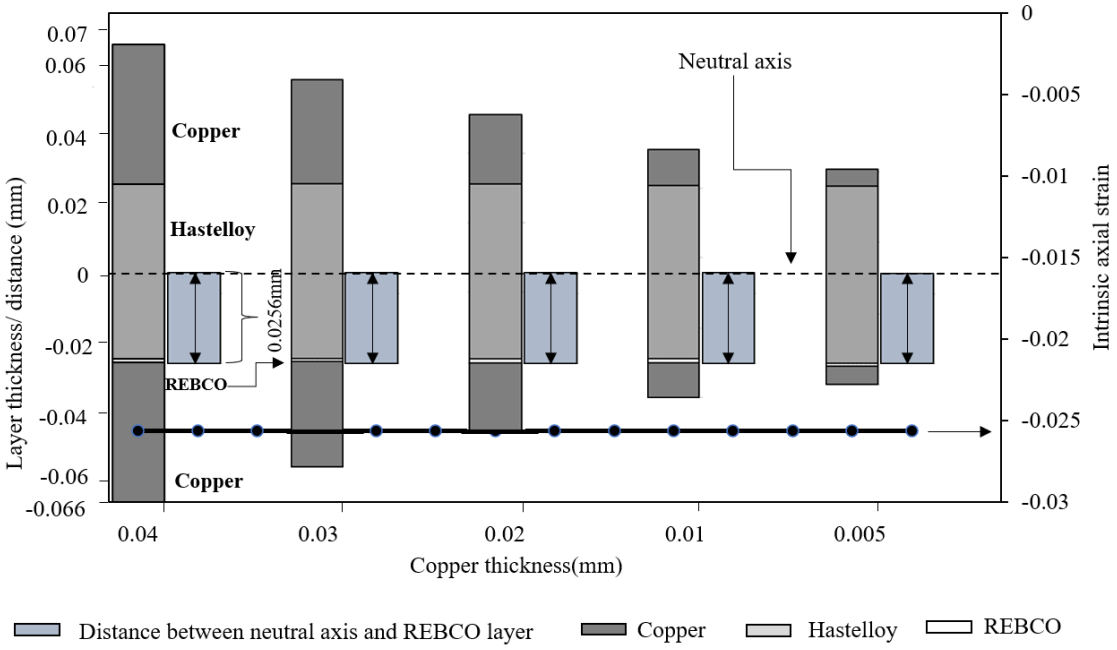

Figure 5.6: Effect of thickness of copper layers on the induced strain in the REBCO for 1 mm bending radius and 0.05 mm Hastelloy thickness

The figure shows that the distance between the neutral axis and the bottom side of the REBCO layer is constant (0.0256 mm) when the thicknesses of copper layers are changed symmetrically on both top and bottom sides (from 0.04 to 0.005 mm). The intrinsic strain that is developed in the REBCO layer is found to be constant for all the copper thicknesses. However, in practice the strain values should change when varying the copper thickness. A constant value is obtained due to the assumption of a single material layer than layers of different materials. Also, the interaction between the layers is ignored in this result.

Another important factor to be considered here is the change in the neutral axis position while varying the bending diameter. Decreasing the bending diameter may give rise to progressive plastic deformation in the different layers of the tape. Therefore, in practice, with the decrease in bending diameter, the strain increases and may exceed the elastic limit of the copper layer. Since the copper layer can no longer take any stress, the neutral axis may shift towards the Hastelloy side to balance the stress between the tensile

and compressive stress. When the bending diameter is further decreased, the Hastelloy may start yielding in tension. The position of the neutral axis may move back to the REBCO layer side to maintain the stress balance. Similar behaviour is obtained even in tapes with asymmetric structure as reported by A. Ben Yahia [125].

The use of Flexure formula and equivalent widths of layers for this type of application can be an oversimplification mainly because of two reasons: 1) The tape is comprised of multiple layers of different materials and 2) when the tape is subjected to smaller bending diameters that there can be significant plastic deformation. These two factors are further investigated in the subsequent parts of the chapter.

5.5. Comparison of analytical approach with numerical modelling for determining the induced strain in REBCO tape

The Flexure formula may provide only a rough approximation of the stresses induced in the REBCO tape because of non-homogeneity in the composite structure and the mutual interaction between the layers. Therefore, the numerical modelling is performed in this section. Parametric studies are carried out to reveal the effects of varying the thickness of Hastelloy substrate and copper layers. The results obtained are compared with those computed using the Flexure formula.

5.5.1. Comparison of analytical and numerical approaches for a given thickness of Hastelloy and copper.

Figure 5.7 depicts the results obtained using the Flexure formula and the numerical model for a REBCO tape of Hastelloy thickness, 0.05 mm and copper thickness, 0.02 mm when subjected to bending stress. The bending radius is decreased from 10 mm to 1 mm in multiple steps. The graph shows that the compressive strain in the REBCO layer increases with decreasing the bending radius. However, it is found that by decreasing the bending radius below 4 mm, the increase in intrinsic axial strain is drastic. Therefore, it may degrade the superconducting tape as the induced stress is more than 1%.

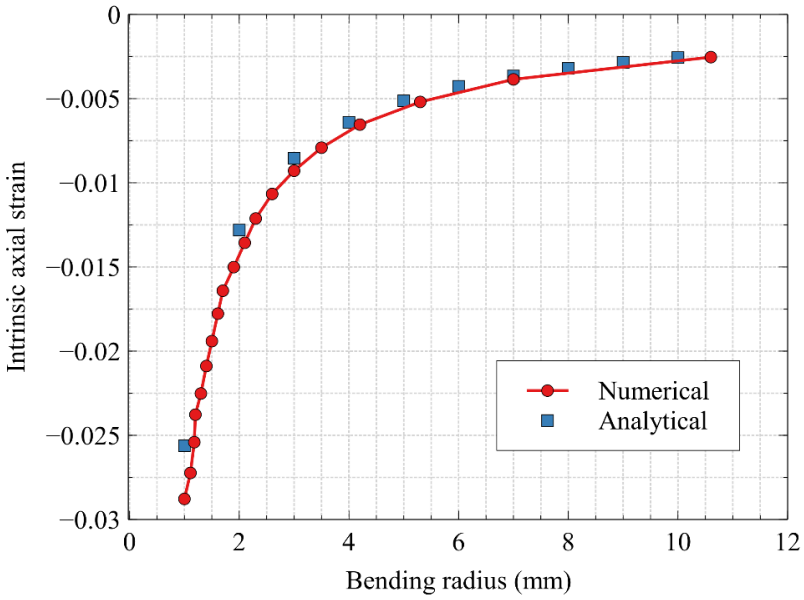

Figure 5.7: Comparison of analytical and numerical approaches on the effect of bending radius on axial strain in the REBCO layer (Hastelloy 0.05 mm, copper 0.02 mm thickness, and 4 mm width tape).

It can be observed from Figure 5.7 that while reducing the bending radius from 10 mm to 4 mm, the increase in induced compressive strain is 156 % (changed from 0.0025 to 0.0064). However, further reduction in radius (from 4 to 1 mm), doubled the strain by 306% (from 0.0064 to 0.026). The analytical approach by the Flexure formula and the numerical method shows the same trend. Results of both are in good agreement at higher bending radii (say above 4 mm, the maximum deviation is 2% only). For bending below 4 mm, there is a maximum 10 % difference between the strain values computed. The numerical approach gives a higher value of strain. The difference is maximum (10%) at a bending radius of 1 mm. It may be noted that both numerical and analytical approaches considered the tape as elastic, but in numerical modelling, the intertwined effects and interaction between the layers are considered. In the analytical approach, the tape is converted to single equivalent material and then the stress is calculated then stress based on the neutral axis position. Therefore, using the Flexure formula for determining the induced strain below 4 mm bending radius may not provide accurate results.

5.5.2. Comparative evaluation of the analytical and numerical approaches under the varying thickness of Hastelloy

The variations in the induced strain with changes in the bending radius for different Hastelloy thicknesses are presented in Figure 5.8.

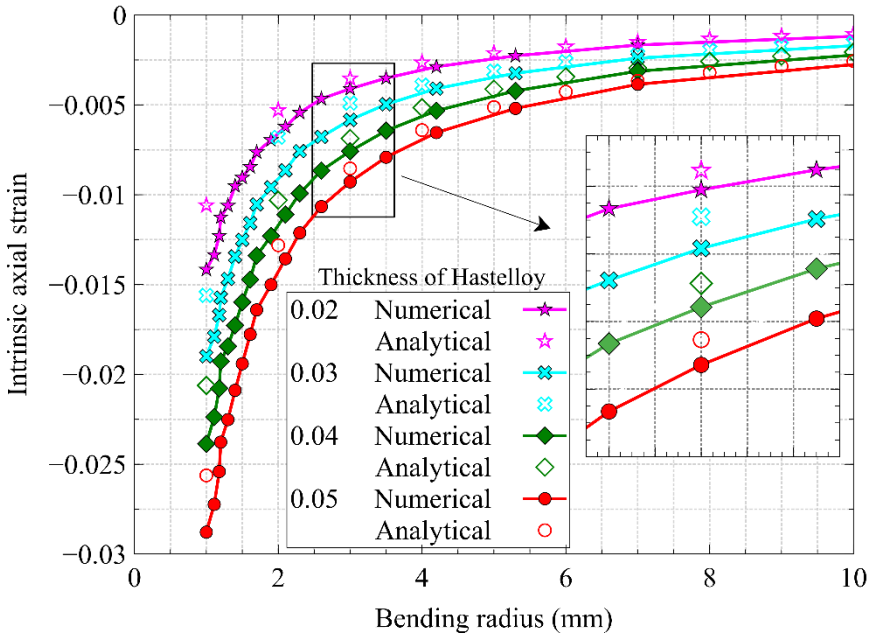

Figure 5.8: Comparison of analytical and numerical approaches on the effect of bending radius on axial strain in the REBCO layer for varying thickness of Hastelloy (thickness of copper 0.02 mm, and 4 mm width tape).

When the bending radius is decreased, the curvature radius increases, leading to the development of more strain in the REBCO layer. At different Hastelloy thicknesses, the result obtained from analytical and numerical simulation is also compared in Figure 5.8. It may be noted that the trend for both numerical and analytical approaches are almost the same. The maximum difference between these results is observed at the smallest bending radius of 1mm, equal to 25%. It is also observed that deviation between the numerical and analytical results increases with decreasing the thickness of the Hastelloy layer. As a result, caution should be exercised because excessive bending of REBCO tapes during the cabling and application phases might induce significant strain in the tapes, causing them to degenerate. At the lower bending radii, the impact of changing the thickness of Hastelloy from 0.05 to 0.02 mm has decreased the induced strain in the REBCO layer by almost 50 %. This means that while making superconducting tapes, the thickness of Hastelloy layer must be carefully decided considering all the influences.

5.5.3. Comparative evaluation of the analytical and numerical approaches under the varying thickness of copper

The variations in the induced strain with changes in the bending radius for different copper thicknesses are presented in Figure 5.9.

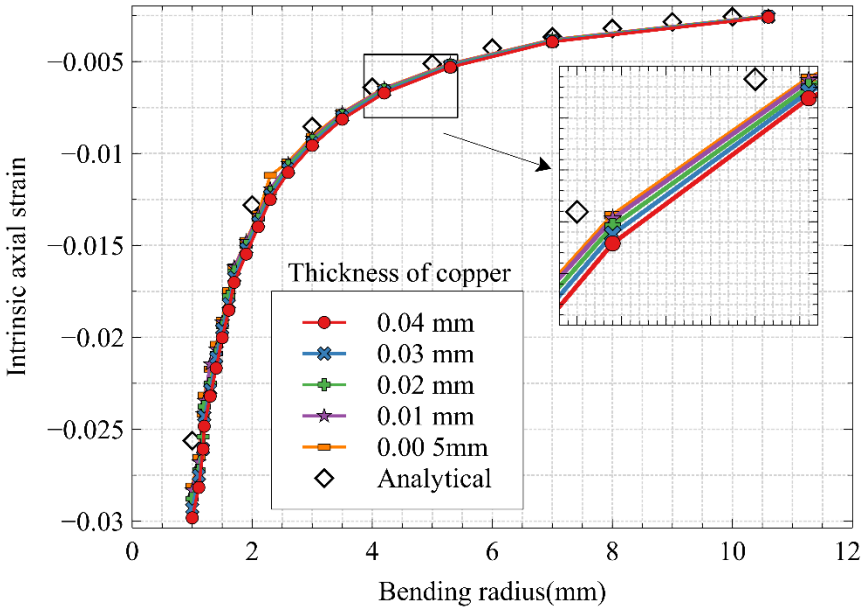

Figure 5.9: Comparison of analytical and numerical approaches for the effect of bending radius on axial strain in the REBCO layer for varying thickness of copper (thickness of Hastelloy 0.05 mm, and 4 mm width tape).

Decreasing the bending radius increases the curvature radius and thereby induces more strain in the REBCO layer. Changing the copper thicknesses on the induced intrinsic axial strain under different bending radii is calculated analytically and numerically. When comparing analytical and numerical approaches to changes in bending radius, the results are almost matching. The maximum difference between the results is about 14% for the lowest bending radius (1 mm). However, the result obtained from the analytical calculation shows that intrinsic axial strain is the same for all the copper thickness. No change is obtained with increase/ decrease of copper thickness in the analytical approach. The numerical approach shows that copper thickness has an influence on the development of intrinsic axial strain in the REBCO layer. Intrinsic axial strain in the REBCO layer increases with increasing the copper thickness.

However, the impact of the changing in the thickness of copper from 0.04 to 0.005 mm has not significantly affected the induced strain in the REBCO layer. It may be noted that the percentage change is only about 5.7%. On the other hand, the change in the thickness of Hastelloy has resulted in about 50 % change in the induced strain. Therefore, it may be concluded that the effect of changing the copper thickness is less significant compared to that of changing the Hastelloy thickness.

Plasticity and the residual strain are two important parameters that influence the development of intrinsic axial strain in the REBCO layer. Therefore, these two factors

are taken into account in numerical modelling, and the simulation is performed again to determine their influence on the intrinsic strain in the superconducting layer. The objective is to obtain more realistic results.

5.5.4. Modelling of the superconducting tape considering residual strain and plastic properties.

The Flexure formula is applied only in the elastic range in the analytical calculation. Even though the tape is considered a composite structure of different constituent layers, it should be converted to equivalent homogeneous material before applying the Flexure formula. In the earlier numerical approach, the tape is assumed elastic. It cannot be assumed that the tape is elastic for entire range of study. So, the non-consideration of plastic properties may affect the results obtained. The tape is subjected to a high temperature of 1020 K during production, and as a result residual strain could develop within the tape. This also affects the development of intrinsic axial strain in the REBCO layer. The plastic behaviour of layers is captured by providing realistic property value for the different constituent materials has given in chapter 4 in TABLE 4.1. The results obtained using the more realistic model considering the plastic properties and residual strain, are compared with that of the previous analytical and numerical approaches. For all three cases, the increase in the induced strain with the decrease in bending radii follow the same trend as evident from Figure 5.10.

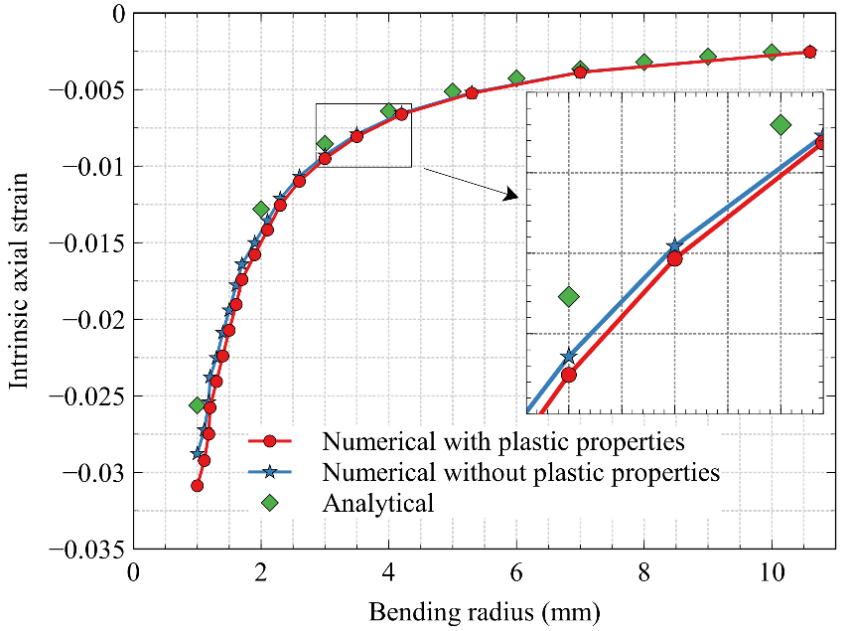

Figure 5.10: Comparison of the improved numerical model considering plastic properties and residual strain with previous analytical and numerical approaches (0.05 mm Hastelloy thickness, 0.02 mm copper thickness and 4 mm width tape).

The difference between the old and new numerical models is approximately 7.6 %, while the difference between the analytical approach and the new simulation model is about 17 %. It may be noted that 17% is the maximum difference obtained and it is at the lowest bending radius (1 mm). The difference decreases with increasing bending radius and may even become insignificant at higher values, especially when the materials are elastic. However, it may be noted that the induced strain increases when plastic properties and residual strain are considered.

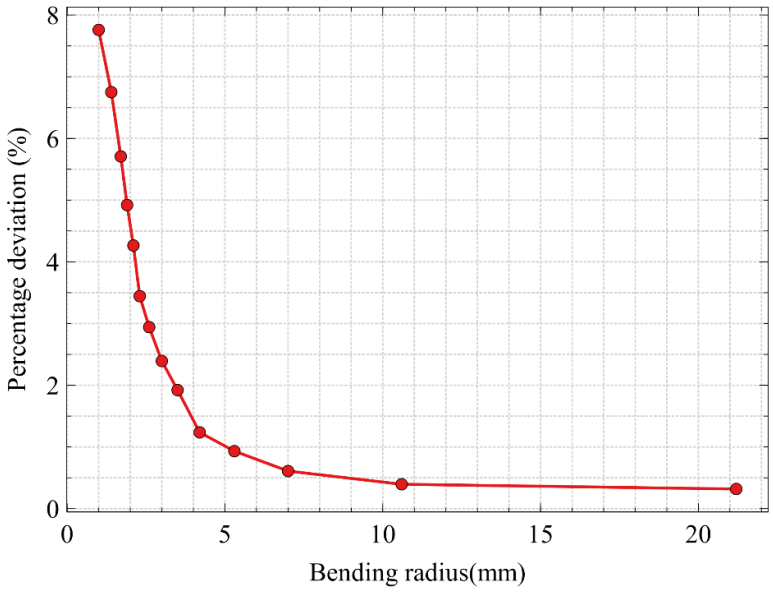

Figure 5.11: Percentage deviation of intrinsic axial strain with plastic and without plastic properties (0.05 mm Hastelloy thickness, 0.02 mm copper thickness and 4 mm width tape).

Figure 5.11 depicts the percentage deviation in intrinsic axial strain in the REBCO layer with and without considering the plastic properties and residual strain into account. The percentage deviation between the new and old numerical model drastically increases with decrease in bending radius. This is because the tape reaches the plastic range at a smaller bending radius. Throughout the paper, 1% axial compressive strain in the REBCO layer (intrinsic axial strain) is considered the maximum degradation limit. It may be noted that bending radii corresponding to the 1% compressive strain for analytical, numerical model not considering and considering plastic properties and residual strain are 2.66 mm, 2.79 mm and 2.86 mm, respectively. This shows that consideration of realistic properties of materials and proper modelling conditions have a significant impact on determining

the degradation limit in terms of bending radius of superconducting tapes, wire, and cables.

5.5.5. Distribution of intrinsic axial strain along the length and width of the superconducting tape

The maximum intrinsic strain developed during bending is studied in previous sections while varying the thickness of the superconducting tape. However, determining the strain distribution along the length and width of the REBCO layer may be useful. This allows for the identification of critical areas with high strain concentrations, in the superconducting tapes.

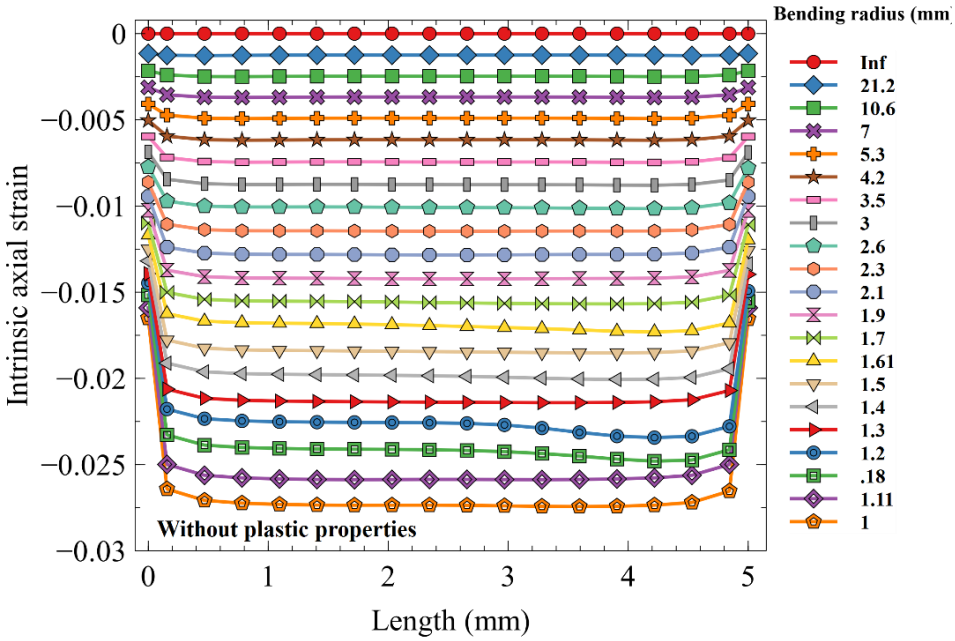

Figure 5.12: Intrinsic axial strain along the length at the centre of the tape without considering plastic properties and residual strain (0.05 mm Hastelloy thickness, 0.02 mm copper layer thickness).

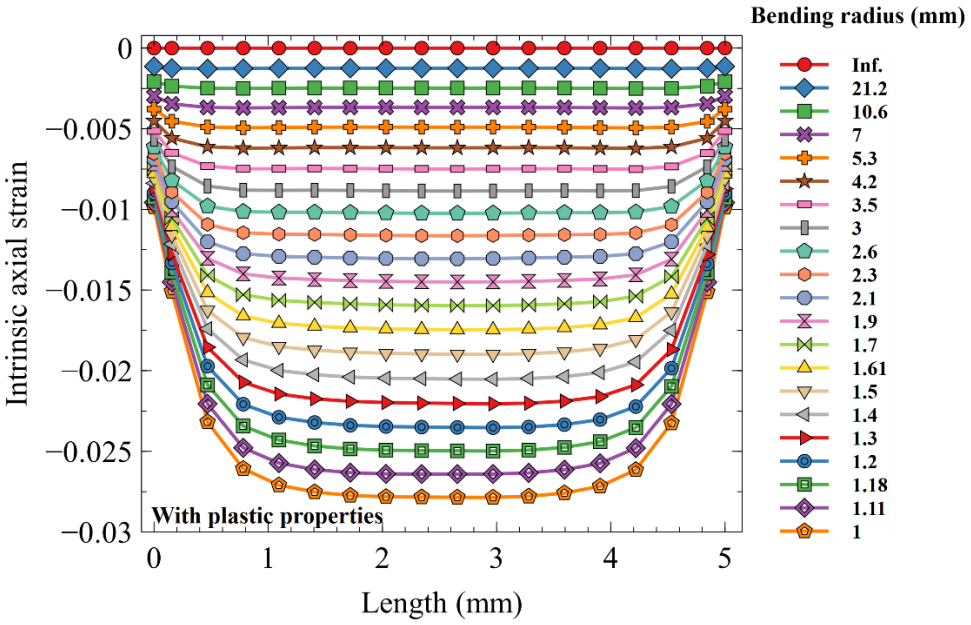

Figure 5.13: Intrinsic axial strain along the length at the centre of the tape with considering plastic properties and residual strain (0.05 mm Hastelloy thickness, 0.02 mm copper layer thickness).

The distribution of induced intrinsic axial strain after bending along the length of the tape for different bending radii at the centre of the width is depicted in Figures 5.12 and 5.13. For comparisons, two numerical models have been used: a) the initial numerical model (without considering the plastic properties) and b) the improved numerical model considering the plastic properties and residual strain. When comparing the improved numerical model to the initial model, it is clear that there is a significant difference in strain distribution, and reveals the effect of plastic properties of the materials on the induced intrinsic axial strain in the REBCO layer. In the improved numerical model, the magnitude of the intrinsic axial strain distribution along the length considered at the centre of the tape has increased only by about 3 %. However, the near uniform strain distribution along the length of the tape has changed to a new distribution with the improved numerical model where the strain at the two ends of the tape is significantly reduced. It may be due to the effect of consideration of plastic properties.

The distribution of the intrinsic axial strain along the width of the tape for different bending radii at 0.05 mm and 0.02 mm Hastelloy thicknesses is depicted in Figure 5.14 and Figure 5.15. Please note that copper thickness is not varied, but kept at 0.01 mm.

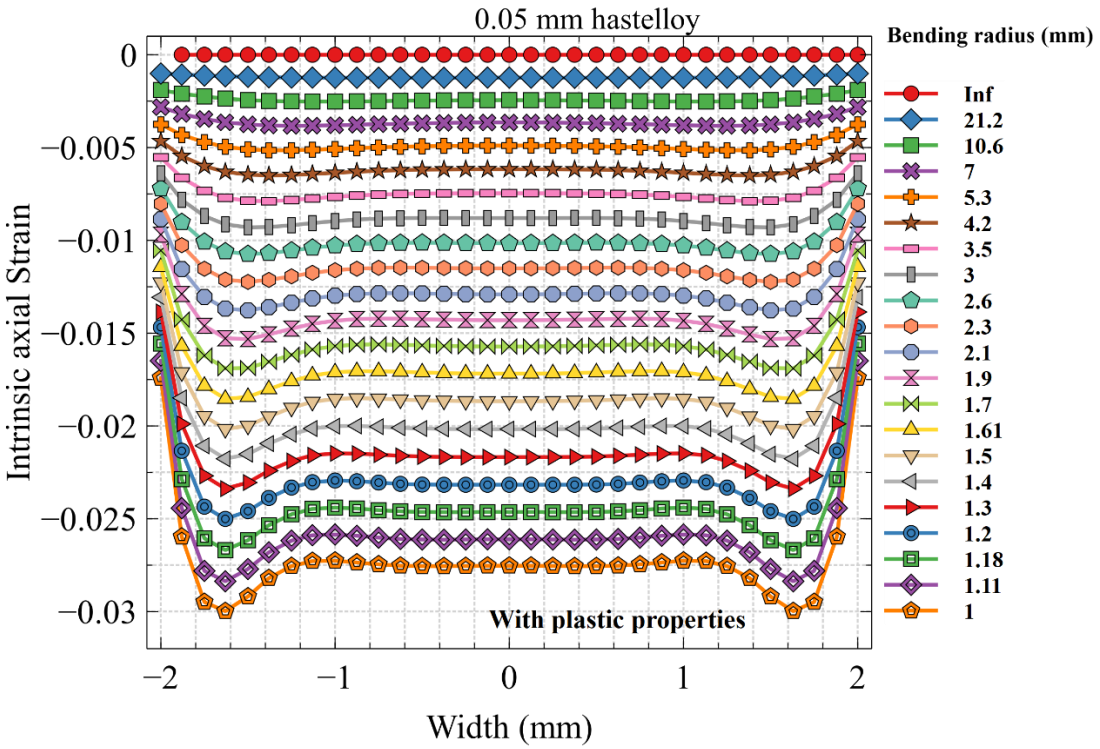

Figure 5.14: Effect of variation in the thickness of Hastelloy on intrinsic axial strain along the width of the tape for different bending radius at a Hastelloy thickness of 0.05 mm. (0.01 mm copper thickness).

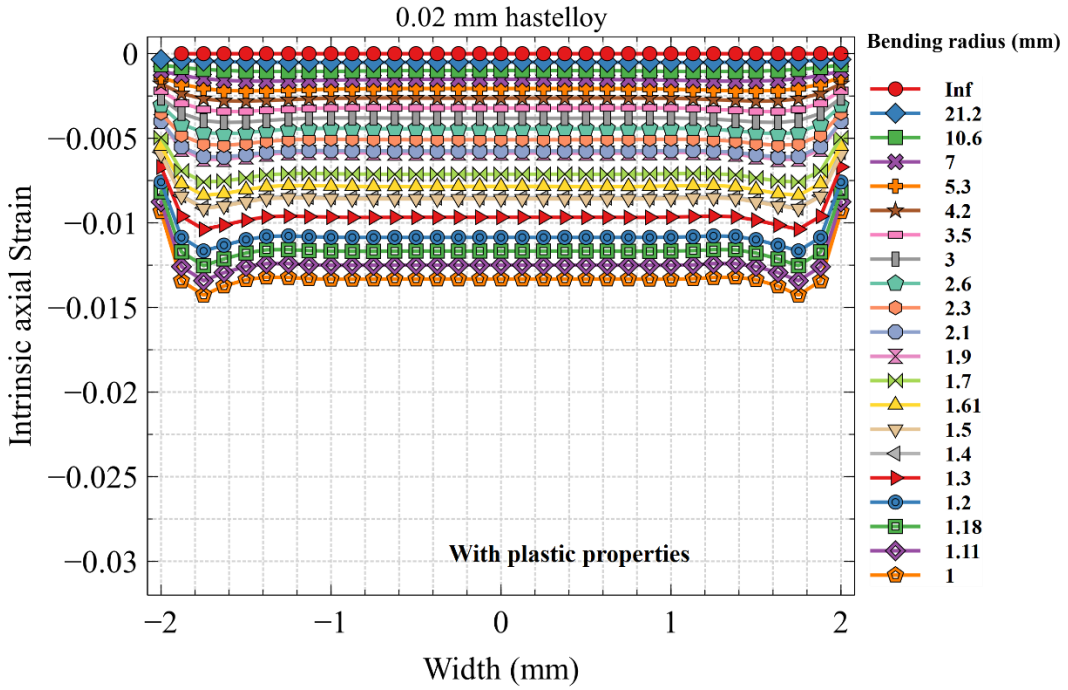

Figure 5.15: Effect of variation in the thickness of Hastelloy on intrinsic axial strain along the width of the tape for different bending radius at a Hastelloy thickness of 0.02 mm. (0.01 mm copper thickness).

The induced strain in the tape appears to increase as the bending radius decreases. The distribution shows that the compressive strain is lowest at the edges compared to the centre. The strain distribution obtained is consistent with prior studies [120, 126]. Even though the magnitude of intrinsic axial strain has decreased with Hastelloy thickness of 0.02 mm, the trend remains the same. Compared to the 0.05 mm case, the induced intrinsic axial strain is nearly half that of Hastelloy, with a thickness of 0.02 mm. This demonstrates the significant influence of Hastelloy thickness on strain-induced irrespective of bending radii. Reason for the same is already discussed in the section 5.41.

Similarly, the effect of varying the thickness of copper layers on the strain-induced is thoroughly investigated. Figure 5.16 depicts the distribution of intrinsic strain along the width of the tape for two different copper thicknesses of 0.02 and 0.01 mm, at a constant thickness of Hastelloy layer (0.05 mm). The figure shows that changing the thickness of copper has a comparatively slight impact on the strain-induced. It is almost insignificant in the infinite bending radius case (both points coincide), and there are only slight differences at the edges in the 5.3 mm bending radius case.

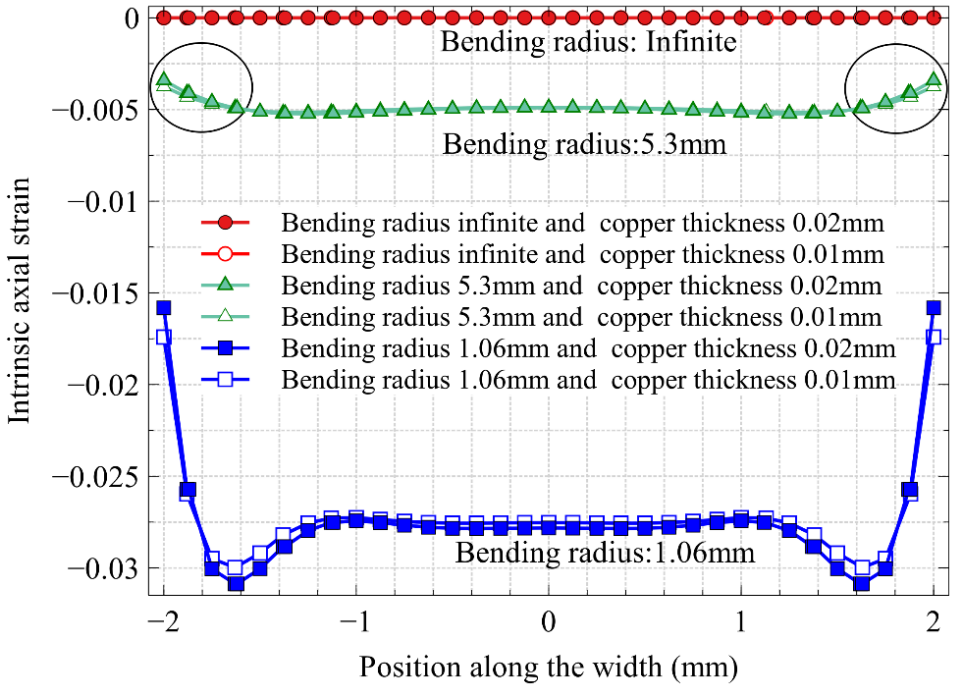

Figure 5.16: Effect of variation in the thickness of copper on intrinsic axial strain along the width of the tape for different core diameters and a given Hastelloy thickness of 0.05 mm.

The maximum increase in intrinsic strain is observed at the smallest bending radius (1.06 mm), and it is more prominent at the edges than in the centre. This type of behaviour is observed because, as the thickness of the sandwich copper layers changes,

the position of the neutral axis does not change significantly. As a result, its influence is minimal in the REBCO layer when bending.

The combined effect of changes in the thicknesses of copper and Hastelloy is presented. Figure 5.17 illustrates the variation of intrinsic strain with bending radius for various thicknesses of copper and Hastelloy layers. When the bending radius is reduced, the intrinsic strain-induced increases. The impact of changing the thickness of the copper layer from 0.02 to 0.01 mm on the strain-induced is not the same for different Hastelloy thicknesses. For a bending radius of 1.06 mm and a Hastelloy thickness of 0.05 mm, the difference in strain-induced is 2.9 %; this increases to 3.9 % for a Hastelloy thickness of 0.04 mm and to a maximum of 5.7 % for a thickness of 0.02 mm.

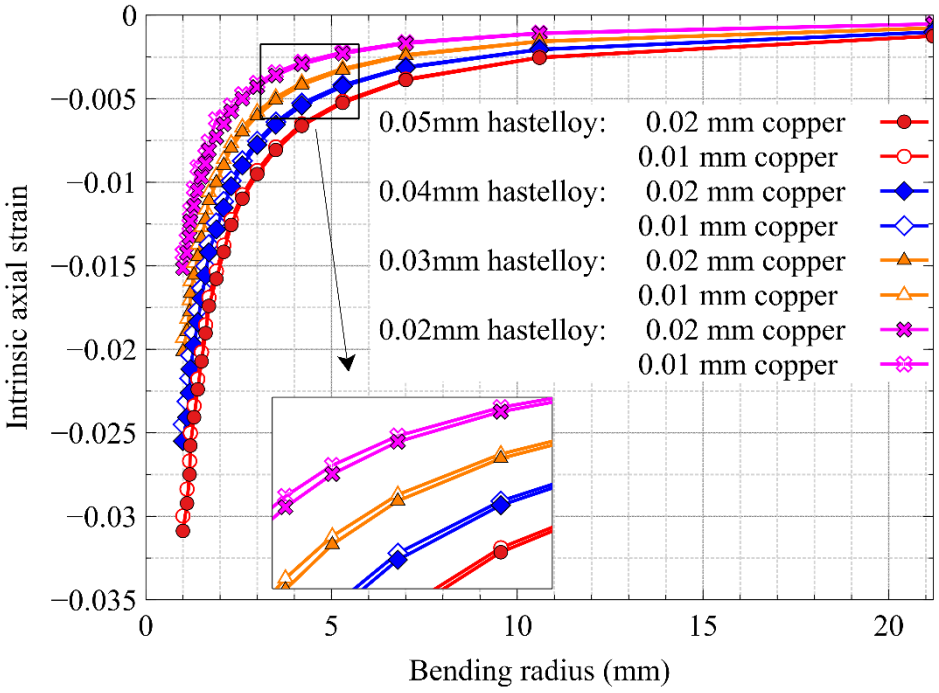

Figure 5.17: Effect of copper and Hastelloy thickness on the induced strain in the REBCO layer.

It may be observed that altering the thickness of the copper layer did not affect the intrinsic axial strain created in the REBCO layer (see figure 5.6). With the consideration of the residual strain generated during the manufacturing process and the plastic properties of the materials taken into account, then there is a considerable effect on the strain induced in the REBCO layer when the thickness of the copper layers is changed.

It may be observed that the lowest bending radius (that can be attained without degradation of the tape) changes with variation in the thickness of Hastelloy. For instance, at 0.03 mm thickness of Hastelloy the minimum bending radius possible is 2 mm.

Similarly, for the lowest thickness taken for the Hastelloy (0.02 mm), the minimum bending radius obtained is 1.5 mm. These findings are consistent with previous research on a similar tape configuration. The experimental study in the literature reported 2.3 and 1.6 mm for 0.03 and 0.02 mm Hastelloy thicknesses, respectively [5].

The changes in the position of the neutral axis of the superconducting tape with changes in the thickness of copper and Hastelloy layers are graphically represented in Figure 5.18. For each thickness of Hastelloy (0.02, 0.03, 0.04, 0.05 mm), the thickness of copper is varied in three steps (0.02, 0.01 and 0.005 mm).

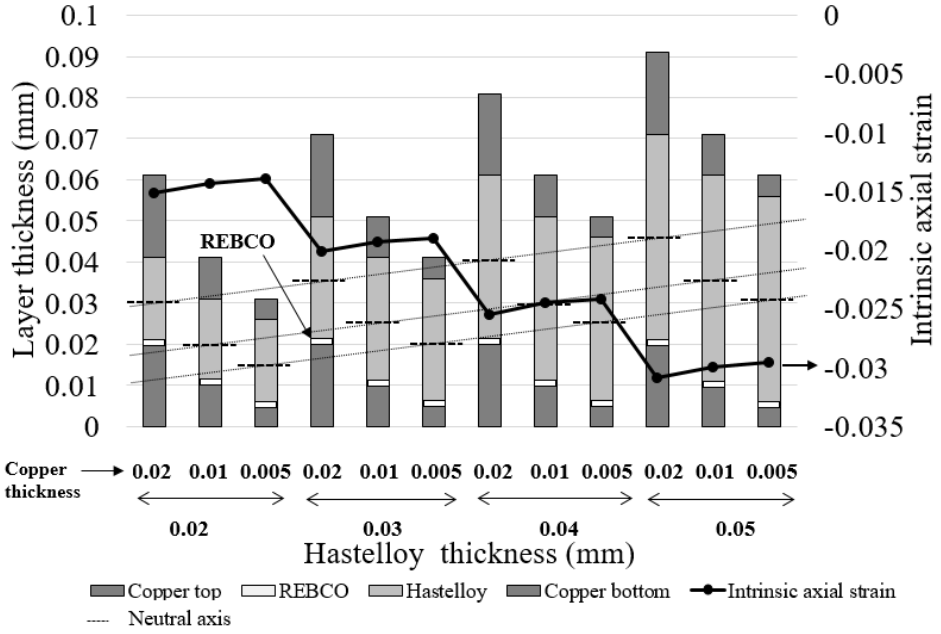

Figure 5.18: Effect of thickness of copper on the induced intrinsic axial strain in the REBCO layer at different Hastelloy thickness (1 mm bending radius).

The neutral axis position is marked on each bar diagram using a bold dashed short line in the diagram. It may be noted that with the increase in the thickness of Hastelloy, there is an almost proportional increase in the intrinsic strain irrespective of the thickness of the copper layers. On the other hand, the reduction in the thickness of the copper layers gives only a slight decrease in the intrinsic strain. This behaviour can be explored from the changes in the relative position of the neutral axis with changes in the thickness of layers. The thin dotted lines marked in the diagram connecting the position of corresponding neutral axes show that the variation is almost linear.

5.6. Electrical performance under bending on REBCO tape

Superconductors are used in systems that require a significant quantity of current to be transmitted. The level of degradation in superconductors can be measured in terms

of their current carrying capacity. This electrical performance of superconductors can be influenced by a variety of mechanical loading, including bending. This section investigates the effect of bending-induced strain on the electrical performance of REBCO-based superconductors. The critical current degradation can be determined using the power law of critical current strain dependency [127-129]. This expression applies to REBCO coated conductors manufactured using the IBAD-MOCVD process. The critical current's power-law strain dependency is expressed as,

$$I_c = I_c(\varepsilon_m)(1-a(\alpha)\left|\varepsilon-\varepsilon_m(\alpha)\right|^{2.18}) \tag{5.13}$$

The critical current for a given strain (ε) is denoted by I_c. The strain at which the critical current reaches its highest value ($I_c(\varepsilon_m)$) is indicated by ε_m, which is the equivalent of the residual strain applied to nullify the residual strain and make the resultant strain zero. $a(\alpha)$ is the strain sensitivity of critical current, and the value is taken straight from the literature [127]. It may be noted that 'α' is the in-plane angle at which strain is applied. The critical current retention is defined as the ratio of the critical current to the maximum value of the critical current, and its change with different bending radii is depicted in Figure 5.19.

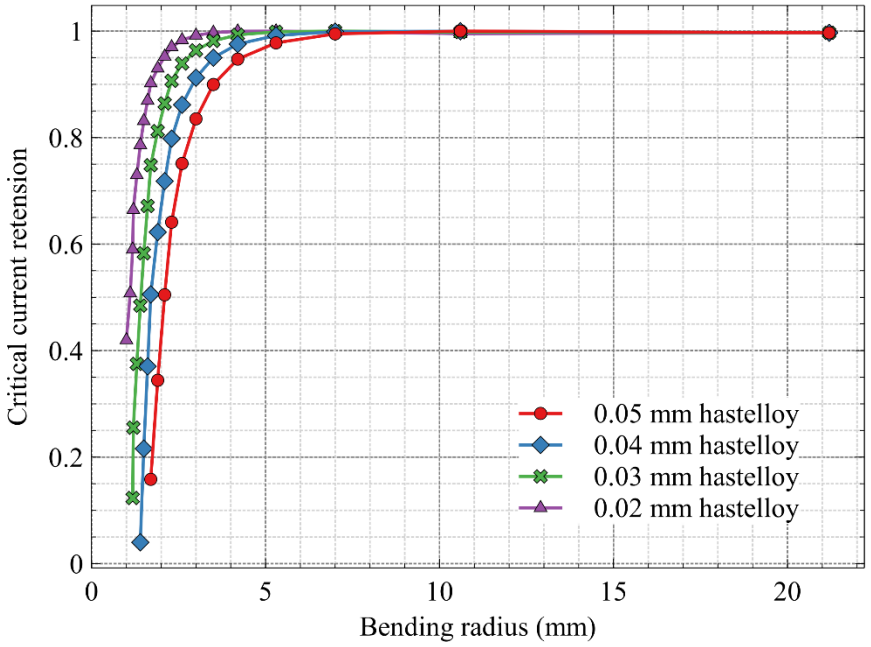

Figure 5.19: Critical current retention with the decrease in bending radius (0.02 mm copper thickness).

It may be noted that the critical current drops with decreasing bending radius. In the case of smaller bending radii, the critical current degradation is dramatic. For instance, when assuring that the critical current degradation is less than 5%, the bending radius can

vary widely. It can be seen that 5% of critical current degradation occurs at 4.3, 3.5, 2.7, and 2 mm bending radius respectively for 0.05, 0.04, 0.03 and 0.02 mm Hastelloy thicknesses. It is observed that the tape's current carrying capability degrades significantly beyond these bending radii. It may be noted that the copper is kept constant at 0.02 mm.

Figure 5.20 depict the direct relationship between the thickness of the Hastelloy layer and the limiting bending radius. When decreasing the bending radius, the thickness of the Hastelloy layers has to be also decreased to keep the critical current degradation constant at 5%. The critical bending radius varies only slightly with changes in copper thickness, and the trend is nearly constant. It may be observed that for smaller Hastelloy thicknesses and bending radii, the copper thickness has a more significant role in causing degradation.

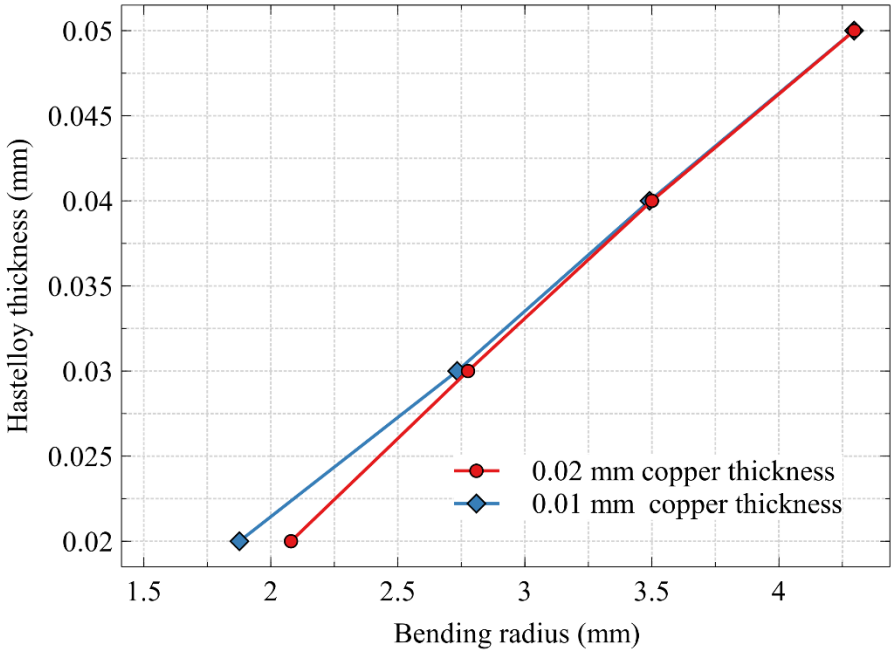

Figure 5.20: Limiting bending radius at 5% critical current degradation for different Hastelloy and copper thicknesses.

Therefore, for any given thickness for Hastelloy and copper layers, there can be a limiting value for the bending radius. Decreasing beyond them will significantly reduce the current-carrying capacity. It should be noted that a critical current degradation of 5% is permissible if the physical change in the superconducting tape is reversible.

These findings are expected to assist manufacturers in making appropriate decisions during the manufacturing of superconducting tapes and conductors. The values obtained

in this work for a critical current degradation of 5% are compared with the available experimental results [36]. The results are represented in Figure 5.21.

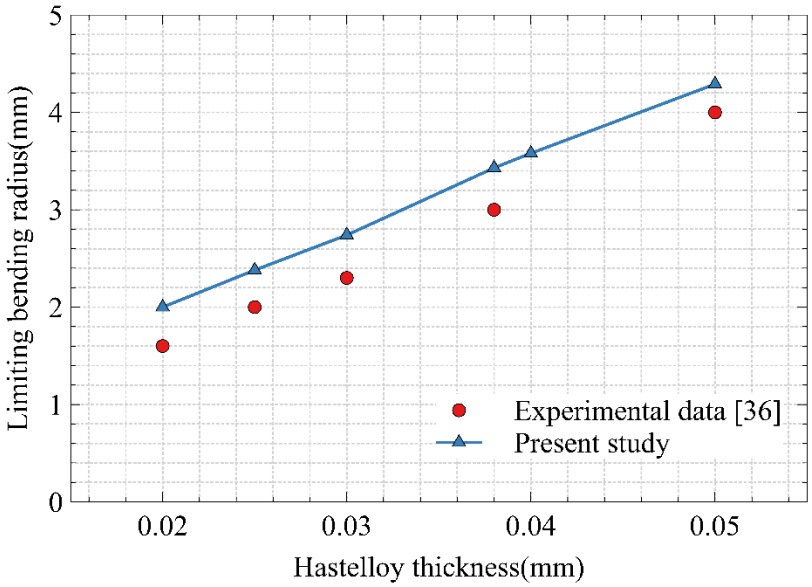

Figure 5.21: Comparison of limiting bending radius for the present study and experimental result [36].

The graph indicates that both experimental and numerical results follow the same trend and the values are comparable. Since the numerical results obtained are slightly higher values, the design is safer and can ensure very few chances of tape degradation during bending. These study's findings are expected to be valuable in the production and application stages of superconducting cables.

5.7. Summary

The effect of bending load on the degradation of the superconducting REBCO tape is investigated. The influence of Hastelloy and copper thickness variation on intrinsic axial strain is further studied, and also found critical bending radii for various situations. The important results may be summarised as follows,

- The effect of induced strain on the degradation of these superconducting properties during bending of REBCO tapes has been numerically explored and compared to the traditional analytical technique.
- The superconducting tape's geometrical configuration varies in terms of the width and thickness of its constituent layers. In all situations, the strain induced in the REBCO layer is computed.

- The conventional analytical technique via the Flexure formula and the numerical approach agree well at a larger bending radius (more than 4 mm), the difference increases below.
- The distance between the neutral axis and the REBCO layer increases linearly as Hastelloy thickness increases. As a result, there is an increase in intrinsic axial strain.
- It is also found that constituent materials' plastic characteristics significantly impact the induced strain in the REBCO layer. The difference between the old (Without plastic characteristics) and new numerical models (With plastic characteristics) is approximately 7.6 %
- With the new numerical model, a 60% reduction in Hastelloy thickness (0.05 mm to 0.02 mm) decreased the induced strain to almost half for all bending radii. This reveals the profound influence of Hastelloy thickness on strain-induced, irrespective of bending radius.
- The thickness of copper has a relatively less impact on the strain-induced; a 50% reduction in copper thickness (from 0.02 mm to 0.01 mm) results in a maximum drop in the strain-induced of just 5.7%.
- For 0.03 mm and 0.02 mm Hastelloy thicknesses, the limiting bending radius beyond which the superconductor may degrade (as per the 1% criterion) is 2 mm and 1.5 mm, respectively.
- It may be observed that the 5% critical current degradation is occurring at bending radii of 4.3, 3.5, 2.7 and 2.0 mm for the Hastelloy thickness of 0.05, 0.04, 0.03 and 0.02 mm, respectively.

The effect of configurational parameters of REBCO-based superconducting tapes under bending and the limiting values obtained would benefit manufacturers trying to make power cables and magnets with smaller core diameters.

The previous chapters investigated the effects of tensile and bending loads on the degradation of REBCO tape. Twisting is another significant load that contributes to degradation. Also, the combined effect of tensile and torsional loads is also investigated in the subsequent chapter.

Publication arising out of this chapter

- **Ashok KB**, Thomas RJ, Prakash MJ, Nijhuis A, "Analytical and Numerical Investigations on the Degradation of REBCO Based Superconducting Tapes Under Bending," in IEEE Transactions on Applied Superconductivity, vol. 31, no. 7, pp. 1-12, Oct. 2021, Art no. 8400712, doi: 10.1109/TASC.2021.3109720. (Impact factor: 1.96)

Chapter 6

Effect of torsional load, and combined tensile and torsional loads on the degradation of REBCO superconducting tape

6.1. Introduction

The effect of thermal, tensile, and bending load on the degradation of REBCO tape has been discussed. This chapter deals with investigations on the effect of torsional load on the degradation of the REBCO tape. The studies reported in the literature on the degradation of HTS tape during winding indicates that the torsional load has a lesser impact than bending and tensile loading [82, 130]. However, when the torsional load is combined with other loads, especially the tensile load, may have an impact on the degradation of the REBCO tape. It is reported that the torsional strain in the tape helps to increase critical current slightly in the initial stage [17]. However, with a further increase

in torsional strain, the critical current density decreases sharply (below the critical twist pitch limit) [17]. It is reported that the role of intrinsic axial strain on critical current degradation of REBCO tape is very much determined by the characteristics of the substrate layer and the thicknesses of different constituting layers [57, 131]. The width of the tape is another crucial parameter when the tape is subjected to torsional loading since the longitudinal strain gets affected [83]. Allen N. C *et al*. has carried out the numerical simulation under different tensile and torsional load for a specific geometry of the tape [132]. But the detailed numerical simulation of REBCO tape subjected to tensile and torsional load for a wide range of geometrical parameters like Hastelloy thickness, copper thickness, and tape width is scarce in the open literature. Therefore, it is worth investigating on the behaviour of REBCO tape under torsional load and combined tensile and torsional loads for different geometrical parameters.

6.2. Modelling

The layers are modelled using a brick element with 27 nodes, as recommended by the COMSOL Multiphysics developers for thin layer geometries. The angle of twist is changed from 0^{o} to 360^{o} in order to provide the torsional load. When the entire 70 mm tape is subjected to the full torsional load with a twist angle of 360^{o}, an equivalent load is produced in 1/4th of the tape (17.5 mm) with a twist angle of 90^{o} in the symmetrical part. A symmetrical boundary condition is provided at one end of the tape. The pictorial representation of the tape symmetry and the part of the tape modelled is presented in Figure 6.1.

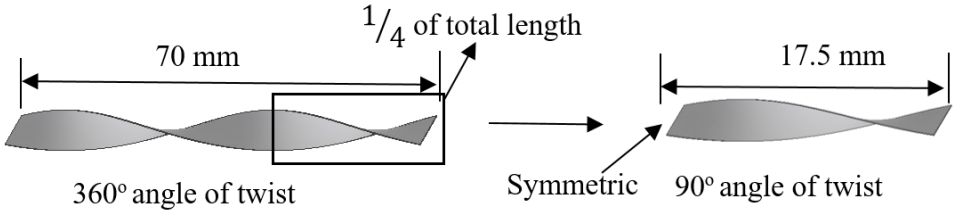

Figure 6.1: Pictorial representation showing the tape symmetry and the section of the tape modelled.

Only a symmetrical portion of the tape is modelled to minimise computing effort. A REBCO tape with a length of 70 mm is considered.

Figure 6.2 shows a schematic of the geometry and dimensions of the modelled REBCO tape section; also the thickness of the constituting layers are shown. The tape, which has dimensions of 17.5x4x0.091 mm (length, width, and thickness), is modelled

with layers of copper, Hastelloy, and REBCO. The tape width is altered from 3 mm to 12 mm to understand the effect of changing the tape width. The mesh dependent study is carried out to find the optimum mesh for the analysis. The mesh size of 72 elements per length, 24 elements per width, and 4 elements per thickness achieved good results that were closer to the experimental work. The thickness of the Hastelloy layer is varied from 0.02 to 0.05 mm, and that of the copper layer varies from 0.005 to 0.04 mm. The intrinsic axial strain generated in the REBCO layer is computed for all tensile and torsional load cases. The tape is considered degraded if the generated axial strain exceeds the reversible limit.

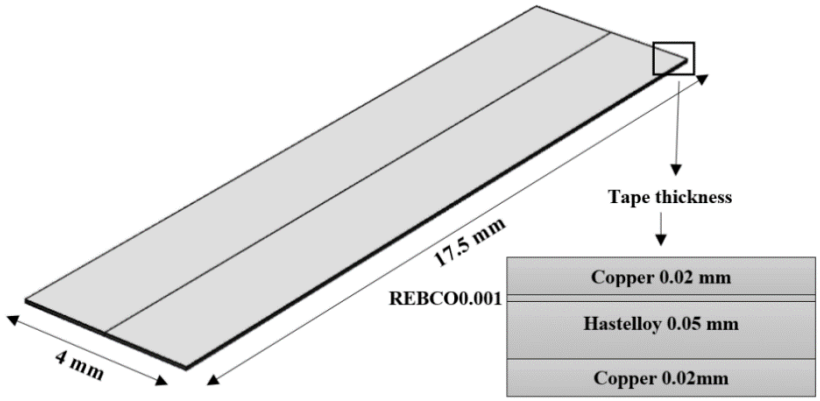

Figure 6.2: Schematic showing the geometry and dimensions of the section modelled and the constituting layers of the REBCO tape

When a finite load is applied to the REBCO tape, the differences in layer properties profoundly influence the intrinsic axial strain developed. The bonding between the layers may influence the eventual force transmitted between the layers. This effect is pictorially represented using a tensile loading case as depicted in Figure 6.3.

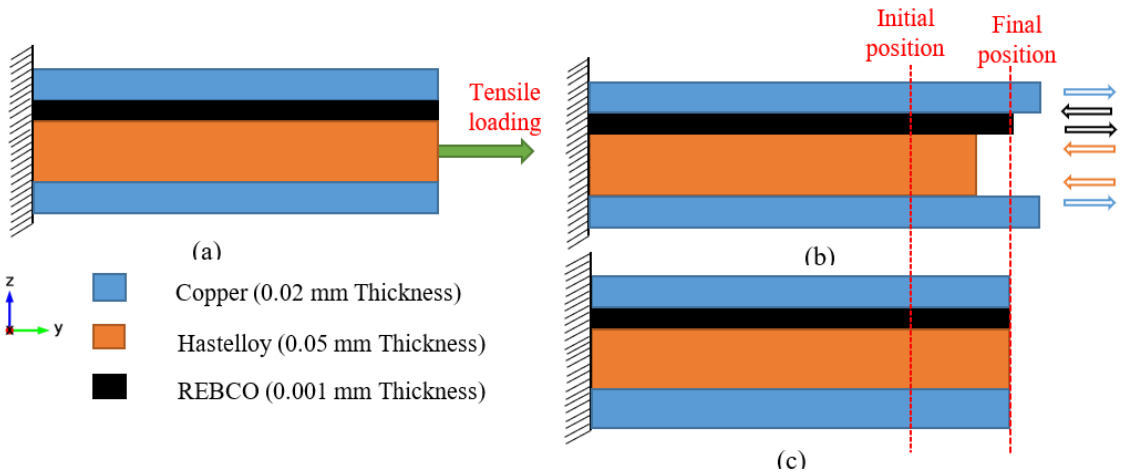

Figure 6.3: Pictorial representation of the effect of different dissimilar material layers on the induced strain in the REBCO tape a) Before loading b) Under loading with no interfacial bonding between the layers c) Under loading with interfacial bonding between the layers

The tensile stress applied is the same for all the layers, then the strain induced in each layer is dependent on Young's modulus of the constituting layers. Hastelloy, which has a high Young's modulus than other layers, will experience less strain than copper and REBCO. The layers having lesser value of Young's modulus, the copper layers will experience the maximum tensile strain due to its lowest Young's modulus value out of all other layers. Under tension, the copper layer tries to pull adjacent REBCO and Hastelloy layers to the right, as marked in Figure 6.3. At the same time, REBCO and Hastelloy layers may resist this pulling of the copper layers. A similar interfacial effect is also observed between the Hastelloy and REBCO. Hastelloy tries to pull the REBCO layer to the left, but the REBCO layer resists this effect and also vice versa. This effect is marked by small arrow marks on the right side of Figure 6.3. Pulling force of each layer has combined impact on the eventual strain under tensile load. Therefore, the dimensions of individual layers, including thickness, length, and width, may affect the strain developed by tensile loading. When the thickness of a layer is changed, the volume fraction of the layer changes. This in turn changes the cross-sectional area on which the stress acts. However, it may be noted that because all layers have the same width and length, the volume fraction of each layer remains constant if the length or width of the tape is changed. When the tape is subjected to pure tensile loading, a change in tape width may have no effect on the development of intrinsic axial strain in the REBCO layer. However,

the associated intertwined effects and interfacial bonding are expected to have a minor influence on the induced strain.

The effects of characteristics of different material layers, bonding between layers, and residual strain would influence the intrinsic axial strain generated in the REBCO layer in the case of pure torsional and combined tensile and torsional loading. However, unlike in a pure tensile situation, the mechanism of action and failure for combined tensile and torsional loading will be different.

The method developed for providing pure torsion, pure tension, and combined tension and torsional stresses are depicted in Figure 6.4. The production process of REBCO tape is first modelled to determine the amount of residual strain induced in the tape. In the second stage, the tensile stress is changed from 0 % to 0.7 % in 15 steps with an increment of 0.05 %. The torsional load is changed in the third stage for each tensile load by varying the angle of twist from 0^o to 90^o about the y axis with a step size of 5^o .

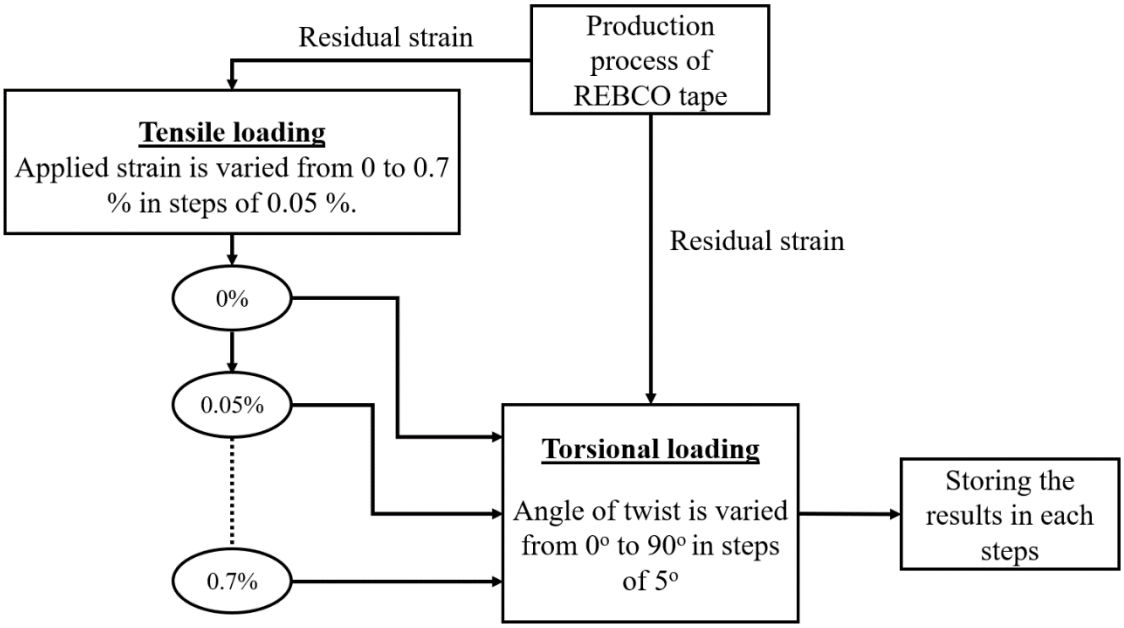

Figure 6.4: Methodology adopted for providing pure torsional, pure tensile and combined tensile and torsional loads on REBCO tape in FE modelling.

In this methodology, the pure tensile, pure torsional, and combined torsion and tension cases are applied.

6.3. Validation

The results obtained using the model are compared with that of the experimental and simulation works mentioned in the literature [17]. The results are plotted in Figure 6.5. Figure also distinguishes the reversible and irreversible regions of the REBCO layer under tension and torsion stress based on critical limit criteria.

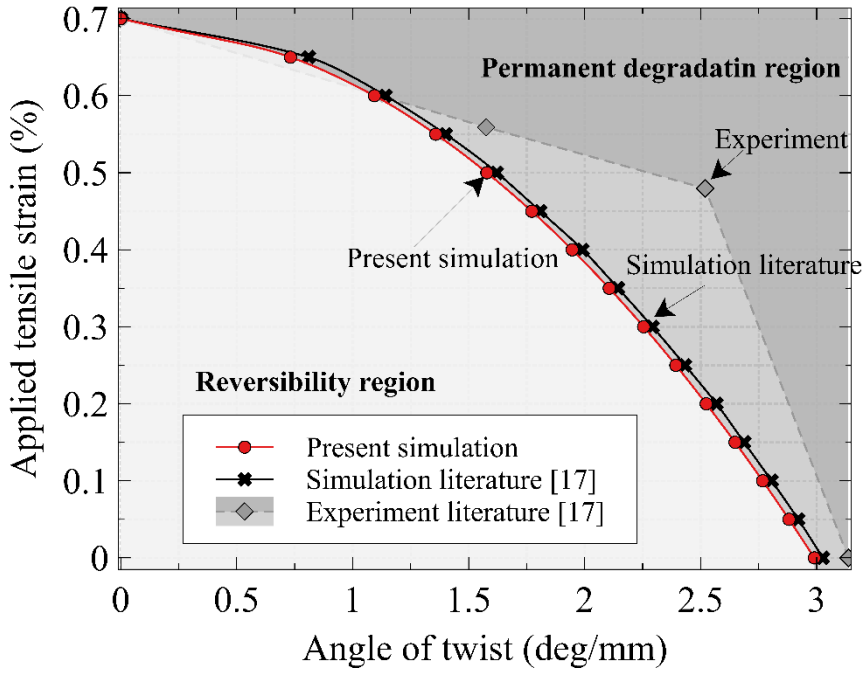

Figure 6.5: Comparison of the simulation results of the present study with experimental and simulation data available in the literature [17].

The present simulation results and the experimental result available in the literature show reasonably good agreement (6 % average difference), except at one point. Similarly, the simulation study mentioned in the literature and the present study are having very close agreement (maximum difference is 1.2%). The difference between the simulation and the experimental results may be due to the sensitivity difference in detecting irreversibility for tensile and torsional loads. K. lin et al. mentioned that the sensitivity is sufficiently high for pure tensile strain but very small for torsional strain at a critical current criterion of 10 μVm^{-1}[17]. It is understood that the created model is adequate for carrying out the studies.

The parametric studies analyse both the individual effects of tensile and torsional loads as well as their combined influences. The parameters changed are the thickness of the copper layer, the thickness of the Hastelloy layer, and the width of the tape. The results

of the parametric studies obtained under pure tensile, pure torsional, and combined tensile and torsional loadings are discussed.

6.4. Results and discussion

The results of pure tensile loading are reported first, followed by the findings of combined tensile and torsional loading. The critical degradation point corresponding to different loading conditions is calculated for various tape dimensions.

6.4.1. Influence of pure tensile loading on the performance of the REBCO tape.

The effects of pure tensile loading on tape degradation and the changes obtained with alterations in the tape's geometry are discussed. Figure 6.6 depicts the changes in applied critical force with variations in geometrical parameters such as the thickness of Hastelloy and copper layers.

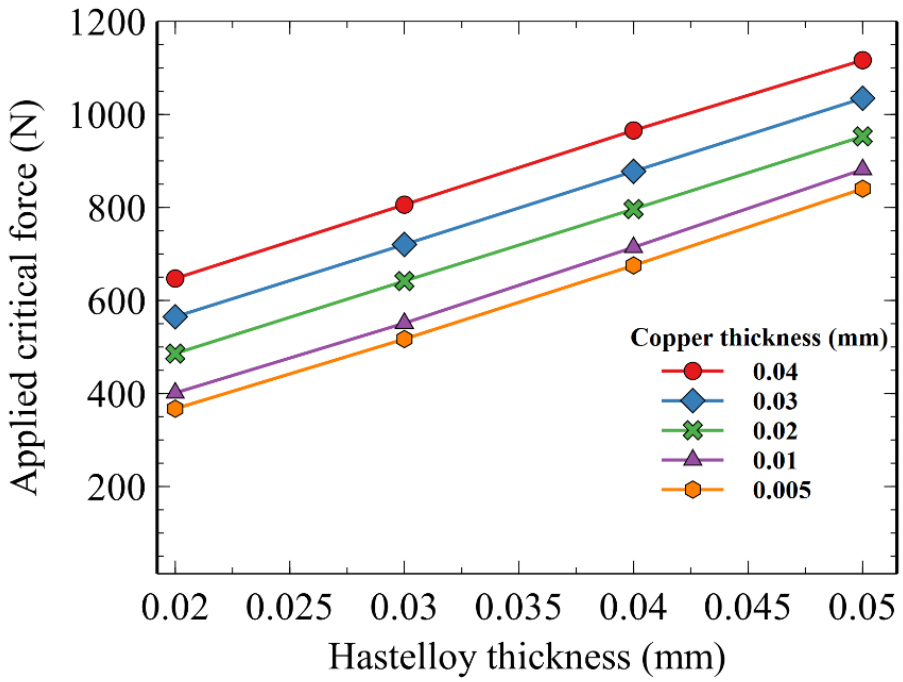

Figure 6.6: Effect of Hastelloy and copper thicknesses on the applied critical force (Tape width = 12 mm).

The applied critical force increase as the thicknesses of the Hastelloy and copper layers are increased. However, increasing the thickness of the Hastelloy layer has been found to have a more significant influence. When the Hastelloy thickness increases from 0.02 mm to 0.05 mm (about 150 % increase) for the thickest copper layer (0.04 mm), the applied critical force increases by 72.5 %. Whereas when the copper thickness is increased from

0.005 mm to 0.04 mm (a 700% increase), the applied critical force only increases by 32.9 % (for the thinnest Hastelloy layer of 0.02 mm).

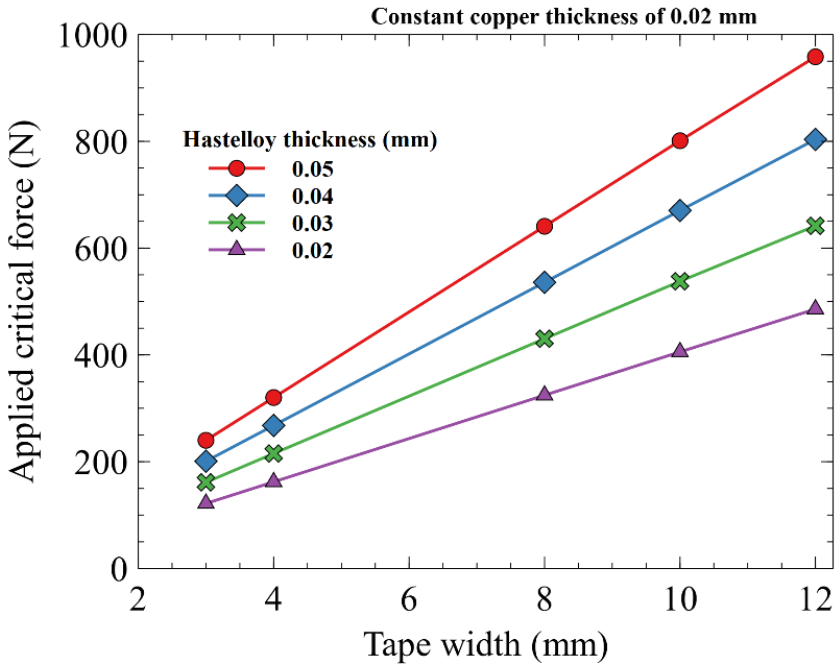

Figure 6.7: Effect of tape width on the applied critical force.

Figure 6.7 depicts the effect of tape width on the applied critical force. It may be noted that as the tape width increases, so does the maximum force that can be applied to the tape. The load-bearing capacity of the REBCO tape increases with the increase in Hastelloy thickness. When the Hastelloy thickness is increased from 0.02 mm to 0.05 mm (about 150 %), the applied critical force increases by 97 % for all tape widths.

6.4.2. Variations in the induced strain in REBCO with change in Hastelloy thickness

The axial force subjected on the REBCO tape induces axial strain in the REBCO layer. As previously stated, intrinsic axial strain developed above a certain limit may have an effect on the performance of the superconducting tape. As a result, the changes in intrinsic axial strain with changes in the thickness of the Hastelloy layers of the tape are determined. Figure 6.8 depicts the effect of pure tensile loading on intrinsic axial strain on the REBCO tape for various Hastelloy thicknesses.

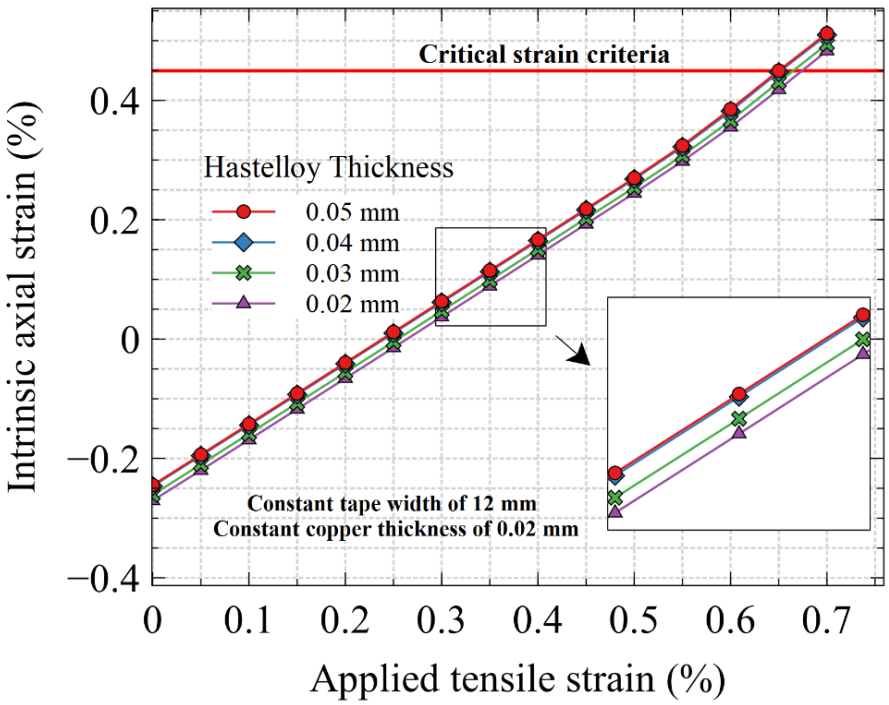

Figure 6.8: Effect of Hastelloy thickness on intrinsic axial strain under pure tensile loading.

For any given Hastelloy thickness, increasing the applied tensile strain produces a directly proportional increase in the intrinsic axial strain in the REBCO layer. It is evident from the graph that, before the application of the tensile load, there is residual strain in the REBCO layer developed during the manufacturing of the tape. It may be noted that the residual strain in the REBCO layer is -0.242 % at zero applied strain (at 0.05 mm Hastelloy thickness). When the Hastelloy thickness is dropped to 0.02 mm, the residual strain rises from -0.242 % to -0.27 % (about 2.7 %.) It is also found that when the applied tensile strain is about 0.25 %, the intrinsic axial strain in the REBCO layer changes from compressive to tensile (negative to positive values). It may be observed that the intrinsic axial strain in the REBCO layer is decreased as the Hastelloy layer thickness is reduced. It is due to the changes in the volume fraction of different layers with increase/ decrease in the Hastelloy thickness. The critical strain criterion is marked by the continuous horizontal line at the top of the graph. Precautions must be taken when using the tape to ensure that the magnitude of the applied tensile strain does not exceed the critical values specified by this degradation limit. It may be noted that as the thickness of Hastelloy is reduced, there is a slight increase in the critical strain value. As the thickness of Hastelloy decreases from 0.05 mm to 0.02 mm (60 % decrease), the applied tensile strain increases

by 3.75 %. In all these cases, the copper layer thickness is kept constant at 0.02 mm and the tape width at 12 mm.

6.4.3. Variation in the induced strain in REBCO with change in copper thickness

The effect of changing copper thickness on intrinsic axial strain in the REBCO layer under pure tensile load is depicted in Figure 6.9. The differences in copper thickness affect the intrinsic axial strain induced in the REBCO layer, and the variations obtained are nearly identical to those obtained for Hastelloy thickness. However, in contrast to the case of Hastelloy thickness, when the copper thickness is increased from 0.005 mm to 0.04 mm, the difference in intrinsic axial strain increases by 4 %. The critical strain value rises by 5.3 % for the same variation in copper thicknesses.

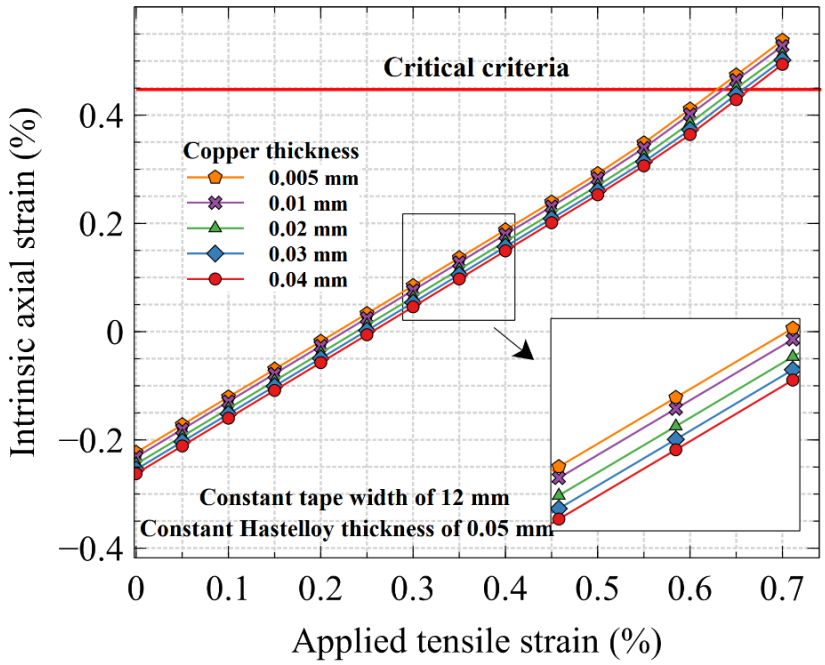

Figure 6.9: Effect of copper thickness on the intrinsic axial strain in the REBCO layer under pure tensile load.

Similar to the Hastelloy variation case, the residuals train values are also dependent on the thickness of the copper. The residual strain value varies from -0.223 to -0.262 % when the copper thickness is changed from 0.005 mm to 0.04 mm, as discussed. The applied tensile strain that may withstand without producing degradation increases as the copper thickness increases.

6.4.4. Variation in the induced strain in REBCO with change in tape width.

Figure 6.10 and 6.11 representing the changes in the applied critical strain with variation in the tape width corresponding to different Hastelloy and copper thicknesses.

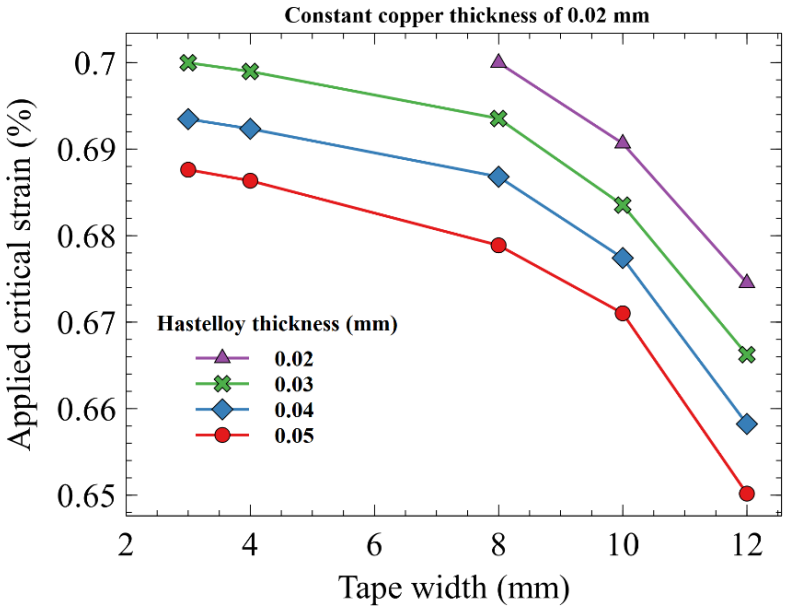

Figure 6.10:Variation in applied critical strain with changes in tape width for different Hastelloy thicknesses under pure tensile loading

Though the trend remains the same for all widths, the magnitude of the critical applied strain decreases as tape width increases. The degradation is faster as the tape width increases (lower values for critical applied strain). Larger tapes can bear higher tensile force without degrading. When the Hastelloy thickness is increased from 0.02 mm to 0.05 mm on a 12 mm tape, the critical applied tensile strain values are reduced by approximately 36%.

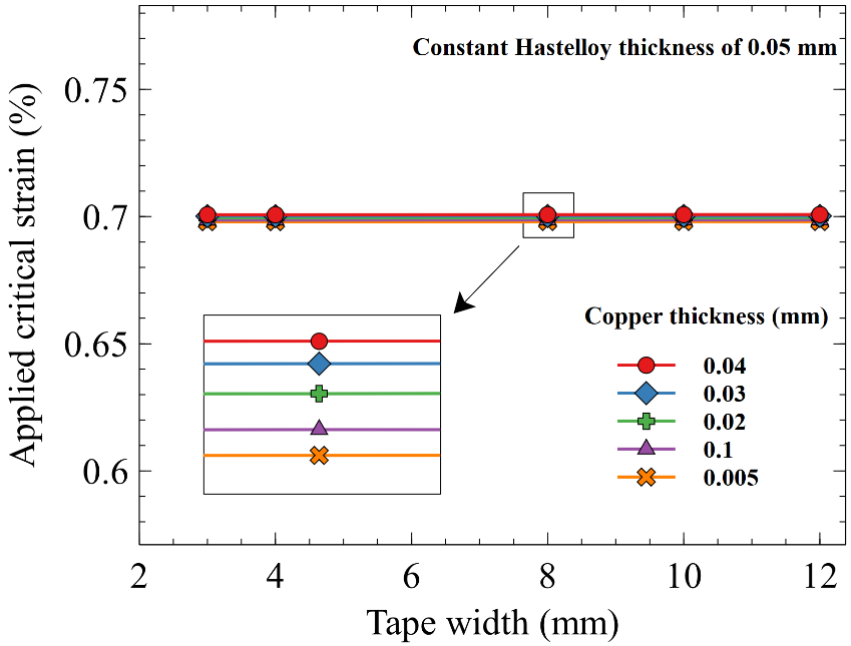

Figure 6.11:Variation in applied critical tensile strain with changes in tape width for different copper thicknesses under pure tensile loading

Figure 6.11 shows the critical applied strain change with tape width variations corresponding to different copper thicknesses under pure tensile loading. It is found that the influence of copper thickness on the induced intrinsic axial strain is not as significant as it is in the Hastelloy case. For instance, increasing the thickness of copper from 0.005 mm to 0.04 mm (approximately 700%) increases the critical applied tensile strain value only by 3.9 %. It can also be noted that the tape width has no significant effect on the development of intrinsic axial strain in the REBCO layer with changes in copper thickness.

6.5. Influence of combined tension and torsion on the performance of the REBCO tape.

The degradation of the superconducting tape under tension and torsional load is important since these tapes are subjected to such loads during the manufacturing of the superconducting cable and the magnets. The impacts of changes in geometrical parameters of the tape when subjected to combined loading is studied. The degradation limits of the tape are plotted as a function of Hastelloy, copper layer thickness and the width of the tape.

6.5.1. Effect of combined tensile and torsional loading on REBCO with changes in Hastelloy thickness.

Figure 6.12 depicts the degradation limits of REBCO tape subjected to the combination of tensile and torsional loads. Torsional and tensile loads are represented in terms of angle of twist and tensile strain. The curve denotes the degradation point corresponding to each combined tensile and torsional load. The shaded area above the curve represents the degradation region, and white region below the curve indicates the safe area. The graph illustrates that when the torsional load (angle of twist) is large, the tensile load that the tape may withstand will be reduced. For instance, if the twist angle is 0.18 deg/mm, the maximum tensile strain applied is 0.65%. When the twist angle increases from 0.18 to 0.72 deg/mm (300 % increase), the maximum value of applied tensile strain is reduced to 0.3 % (about 54 % decrease). The applied tensile strain can be as high as 0.7 % when the twist angle is zero (pure tension case). Similarly, when no tensile load is applied, the highest twist angle available is 0.93 deg/mm (the pure torsion case).

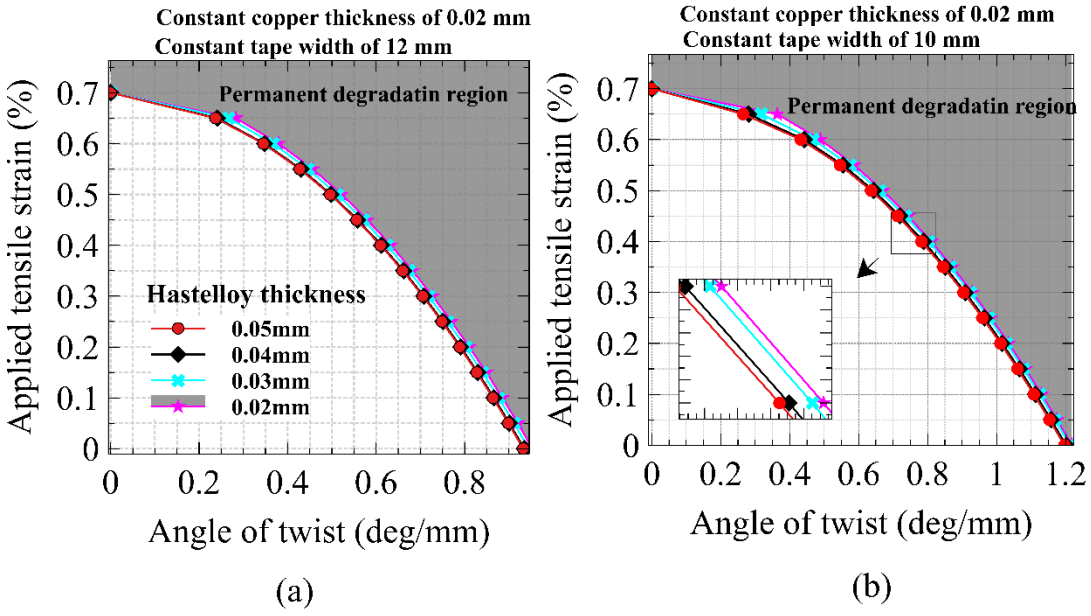

Figure 6.12: Critical strain in the REBCO layer under the combined loading of tension and torsion at different Hastelloy thicknesses for a) 12 mm tape width b) 10 mm tape width

Increases in the thickness of the Hastelloy layer have less effect on the critical limits, as shown in Figure 6.12. In the pure torsion situation, the angle of twist can only be increased by 2.2 % when the Hastelloy thickness is decreased from 0.05 mm to 0.02 mm (approximately 60% reduction). It may be noted that in all these cases mentioned, the

thickness of copper is kept constant at 0.02 mm. In the case of Figure 12 (a), the tape width is kept constant at 12 mm. Figure 12 (b) shows the effect of decreasing the tape width to 10 mm. Figures 12(a) and 12(b) show that a tape with a 12 mm width degrades faster than one with a 10 mm width. In the pure torsion scenario, it is also found that a 10 mm wide tape can sustain 1.2 deg/mm of twist angle. This is approximately 28% higher than the tape with 12 mm width.

6.5.2. Effect of combined tensile and torsional loading on REBCO with change in copper thickness.

The impact of copper thickness on the degradation of REBCO tape under combined tension and torsional loads is studied. A similar result as that of the Hastelloy study is obtained; when the angle of twist that can be applied is large, the tensile load that the tape can sustain is smaller. The results indicate the critical limits; the intrinsic axial strain values beyond this value are not acceptable. For instance, it is found that the maximum angle of twist that can be applied is 0.92 deg/mm when the tensile load is zero (pure torsion). On the other hand, the maximum applied tensile strain that can be applied is 0.65 % when the torsional load is zero (pure tension). This is for the case where the copper thickness is the minimum (0.005 mm).

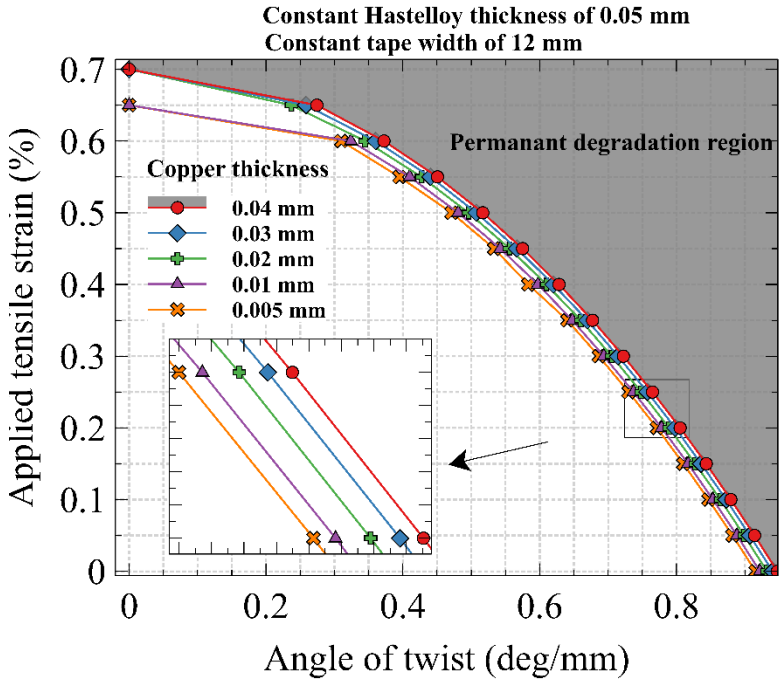

Figure 6.13: Effect of copper thickness on critical strain under combined tension and torsion

Figure 6.13 depicts the effect of changing the thickness of copper layers. The curve denote the degradation points corresponding to each combined tension and torsion load. Under pure torsion, the angle of twist that can be applied increases to 0.95 deg/mm for the maximum copper thickness (0.04 mm) (about 3.2 %). Under pure tension, the applied tensile strain increases to 0.7 %, which is approximately 7.7 % for the same copper thickness. Tapes with the smaller copper thickness degrades faster and this comparison bring out the importance of copper layer in maintaining the strength of the tape for a wide range of operations.

6.5.3. Effect of combined tensile and torsional loading on the REBCO with changes in the tape width

The effect of reducing the tape width on degradation under combined tension and torsional loads is investigated. Figure 6.14 depicts the critical limits for each tape width, for a wide range of torsional and tensile loads as well as their combinations. The area above each curve in the degradation region and it is safe to keep the tape below the curve.

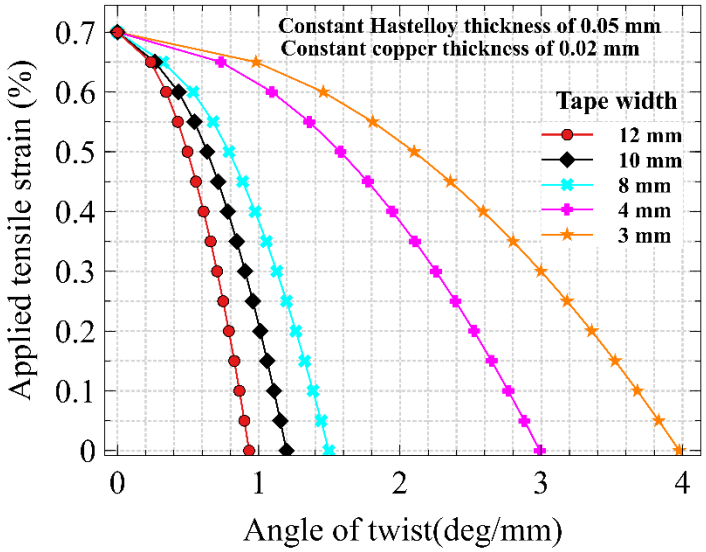

Figure 6.14: Effect of tape width on critical strain under combined tension and torsion

Figure 6.14 shows that when the width of the tape decreases, the critical limits are moved further out, offering manufacturers more flexibility in terms of combined tensile and torsional loads. For the pure torsion the situation of reducing the tape width from 12 mm to 3mm (75 % decrease) increased the maximum permitted angle of twist from 0.93 to 4 deg/mm (326 % increase). However, in the case of pure tension, the change in tape width has no significant effect. The tape degraded at 0.7 % applied tensile strain irrespective of

tape width. With an increase in the angle of twist, the influence of tape width becomes more noticeable in the combined tensile and torsional cases. On the other hand, in pure torsional loading, increasing the width of the tape has a very significant effect on the generated intrinsic axial strain. The cross-sectional area increases proportionally as the tape width increases; whereas, the volume fraction remains the same. In the case of torsional loading, it is found that the cracks develop at the edges. A smaller tape width results in a lesser strain on the tape. Therefore, the width of the tape is found to have a very significant influence on the combined tensile and torsional loading as well as the pure torsional loading. If the tape is wider, under combined tensile and torsional loading, the tape will fail quickly with an increase in the load. This is evident from the Figure as the slope becomes steeper with the increase in tape width.

6.6. Electrical performance of REBCO tape subjected to combined tension and torsion.

The electrical performance of superconducting REBCO tape when subjected to torsional loading is investigated. The effect of combined tension and torsion forces on the induced strain and the associated amount of degradation of the superconducting tape is presented in terms of its current carrying capacity. After being converted to cables/wires, superconducting tapes find use in a variety of systems, including magnets, where a huge quantity of current must be transmitted through them without causing any Joule heating. However, induced strain due to mechanical loads on them can degrade the superconducting tape; thus producing some electrical resistance. Though the value of such electrical resistance will be very small, the resulting heating would be enormous due to the large quantity of high current being passed through them. This result in situation like quenching and can permanently damage the superconducting cable/ wire. Each superconducting tape has a maximum current carrying capacity, called as the critical current limit and this capacity decreases as the tape degrades. Therefore, the current-carrying capacity of superconducting tape may be used to determine the extent of degradation. This changes the electrical performance of superconductors when subjected to tension, torsion, and combined tension and torsion are important and need to be monitored.

6.6.1. Changes in the critical current retention under pure torsional loads

The critical current depends upon the intrinsic axial strain. In pure torsion and combination tension and torsional cases, the intrinsic axial strain is not constant over the width of the tape. Under torsion the strain-induced will be more at the edges of the tape and when moved to the centre line along the width direction, the strain is reduced. Consequently,The current-carrying capacity will change according to the strain-induced, Equation 6.1 may be used to calculate the overall current carrying capacity of the tape [83].

$$I_c = t_s \int_{-\frac{w}{2}}^{\frac{w}{2}} j_c(\varepsilon_x) dx \quad (6.1)$$

Where the critical current 'I_c' of a twisted tape is represented as a sum of critical current densities '$j_c(\varepsilon_x)$' over the width 'w' and thickness 't_s' of the tape cross-section, the critical current density is the function of the intrinsic axial strain in this expression. A more precise empirical expression (Equation 6.2) is reported in the literature [83], and it is based on SuperPower data on Yttrium Barium Cupric Oxide (YBCO) [121].

$$\frac{I_c}{I_{co}} = 0.057713x10^{12}\,\varepsilon_x^6 - 0.03979215x10^{10}\,\varepsilon_x^5 - 0.02090279x10^{8}\,\varepsilon_x^4 + 0.02385557x10^{6}\,\varepsilon_x^3 - 0.1668065\,x10^{4}\,\varepsilon_x^2 - 0.003662115\,x10^{2}\,\varepsilon_x + 1 \quad (6.2)$$

Where 'I_{co}' is the critical current density at zero intrinsic axial strain. Critical current retention at a particular strain is the ratio of critical current at that strain to the critical current value when the intrinsic axial strain is zero. The above expression is used for calculating the critical current retention ($\frac{I_c}{I_{co}}$) of different cases.

6.6.2. Effect of thickness of Hastelloy on the critical current retention

Figure 6.15 describes the influence of Hastelloy layer thickness on critical current retention under pure torsion (zero applied tensile strain).

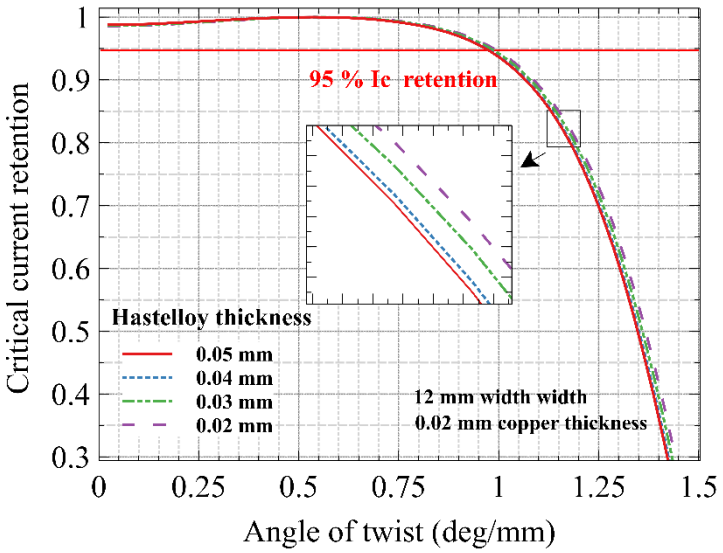

Figure 6.15: Critical current degradation at different Hastelloy thicknesses under pure torsion

The torsional load is changed by varying the angle of twist, which is represented on the X-axis. The Y-axis represent the the critical current retention. The maximum critical current retention allowable is 95 % and it is marked by the horizontal straight line at the top. The graph shows that as the angle of twist increases, the critical current retention is good until about 0.9 deg/mm, beyond which it decreases significantly. A 50% increase in the angle of twist beyond 0.9 deg/mm (0.9 deg/mm to 1.35 deg/mm) reduces critical current retention by nearly 50%. The similar trends can be seen for other Hastelloy thicknesses (from 0.05 mm to 0.02 mm). Initially, as the angle of twist increases, so does the critical current retention. This is due to the influence of residual strain as discussed earlier. When the twist angle is about 0.54 deg/mm, the critical current retention is near 1.

The graph also illustrates that by decreasing the thickness of Hastelloy, the tape may not be able endure a higher angle of twist without affecting critical current retention. For instance, at 0.05 mm thickness of Hastelloy, critical current retention of 95 % is only possible up to a twist angle of 0.96 deg/mm. When the thickness of Hastelloy is reduced from 0.05 mm to 0.02 mm (a 60% reduction), the angle of twist possible (torsional load) increases to just 0.99 deg/mm, which is about 2 % increase only. The results suggest that it is possible to reduce the thickness of Hastelloy without significantly affecting its electrical performance.

6.6.3. Effect of thickness of copper on the critical current retention

The thickness of the copper layers' is changed in this case and Figure 6.16 shows its corresponding the changes in critical current retention under pure torsional loading.

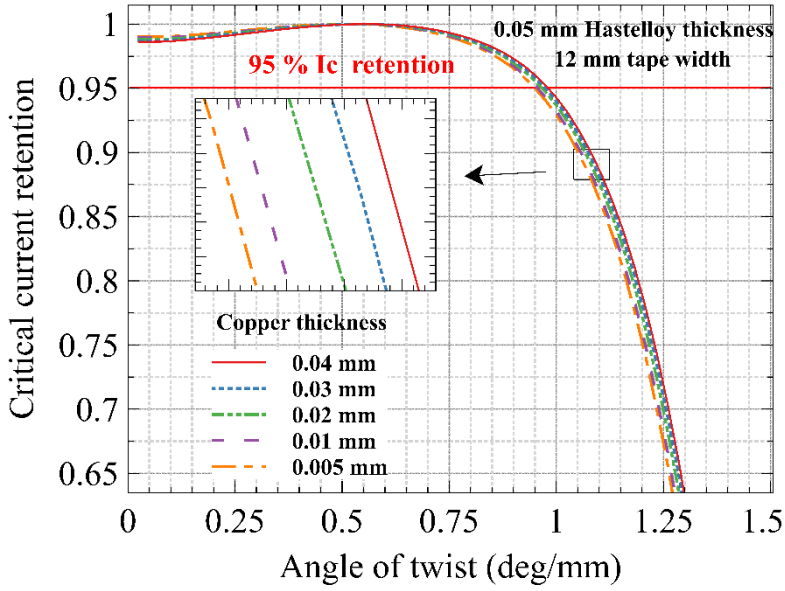

Figure 6.16: Critical current degradation at different copper thicknesses under pure torsion

The copper layers' thickness is increased and then decreased from the given value of 0.02 mm. When increasing the angle of twist, the critical current retention under pure torsion is better with the thicker copper layers. When the copper thickness is decreased, the critical current retention is slightly reduced. At a copper layer thickness of 0.04 mm, the critical current retention of 95% is possible only up to an angle of twist equal to 0.98 deg/mm. The maximum angle of twist is reduced to 0.95 deg/mm when the thickness of the copper layers is decreased to 0.005 mm. For almost all the copper thicknesses, the degradation limit in terms of torsional load demarcated by limit in terms of 95 % critical current retention beyond 0.9 deg/mm for the given configuration.

For all cases, the critical current retention becomes 1, when the angle of twist is nearly 0.54 deg/mm. With an initial torsional load of up to 0.54 deg/mm, tapes with thicker copper layers can hold more residual strain. On the other hand, a torsional load above 0.54 deg/mm has high critical retention for tapes with larger copper thickness.

6.6.4. Effect of tape width on the critical current retention

Figure 6.17 depicts the impact of tape width on critical current retention under pure torsion (zero applied tensile strain). The width of the tape is reduced from the given value to understand its impact on the electrical performance.

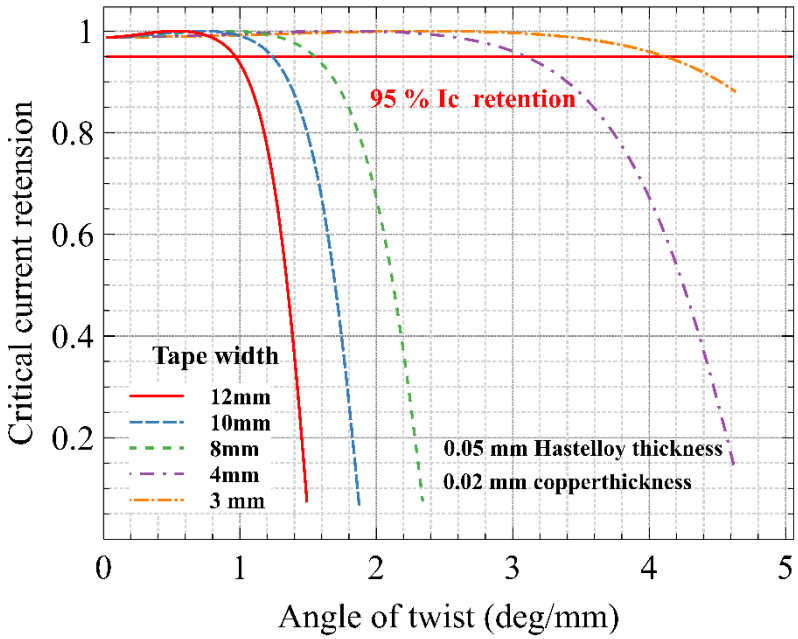

Figure 6.17: Critical current degradation at different tape widths under pure torsional load

The findings indicate that the width of the tape has a considerable impact on critical current retention. When the width of the tape is reduced from 12 mm to 3 mm (75% reduction), the maximum angle of twist possible without degradation increases from 0.93 to 4.1 deg/mm (about 326 % increase). The 95 % critical current retention is marked by the straight horizontal line at the top. It is evident from the graph that the impact of tape width on critical current retention is more crucial at higher tape widths.

6.6.5. Changes in the critical current retention under combined tensile and torsional loads

The critical current retention of the REBCO superconducting tape under combined tensile and torsional loads is shown in Figure 6.18. The changes in torsional load is indicated on the x-axis in terms of the angle of twist, and the various tensile loads applied are marked in the legend of the graph. The critical current retention varies from around 100 % to 65 % for the given range of parameters, as shown in the graph. If the

critical current retention is less than 95 %, the tape is considered to lose its superconductivity and so degraded. The horizontal line at the top of the graph shows this limit. The region above this line can be considered as safer region. As expected the critical current retention considerably decreases with a significant increase in tensile and torsional loads.

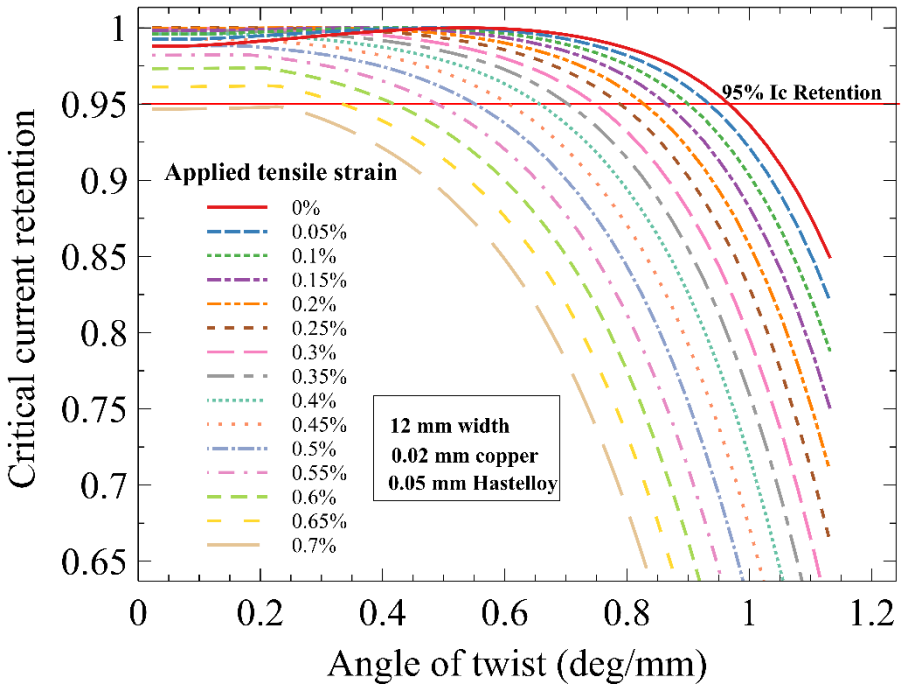

Figure 6.18: Critical current degradation under combined tensile and torsional load

The shapes of the different graphs show that as the applied tensile strain increases, the rate at which the critical current retention decreases increases. It may be noted that even without any torsional load (0 deg/mm angle of twist), the critical current retention is less than 95 % at the maximum applied tensile strain (0.7 % curve). When a more torsional load is applied, the entire tape enters the degraded region. On the other hand, the highest angle of twist that can be provided without degradation is 0.97 deg/mm in the absence of any tensile load (0 % applied tensile strain). It may also be observed that the critical current value first increases with an increase in the angle of twist. Once it reaches a particular strain value, it starts decreasing for each case of applied tensile strain. Similar results were obtained by other researchers earlier [8]. It may be due to the relief of the residual strain in the tape.

The numerical simulation done by llin et al. [17] reported that, when the applied strain is 0.3%, then the maximum angle of twist that can withstand without any

degradation is 2.29 °/mm. This study also found a similar result, the maximum allowable angle of twist without any degradation at 0.3% applied strain is 2.25 °/mm. The critical current degradation under combined tension and torsion is reported in another literature [88]. However, a direct comparison of these two studies is not possible, because the present study is using 12 mm wide tape, and the literature use 4 mm wide tape. At 0.6% applied strain, 4 mm width tape can accommodate 1.8 °/mm angle of twist [88]. In this study, 12 mm width tape at 0.6% applied strain can accommodate 0.42 °/mm. Another study by Gorospe et al. reported that 5% critical current degradation occurred for 4.01 mm GdBCO tape at 2.96 °/mm [133]. However, in the present study, 5% critical current degradation is observed at 0.97 °/mm (12 mm width tape). In all the cases, a direct comparison of this 12 mm and 4 mm width tape is not possible, even though it is clear that 12 mm width tape fails first compared to 4 mm width one under pure torsion and combined tension and torsion.

6.7. Summary

The influence of intrinsic axial strain induced on the degradation of REBCO tape under combined twisting and torsion has been studied. The tape parameters, such as the thickness of Hastelloy and copper layers, the width of the tape, etc., are varied to evaluate the amount of degradation under pure tension, pure torsion and combined tension and torsion loads. From the results obtained from the study, the following conclusions can be derived.

- Under pure tensile loading, the applied tensile strain on the tape is directly proportional to intrinsic axial strain developed in the REBCO layer irrespective of the thickness of Hastelloy and copper layers and the width of the tape. For the given configuration, the applied tensile strain beyond which the tape degrades is between 0.6 %, and 0.7 % applied tensile strain for any thickness of layers and tape width.
- Under combined tension and torsion, there is an inverse relationship between the applied tensile strain and the angle of twist that can be applied. When the angle of twist is increased from 0.18 to 0.72 deg/mm (300 % increase), the maximum value of applied tensile strain that can be applied, is to be decreased from 0.65 % to 0.3 % (about 54 % decrease). Decreasing the tape width further decreases the maximum value of applied tensile strain for the same increase in the angle of twist.

Changing the thickness of Hastelloy and copper layers is not found to have much significant influence on the degradation of the tape.

- It is found that under pure torsional as well as combined tensile and torsional loads, the applied tensile strain that can be applied on the tape can be increased by decreasing the width of the tape. By decreasing the tape width, the critical limits can be pushed further, giving more flexibility for the manufacturers to accommodate combined tensile and torsional loads. By decreasing the tape width from 12 mm to 3mm (75 % decrease), the maximum allowable angle of twist can be increased from 0.93 to 4 deg/mm (326 % increase) under pure torsional loading.
- The study found that under pure torsion, the influence of Hastelloy thickness on the degradation limits are not appreciable in the given range. Decreasing the Hastelloy thickness from 0.05 mm to 0.02 mm (about a 60 % decrease) has increased the maximum allowable angle of twist by only 2.2 %.
- Observation of the critical current retention under combined tension and torsion revealed that the critical current value first increases with an increase in the angle of twist. However, further increase will decrease the critical current retention.
- Changing the thickness of Hastelloy and copper layers is not found to have any significant influence on the critical current retention in the REBCO tape. When reducing the thickness of Hastelloy from 0.05 mm to 0.02 mm (60% decrease), angle of twist can only be increased from 0.96 to 0.99 deg/mm (2.2%). Similarly, when the copper thickness is reduced from 0.04 mm to 0.005 mm (87.5 % decrease), the maximum allowable angle of twist decreases from 0.98 to 0.95 deg/mm (3.1 % decrease).
- It is found that under pure torsion, the width of the tape has significant influence. The angle of twist has to be decreased from 4.1 to 0.97 deg/mm (326 %) with the increase of tape width from 3 to 12 mm (300 % increase).

The results generated are expected to help the manufacturers of superconductors when developing REBCO based tapes and cables subjected to tensile, torsional, combined tensile and torsional loads.

Publication arising out of this chapter

- **K. B. Ashok**, R. J. Thomas, M. J. Prakash, and A. Nijhuis, "Influence of combined tension and torsion on the performance of REBCO superconducting tapes," IEEE Trans. Appl. Supercond., vol. 33, no. 3, pp. 1–11, 2023, doi: 10.1109/tasc.2023.3236010 (Impact factor: 1.96).

Chapter 7

Effect of winding on the degradation of REBCO superconducting tape

7.1. Introduction

This chapter studies the influence of the winding process on simple superconducting CORC® cable while changing tape parameters like substrate thickness, copper stabiliser layer thickness, winding angle, and centre core diameter. D. C. van der Laan developed the CORC cable in 2009 [35, 127], and a detailed discussion on this type of cable has been provided in section 1.5.5. The previous chapters discussed the effect of different mechanical loads such as tension, bending load, twisting load and combined tension and twisting on the degradation of the REBCO tape. The winding process has the combination of all three mechanical forces applied simultaneously. In the CORC type cable, winding of the superconducting REBCO tape is performed on a central core. One of the advantages of CORC® cable over other cable types is the possibility of using a

central core with a small diameter, thereby reducing the cable size. It is essential to calculate the lowest possible core diameter of the cable without any degradation of the HTS layer. Smaller the core diameter, more profound would be the effect of the critical parameters. In addition to this, parameters such as Hastelloy thickness, copper thickness, tape width and the winding angle also influence the degradation of the superconducting tape.

Winding of simple superconducting cable is earlier reported in the literature by Wang *et al.* [126]. They have treated the multi-layered tape made of various materials such as copper, Hastelloy, REBCO as a single homogeneous material for their analysis. They have also considered the materials as completely elastic. Young's moduli of the superconducting substrate, and copper layers were weighted according to the volume fraction of each material to calculate the equivalent Young's modulus. The residual strain presents in the material is a crucial component determining the tape performance under structural loading; however, their work did not consider the effect of residual strain.

When considering the tape as a homogeneous material with elastic properties, the modelling would be easier [3]. However, since the tape is constituted of different layers made of different materials consideration of homogeneous materials may not generate accurate results especially when modelling of more involved process like the winding. In addition to this, most of the layer materials are plastic in nature and the consideration of elastic properties will have an impact on the induced strain in the tape during the winding process. In the present study, the influence of these aspects is studied in detail.

7.2. Modelling approach

Winding the superconducting cable is a crucial process. The experimental investigation to find the critical limit would be time-consuming and costly. In addition to this, winding for various central core diameters with different REBCO tape configurations is practically difficult to execute. The numerical model of single-layer superconducting CORC cable is developed with the help of the Solid Mechanics module in COMSOL Multiphysics® software. The numerical model created is used to determine the range of each parameter within which the cable is not degraded. The numerical model helps to conduct the analysis for a series of winding processes so as to find the degradation limit of each parameter. Figure 7.1 shows the configuration of the Superpower REBCO tape used in the analysis. The layer' details and their functions are already discussed in the initial Chapters.

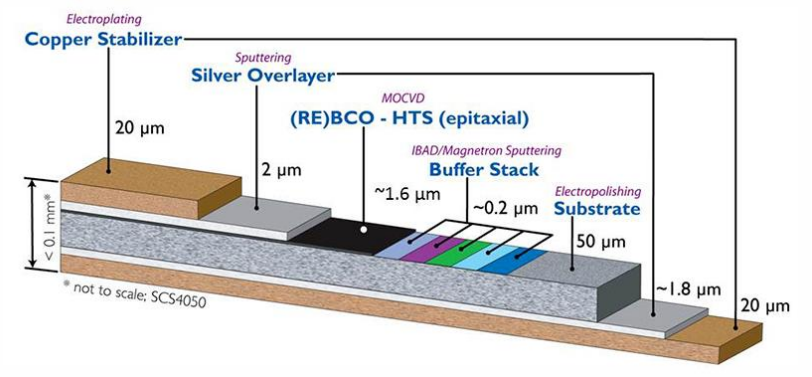

Figure 7.1: Configuration of SuperPower® 2G HTS Tape SCS4050 [121]

The strain developed in the REBCO layer due to the effect of other layers under different loading situations is a concern when using superconducting tape. However, it may be observed that the thickness of the Hastelloy substrate and copper stabiliser is dominant among the different layers. As a result, their impact on the strain generated in the REBCO layer will be significant compared to the other much thinner layers. REBCO, copper, and Hastelloy layers are considered for modelling, but the remaining layers are ignored, as mentioned in the previous chapters [17, 91]. The simple superconducting CORC cable and the winding machine is depicted in the Figure 7.2.

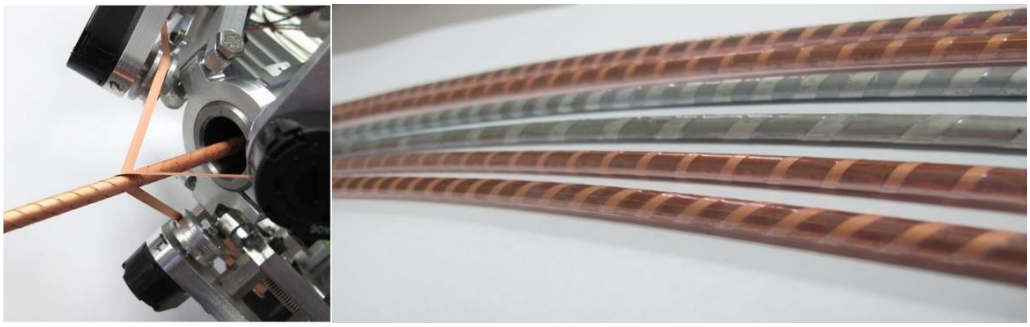

Figure 7.2: a) CORC cable winding machine [126] b) Simple superconducting CORC cable

In actual practice, the winding process is carried out at room temperature, and residual strain is calculated similarly as provided in the previous chapters. The lower limit of temperature is 293.15 K. The material properties and assumptions used are already mentioned in chapter 4. Also, REBCO is considered elastic in the whole range of temperature, and the plastic properties of Hastelloy and copper are considered throughout the modelling. The residual strain already present in the tape is also considered.

7.3. Mesh and boundary conditions

The numerical modelling of the winding process of the REBCO tape over the central core is challenging due to the contact involved. Contact pair is defined in COMSOL Multiphysics in two ways; the Augmented Lagrangian and Penalty methods. The system of equations is solved segregated way in the augmented Lagrangian approach. Augmentation components for contact pressure and friction traction vector components are introduced. There is an additional iteration level in which the normal displacement variables are solved independently of the contact pressure and traction variables. This process is repeated until the algorithm satisfies a convergence criteria. There are no additional degrees of freedom required for the contact pressure or the friction traction vector when using the penalty technique. These results are calculated from the displacements and the penalty stiffness. This means that no additional solver strategies are required. Although the enhanced Lagrangian technique is more accurate, it has a higher computing cost and requires more fine-tuning to converge [117]. The Penalty technique is less accurate but more robust and requires less solver tuning. Therefore, in this study the penalty method is used to define the contact pair between the tape and central core to achieve a faster convergence.

Contact pair is defined by taking the bottom side of the tape as the destination, and the periphery of the central core is the source. The mesh in the contact layer of the tape is refined by inserting diagonal elements to ensure proper contact during winding. The tape has meshed finer than the central core to achieve better contact. The mesh independent investigation is performed by altering the number of elements in width and length. Taking 8 elements width wise and 200 elements lengthwise provide good results for all winding angles. These findings are comparable to those obtained with finer meshes. The tape has been meshed with 200 elements along the length and 8 elements along the width for all of the following models. The tape thickness is selected so that each material selected has one element in thickness. one layer of Hastelloy and REBCO and two layers of copper. It may be noted that because geometry comprises the thin layer of materials, the tape will have a high aspect ratio. The attempt to lower the aspect ratio will result in a larger number of elements and a more extensive computation.

The following boundary conditions are provided for the modelling: the rigid connector boundary condition is applied to one surface of the central core to provide the rotation and translational movement to the central core. Rotational and translational

motions are applied to the REBCO tape surfaces as pictorially represented in Figure 7.3. The opposite end of the REBCO tape is subjected to a boundary load of 50-100 MPa, and the displacement perpendicular to the tape surface is limited to zero. It may be noted that, in practice, winding stress is usually kept between 50 and 100 MPa.

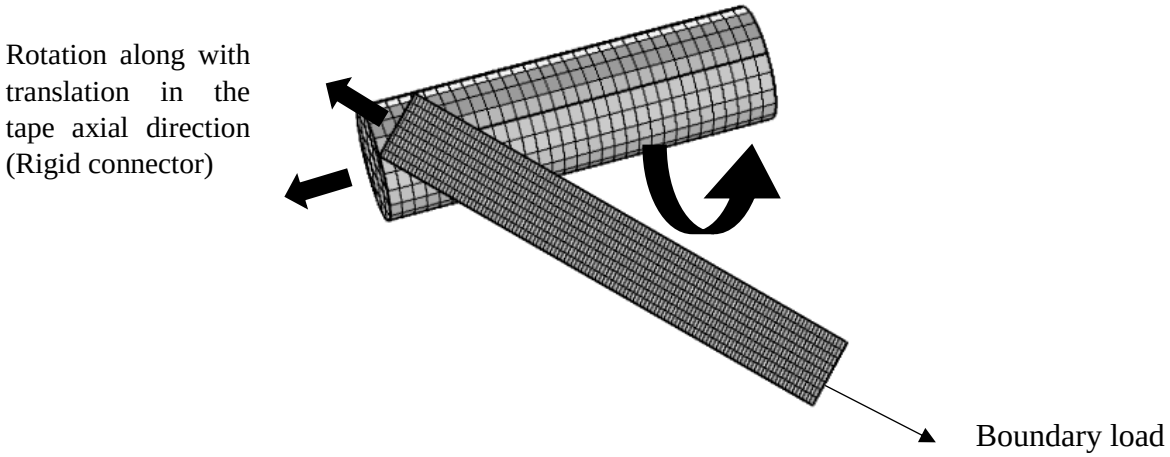

Figure 7.3: Mesh and boundary conditions: REBCO tape and central core.

The convergence is verified using mesh-independent analysis and constant monitoring of the convergence plot. To achieve better convergence, the damping factor is adjusted. The tolerance limit is initially set at 0.001 and later raised to 10^{-6}. Figure 7.3 also depicts the relative movements of the central core and the tape during the winding process.

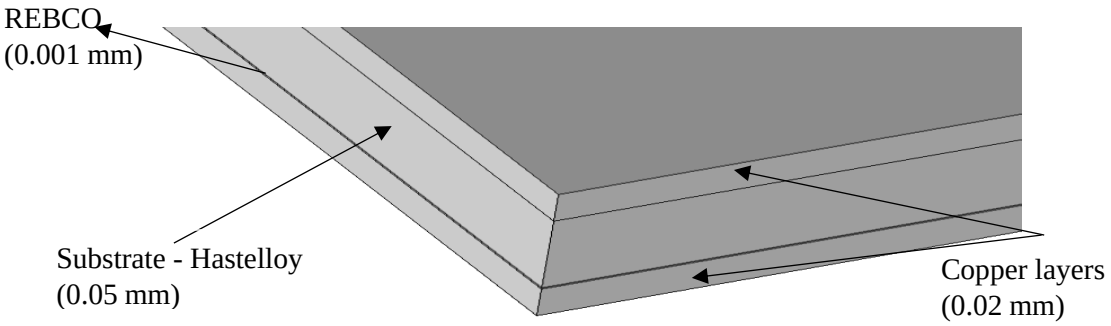

Figure 7.4: Enlarged sectional view of the REBCO Tape.

Figure 7.4 shows a magnified sectional view of the tape. The REBCO layer is placed on the Hastelloy substrate and covered by copper layers on the top and bottom sides. It may be noted that while winding, the side with the REBCO layer faces the central core.

7.4. Results and discussion

7.4.1. Comparison of the present study with literature

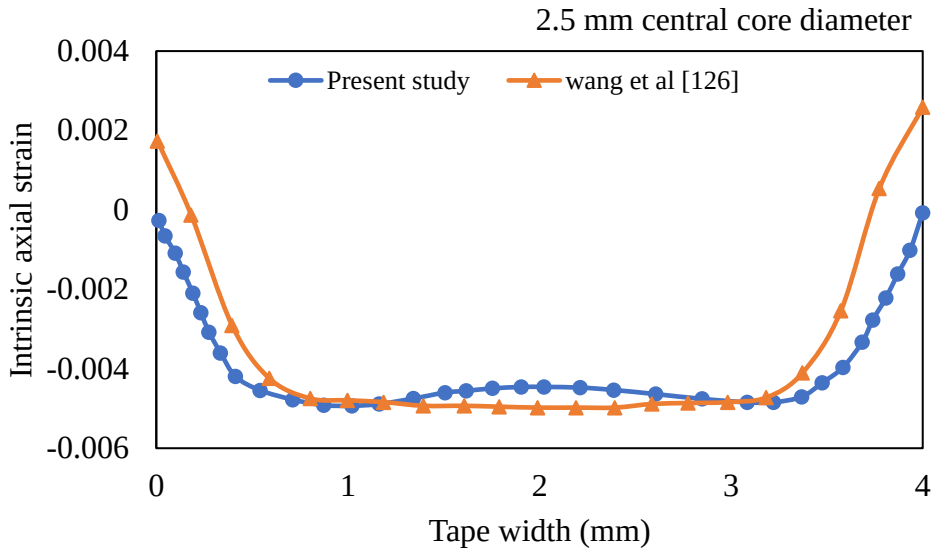

Figure 7.5: Comparison of present study with result published in the literature, Distribution of intrinsic axial strain across the width of the tape when subjected to winding load.

The winding of REBCO tape over a 2.5 mm core diameter shows good agreement with the result published in the literature [126]. It may be observed that there is difference in the edges and the middle portion may be due to the consideration of layered structure, residual strain and consideration of plastic properties in the present study. In both the results, the amplified axial strain can be observed at the centre of the tape. The same has been reported by other studies too [126]. The lack of adjacent support at the edges will result in decreased strain. There is about 11 % difference at the centre of the tape and this increases to about 100 % at the edges. This behaviour is discussed in detail in the subsequent sections.

7.4.2. Development of strain during the cabling

The winding stage is crucial in developing CORC cable because it contributes to strain variations in the superconducting material. Compressive strain is created in the REBCO layer during winding because the side of the tape with the REBCO layer below the neutral axis faces the central core. The winding is initially modelled using an arbitrary central core diameter of 3 mm, using a tape width of 4 mm, with a winding angle of 45°. Figure 7.6 depicts the distribution of intrinsic strain in the REBCO layer after winding. The varied strain pattern generated at the end of the tape is owing to its boundary condition provided.

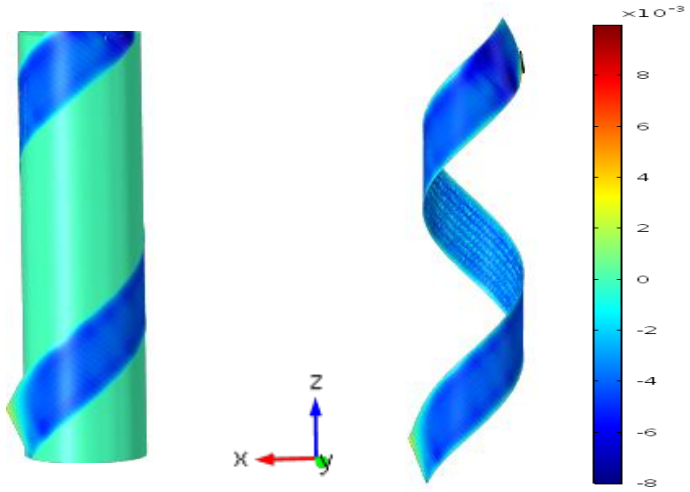

Figure 7.6: Intrinsic axial strain distribution of the REBCO layer for a 3 mm diameter central core, 4 mm tape width, and 45° winding angle

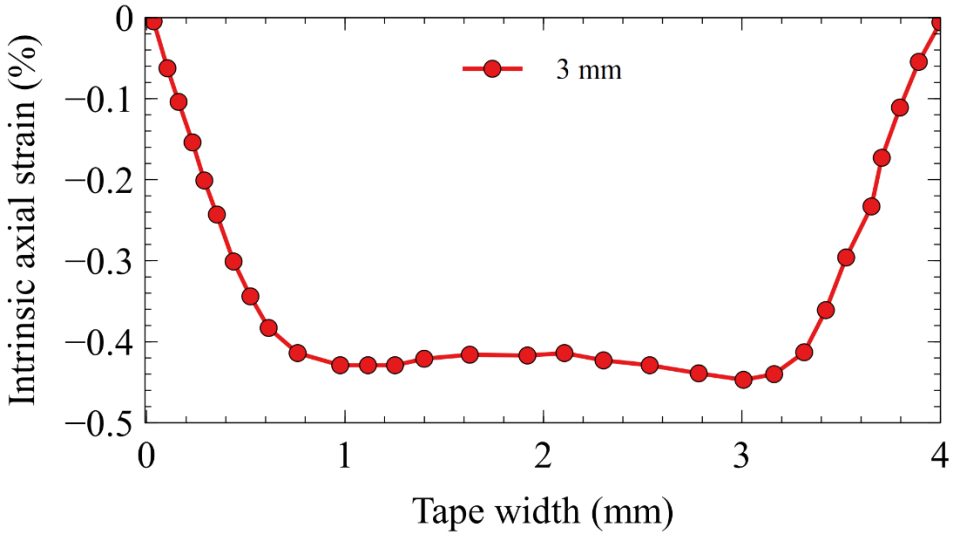

Figure 7.7: Intrinsic axial strain in the REBCO layer vs tape width for a 3 mm diameter central core CORC cable.

Figure 7.7 indicates the strain distribution across the width of the tape. The strain value is varied from -0.06 % to -0.45% across the width of the tape. These values are almost constant at the centre. This variation is mainly due to the combined effect of tension, bending and twisting load during the winding. It may be observed that the maximum intrinsic axial strain developed is -0.45 % and is more predominant at the central portion of the tape compared to the side end. It is also clear that the strain distribution are almost axially symmetric over the width of the tape. This is because REBCO tape is subjected mainly to bending, as it is eccentrically located at the inner side of the tape, closer to the central core.

7.4.3. Variation of central core diameter

The size of the central core is an important parameter during the manufacturing stage of the CORC cable. Smaller the diameter for central core, higher would be the strain development. The diameter of the centre former is varied in five steps, from 7 to 1 mm and the results obtained are presented in Figure 7.8. It may be noted that the tape considered has a width of 4 mm, Hastelloy thickness of 0.05 mm, and copper thickness of 0.02 mm.

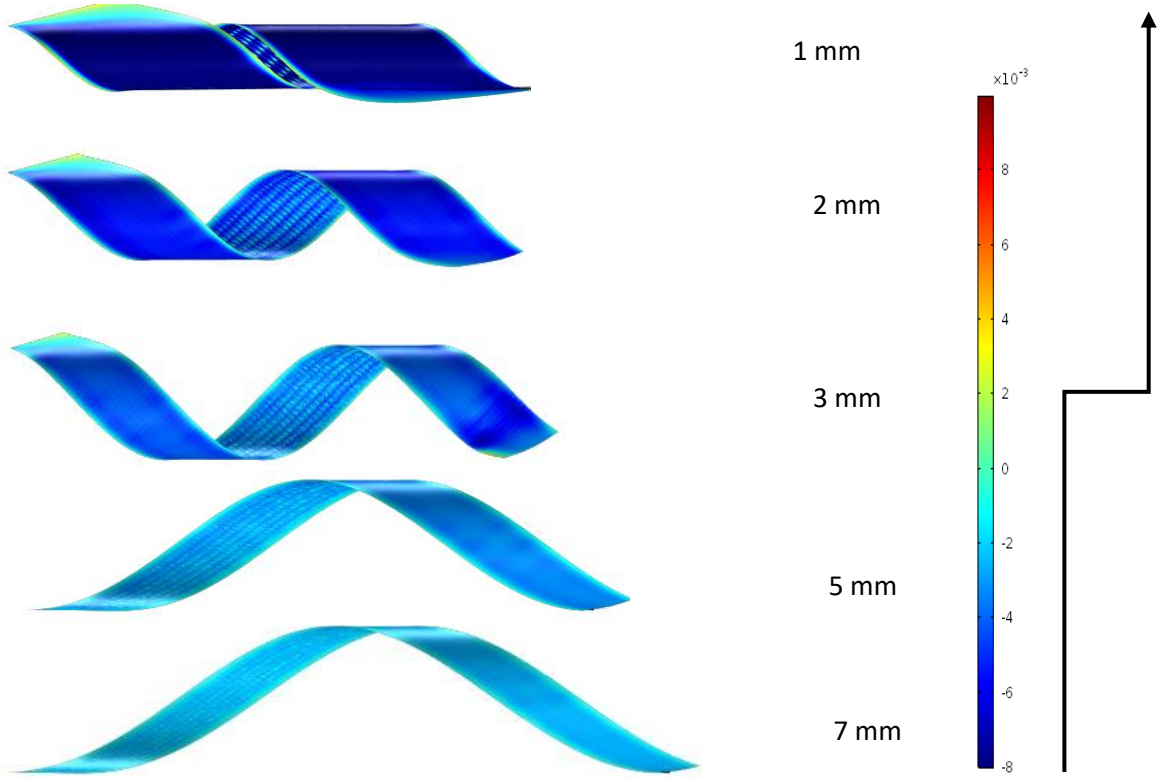

Figure 7.8: Intrinsic axial strain pattern in the REBCO layer for different central core diameters.

Figure 7.9 depicts the effect of variation in intrinsic axial strain in the REBCO layer across width when wound on central core of different diameters. The graph illustrates that for all diameters, the distribution of intrinsic axial strain across the width of the tape is axi-symmetric. It may be noted that the compressive strain generated in the REBCO layer increases as the central core diameter decreases. The bending radius decreases with increasing the radius of curvature of the central core and leads to more strain. Therefore, to reduce the induced strain, central core with higher diameters can be used. For instance, when increasing the core diameter from 1 mm to 7 mm, while the intrinsic axial strain in the REBCO layer drops by 75%.

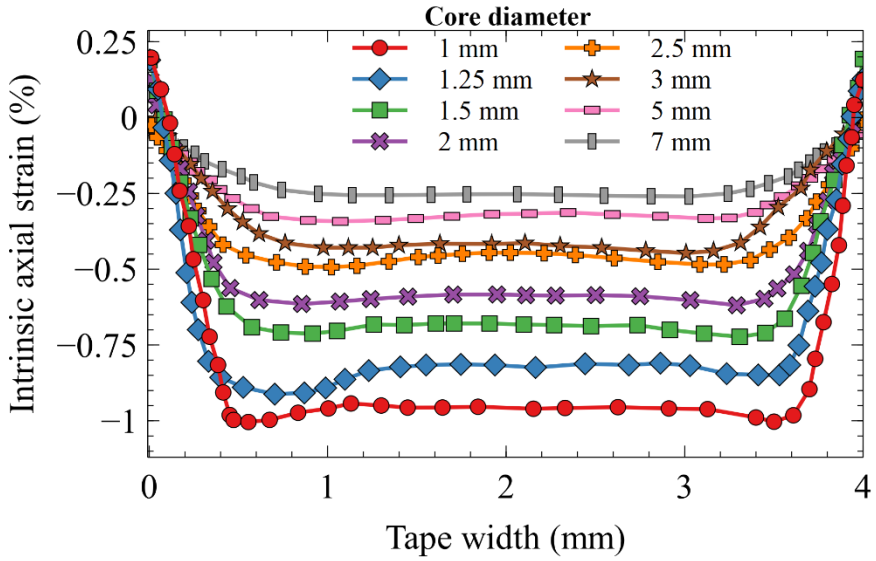

Figure 7.9: Intrinsic axial strain of REBCO layer with different central core diameters

The findings are in good agreement with those of a previous study published in the literature [126]. Both studies show the same trend in the variation of axial strain along the width of the tape for different core diameters. However, as compared to earlier studies, the axial strain values obtained in this work are slightly higher in most cases. This may be because the maximum strain developed in this study is plotted rather than the average strain developed. The differences in values may be also due to the consideration of different material layers than the homogeneous single material assumption of the tape. The consideration of residual strain is also may increase the strain induced in the tape.

It is understood that decreasing the central core diameter results in the development of greater compressive strain. The compressive strain increases with decreasing the central core diameter. However, in practice, using a smaller central core can be significantly advantageous since it approaches the required small round wire

diameter range with a high current density [37]. An attempt is made to determine the limiting diameter for the central former beyond which the strain produced is not within the acceptable limits. This result is presented in Figure 7.10. The diameter of the central former is varied from 7 to 1 mm in eight steps.

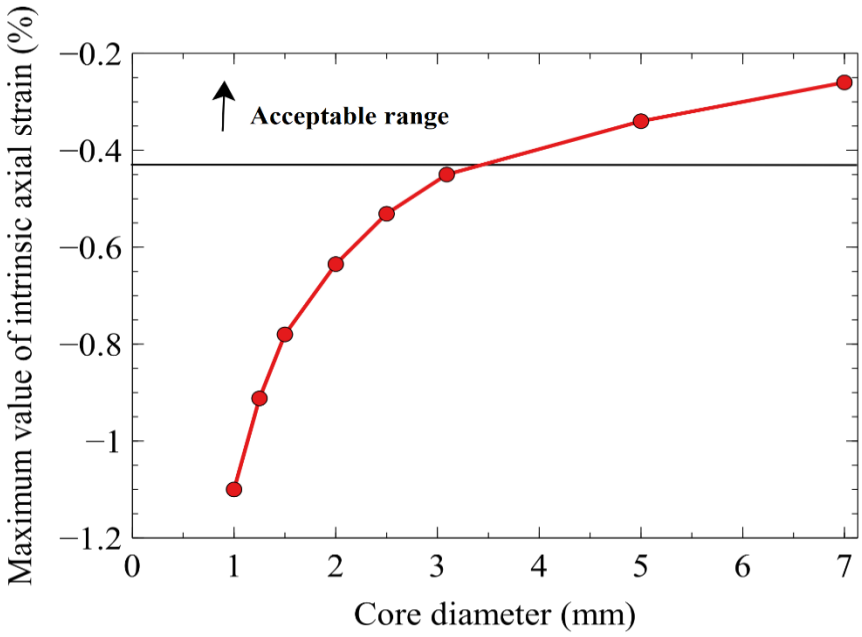

Figure 7.10: Maximum intrinsic axial compressive strain across the width of the REBCO layer with a different central former diameter

It may be observed that when the core diameter decreases beyond 3.43 mm, there is a sudden increase in the intrinsic compressive strain. This is observed at about -0.42 % intrinsic axial strain. So, care must be taken not to reduce the core diameter below 3.43 mm for the given tape configuration and loading conditions.

7.4.4. Variation in winding angle

The angle of winding considerably impacts the strain generation in REBCO tape. The generation of strain for five different winding angles, ranging from 0^o to 60^0 in steps of 15^0 has been found. The thickness of the Hastelloy substrate is 50 mm, and the thickness of the copper stabiliser is 20 mm for this tape configuration. The bending curvature of the superconducting tape gradually reduces as the helix angle rises, as depicted in Figure 7.11. As a result, the axial compressive strain in the REBCO layer decreases as it is visible from Figure 7.11. The induced intrinsic axial strain over the width of the tape is maximum at 0^o winding angle, where the influence of layer twisting is absent.

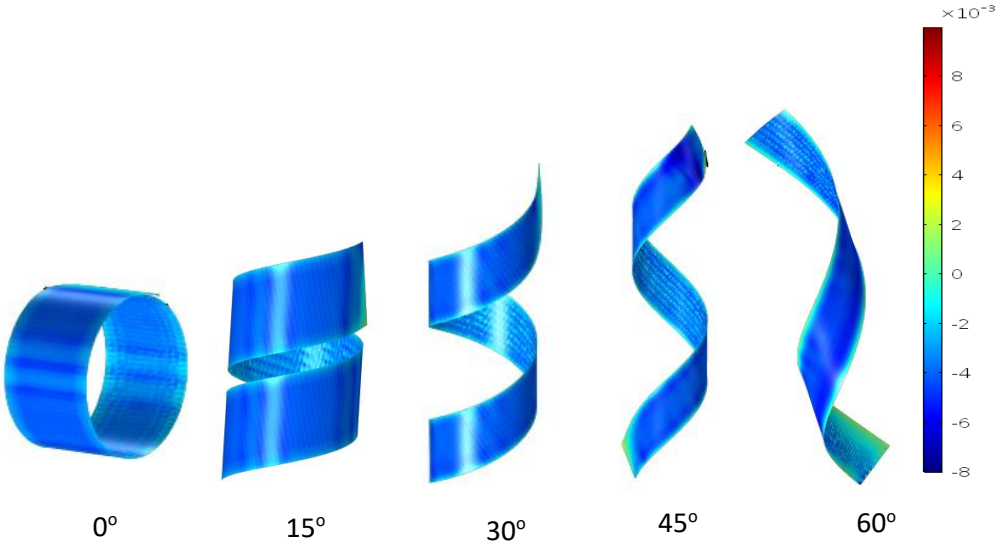

Figure 7.11: Axial strain in the REBCO layer for different winding angles.

Figure 7.12 shows the detailed strain distributions across the width of the tape under different winding angles. It may be observed the strain values are lower for 30° and 45° winding angles.

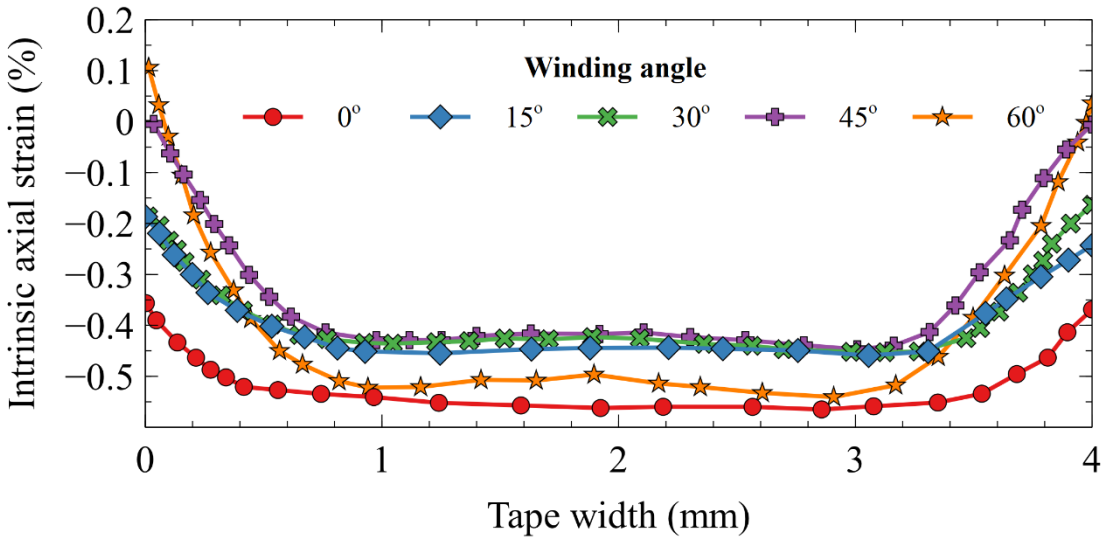

Figure 7.12: Axial strain in the REBCO layer with different winding angles (central former diameter = 3 mm).

D.C.Van der Laan *et al*. reported that the strain sensitivity is maximum when the strain is applied parallel to 0° and 90° directions [17, 37]. It is reported that the critical current is independent of strain when the strain is applied at 45° direction [17, 37]. At 0° winding angle, where there is no influence of twisting and hence torsion strain is the least, the strain distribution is most uniform across the width, indicating close to pure bending

strain. Eventually, the best choice for the winding angle would depend on the application and the anticipated bending radius of the CORC cable.

7.4.5. Substrate thickness variation

The strain generated in the REBCO layer is affected by variations in the thickness of the substrate used to make the superconducting tape. It may be noted that the relative position of the REBCO layer would shift away from the neutral axis if the thickness of the substrate (made of Hastelloy) is increased. As a result, given a thicker substrate the intrinsic axial strain induced during winding increases. Figure 7.13 depicts the difference in strain generation with decreasing substrate thickness for different core diameters.

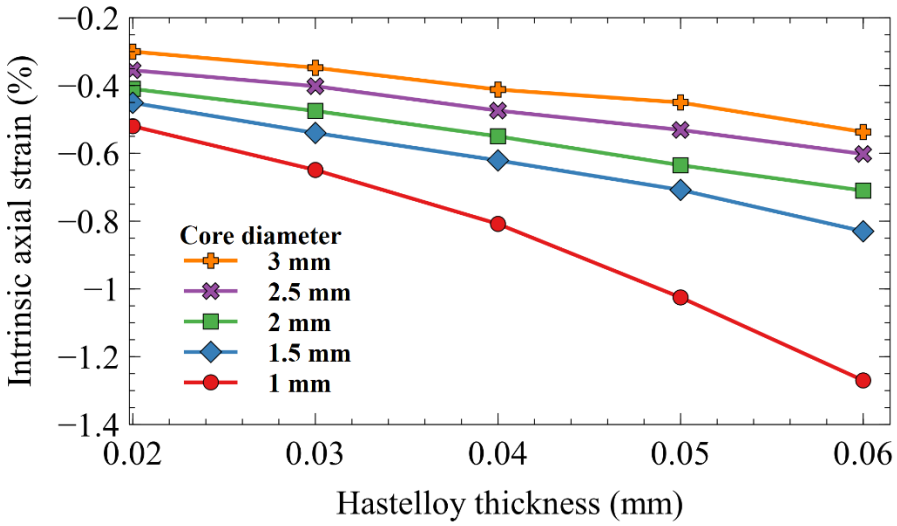

Figure 7.13: Maximum axial tensile strain in the REBCO layer vs substrate thickness for different central former diameters from 1 to 3 mm and α =45°

It may be noted that winding involves both bending and twisting effects in the tape. Compression occurs in the layer below the neutral axis, and tension occurs in the layer above the neutral axis during bending. The graph illustrates that decreasing the thickness of Hastelloy reduces compressive strain in the REBCO. This is observed for all core diameters. It may also be observed that reducing the thickness of the substrate has a greater impact when the core diameter is small. Therefore, using a thinner substrate to reduce the total thickness of the wire is an effective way to increase the critical current density of the REBCO tape [80]. It may be noted that when reducing the Hastelloy thickness from 0.06 mm to 0.02 mm at 1 mm core diameter, the compressive strain decreases by 59 %, and by 44 % at 3 mm core diameter. For a previous study reported in the literature [126], the results follow the same pattern. However, the graphs are steeper

than the current one. This could be due to a variation in modelling technique and the relaxation of homogeneity.

7.4.6. Effect of tape width

The effect of tape width on strain in the REBCO layer is studied. The tape width is varied from 1 to 5 mm in steps of 0.5 mm. The thickness of the Hastelloy substrate is kept as 0.05 mm, the thickness of the copper stabiliser at 0.02 mm, and the winding angle at 45^{o}. The results are depicted in Figure 7.14. Results show that the difference and distribution of strain caused differ with tape width. In addition, a wavering strain pattern is visible in the strain distribution plot. The reason for this pattern could be due to plastic deformation, as observed in a long membrane. Lin and Wickert also report similar observations in the open literature [134].

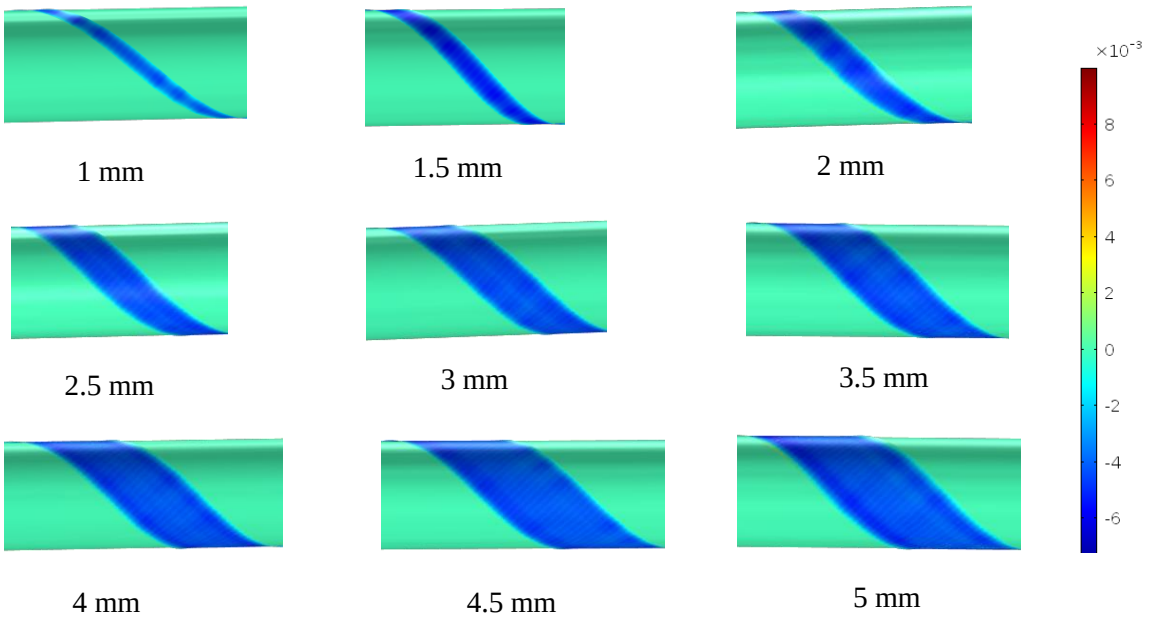

Figure 7.14: Axial strain distribution in REBCO layer for different tape width

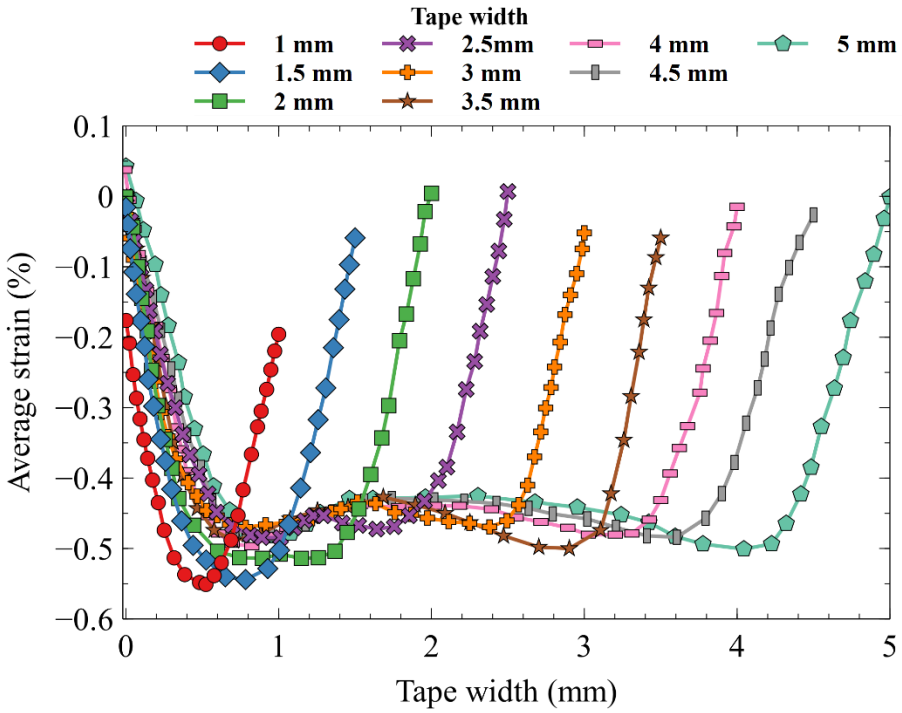

Figure 7.15: Average axial strain in the REBCO layer vs tape thickness (central former diameter = 3 mm and α =45^{o}).

Figure 7.15 depicts the variation of the intrinsic strain in the REBCO layer across the width of the tape for each tape width. It may be noted that when the tape width is increased, the maximum strain produced decreases at the centre portion. For all tape widths, the maximum strain in the tapes remains near about 0.5 %. The warpage effect is more prominent in tapes having smaller width, and the compressive strain level decreases as tape width increases especially at smaller widths. The findings are in agreement with a previous study published in the literature [126]. As the width of the tape increases, the strain level in the superconducting layer drops. Further, as the tape width increases, the maximum strain caused reduces at the centre portion, but the maximum value remains nearly constant in all cases.

7.4.7. Combined variation of thickness of copper, Hastelloy layers, and tape width on winding for different core diameters

It may be observed that the compressive strain in the REBCO layer increases as the Hastelloy thickness increases. Figures 7.16 and 7.17 show how the maximum compressive strain varies with changes in Hastelloy thickness from 0.05 to 0.02 mm at 0.02 mm and 0.01 mm copper thickness, respectively. The maximum strain value appears to converge to a single point as the Hastelloy thickness reduces from 0.05 mm to lower

values. It is also evident that the variation in maximum strain in the REBCO layer is more significant for smaller core diameters. When the Hastelloy thickness is reduced from 0.05 to 0.02 mm, the change of maximum strain at 1 mm core diameter is 47 %.

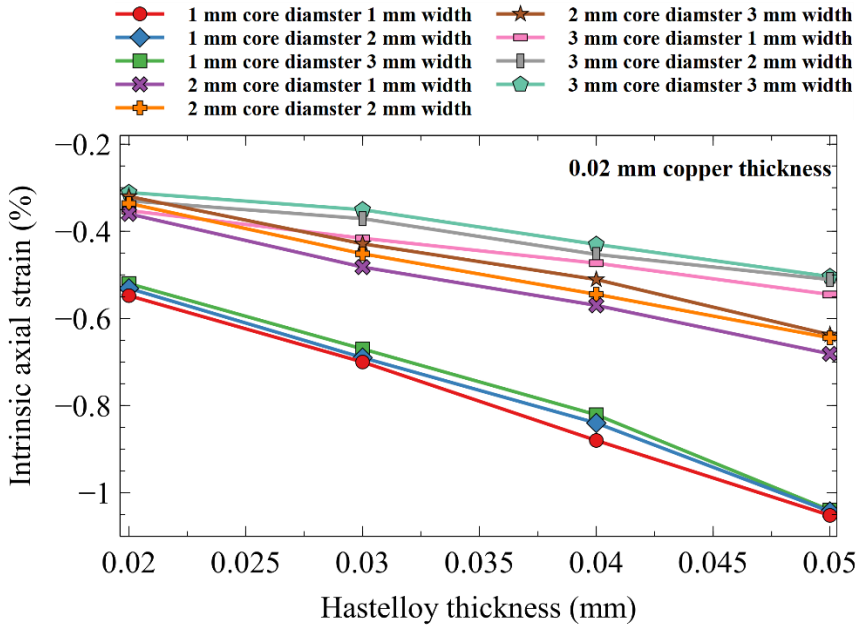

Figure 7.16: Maximum intrinsic compressive strain in REBCO layer vs Hastelloy thickness (0.02 mm copper thickness)

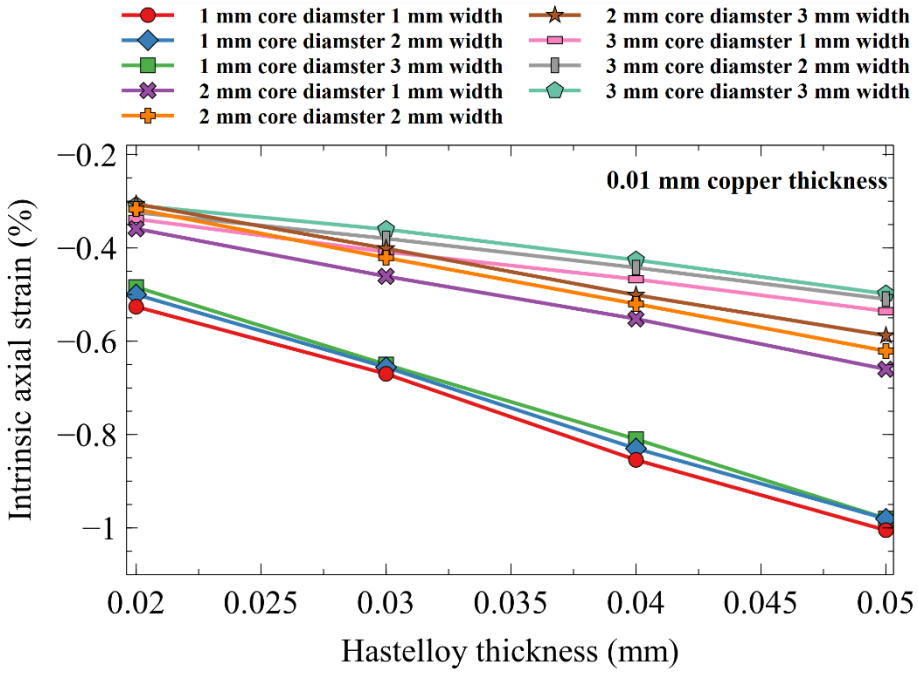

Figure 7.17: Maximum intrinsic compressive strain in REBCO layer vs Hastelloy thickness (0.01 mm copper thickness)

A maximum strain variation of 52 % is reported for 0.02 mm copper and 0.05 mm Hastelloy thickness (at 1 mm core diameter). When the core diameter increases from 1 to 3 mm for the Hastelloy thickness of 0.02 mm, the variation reaches its maximum of 43%. Similarly, when the core diameter increases from 1 to 3 mm, the maximum strain variation is 50% for 0.01 mm and 0.05 mm copper and Hastelloy thickness respectively. These variations are more significant as the copper thicknesses is increased.

7.5. Electrical performance of simple CORC cable/ wire

The electrical performance of superconducting CORC cable with the help of data published by SuperPower on Yttrium Barium Cupric Oxide (YBCO) is discussed. Electrical performance of the superconducting tape may get affected during the winding process because of the strain induced. Therefore, the induced strain is computed for different cases of core diameter, winding angle and thickness of various layers of the tape. The results obtained are substituted in the empirical equation to determine critical current retention of the tapes. Detail explanation of the empirical equation is provided in section 6.6.1. [83].

Figure 7.18 depicts the variation in critical current retention with changes in core diameter. The critical current retention drops as the core diameter decreases. This is due to an increase in the radius of curvature, which results in higher compressive bending strain in the REBCO layer. This strain causes the tape to degrade. For instance, it can be observed from the figure that when the core diameter is reduced from 7 mm to 1 mm, the critical current retention is decreased by nearly 40%.

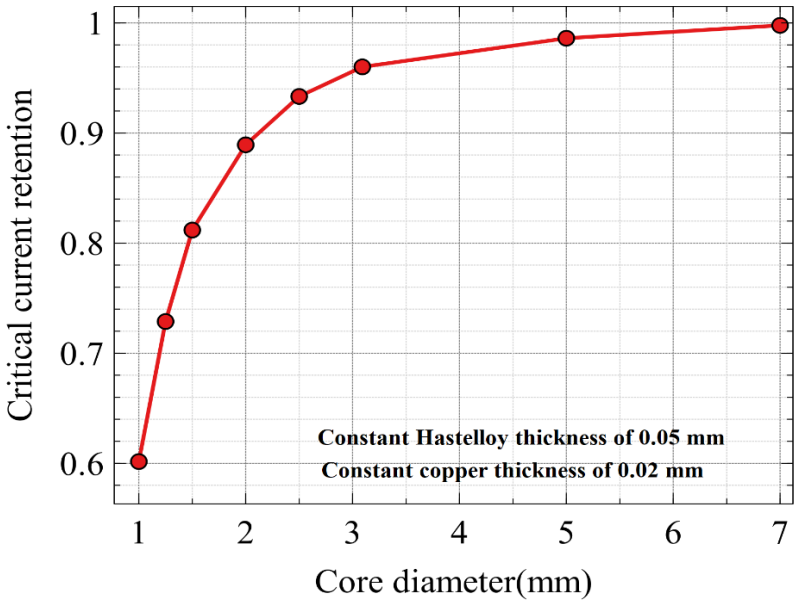

Figure 7.18: Variation in critical current retention with changes in core diameter.

The winding angle is varied from 0° to 60°, and the critical current retention is plotted against the winding angle, as shown in Figure 7.19. When the winding angle is changed from 0° to 45°, it can be observed that the critical current retention capacity of the cable/wire increases. When the winding angle is increased beyond 45°, the critical current retention capacity drops.

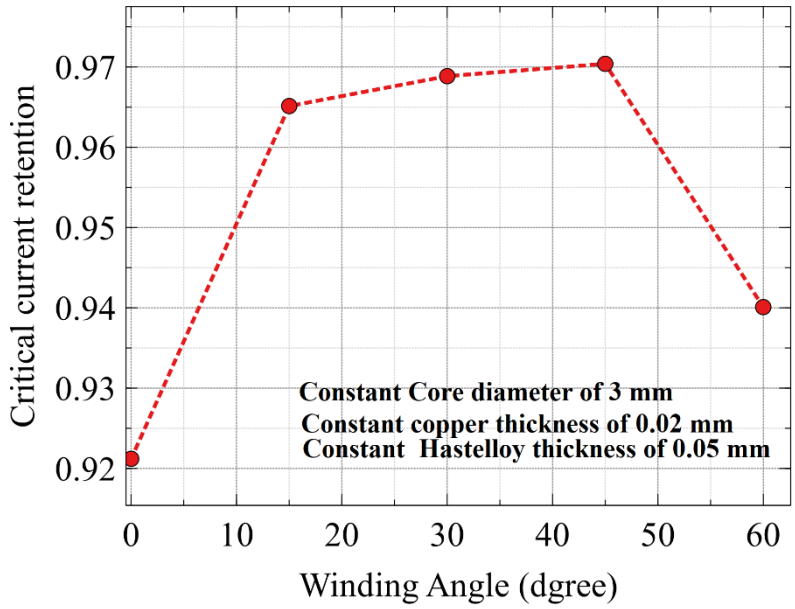

Figure 7.19: Variation of critical current retention with change in winding angle

It may be observed that when the REBCO tape is wound on a 3 mm central core, the critical current retention capacity drops only by 3% at a 45° winding angle. The maximum degradation is occurring at a 90°/0° winding angle. Therefore, it may be understood that 45° is the best angle for winding. Similar findings are also reported by D. C. van der Laan *et al*. [37].

Figure 7.20 illustrates the critical current retention in the REBCO tape for various Hastelloy thicknesses. As the Hastelloy thickness increases, the critical current retention in the REBCO layer reduces. When the Hastelloy thickness is increased from 0.02 mm to 0.06 mm, the critical current retention drops by 47.4 % and 6.2 % for 1 mm and 3 mm core diameters, respectively.

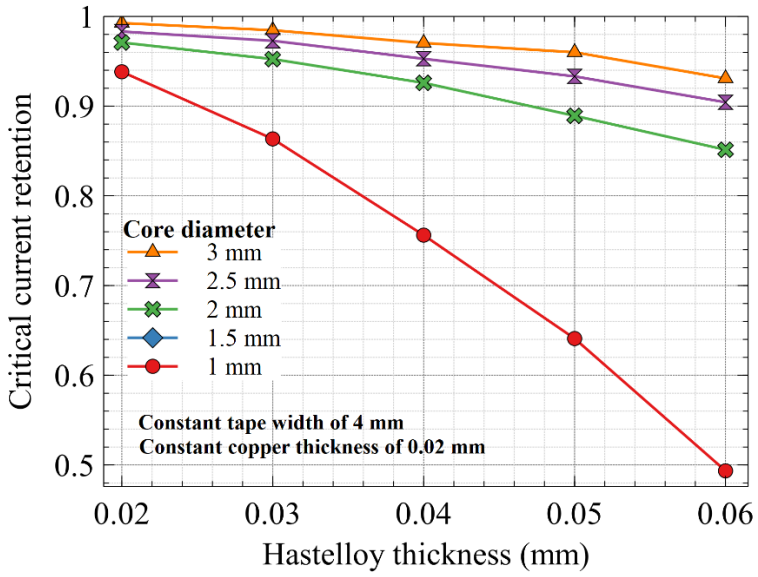

Figure 7.20: Variation in critical current retention with changes in Hastelloy thickness for different core diameters

Therefore, CORC cables with smaller core diameters degrade faster than those with larger ones. The radius of curvature for the winding increases as the core diameter decreases during winding. More strain is developed in the REBCO layer as the radius of curvature increases, resulting in higher level of degradation in the critical current.

Figure 7.21 depicts the variation in critical current retention with changes in Hastelloy thickness for various core diameters and tape widths. The critical current retention increases as the Hastelloy thickness is decreased from 0.05 mm to 0.02 mm. It also be observed that the change in critical current retention in the REBCO layer with changes in Hastelloy thickness is more significant for small core diameters.

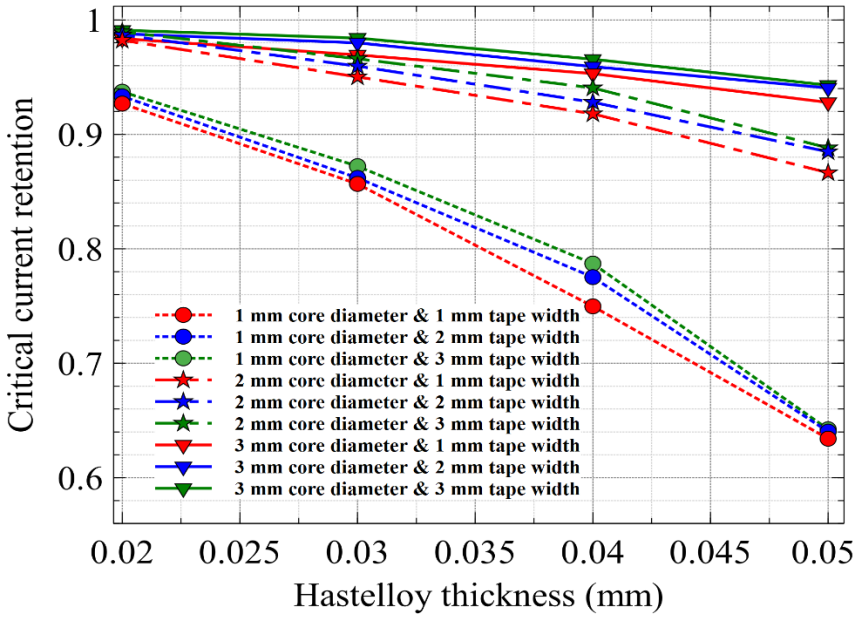

Figure 7.21: Variation in critical current retention with changes in Hastelloy thickness for different core diameters and tape widths.

Therefore, consideration have to be taken while increasing the thickness of the Hastelloy layer. When the Hastelloy thickness is increased from 0.02 to 0.05 mm, the critical current is reduced by 31.6 % for 1 mm core diameter. This is because as the Hastelloy thickness increases the distance between the neutral axis and the REBCO layer increases. As a result, the intrinsic axial strain induced during winding increases, and hence affects the critical current retention. Changes in tape width is found to have minor influences on critical current degradation than changes in core diameter. When the core diameter is reduced from 3 mm to 1 mm, the critical current is reduced by 31.9 % and 5.5 % at 0.05 mm and 0.02 mm Hastelloy thicknesses. Figure 7.22 depicts the variation in critical current retention with modifications in Hastelloy thickness for various copper thicknesses. The critical current retention in the REBCO layer lowers as the Hastelloy thickness increases.

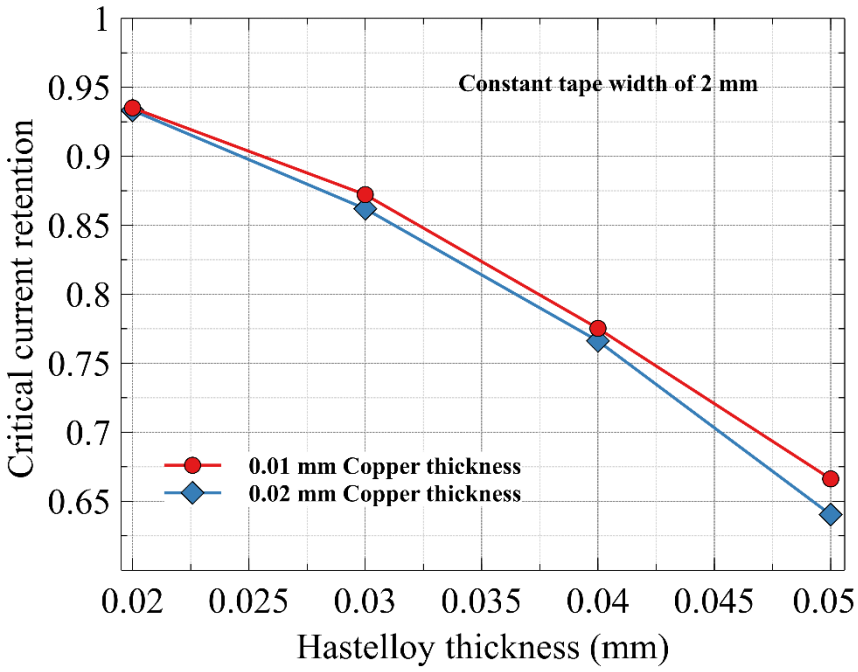

Figure 7.22: Variation in critical current retention with changes in Hastelloy thickness for different copper thicknesses

It has also been found that increasing the copper thickness leads to critical current degradation. It can be related to the neutral axis shift as well as interfacial bonding between various layers. When the Hastelloy thickness is increased from 0.02 mm to 0.05 mm, the critical current is reduced by 31.4 % and 28.7 % for 0.02 mm and 0.01 mm copper thicknesses, respectively. This is also shows that when compared to Hastelloy thickness, the influence of the copper thickness on critical current retention is less significant.

7.6. Summary

Modelling of REBCO tape is performed to examine its degradation upon winding loads for different winding patterns and tape parameters. The strain created in the REBCO layer is the result of the combined effects of axial tension, compression, bending, and torsion. The strain generated under various conditions is estimated and compared to ensure that the strain remains within the degradation limits. The result indicates that the compressive intrinsic axial strain in the REBCO layer increases when the central core diameter decreases. When the thickness of the substrate is reduced, the compressive strain in the superconducting tape decreases. It is also observed that the best winding angle is 45^{o}. The strain in the superconducting layer decreases as the tape width increases and

warpage caused by twisting is more evident on tapes with a smaller width. The influence of Hastelloy thickness and core diameter on winding is determined. When the Hastelloy thickness decreases from 0.05 to 0.02 mm, at 1 mm core diameter, the variation of maximum strain is 47 % and 52%, at 0.01 and 0.02 copper thickness, respectively. The compressive strain increases by 43 % when the core diameter decreases from 3 to 1 mm, at 0.02 mm Hastelloy thickness. Varying the thickness of copper layer is found to have comparatively less significance on the REBCO tape. A similar trend is observed in the case of critical current retention as well.

Publication arising out of this chapter

- **Ashok KB**, Thomas RJ, Prakash MJ, Nijhuis A (2021) Performance limits in REBCO tape for variation in winding parameters of CORC cable and wire, Elsevier, Physica C: Superconductivity and its applications, vol 582, 15 March 2021:1353828. https://doi.org/10.1016/j.physc.2021.1353828. (Impact factor: 1.54)

Chapter 8

Effect of different fatigue loads on the degradation of the REBCO superconducting tape

8.1 Introduction

The effect of different mechanical loads on the degradation of REBCO tape is investigated in chapters 4-7. Apart from these normal mechanical loads, another significant load is the fatigue type of loading. One of the sources of fatigue type of load is repeated thermal cycling during the usage phase, where the tape temperature changes from room condition to cryogenic temperature. In addition to this, the tape may be subjected to repeated mechanical loads during its installation and operating stage. The repeated thermal and mechanical load cycles affect superconductor performance and cause the tape to degrade. Another source for fatigue load is due to the Lorentz force developed when alternating current passes through the superconductor. Fatigue load is

experienced in the case where REBCO tape is used in rotating machines like motors and generators. This is happening due to the development of centrifugal stress. Carrying out the high-cycle fatigue at cryogenic temperature is costly and time-consuming. Numerical modelling has huge potential to overcome this challenge and avoid the use of sophisticated experimental facilities. This chapter investigates the fatigue strength or limit of superconducting REBCO tape subjected to different cyclic mechanical loads, such as tension, bending, and torsion. The influence of changing the thickness of Hastelloy and copper layers on fatigue strength is also studied.

8.2 Modelling

The phenomenon of a component failing after repetitive loading and unloading is referred to as fatigue. However, the magnitude of each load applied under repeated loadings is smaller than the material's ultimate stress. The numerical simulation model is developed using the fatigue module of COMSOL Multiphysics. In the first stage, the mechanical load is applied using the solid mechanics module in COMSOL Multiphysics. The repeated load is applied using the fatigue module to calculate the Fatigue strength/ Fatigue usage factor. Different type of fatigue modelling approaches are used to carried out the fatigue analysis. The major models are stress based, strain based, stress life based, strain life based, energy based etc. [135]. Stress based and stress life-based approaches are best suited for high cycle fatigue analysis. However, this work is concentrated on stress-based approach. Findley Criterion, Matake Criterion, and Maximum Normal Stress Criterion are most widely used stress-based approaches. Matake approach is best suited for the brittle and ductile materials so the work is further concentrated on the same [115]. For stress based High Cycle Fatigue, Matake criteria are used to evaluate the Fatigue usage factor (FUS). Utilizing the critical plane approach, multiple orientations in space are evaluated to determine the critical plane where fatigue is anticipated to occur. Stress-Based Fatigue Models predict a fatigue usage factor (FUS), which is the ratio of the applied stress to the stress limit. This implies that the stress limit has been exceeded and failure is expected, or that the component will maintain its quality throughout the anticipated fatigue life. The fatigue usage factor is opposite to the safety factor.

$$Fatigue\ Usage\ Factor\ (FUS) = \frac{Applied\ stress}{Fatigue\ Strength} \tag{8.1}$$

In this criteria, the critical plane is calculated based on the shear stress value in each plane. When the shear stress value is maximum, it is considered the critical plane, and the maximum normal stress is evaluated on that plane.

$$\left(\frac{\Delta\tau}{2}\right)_{max} + k\sigma_n = f \tag{8.2}$$

Where '$\Delta\tau$' is the maximal shear stress range on a plane, 'σ_n' is the normal stress on the same plane, 'k' and 'f' are material properties.

$$\frac{\sigma_a}{2}\left(1 + \frac{k\sigma_{max}}{\sigma_a}\right) = f \tag{8.3}$$

Material properties 'k' and 'f' values are calculated using the experimental data available in the literature (σ_{max} = 669 MPa, and the stress ratio is 0.1) [106]. 'σ_{max}' and 'σ_a' are maximum stress and stress amplitude respectively. The geometry and dimension of the REBCO tape considered for the study are shown in Figure 8.1. A tape of 5 mm length, 4 mm width, and 0.093 mm thickness is modelled to carry out the numerical simulation. Compared with previous mechanical analyses, here silver overlayer is also considered for the analysis to measure its influence on the REBCO tape's degradation.

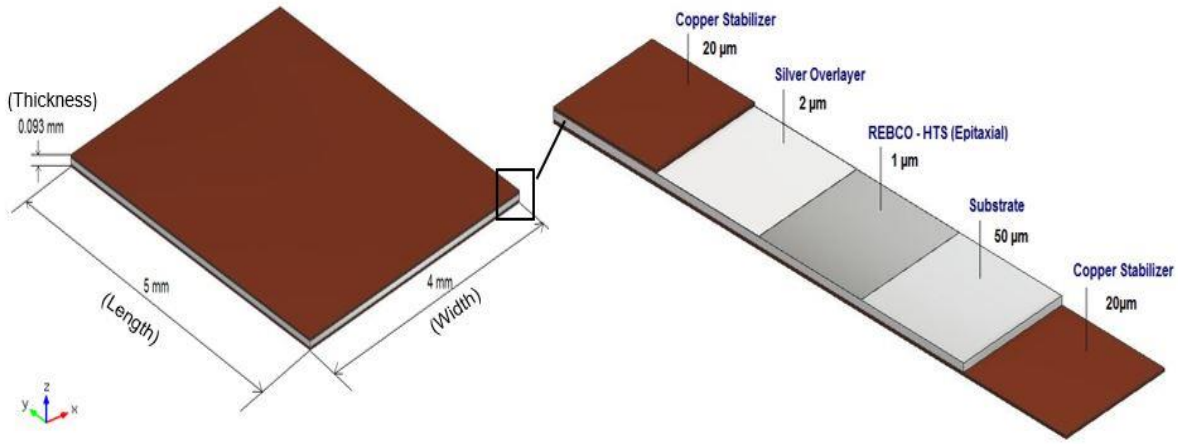

Figure 8.1. HTS REBCO tape modelled and its constituent layers

The tape production process and mechanical loading are similar to tensile, bending and twisting cases investigated earlier in this study. However, for providing the fatigue type of loading, a repeated load of 10^6 cycles is applied and the FUS values are evaluated using the fatigue module. The material parameters, 'f' and 'k' are calculated using a dedicated Matlab code.

Figure 8.2 shows the relationship between the limit and normal sensitivity coefficient. It may be observed that the limit factor increases linearly with the normal sensitivity coefficient.

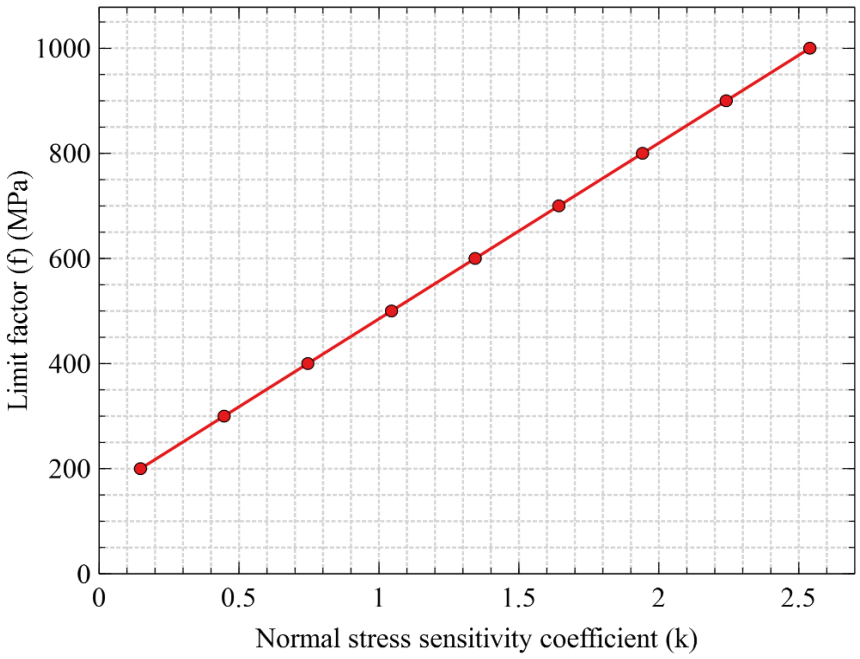

Figure 8.2. k and f material parameter function for Matake criterion

The mesh independent study is carried out to fix the mesh in the analysis. For tensile cyclic loading, 30x24x6 mesh size, and for bending and twisting loads, 42x30x6 mesh size are taken for the analysis

8.3 Comparison of numerical and experiment results

The numerical simulation result is successfully validated with the experimental data from the literature [106], as depicted in Figure 8.3. Applied stress is provided on the x-axis and fatigue strength on the primary y-axis. The percentage deviation of experimental and numerical simulation results is represented on the secondary y-axis. The fatigue strength of REBCO layer calculated experimentally is reported in the literature and the value is 609 MPa [106].

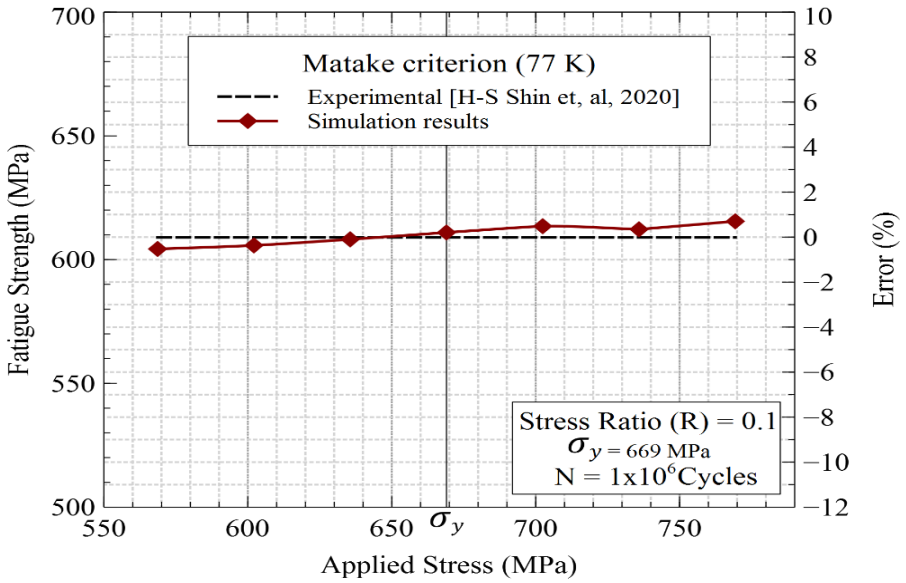

Figure 8.3: Comparison between simulation (Matake) and experimental results [106]

The comparison between the two sets of data shows that the maximum percentage deviation between the experimental and numerical simulation results is less than 1 %.

8.4 Results and discussion

Unlike simple tension, bending or torsional loading, the repeated cyclic loading has multiple influences on the degradation of the superconducting tape. Changes in the FUS values of the REBCO tape subjected to tensile, bending and torsional repeated cyclic load are discussed in detail as separate sections. The impact of changing the thickness of Hastelloy and copper layers on the FUS value is also investigated in each case of tensile, bending and torsional fatigue loading.

8.4.1 Cyclic tensile loading

While maintaining temperature at 77 K, repeated cyclic tensile loads are applied to the superconducting tape in terms of stress value. The maximum applied stress is varied from 569 to 769 MPa in 6 steps by keeping the stress ratio constant at 0.1. The results show that upon cyclic tensile loading, the values of FUS are different for different layers and this is depending on the type of the layer material. Also, it is found that the FUS values are not the same within a layer and they change with their position in the layer. The degradation of the superconducting tape is expected to get initiated at the point where

the FUS values are maximum. Figure 8.4 shows the variation of maximum FUS values for each layer while changing the applied stress.

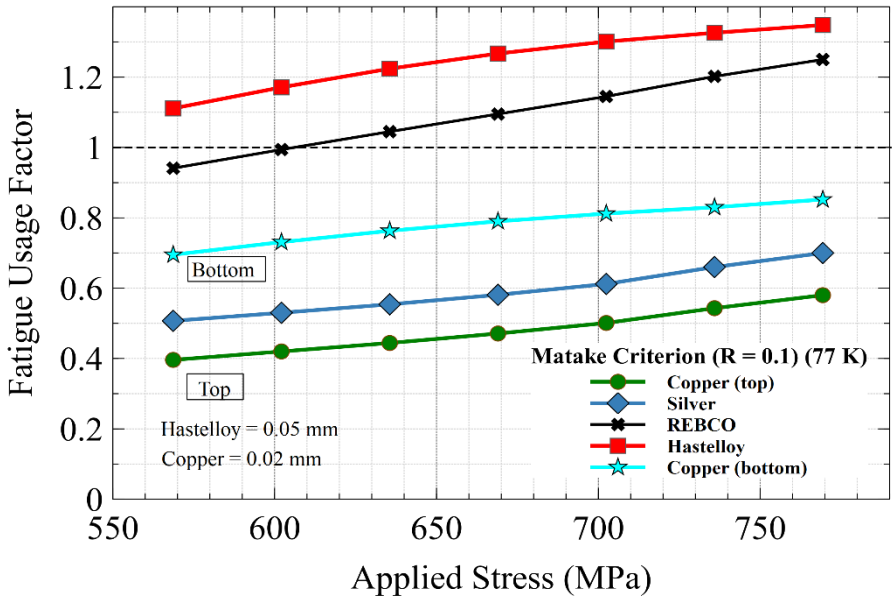

Figure 8.4. FUS variations of different layers with applied tensile stress

It may be observed that the maximum value of FUS increases with the increasing applied stress in all the layers. The FUS value and the applied stress seem to have an almost linear relationship. It is also observed that in the entire load range, the FUS values of the Hastelloy and REBCO layers have crossed their fatigue strength (FUS > 1). Beyond this point, cracks may be found in the layers and may propagate into other layers, eventually degrading the entire tape. The order in which each layer may fail can be predicted from their relative maximum FUS values. Accordingly, from Figure 8.4, it may be understood that the Hastelloy layer that has the highest FUS is the first to fail. This is followed by REBCO, bottom copper, silver and top copper layers. Since there is no degradation found in the REBCO layer up to 609 MPa, the tape would be able to carry the same amount of electrical power through the intact REBCO layer. For loads beyond 609 MPa, the tape will fail as the maximum FUS values of the REBCO layer is above its fatigue strength. It may be noted that this is in spite of the fact that the maximum FUS values of copper and silver layers are less than one for the entire range.

It may be observed from Figure 8.4 that though the FUS values on the Hastelloy layer cross the limit (value > 1), there is no degradation found in the REBCO layer. Similar results have been obtained in an experimental study reported in the literature [7].

It was found that though there is a failure in the Hastelloy layer, a corresponding degradation in the current carrying capacity is not observed in the REBCO tape. Results of this simulation study also substantiate this finding. Therefore, tape would be able to carry the same amount of electrical power through the intact REBCO layer.

Upon the application of cyclic tensile load the maximum FUS values are changing. Therefore, it is interesting to find out the distribution of FUS values within an entire layer. Such a graph will help us to identify the critical regions within a layer that may be expected to fail first. The FUS distribution over the surface of the REBCO and Hastelloy layers only are taken into consideration as the FUS values of other layers are below one. The changes in the FUS values under cyclic tensile load for REBCO and Hastelloy are depicted in Figures 8.5 and 8.6 respectively. For these cases, a repeated cyclic tensile load of 669 MPa is applied to the superconducting tape at 77 K, and for a stress ratio of 0.1. It may be noted that the same case is used for the validation. The adjacent layers and the properties of each layer influence the FUS values within a given layer. As a result, the FUS values would be different for the top and bottom surfaces of each layer. Therefore, in Figures 8.5 and 8.6, the distributions of FUS values are separately plotted for the top and bottom surfaces of the REBCO and Hastelloy layers. It may be noted that the REBCO layer is deposited above the Hastelloy substrate. Therefore, the FUS values in the bottom layer of REBCO will also be influenced by the changes in the top surface of the adjacent Hastelloy layer. Similarly, the FUS distribution in the top surface of the REBCO layer will be affected by the bottom surface of the silver layer, which is above it. Figure 8.5 shows the distribution of FUS values of the top and bottom surfaces of the REBCO layer.

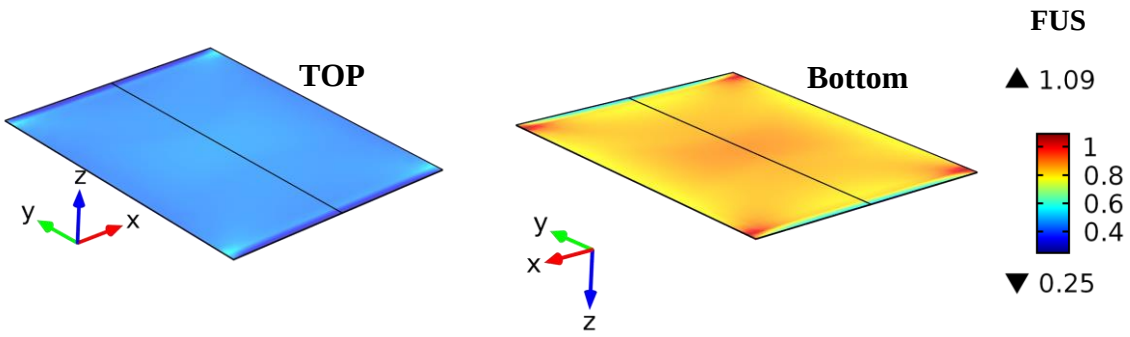

Figure 8.5. Distribution of FUS value of REBCO layer on it's a) top layer surface b) bottom layer surface.

It may be observed that the FUS values in the top surface of the REBCO layer is lower than those in the bottom layer. This is due to the fact that the maximum FUS values in the Hastelloy layer is higher than those in the REBCO layer as evident from Figure 8.4. In addition to this Figure 8.5 depicts that the FUS values are at their maximum at the corners of the tape; this is true for both the top and bottom layers. Therefore, it may be expected that the failure in these layers may get initiated from the corners. It may be due to the higher stress concentration at the edges because of absence of the side support at any edge. The maximum FUS value experienced in the REBCO layer is 1.09 and are at the corners of bottom surface.

The distribution of FUS values of the top and bottom surfaces of the Hastelloy layer is shown in Figure 8.6. It may be noted that the adjacent layer to the top surface of the Hastelloy layer is the REBCO layer. And the adjacent layer of the bottom surface of Hastelloy is the bottom copper layer.

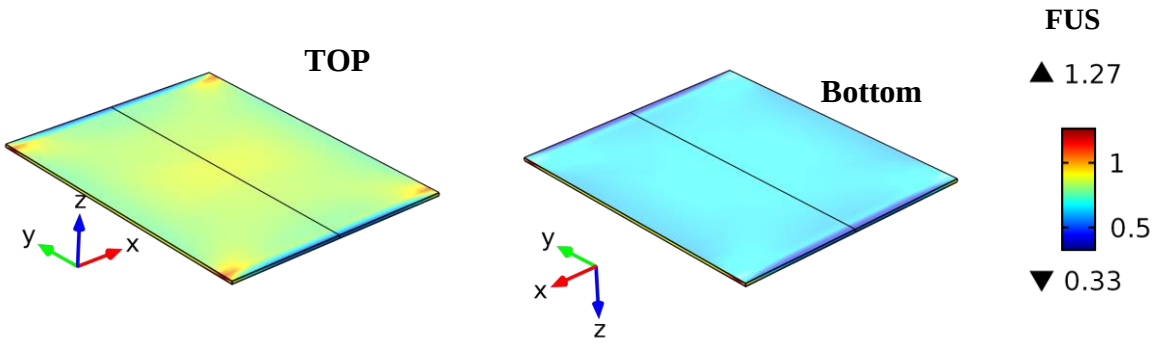

Figure 8.6: Distribution of FUS value of Hastelloy layer on it's a) top layer surface and b) bottom layer surface.

It may be observed that the FUS values in the top surface of the Hastelloy layer is higher than those in the bottom layer. The FUS values in the bottom layer of Hastelloy is not much influenced by the top surface of the adjacent copper layer. However, the FUS distribution in the top surface of the Hastelloy layer is affected by the bottom surface of the REBCO layer above it. This is due to the fact that the maximum FUS values in the REBCO layer is higher than those in the bottom copper layer (as evident from graph shown as Figure 8.4). For both the top and bottom surfaces of Hastelloy, the FUS values are maximum at the corners. The maximum FUS value experienced in the entire Hastelloy layer is 1.27 at the corners near to the top layer.

8.4.2 Parametric studies under cyclic tensile loading

The cyclic tensile load has been provided with a stress ratio of 0.1 to determine the FUS values. However, a more realistic fatigue loading would be with a stress ratio of -1 where the tape is subjected to alternatively to tensile and compressive loads in a cyclic manner. This would be the worst-case scenario and it is necessary to determine the region where the FUS values cross their fatigue limit and may get degraded. At the load of 669 MPa and 0.1 stress ratio, REBCO tape is already in the degraded region. For providing a stress ratio of -1, the load is reduced to half (669/2 MPa) and the FUS values are calculated. However, for this case, it is found that the tape is in the degraded area. Therefore, the load is further reduced to almost one by forth of 669 MPa so that the region for degradation can be identified. At a tensile load of 130 MPa (669/4), the tape is found to be in the transition region for degradation. Under these conditions the effect of changing the geometrical parameters of the tape is carried out. The thickness of the Hastelloy layer is varied from 0.02 mm to 0.05 mm and copper thickness is varied from 0.01 mm to 0.04 mm. While varying thickness of one layer, that of the other layers are kept constant. The individual parametric studies are presented in the subsequent sub-sections.

8.4.2.1 Effect of Hastelloy thickness on FUS value

The effect of variation of FUS value with changes in Hastelloy thickness for Hastelloy, REBCO and silver layers are represented in Figure 8.7. It can be observed that a thicker layer of Hastelloy can bear more load compared to thinner one as the FUS value increases with decreasing the Hastelloy thickness.

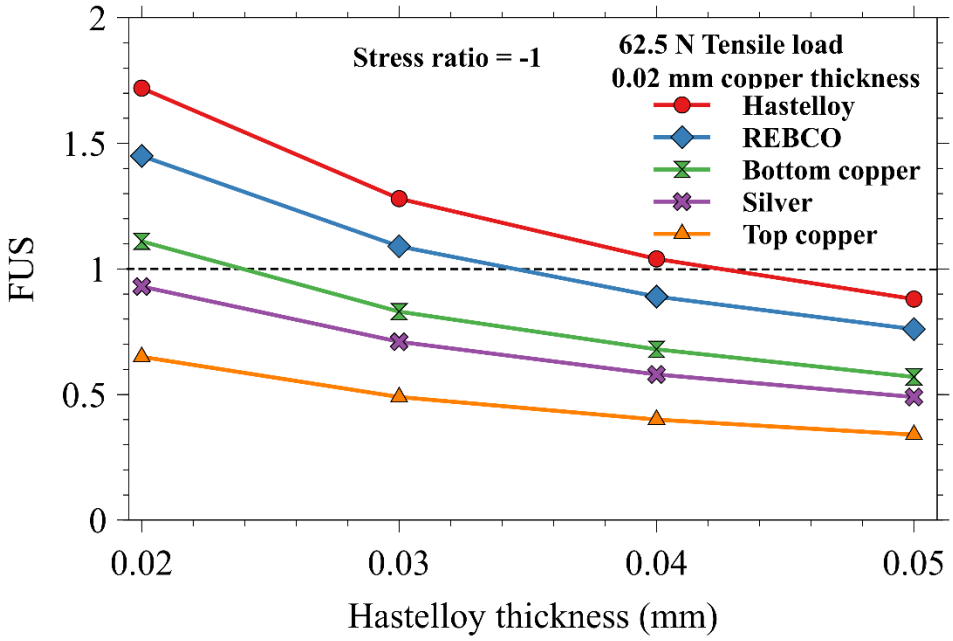

Figure 8.7: Variation of FUS value with changes in Hastelloy thicknesses

When the Hastelloy thickness increases from 0.02 mm to 0.05 mm, the FUS value decreases by about 48 %. It can be seen that at least 0.0425 mm of Hastelloy thickness is needed to tolerate a 62.5 N cyclic tensile load and beyond that there can be the propagation of crack in the Hastelloy layer. It can be also seen that for the REBCO and silver layers, the failure may happen for Hastelloy layer with lower thicknesses. Please note that the copper thickness is kept constant at 0.02 mm. Since no degradation is observed in the copper layers at the given load range, the changes in the FUS values within the copper layers are not plotted.

8.4.2.2. Effect of copper thickness on FUS value

The variation of FUS value with changes in copper thickness for Hastelloy, REBCO and silver layers is depicted in Figure 8.8.

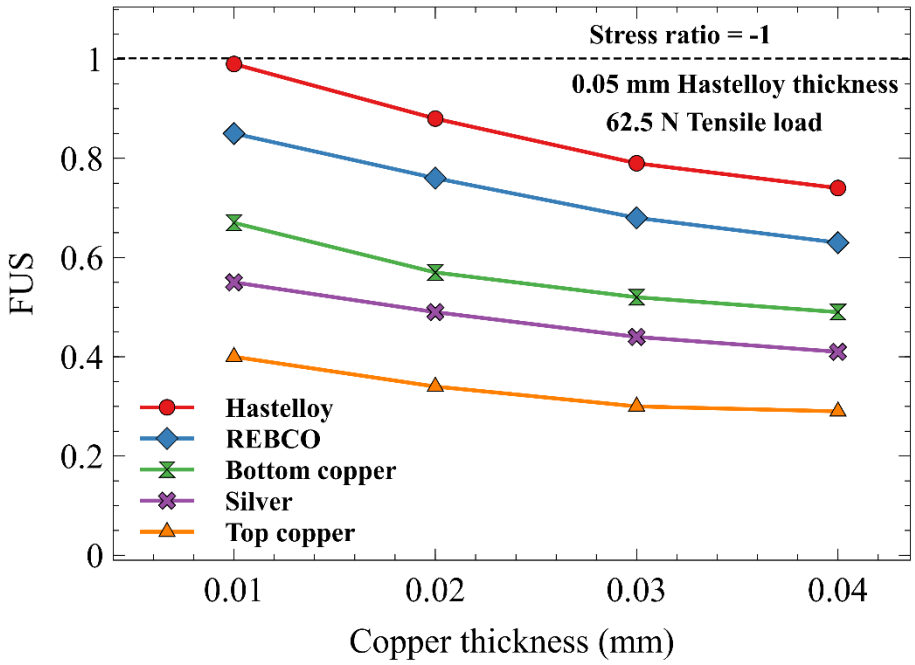

Figure 8.8: Variation of FUS value with changes in copper thicknesses

It can be observed that thicker copper layers can withstand more load as the FUS value decreases with increasing the copper thickness. There is a 25 % reduction in the FUS value in the all the three layers when the copper thickness is increased from 0.01 to 0.04 mm. Since the tape is in the safe area when subjected to a 62.5 N cyclic tensile load till 0.01 mm copper thickness, a degradation in the tape can be observed at much lesser copper thicknesses. However, the thicknesses of copper cannot be reduced beyond a certain limit due to stability reasons [136]. It is found that changing the Hastelloy thickness has a more significant influence than changing the copper thickness. For instance, 150 % increase in the thickness of Hastelloy layer resulted in 48 % reduction in the FUS value; whereas, 300 % increase in the thickness of copper layer has reduced the FUS value by only 25%.

8.4.2.3 FUS distribution under repeated cyclic tensile load with stress ratio -1.

The distributions of FUS values at top and bottom surfaces of the Hastelloy and REBCO layers corresponding to the 62.5 N and -1 stress ratio for a specific geometrical condition (0.05 mm Hastelloy thickness and 0.02 mm copper thickness) are plotted in Figure 8.9 and 8.10. The results obtained have a similar trend as that of the distribution obtained for a higher load of 669 MPa (N) and for a stress ratio of 0.1 depicted earlier in Figures 8.5 and 8.6. The regions of maximum FUS values, the distribution of FUS in

different surfaces, the relative values of FUS in different layers, etc. remains the same in both cases. However, there are differences in the magnitude of FUS values due to changes in the load applied and the stress ratio.

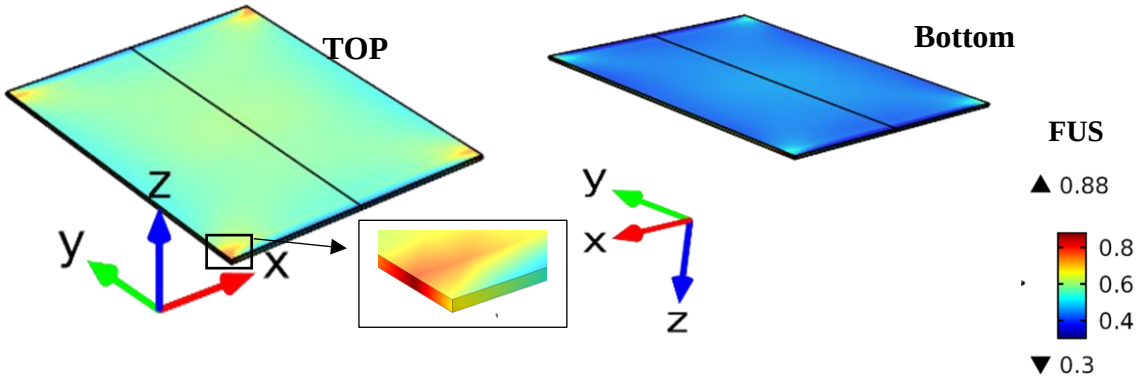

Figure 8.9: FUS distributions in the Hastelloy layer under repeated cyclic tensile load

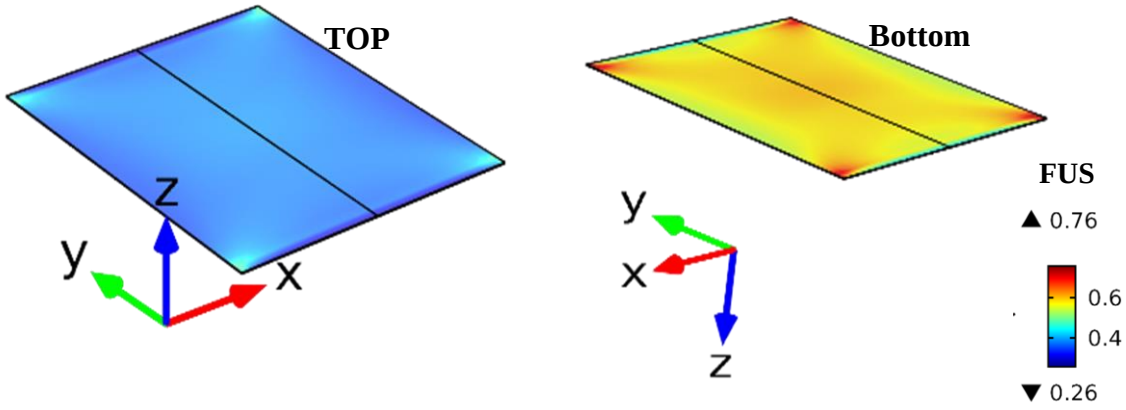

Figure 8.10: FUS distribution in the REBCO layer under repeated cyclic tensile

It is understood that the location of the critical region where the cracks are initiated depends on the bonding between the layers and the yield strength of the material layers [110]. It may be observed that the maximum value of the FUS observed at the edges. Same results have been reported by other researchers [1, 2]. However, it is observed that the maximum value of FUS is found not to be at the surface but a little below the interfacing surface between the Hastelloy and REBCO layers. This is depicted as a zoomed image in the inset of Figure 8.9. Therefore while performing the experimental investigation on the fatigue failures of superconducting tapes, the surface imaging

technique may not be sufficient enough to grab the exact picture of crack propagation. It may also be observed that the FUS distribution in the top surface of the REBCO layer is lower than that on the bottom surface, as depicted in Figure 8.10. This again shows the influence of the interfacing surface between Hastelloy and REBCO layers on the overall fatigue performance of the tape.

8.4.3 Cyclic bending load

The repeated cyclic bending loads are applied to the superconducting tape. The maximum value of bending moment is varied from 0.1 to 0.6 N-mm in 5 steps by keeping the stress ratio constant at -1. In the initial model, REBCO tape of 0.05 Hastelloy and 0.02 mm copper thickness is considered. The variation of the FUS value with changes in bending moment is illustrated in Figure 8.11. The results show that as similar to the tensile fatigue study, under bending loading the Hastelloy material fails first, followed by the REBCO material.

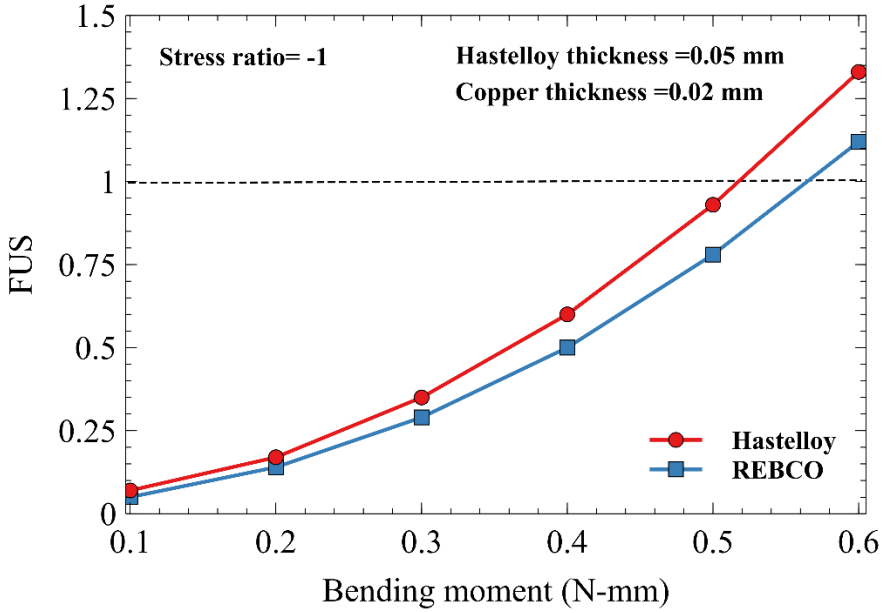

Figure 8.11: Variation of FUS value with changes in bending moment.

The figure shows that with the increase in bending moment, the FUS value is also increased. It is also found that up to 0.52 N-mm bending moment, for the given tape configuration and size, the tape is in the safer region. Beyond 0.52 N-mm, the tape may start to degrade. This study is further extended by varying the thickness of Hastelloy and copper layers. To get the FUS values close to one, the maximum value of bending moments is kept as 0.2 N-mm and 0.4 N-mm, respectively, for Hastelloy and copper layers by trial and error approach.

8.4.3.1 Effect of thickness of Hastelloy layer under repeated cyclic bending load

The variation of FUS values with changes in Hastelloy thickness when the tape is subjected to cyclic bending load is plotted in Figure 8.12.

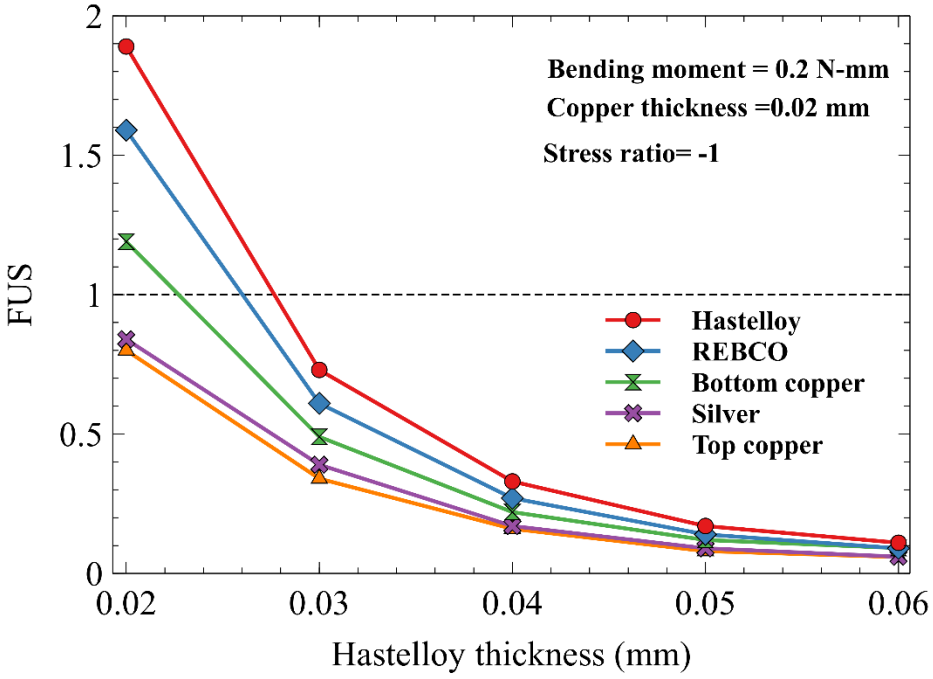

Figure 8.12: Variation of FUS value with changes in Hastelloy thickness under bending

It may be observed that with increasing thickness of the Hastelloy layer, the FUS values in all the layers (Hastelloy, REBCO silver and copper) decrease asymptotically. A similar trend is obtained for the tensile load case. When increasing the thickness of Hastelloy from 0.02 mm to 0.03 mm (0.01 mm increase), the FUS value is decreased by 61 %. Whereas, increasing the thickness from 0.02 to 0.06 mm (0.04 mm increase), the decrease in the FUS value is 94 %. It is found that the tape starts to degrade, for the given applied load and tape configuration, when the Hastelloy thickness is reduced beyond 0.028 mm (the region where the FUS values are more than one).

8.4.3.2 Effect of thickness of copper layer thickness under repeated cyclic bending load

The decrease in the FUS value with an increase in copper thickness is shown in Figure 8.13. When the thickness of the copper layer is increased from 0.01 mm to 0.04 mm, the REBCO tape is found to be safe up to 0.016 mm for the given bending moment of 0.4 N-mm and 0.05 mm thickness for the Hastelloy layer. Below this point, since the FUS value is more than one, the Hastelloy layer may start to degrade, followed by the REBCO layer (at a copper thickness of 0.147 mm). The total reduction in the FUS value

is found to be 93 % for the given configuration and conditions. It may be noted that the thickness of copper layer can not be substantially reduced because of stability reasons [136].

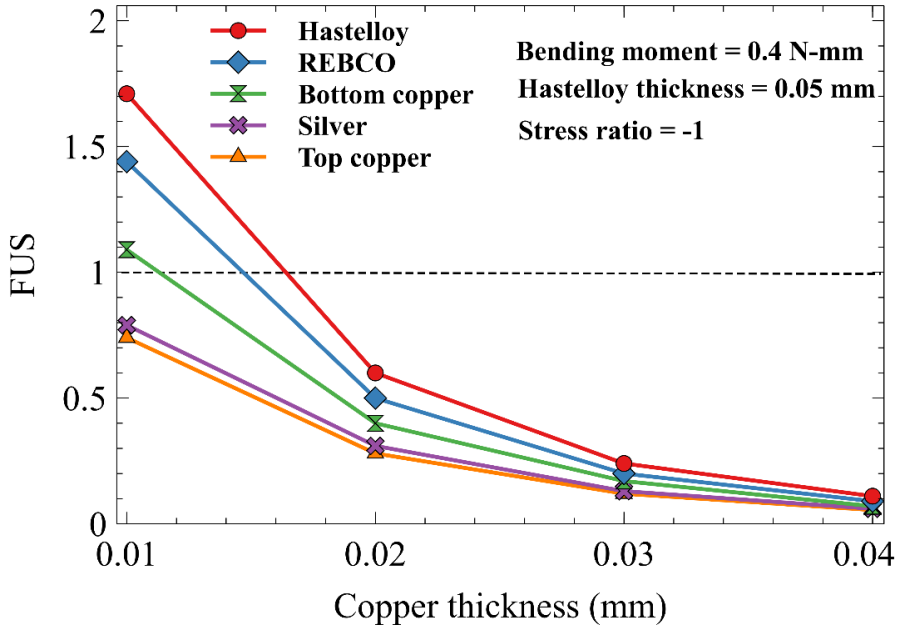

Figure 8.13: Variation of FUS value with changes in copper thickness under bending.

It may be also observed that under cyclic bending loading, the Hastelloy material fails first, followed by the REBCO and silver layers

8.4.3.3 FUS distribution under repeated cyclic bending load

To visualise the changes in the FUS values in the top and bottom surfaces of Hastelloy and REBCO layers, their distribution are plotted in Figures 8.14 and 8.15 respectively. The maximum bending moment applied, in this case, is 0.5 N-mm, and the stress ratio is -1.

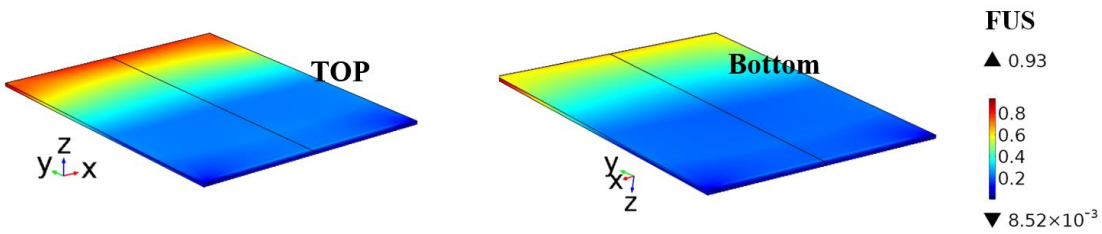

Figure 8.14: FUS distribution of Hastelloy under repeated cyclic bending loading

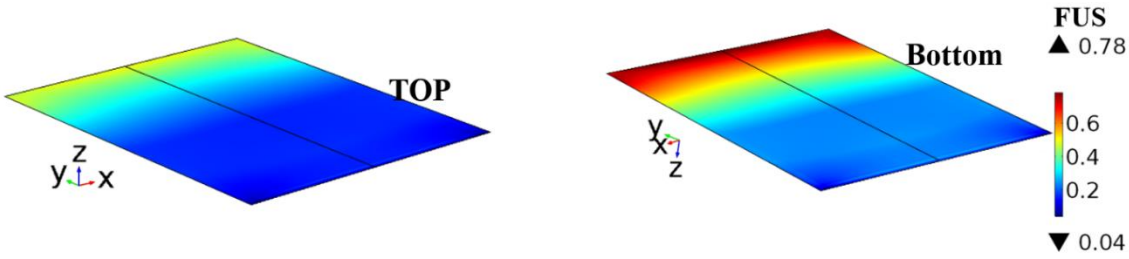

Figure 8.15: FUS distribution of REBCO under repeated cyclic bending load

It may be observed that under cyclic repeated bending load, the higher value of FUS occurs at the loading end of the tape. It may be due to the continuous changing of the nature of load (tensile to compressive and backforth) above and below the neutral axis.

8.4.4 Cyclic torsional loading

The effect of variation in the twisting moment on the degradation of the REBCO tape is studied. The twisting moment is varied from 0.02 N-m to 0.07 N-m with 0.01 N-m increment and its effect on the FUS values in the Hastelloy and REBCO layers is depicted in Figure 8.16.

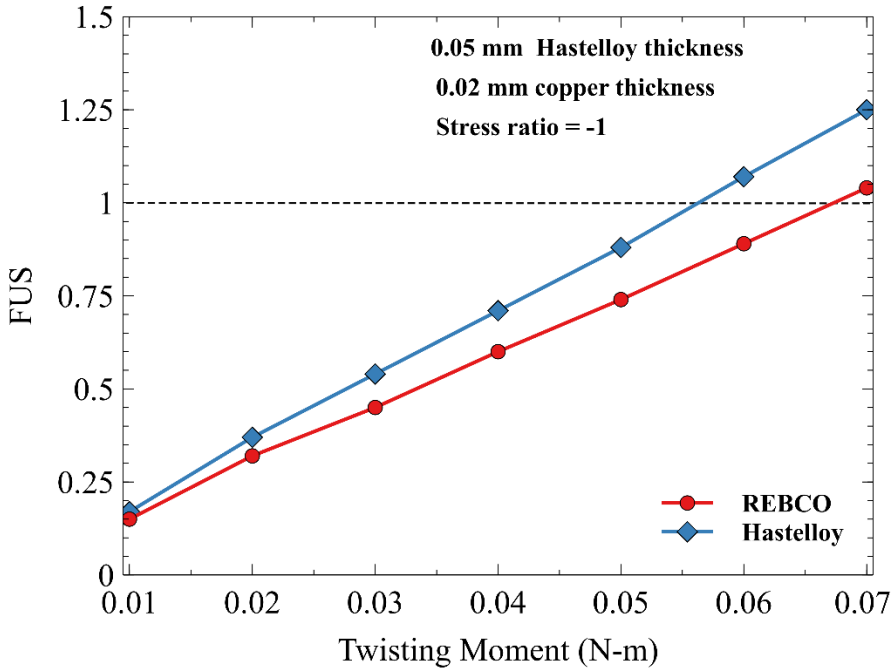

Figure 8.16: Variation of FUS value with changes in the torsional moment.

With increasing the twisting moment, the FUS values are increased both in the Hastelloy and REBCO layers. However, beyond value of 0.056 N-m, since the FUS value is more than one and the Hastelloy layer may start to degrade. The Hastelloy layer fails first, followed by the REBCO layer at 0.067 N-m. It may be noted that, similar type of behaviour is obtained for repeated tensile and bending load as well.

8.4.4.1. Effect of Hastelloy thickness under repeated cyclic torsional load

The changes in FUS value with increase in Hastelloy thickness are depicted in Figure 8.17. The twisting moments are changed by the trial-and-error method to obtain the region where FUS values are near to one. Correspondingly, for Hastelloy and copper variation the moments obtained are 0.04 N-m and 0.05 N-m respectively.

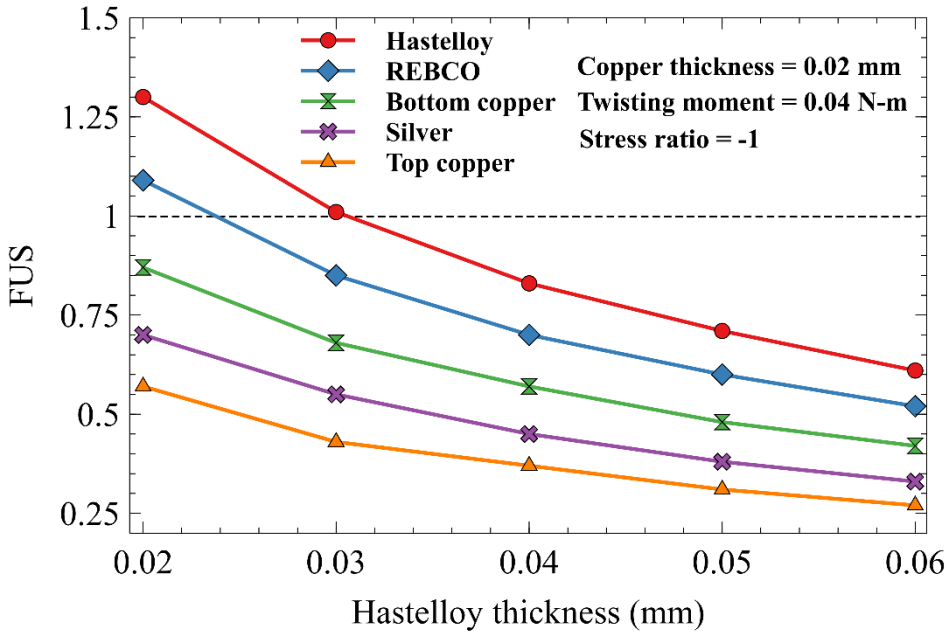

Figure 8.17: Variation of FUS with changes in Hastelloy thickness under cyclic torsional load

Similar to earlier cases, as Hastelloy thickness increases, the FUS value decreases. For instance, as the Hastelloy thickness increased from 0.02 mm to 0.05 mm, the FUS value decreased by almost 45 %. For a given configuration and applied twisting moment, the REBCO tape is found to be safe up to 0.03 mm of Hastelloy thickness.

8.4.4.2. Effect of copper thickness under repeated cyclic torsional load

The variation of FUS value with changes in the thickness of copper layer under cyclic torsional load is depicted in Figure 8.18. It may be noted that the thickness of copper is not reduced beyond 0.01 mm due to stability issues.

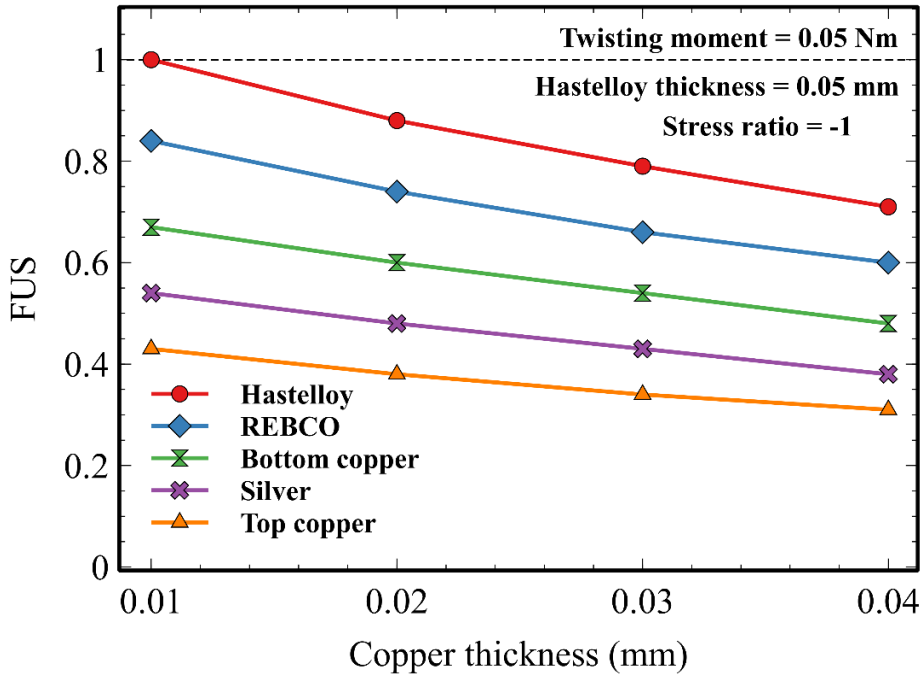

Figure 8.18: Variation of FUS with changes in copper thickness under cyclic torsional load

When decreasing the thickness of copper layer, as expected, the FUS values decrease. When copper thickness changes from 0.01 mm to 0.04 mm, the FUS value decreases by about 29 %. It may be observed that for the entire range of copper thicknesses, all the three layers remain in the safer region up to 0.01 mm copper thickness.

8.4.4.3 The FUS distribution under repeated cyclic torsional load

FUS distribution of Hastelloy and REBCO are plotted in Figures 8.19 and 8.20 respectively. It may be observed that under cyclic repeated torsional loading, the higher value of FUS is observed in the two sides of the REBCO tape. Similar results are reported for normal torsional loading cases in the literature [17].

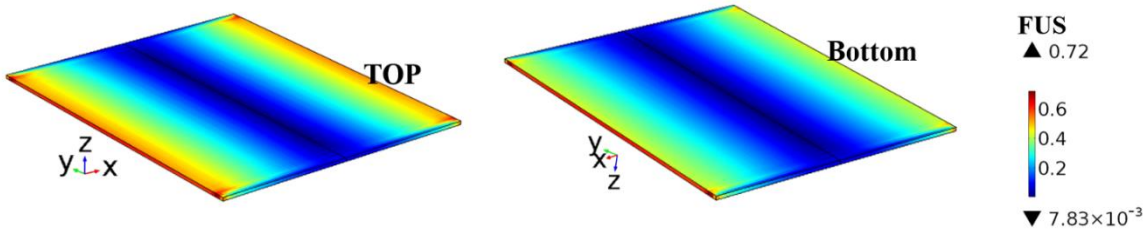

Figure 8.19: FUS distribution in the Hastelloy layer under repeated cyclic torsional loading

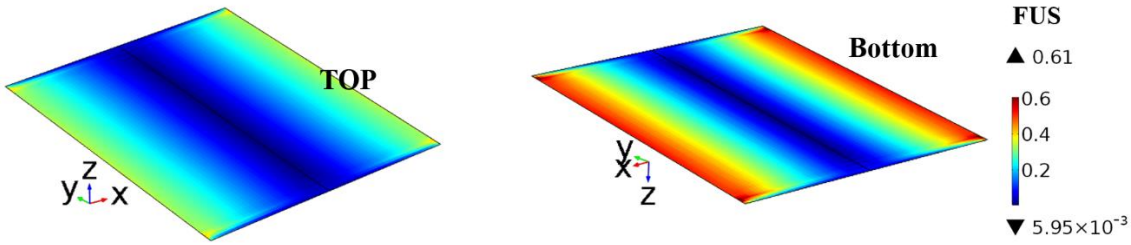

Figure 8.20: FUS distribution in the REBCO layer under repeated cyclic torsional loading

As compared to the FUS values in the bottom surface of Hastelloy layer, those in the top surface are higher. It may be noted that the REBCO material is coated on the top surface of the Hasetlloy layer. Correspondingly, the FUS values in the bottom surface of the REBCO layer is higher than those in the top layer.

8.4.5 Comparative analysis of FUS value under different cyclic repeated mechanical loads

The way in which each layer of materials and their interface surfaces are affected by fatigue loading is compared under tension, bending and twisting loads. In order to compare the FUS values at different interface and inner surfaces, they are divided by the maximum FUS value obtained. This ratio is multplied by 100 to obtain the 'Percentile of FUS'. For each case of repeated cyclic tensile, bending, and twisting loads the 'Percentile of FUS' is plotted in the y-axis as represented in Figure 8.21.

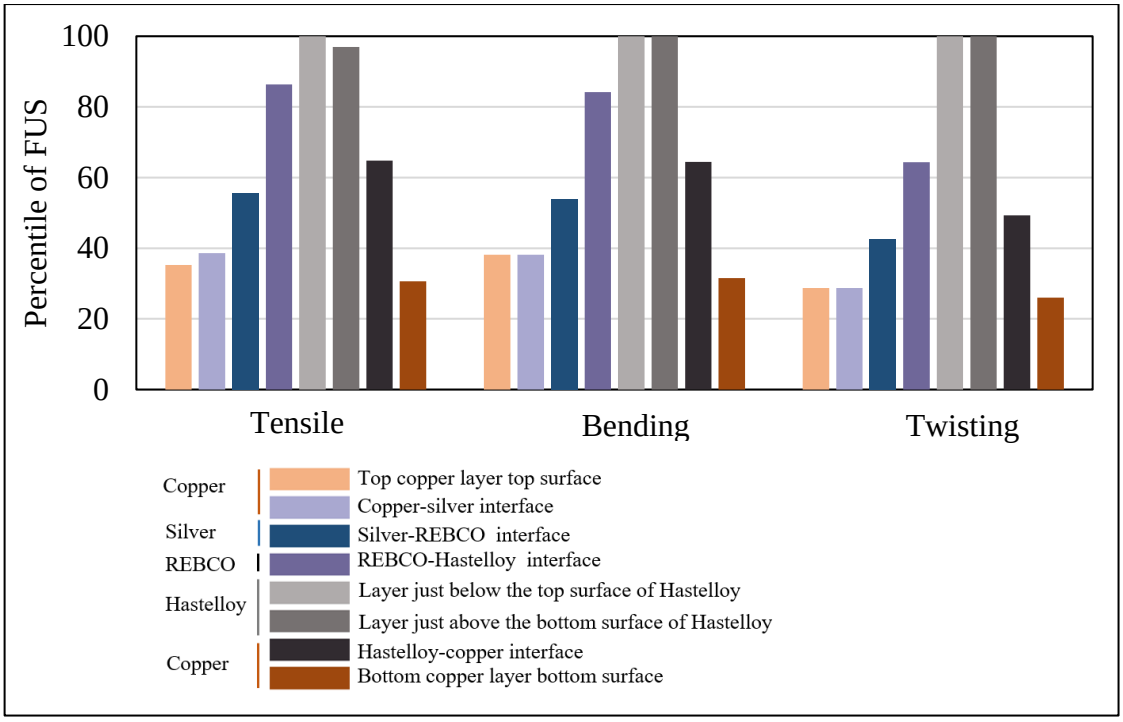

Figure 8.21: Percentile of FUS under repeated cyclic tension, bending, and twisting loads

The figure shows that, irrespective of repeated cyclic tension, bending, or twisting loads, the distribution of the maximum FUS values in the different layers of the tape are almost in the same order. The layer surfaces in the descending order of maximum FUS values are as follows: 1) layer just below the top surface of Hastelloy, 2) layer just above the bottom surface of Hastelloy, 3) REBCO-Hastelloy interface, 4) Hastelloy-copper interface, 5) silver-REBCO interface, 6) copper-silver interface, 7) top copper layer top surface, and 8) bottom copper layer bottom surface. The same order is followed for tension, bending and twisting cases.

It may be understood that the maximum values of FUS is not only dependent upon type of layer material but also influenced by the material properties of the adjacent layers. The maximum FUS value is observed inside the Hastelloy in all three scenarios. It may be either in the layer directly below or above the top and bottom interfacing layers of Hastelloy with its adjacent layers. The FUS value is decreased in the interface between Hastelloy and copper. The point where the FUS value is increased is in the interfacing layer between REBCO and silver. The FUS value further decreases the interface between silver and copper layers. Then the FUS value decreases further at the top surface of the

upper copper layer. The lowest value is found to be at the bottom surface of the bottom copper layer.

8.4.5.1. Percentage variation of FUS with changes in Hastelloy and copper thickness under different repeated cyclic loading

The percentage variations of FUS value with changes in Hastelloy and copper thicknesses for tensile, bending and torsional loads are depicted in Figure 8.22. The y-axis depicts the percentage decrease in the FUS values when increasing the thickness of Hastelloy and copper layers from the initial value to a final value of the range considered in this study.

$$|\text{Variation of FUS value}| = \left|\frac{(\text{FUS at initial thickness of the layer} - \text{FUS at final thickness of the layer})}{\text{FUS at initial thickness of the layer}}\right| \times 100$$

The force applied in the each case of tensile, bending and twisting is also provided in the legend of the graph.

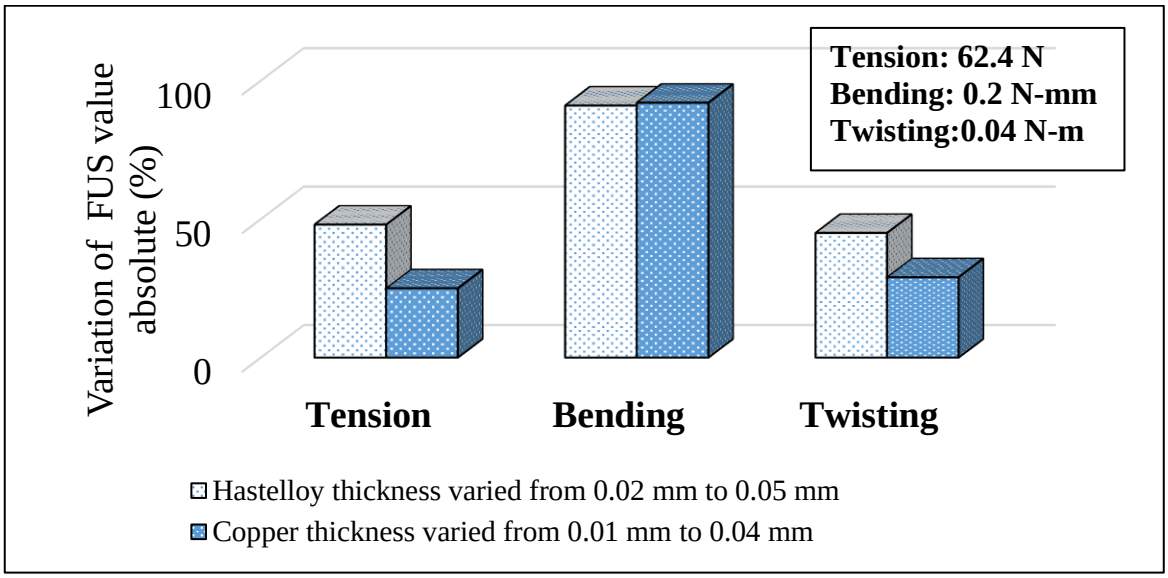

Figure 8.22: Variation of FUS with changes in Hastelloy and copper thickness under cyclic tensile (62.4N), bending (0.2 N-mm) and twisting loads (0.04 N-m)

Compared to tensile and torsional loads, the variation in FUS value with changes in the Hastelloy and copper thickness is more predominant under cyclic bending loading. As the Hastelloy thickness increased from 0.02 mm to 0.05 mm, the FUS value is decreased by 48 %, 91 %, and 45 %, respectively, for tensile, bending and torsional loads. A similar kind of variation is also observed with changes in the copper thickness. When the copper thickness changes from 0.01 mm to 0.04 mm, the FUS value decreases by 25 %, 92 %,

and 29 %, respectively, under cyclic tensile, bending and torsional loads. Therefore, it can be understood that out of the three loading conditions, repeated cyclic bending load has more influence on the degradation of the superconductor.

8.4.5.2. Limiting load for different Hastelloy and copper thicknesses under different repeated cyclic loading

The maximum load that can be applied without any degradation (at FUS =1) is denoted as the limiting load. The limiting tensile, bending, and twisting load for 0.02 mm and 0.05 mm Hastelloy thicknesses are given in Table 8.1. As the Hastelloy thickness increases from 0.02 mm to 0.05 mm (60 % increase), there is 88.5 % increase in the limiting tensile force, 256 % increase in limiting bending moment and 81% increase in the limiting twisting moment are observed under different cyclic loadings.

Table 8.1: Limiting load at 0.02 and 0.05 mm Hastelloy thicknesses for a constant copper thickness of 0.02 mm

Mechanical cyclic load	***Hastelloy thickness (mm)***	
	0.02	*0.05*
Tension	*37.60 N*	*70.88 N*
Bending	*N-mm*	*0.52 N-mm*
Twisting	*0.031N-m*	*0.056 N-m*

Table 8.2: Limiting load at 0.01 and 0.04 mm copper thicknesses for a constant Hastelloy thickness of 0.05 mm

Mechanical cyclic load	***Copper thickness (mm)***	
	0.01	*0.04*
Tension	*62.91 N*	*83.38 N*
Bending	*0.28 N-mm*	*1.31 N-mm*
Twisting	*0.05 N-mm*	*0.071 N-mm*

The limiting force/ moments corresponding to 0.01 mm and 0.04 mm copper thicknesses are given in Table 8.2. As the copper thickness increases from 0.01 mm to 0.04 mm, there is 32.5 % increase in the limiting tensile force, 367 % increase in the limiting bending moment and 42 % increase in the limiting twisting moment are observed under different cyclic loadings.

It may also be understood that the thickness of Hastelloy and copper layers are significant parameters under fatigue loading irrespective of the nature of cyclic load (Tensile, bending, twisting).

8.5 Summary

The fatigue analysis on superconducting REBCO tape is carried out under tensile, bending, and twisting cyclic load. The results may be summarised as follows,

- The thickness of Hastelloy also has a significant influence on the degradation of the tape under cyclic tensile loading. The Hastelloy thickness increased from 0.02 mm to 0.05 mm (60 % increase); fatigue usage factor value decreased by 48 % (maximum value of applied stress = 62.4.5N, R = -1). It is also found that at least 0.425 mm of Hastelloy thickness is needed to tolerate a 62.5 N cyclic tensile load, and beyond that, there would be crack propagation in the Hastelloy layer.
- There is a linear relationship between the maximum value of the applied bending moment and the fatigue usage factor. It is found that the tape is in the safer region for bending moments up to 0.52 N-mm for the given configuration and size. Also, it is found that at least 0.028 mm Hastelloy thickness is needed to accommodate 0.2 N-mm bending moment with Copper layer thickness of 0.02 mm. Similarly, 0.016 mm copper thickness is required to tolerate 0.4 N-mm bending moment for tape with the Hastelloy thickness of 0.05 mm.
- REBCO tape is subjected to repeated torsional load is in the safer region up to 0.056 N-m twisting moment for a given tape configuration (0.05 mm Hastelloy thickness and 0.02 mm copper thickness). Use of thicker Hastelloy layer helps to withstand more twisting moments under cyclic loading. When the Hastelloy thickness is increased from 0.02 mm to 0.05 mm (150 % increase), the Fatigue usage factor decreases by almost 44 %. It is found that at least 0.03 mm Hastelloy thickness is required to accommodate 0.04 N-m twisting moment for REBCO tape with a Copper thickness of 0.02 mm without any degradation.
- It can be concluded that the variation of FUS value with changes in the Hastelloy and copper thickness is more predominant under cyclic bending loading than in the tensile and torsional fatigue loads. When the Hastelloy thickness is increased from 0.02 mm to 0.05 mm, there is 88.5 % increase in the limiting tensile force, 256 % increase in the limiting bending moment, and 81 % increase in the limiting

twisting moment under different cyclic loadings. Similarly, when the copper thickness is increased from 0.01 mm to 0.04 mm, the limiting values are increased by 32.5 %, 367 %, and 42 % respectively for repeated cyclic tension, bending and twisting loads.

- Under repeated loading, it is obtained that the Hastelloy layer is the first to fail, followed by REBCO, bottom copper, silver, and finally top copper, irrespective of the nature of the load. This is true for fatigue type tensile, bending and torsional loads.

Publication arising out of this chapter

- **K. B. Ashok**, R. Jacob Thomas, M. Jose Prakash, and A. Nijhuis, "Influence of fatigue on superconducting REBCO tapes under repeated cyclic tensile, bending and twisting loads: A simulation-based investigation," Cryogenics, vol. 132, no. January, p. 103672, 2023, doi: 10.1016/j.cryogenics.2023.103672. (Impact factor: 2.13)

Chapter 9

Conclusions

The present work has attempted to find the degradation in the superconducting REBCO tape under different mechanical loads, such as tensile, bending, and torsion, both in normal and fatigue loading conditions. The effect of the combination of these loads are also evaluated. The COMSOL Multiphysics finite element tool is used to model the tape configuration and simulate the mechanical loads and other loading conditions. The mathematical model is customized and also validated with experimental data available in the open literature.

Parametric analysis is carried out by varying the tape parameters like tape width, copper, and Hastelloy thicknesses. The magnitude of the mechanical loads are varied for both normal and fatigue loading conditions. The winding of the REBCO tape in superconducting CORC cable is carried out for various central core diameters and winding angles. Under repeated cyclic loading, the high-cycle fatigue analysis is carried out for tensile, bending, and torsional loads. The tape parameters like Hastelloy and

copper thicknesses are varied to evaluate their influence on the fatigue type of loading. The findings of the normal and fatigue types of loading under tension, bending, and torsion loads are consolidated.

- The study has found that residual strain is developed in the REBCO tape during its production stage. It is also found that the quantity of residual strain induced is significant and is about 50 % of the critical strain beyond which the tape degrades.
- Also it is found that the residual strain developed is dependent on its operating temperature. For the given tape configuration, it is about 0.25% and 0.17% at 77 K and 293 K, respectively. The main reason for the residual strain development in the tape is the lattice mismatch between the adjacent layers.
- The residual strain developed in the tape is compressive in nature, therefore it helps to withstand more load when subjected to tension.
- Varying the thicknesses of the Hastelloy and copper layers has affected the residual strain value and in turn provided the opportunity to modify the load-bearing capacity of the tape.
- The critical force, which is the maximum force that tape can withstand without any degradation is significantly affected by changes in the thickness of Hastelloy and copper layers. The critical force for the SCS4050® tape that has been used is 313 N. The changes in critical force with layer thickness is captured and is as shown in Table 9.1.

Table 9.1: Changes in the critical force under different thickness of constituting Hastelloy and copper layers

		Critical Force (N)		
Hastelloy Thickness (mm)	***Copper thickness (mm)***	***0.02***	***0.01***	***0.005***
0.06		*365*	*337*	*323*
0.05		*313*	*286*	*272*
0.04		*260*	*234*	*221*
0.03		*211*	*184*	*166*
0.02		*157*	*131*	*118*

- The influence of bending loads on REBCO tapes is investigated numerically and also compared with the traditional analytical approach. The results of the traditional analytical approach using the Flexure formula show good agreement

with that of the numerical approach only at a higher bending radius greater than 4 mm. With smaller bending radii, the deviation between the two approaches are found to be increasing. This implies the need for more accurate numerical approach in capturing the strain induced upon bending than relying on the traditional analytical approach.

- It is found that upon bending the tapes with thicker Hastelloy layer degrade faster. When increasing the thickness of the Hastelloy layer, the distance between the neutral axis and the REBCO layer increases and thereby induces more strain in the REBCO layer while bending. Strain reduced to almost half when the thickness of the Hastelloy layer was decreased by 60% irrespective of the bending radius.
- The thickness of copper is found to have comparatively lesser influence on the strain-induced. For a 50% decrease in the thickness of copper, the maximum decrease in the strain-induced obtained is only 5.7%. This is because when changing, both the top and bottom copper layers uniformly changes. The resulting size change in the tape is symmetrical with respect to the neutral axis.
- The lowest bending radius possible for SCS4050® tape for the given configuration is found to be 2.8 mm. The smallest bending radius possible for a tape width of 4 mm and copper thickness of 0.02 mm for different Hastelloy thicknesses is determined and presented in Table 9.2.

Table 9.2: Changes in the critical bending radius with changes in thickness of constitute Hastelloy

Hastelloy (mm)	***Critical bending radius***
0.05	*2.8 mm*
0.04	*2.4 mm*
0.03	*2 mm*
0.02	*1.5 mm*

- Investigation on the effects of torsion loads on the tape has found that the tape width has a significant impact on the degradation of the tape. Decreasing the tape width from 12 mm to 3 mm (75 % decrease), increases the maximum allowable angle of twist from 0.93 to 4 deg/mm (326 % increase) under pure torsional

loading. When the tape width is increased, the distance from the centre line of the tape centre to the side increases, resulting in more strain in the tape.

- It is also understood that the thickness of the Hastelloy and copper layers have only slight impact upon torsional loads. The critical angle of twist for SCS4050® tape configuration for different tape widths is given in Table 9.3.

Table 9.3: Changes in the critical angle of twist with changes in tape width

Tape width (mm)	***Critical angle of twist (deg/mm)***
12	*0.93*
10	*1.2*
8	*1.5*
4	*3*
3	*4*

- It is found that decreasing the tape width provides more flexibility for the manufacturers to accommodate combined tensile and torsional loads.
- The combined tension and torsional loading study revealed that tension have more profound effect than torsion. When the torsional load is increased by 300 % (angle of twist from 0.18 deg/mm to 0.72 deg/mm) the corresponding decrease in the tensile load so as to keep the tape within the degradation limit is only 54 % (applied strain from 0.65 % to 0.3 %).
- Winding of REBCO tape on the central core is carried out, and it is found that the central core diameter, winding angle, and thickness of the Hastelloy layer significantly impact the degradation of the REBCO tape. Under winding, for the given tape configuration, for any central core diameter below 1 mm, the tape fails.
- The best angle of winding for the CORC cable configuration is found to be 45º. Moreover, the thickness of the Hastelloy layer has got more influence on induced strain than that of the copper layer.
- Fatigue analysis found that the Hastelloy layer is the most critical one among different constituents of the tape irrespective of the type of loading. In all three types of loading, the degradation first happens within the Hastelloy layer.

- The layer that fails under fatigue loading after the Hastelloy layer is the REBCO layer; it is followed by the bottom copper layer, then the silver layer, and finally the top copper layer for the given tape configuration and loading conditions.
- For the SCS4050® tape under fatigue loading, it is found that minimum Hastelloy thickness of 0.0425 mm, 0.028 mm, and 0.03 mm is required respectively so as to accommodate 62.5 N tensile, 0.2 N-mm bending, and 40 N-mm torsional loads.
- In fatigue loading, among the three types of loads, the most detrimental one is found to be the bending. Also, the thickness of the constituting layers is found to have a significant influence under the fatigue type of loading.
- When the thickness of the Hastelloy layer is increased by 150 %, upon fatigue the degradation in the tape decreases by 48 %, 91 %, and 45 %, respectively, for tensile, bending, and torsional loads. When the thickness of the copper layers are increased by 300 %, the degradation in the REBCO tape decreases by 25 %, 92 %, and 29 %, respectively for tension, bending, and torsion loads.

This investigation conducted helped in the fine-tuning of different parameters like the maximum load applied, bending radii, angle of twist, central core diameter, winding angle etc. for HTS. Based on these findings, special care has to be taken while deciding the thickness of the constituting layers and the width of the tape during the manufacturing and application stages. The knowledge obtained is expected to help the manufacturers and researchers in developing better HTS tapes and cables.

Future scope

- Determining the degradation of the REBCO tape under the combined influence of magnetic Lorentz force and mechanical loads may help to bring out a more realistic picture
- The combined influence of magnetic Lorentz force and mechanical loads on the degradation of CORC cables may be performed with multiple layers to find the intertwined effect between the layers.
- It may be more revealing if the degradation of the REBCO tape, when subjected to various fatigue loads, are carried out using different modelling approaches reported in the literature.
- Fatigue analysis may extended to other commercial cabling configuration as well as to combined magnetic Lorentz force and mechanical loads.

List of publications arising out of this research work

International Journals

- **Ashok KB**, Thomas RJ, Prakash M J, Nijhuis A, "Analytical and Numerical Investigations on the Degradation of REBCO Based Superconducting Tapes Under Bending," in IEEE Transactions on Applied Superconductivity, vol. 31, no. 7, pp. 1-12, Oct. 2021, Art no. 8400712, doi: 10.1109/TASC.2021.3109720. (Impact factor: 1.96)
- **Ashok KB**, Thomas RJ, Prakash MJ, Nijhuis A (2021) Performance limits in REBCO tape for variation in winding parameters of CORC cable and wire, Elsevier, Physica C: Superconductivity and its applications, vol 582, 15 March 2021:1353828. https://doi.org/10.1016/j.physc.2021.1353828. (Impact factor: 1.54)
- **K. B. Ashok**, R. J. Thomas, M. J. Prakash, and A. Nijhuis, "Influence of combined tension and torsion on the performance of REBCO superconducting tapes," IEEE Trans. Appl. Supercond., vol. 33, no. 3, pp. 1–11, 2023, doi: 10.1109/tasc.2023.3236010. (Impact factor: 1.96)
- **K. B. Ashok**, R. Jacob Thomas, M. Jose Prakash, and A. Nijhuis, "Influence of fatigue on superconducting REBCO tapes under repeated cyclic tensile, bending and twisting loads: A simulation-based investigation," Cryogenic, vol. 132, no. January, p. 103672, 2023, doi: 10.1016/j.cryogenics.2023.103672. (Impact factor: 2.13)

International conferences

- **Ashok KB**, Thomas RJ, Prakash MJ, Nijhuis A, Investigation of Magnetostriction in Second generation High Temperature Superconductors, presented at International Conference On Aerospace And Mechanical Engineering, ICAME 2018, Organized By Department Of Mechanical Engineering, Kollam, December 17-19,2018 and published in Journal of Physics: Conference Series. 1355. 012036. 10.1088/1742-6596/1355/1/012036. (Scopus)

- **Ashok, K. B**., Purushothaman, S. J., Jacob Thomas R., Jose Prakash, M., & Nijhuis, A. (2020). Parametric investigation on the thermal aspects of superconducting REBCO tapes used in CORC cables. Elsevier, Materials Today: Proceedings. doi:10.1016/j.matpr.2020.05.381. (Scopus) (icee)
- Justin Robert, **Ashok KB** and Thomas RJ, Simulation Of Fatigue In High-Temperature Superconductor Using Matake Criterion, Proceedings of International e-Conference on Recent Innovations in Mechanical Engineering (RIME) 2021, ISBN: 978-93-5473-550- 9. 25
- Justin Robert, **Ashok KB** and Thomas RJ , Simulation of Fatigue in High-Temperature Superconductor using Findley criterion, Proceedings of International Conference on Aerospace And Mechanical Engineering, ICAME 2021, Organized By Department of Mechanical Engineering, TKM College of Engineering, Kollam, December 16- 18,2021.
- **Ashok KB**, Thomas RJ, Prakash MJ, Nijhuis A, Effect of Winding on the Electrical Performance of REBCO based CORC® Superconducting Cable/Wire, Proceedings of International Conference on Aerospace And Mechanical Engineering, ICAME 2021, Organized By Department Of Mechanical Engineering, TKM College of Engineering, Kollam, December 16-18,2021

References

[1] I. E. Agency, “India Energy Outlook 2021,” *India Energy Outlook 2021*, 2021, doi: 10.1787/ec2fd78d-en.

[2] K. Fiore, “Nuclear energy and sustainability: Understanding ITER,” *Energy Policy*, vol. 34, no. 17, pp. 3334–3341, 2006, doi: 10.1016/j.enpol.2005.07.008.

[3] P. F. Dahl, “Kamerlingh Onnes and the Discovery of Superconductivity : The Leyden Years , 1911-1914: Historical Studies in the Physical Sciences , Vol . 15 , No . 1 (1984), pp . 1-37 Published by : University of California Press St,” *Hist. Stud. Phys. Sci.*, vol. 15, no. 1, pp. 1–37, 1984.

[4] D. van Delft and P. Kes, “Experimenting in liquid helium,” *Phys. Today*, vol. 63, no. 9, pp. 38–42, 2010, [Online]. Available: http://snf.ieeecsc.org/sites/ieeecsc.org/files/RN16e.pdf

[5] W. Meissner and R. Ochsenfeld, “Ein neuer Effekt bei Eintritt der Supraleitfähigkeit,” *Naturwissenschaften*, vol. 21, no. 44, pp. 787–788, 1933, doi: 10.1007/BF01504252.

[6] J. E. Hirsch, “Spin Meissner effect in superconductors and the origin of the Meissner effect,” A Letters Journal Exploring the Frontiers of Physics (*Epl)*, vol. 81, no. 6, 2008, doi: 10.1209/0295-5075/81/67003.

[7] H. Essén and M. C. N. Fiolhais, “Meissner effect, diamagnetism, and classical physics—a review,” *Am. J. Phys.*, vol. 80, no. 2, pp. 164–169, 2012, doi: 10.1119/1.3662027.

[8] Y. Oda, A. Sumiyama, and H. Nagano, “Meissner Effect and Magnetic Field Dependence of Cu clad Nb in mK region.,” *Japanese J. Appl. Physics, Part 1 Regul. Pap. Short Notes*, vol. 22, no. 3, pp. 464–466, 1983, doi: 10.1143/jjap.22.464.

[9] F. London and H. London, “Superconduction and Diamagnetism,” *Physica*, vol. 2, no. 1–12, pp. 341–354, 1935, doi: 10.1016/S0031-8914(35)90097-0.

[10] J. Bardeen and J. R. Schrieffer, “Chapter VI Recent Developments in Superconductivity,” *Prog. Low Temp. Phys.*, vol. 3, no. C, pp. 170–287, 1961, doi: 10.1016/S0079-6417(08)60137-7.

[11] M. Cyrot, “Ginzburg-Landau theory for superconductors,” *Reports Prog. Phys.*, vol. 36, no. 2, pp. 103–158, 1973, doi: 10.1088/0034-4885/36/2/001.

[12] J. E. Hirsch, “BCS theory of superconductivity: It is time to question its validity,” *Phys. Scr.*, vol. 80, no. 3, 2009, doi: 10.1088/0031-8949/80/03/035702.

[13] C. Barth, “High temperature superconductor cable concepts for fusion magnets,” *High Temp. Supercond. Cable Concepts Fusion Magnets*, pp. 1–232, 2013, doi: 10.5445/KSP/1000035747.

[14] Autoridad Nacional del Servicio Civil, “Stability of Superconductors,” *Angew. Chemie Int. Ed. 6(11), 951–952.*, pp. 2013–2015, 2021.

[15] V. L. Tanna, “Design and Analysis of the Superconducting Current Feeder System

for the International Thermonuclear Experimental Reactor (ITER),” page. 1-152, 2006, [Online]. Available: http://bibliothek.fzk.de/zb/berichte/FZKA7256.pdf

[16] C. Barth, “High Temperature Superconductor Cable Concepts for Fusion Magnets,” page: 1-258, 2013, doi: http://dx.doi.org/10.5445/KSP/1000035747.

[17] K. Ilin *et al.*, “Experiments and FE modeling of stress-strain state in ReBCO tape under tensile, torsional and transverse load,” *Supercond. Sci. Technol.*, vol. 28, no. 5, p. 55006, 2015, doi: 10.1088/0953-2048/28/5/055006.

[18] D. C. Van Der Laan and J. W. Ekin, “Large intrinsic effect of axial strain on the critical current of high-temperature superconductors for electric power applications,” *Appl. Phys. Lett.*, vol. 90, no. 5, pp. 6–9, 2007, doi: 10.1063/1.2435612.

[19] A. Roque, D. M. Sousa, V. Fernão Pires, and E. Margato, “Superconductivity and their applications,” *Renew. Energy Power Qual. J.*, vol. 1, no. 15, pp. 322–327, 2017, doi: 10.24084/repqj15.308.

[20] H. Thomas, A. Marian, A. Chervyakov, S. Stückrad, D. Salmieri, and C. Rubbia, “Superconducting transmission lines - Sustainable electric energy transfer with higher public acceptance?,” *Renew. Sustain. Energy Rev.*, vol. 55, pp. 59–72, 2016, doi: 10.1016/j.rser.2015.10.041.

[21] W. H. Fietz, R. Heller, S. I. Schlachter, and W. Goldacker, “Application of high temperature superconductors for fusion,” *Fusion Eng. Des.*, vol. 86, no. 6–8, pp. 1365–1368, 2011, doi: 10.1016/j.fusengdes.2010.11.018.

[22] R. J. Cava *et al.*, “Bulk superconductivity at 91 K in single-phase oxygen-deficient perovskite Ba2YCu3O9-,” *Phys. Rev. Lett.*, vol. 58, no. 16, pp. 1676–1679, 1987, doi: 10.1103/PhysRevLett.58.1676.

[23] A. K. Jha and K. Matsumoto, “Superconductive REBCO thin films and their nanocomposites: The role of rare-earth oxides in promoting sustainable energy,” *Front. Phys.*, vol. 7, no. JUN, pp. 1–21, 2019, doi: 10.3389/fphy.2019.00082.

[24] F. N. Werfel *et al.*, “Superconductor bearings, flywheels and transportation,” *Supercond. Sci. Technol.*, vol. 25, no. 1, 2012, doi: 10.1088/0953-2048/25/1/014007.

[25] K. B. Ma, Y. V. Postrekhin, and W. K. Chu, “Superconductor and magnet levitation devices,” *Rev. Sci. Instrum.*, vol. 74, no. 12, pp. 4989–5017, 2003, doi: 10.1063/1.1622973.

[26] Stadt Mannheim. Der Roebelstab von Ludwig Roebel (1878 -1934) In:, http: //www. mannheim. De/wirtschaft-entwickeln/, and R.-1878-1934 . 2012, “The Roebel Wand by Ludwig Roebel,” 1912.

[27] W. Goldacker, “Improvement of superconducting properties in ROEBEL assembled coated conductors (RACC),” *IEEE Trans. Appl. Supercond.*, vol. 19, no. 3, pp. 3098–3101, 2009, doi: 10.1109/TASC.2009.2018284.

[28] “ROEBEL Assembled Coated Conductors (RACC): Preparation, properties and progress,” *IEEE Trans. Appl. Supercond.*, vol. 17, no. 2, pp. 3398–3401, 2007, doi: 10.1109/TASC.2007.899417.

[29] W. Goldacker, F. Grilli, E. Pardo, A. Kario, S. I. Schlachter, and M. Vojenčiak, “Roebel cables from REBCO coated conductors: A one-century-old concept for the superconductivity of the future,” *Supercond. Sci. Technol.*, vol. 27, no. 9, 2014, doi: 10.1088/0953-2048/27/9/093001.

[30] S. Schuller, W. Goldacker, A. Kling, L. Krempasky, and C. Schmidt, “Ac-loss measurement of a DyBCO-Roebel assembled coated conductor cable (RACC),” *Phys. C Supercond. its Appl.*, vol. 463–465, no. SUPPL., pp. 761–765, 2007, doi: 10.1016/j.physc.2007.01.063.

[31] S. I. Schlachter, W. Goldacker, F. Grilli, R. Heller, and A. Kudymow, “Coated conductor rutherford cables (CCRC) for high-current applications: Concept and properties,” *IEEE Trans. Appl. Supercond.*, vol. 21, no. 3 PART 3, pp. 3021–3024, 2011, doi: 10.1109/TASC.2010.2095811.

[32] M. Takayasu, L. Chiesa, L. Bromberg, and J. V. Minervini, “Cabling method for high current conductors made of HTS tapes,” *IEEE Trans. Appl. Supercond.*, vol. 21, no. 3 PART 2, pp. 2340–2344, 2011, doi: 10.1109/TASC.2010.2094176.

[33] M. Takayasu, L. Chiesa, L. Bromberg, and J. V. Minervini, “HTS twisted stacked-tape cable conductor,” *Supercond. Sci. Technol.*, vol. 25, no. 1, 2012, doi: 10.1088/0953-2048/25/1/014011.

[34] M. Takayasu, L. Chiesa, N. C. Allen, and J. V. Minervini, “Present status and recent developments of the twisted stacked-tape cable conductor,” *IEEE Trans. Appl. Supercond.*, vol. 26, no. 2, pp. 25–34, 2016, doi: 10.1109/TASC.2016.2521827.

[35] D. C. Van Der Laan, “YBa2Cu3O7-δ coated conductor cabling for low ac-loss and high-field magnet applications,” *Supercond. Sci. Technol.*, vol. 22, no. 6, 2009, doi: 10.1088/0953-2048/22/6/065013.

[36] D. C. Van Der Laan, J. D. Weiss, and D. M. McRae, “Status of CORC® cables and wires for use in high-field magnets and power systems a decade after their introduction,” *Supercond. Sci. Technol.*, vol. 32, no. 3, 2019, doi: 10.1088/1361-6668/aafc82.

[37] D. C. Van Der Laan *et al.*, “Anisotropic in-plane reversible strain effect in Y0.5Gd 0.5Ba2Cu3O7 - δcoated conductors,” *Supercond. Sci. Technol.*, vol. 24, no. 11, 2011, doi: 10.1088/0953-2048/24/11/115010.

[38] D. C. Van Der Laan, P. D. Noyes, G. E. Miller, H. W. Weijers, and G. P. Willering, “Characterization of a high-temperature superconducting conductor on round core cables in magnetic fields up to 20 T,” *Supercond. Sci. Technol.*, vol. 26, no. 4, 2013, doi: 10.1088/0953-2048/26/4/045005.

[39] M. Daibo *et al.*, “Development of a 66 kV-5 kA Class HTS Power Cable with IBAD/PLD REBCO Tapes,” *Phys. Procedia*, vol. 58, pp. 314–317, 2014, doi: 10.1016/j.phpro.2014.09.078.

[40] “SuperPower® 2G HTS Wire Specifications (www.superpower-inc.com/system/files/SP_2G+Wire+Spec+Sheet_for +web_2012FEC_v2_1.pdf).”

[41] J. H. Cheon, P. S. Shankar, and J. P. Singh, “Influence of processing methods on residual stress evolution in coated conductors,” *Supercond. Sci. Technol.*, vol. 18,

no. 1, pp. 142–146, 2005, doi: 10.1088/0953-2048/18/1/022.

[42] D. P. Norton *et al.*, “Epitaxial YBa2Cu3O7 on biaxially textured nickel (001): An approach to superconducting tapes with high critical current density,” *Science (80-.).*, vol. 274, no. 5288, pp. 755–757, 1996, doi: 10.1126/science.274.5288.755.

[43] Y. Iijima, N. Tanabe, Y. Ikeno, and O. Kohno, “Biaxially aligned YBa2Cu3O7-x thin film tapes,” *Phys. C Supercond. its Appl.*, vol. 185–189, no. PART 3, pp. 1959–1960, 1991, doi: 10.1016/0921-4534(91)91104-C.

[44] Y. Iijima, N. Tanabe, O. Kohno, and Y. Ikeno, “In-plane aligned YBa2Cu3O7-x thin films deposited on polycrystalline metallic substrates,” *Appl. Phys. Lett.*, vol. 60, no. 6, pp. 769–771, 1992, doi: 10.1063/1.106514.

[45] C. Cantoni *et al.*, “Reflection high-energy electron diffraction studies of epitaxial oxide seed-layer growth on rolling-assisted biaxially textured substrate Ni(001): The role of surface structure and chemistry,” *Appl. Phys. Lett.*, vol. 79, no. 19, pp. 3077–3079, 2001, doi: 10.1063/1.1407857.

[46] U. Balachandran, M. Li, R. E. Koritala, B. F. Fisher, and B. Ma, “Development of YBCO-coated conductors for electric power applications,” *Phys. C Supercond. its Appl.*, vol. 372–376, no. PART 2, pp. 869–872, 2002, doi: 10.1016/S0921-4534(02)00881-X.

[47] B. Ma *et al.*, “Pulsed laser deposition of YBCO films on ISD MgO buffered metal tapes,” *Supercond. Sci. Technol.*, vol. 16, no. 4, pp. 464–472, 2003, doi: 10.1088/0953-2048/16/4/308.

[48] V. Selvamanickam *et al.*, “High performance 2G wires: From R&D to pilot-scale manufacturing,” *IEEE Trans. Appl. Supercond.*, vol. 19, no. 3, pp. 3225–3230, 2009, doi: 10.1109/TASC.2009.2018792.

[49] M. Mori *et al.*, “Development of long YBCO coated conductors by multiple-stage CVD,” *Phys. C Supercond. its Appl.*, vol. 445–448, no. 1–2, pp. 515–520, 2006, doi: 10.1016/j.physc.2006.04.046.

[50] P. Skov-Hansen and Z. Han Nordic, “Stresses and strains in multi-filament hts tapes,” *IEEE Trans. Appl. Supercond.*, vol. 9, no. 2 PART 2, pp. 2617–2620, 1999, doi: 10.1109/77.785023.

[51] J. W. Ekin, “Strain Effects in Superconducting Compounds.,” *Adv. Cryog. Eng.*, vol. 30, pp. 823–836, 1984, doi: 10.1007/978-1-4613-9868-4_90.

[52] K. Osamura, M. Sugano, S. MacHiya, H. Adachi, S. Ochiai, and M. Sato, “Internal residual strain and critical current maximum of a surrounded Cu stabilized YBCO coated conductor,” *Supercond. Sci. Technol.*, vol. 22, no. 6, 2009, doi: 10.1088/0953-2048/22/6/065001.

[53] K. Osamura *et al.*, “Reversible strain limit of critical currents and universality of intrinsic strain effect for REBCO-coated conductors,” *Supercond. Sci. Technol.*, vol. 22, no. 2, p. 025015, 2009, doi: 10.1088/0953-2048/22/2/025015.

[54] H. S. Shin, K. H. Kim, J. R. C. Dizon, T. Y. Kim, R. K. Ko, and S. S. Oh, “The strain effect on critical current in YBCO coated conductors with different stabilizing layers,” *Supercond. Sci. Technol.*, vol. 18, no. 12, 2005, doi: 10.1088/0953-2048/18/12/023.

[55] J. Xiong, W. Qin, X. Cui, B. Tao, J. Tang, and Y. Li, “Effect of processing conditions and methods on residual stress in CeO2 buffer layers and YBCO superconducting films,” *Phys. C Supercond. its Appl.*, vol. 442, no. 2, pp. 124–128, 2006, doi: 10.1016/j.physc.2006.05.024.

[56] J. Ullmann, A. J. Kellock, and J. E. E. Baglin, “Reduction of intrinsic stress in cubic boron nitride films,” *Thin Solid Films*, vol. 341, no. 1, pp. 238–245, 1999, doi: 10.1016/S0040-6090(98)01766-0.

[57] M. Sugano, K. Osamura, W. Prusseit, R. Semerad, K. Itoh, and T. Kiyoshi, “Tensile fracture behaviour of RE-123 coated conductors induced by discontinuous yielding in Hastelloy C-276 substrate,” *Supercond. Sci. Technol.*, vol. 18, no. 12, 2005, doi: 10.1088/0953-2048/18/12/020.

[58] K. Osamura *et al.*, “Reversibility of micro-yielding and critical current in a YBCO-coated conductor caused by a uniaxial tensile load,” *Supercond. Sci. Technol.*, vol. 20, no. 9, 2007, doi: 10.1088/0953-2048/20/9/S15.

[59] M. Sugano, K. Osamura, W. Prusseit, R. Semerad, K. Itoh, and T. Kiyoshi, “Intrinsic strain effect on critical current and its reversibility for YBCO coated conductors with different buffer layers,” *Supercond. Sci. Technol.*, vol. 18, no. 3, pp. 369–372, 2005, doi: 10.1088/0953-2048/18/3/027.

[60] C. Barth, G. Mondonico, and C. Senatore, “Electro-mechanical properties of REBCO coated conductors from various industrial manufacturers at 77 K, self-field and 4.2 K, 19 T,” *Supercond. Sci. Technol.*, vol. 28, no. 4, p. 45011, 2015, doi: 10.1088/0953-2048/28/4/045011.

[61] N. Cheggour, J. W. Ekin, C. L. H. Thieme, Y. Y. Xie, V. Selvamanickam, and R. Feenstra, “Reversible axial-strain effect in Y-Ba-Cu-O coated conductors,” *Supercond. Sci. Technol.*, vol. 18, no. 12, 2005, doi: 10.1088/0953-2048/18/12/016.

[62] M. Sugano, K. Shikimachi, N. Hirano, and S. Nagaya, “The reversible strain effect on critical current over a wide range of temperatures and magnetic fields for YBCO coated conductors,” *Supercond. Sci. Technol.*, vol. 23, no. 8, p. 085013, 2010, doi: 10.1088/0953-2048/23/8/085013.

[63] D. C. Van Der Laan and J. W. Ekin, “Large intrinsic effect of axial strain on the critical current of high-temperature superconductors for electric power applications,” *Appl. Phys. Lett.*, vol. 90, no. 5, pp. 18–20, 2007, doi: 10.1063/1.2435612.

[64] J. X. Jin, S. X. Dou, H. K. Liu, T. Hardono, C. Cook, and C. Grantham, “Critical current degradation caused by winding process of Bi-2223/Ag HTS wire in the form of a coil,” *IEEE Trans. Appl. Supercond.*, vol. 9, no. 2 PART 1, pp. 138–141, 1999, doi: 10.1109/77.783255.

[65] C. Park *et al.*, “Bend strain tolerance of critical currents for YBa2Cu3O7 films deposited on rolled-textured (001)Ni,” *Appl. Phys. Lett.*, vol. 73, no. 13, pp. 1904–1906, 1998, doi: 10.1063/1.122321.

[66] H. S. Shin and K. Katagiri, “Critical current degradation behaviour in Bi-2223 superconducting tapes under bending and torsion strains,” *Supercond. Sci. Technol.*, vol. 16, no. 9, pp. 1012–1018, 2003, doi: 10.1088/0953-2048/16/9/309.

[67] M. B. de Leon, A. R. Nisay, M. A. Diaz and H. S. Shin, "Bending Strain Sensitivity of Critical Current in REBCO Coated Conductor Winding for Coil Application at 77 K," in IEEE Transactions on Applied Superconductivity, vol. 32, no. 6, pp. 1-5, Sept. 2022, Art no. 8400605, doi: 10.1109/TASC.2022.3183954.

[68] H. S. Shin, S. Y. Choi, D. K. Ko, H. S. Ha, D. W. Ha, and S. S. Oh, "A comparison of strain effect on critical current in Bi-2223 superconducting tapes in different bending modes," *IEEE Trans. Appl. Supercond.*, vol. 13, no. 2 III, pp. 3526–3529, 2003, doi: 10.1109/TASC.2003.812388.

[69] M. B. de Leon, M. J. Dedicatoria, and H. S. Shin, "Determination of winding diameter based on bending strain analysis for REBCO coated conductor tapes," *J. Korea Inst. Appl. Supercond. Cryog.*, vol. 14, no. 2, pp. 8–11, 2012, doi: 10.9714/psac.2012.14.2.008.

[70] Y. Wang, H. Zhang, Y. Fu, C. T. Kan, C. Xue, and T. Hasegawa, "Experimental Research on Bending Characterization of 2G Tapes and Strand Consisting of 2G Tapes," *IEEE Trans. Appl. Supercond.*, vol. 26, no. 7, pp. 7–11, 2016, doi: 10.1109/TASC.2016.2591962.

[71] Y. Fu, Y. Wang, Y. Hou, C. Kan, and H. Zhang, "Out-of-plane bending characteristics of second generation high temperature superconducting tapes," *Supercond. Sci. Technol.*, vol. 30, no. 7, 2017, doi: 10.1088/1361-6668/aa7108.

[72] Y. Sutoh, K. Kakimoto, N. Kaneko, Y. Iijima, and T. Saitoh, "Mechanical bending property of YBCO coated conductor by IBAD/PLD," *Phys. C Supercond. its Appl.*, vol. 426–431, part. II, pp. 933–937, 2005, doi: 10.1016/j.physc.2005.02.086.

[73] D. C. Van Der Laan and J. W. Ekin, "Dependence of the critical current of YBa2Cu3O 7-δ coated conductors on in-plane bending," *Supercond. Sci. Technol.*, vol. 21, no. 11, 2008, doi: 10.1088/0953-2048/21/11/115002.

[74] R. L. Holtz, S. Fleshler, and D. U. Gubser, "Fatigue of a reinforced high temperature superconducting tape," *Adv. Eng. Mater.*, vol. 3, no. 3, pp. 131–134, 2001, doi: 10.1002/1527-2648(200103)3:3<131::aid-adem131>3.3.co;2-i.

[75] S. Kar, W. Luo, and V. Selvamanickam, "Ultra-Small Diameter Round REBCO Wire With Robust Mechanical Properties," *IEEE Trans. Appl. Supercond.*, vol. 27, no. 4, 2017, doi: 10.1109/TASC.2017.2669727.

[76] D. Verebelyi *et al.*, "Practical neutral-axis conductor geometries for coated conductor composite wire," *Supercond. Sci. Technol.*, vol. 16, no. 10, pp. 1158–1161, 2003, doi: 10.1088/0953-2048/16/10/306.

[77] X. Li *et al.*, "Effects of bending and torsion behavior on I c degradation and microstructure of ReBCO coated conductors," *Cryogenics (Guildf).*, vol. 126, no. July, p. 103523, 2022, doi: 10.1016/j.cryogenics.2022.103523.

[78] L. Lai *et al.*, "Characterization of Ic Degradation in Bent YBCO Tapes," *IEEE Trans. Appl. Supercond.*, vol. 29, no. 5, pp. 2–6, 2019, doi: 10.1109/TASC.2019.2900354.

[79] D. W. Jeremy, M. Tim, J. ten K. Herman, and C. van der L. Danko, "Introduction of CORC ® wires: highly flexible, round high-temperature superconducting wires

for magnet and power transmission applications," *Supercond. Sci. Technol.*, vol. 30, no. 1, p. 14002, 2017, [Online]. Available: http://stacks.iop.org/0953-2048/30/i=1/a=014002

[80] T. F. and D. W. H. A Sundaram, Y Zhang, A R Knoll, D Abraimov, P Brownsey, M Kasahara, G M Carota, R Nakasaki, J B Cameron, G Schwab, L V Hope, R M Schmidt, H Kuraseko, "2G HTS wires made on 30 μm thick Hastelloy substrate," *Supercond. Sci. Technol.*, vol. 29, no. 10, 2016, doi: 10.1088/0953-2048/29/10/104007.

[81] H. S. Shin, J. R. C. Dizon, T. H. Kim, D. W. Ha, and S. S. Oh, "Critical current degradation behavior in YBCO coated conductors under torsional strain," *IEEE Trans. Appl. Supercond.*, vol. 17, no. 2, pp. 3274–3277, 2007, doi: 10.1109/TASC.2007.897458.

[82] T. Takao *et al.*, "Influence of bending and torsion strains on critical currents in YBCO coated conductors," *IEEE Trans. Appl. Supercond.*, vol. 17, no. 2, pp. 3513–3516, 2007, doi: 10.1109/TASC.2007.899648.

[83] M. Takayasu, J. V. Minervini, and L. Bromberg, "Torsion strain effects on critical currents of HTS superconducting tapes," *AIP Conf. Proc.*, vol. 1219, no. 2010, pp. 337–344, 2010, doi: 10.1063/1.3402320.

[84] N. C. Allen, L. Chiesa, and M. Takayasu, "Combined tension-torsion effects on 2G REBCO tapes for twisted stacked-tape cabling," *IEEE Trans. Appl. Supercond.*, vol. 25, no. 3, pp. 2–6, 2015, doi: 10.1109/TASC.2014.2364401.

[86] G. Majkic, R. J. Mensah, V. Selvamanickam, Y. Y. Xie, and K. Salama, "Electromechanical behavior of IBAD/MOCVD YBCO coated conductors subjected to torsion and tension loading," *IEEE Trans. Appl. Supercond.*, vol. 19, no. 3, pp. 3003–3008, 2009, doi: 10.1109/TASC.2009.2018825.

[86] L. Chiesa, M. Takayasu, N. C. Allen, and L. Bromberg, "Electromechanical investigation of different type YBCO tapes for twisted stacked-tape cabling," *IEEE Trans. Appl. Supercond.*, vol. 23, no. 3, pp. 23–27, 2013, doi: 10.1109/TASC.2012.2233838.

[87] J. Fleiter, M. Sitko, and A. Ballarino, "Analytical formulation of Ic dependence on torsion of YBCO and BSCCO conductors," *IEEE Trans. Appl. Supercond.*, vol. 23, no. 3, pp. 3–6, 2013, doi: 10.1109/TASC.2012.2228292.

[88] P. Gao, J. Mao, J. Chen, X. Wang, and Y. Zhou, "Electromechanical degradation of REBCO coated conductor tapes under combined tension and torsion loading," Int. J. Mech. Sci., vol. 223, no. April, p. 107314, 2022, doi: 10.1016/j.ijmecsci.2022.107314.

[89] D. C. Van Der Laan *et al.*, "Engineering current density in excess of 200 A mm-2 at 20 T in CORC® magnet cables containing RE-Ba2Cu3O7-δ tapes with 38 μm thick substrates," *Supercond. Sci. Technol.*, vol. 28, no. 12, p. 124001, 2015, doi: 10.1088/0953-2048/28/12/124001.

[90] D. C. Van Der Laan *et al.*, "Record current density of 344 A mm-2 at 4.2 K and 17 T in CORC® accelerator magnet cables," *Supercond. Sci. Technol.*, vol. 29, no. 5, pp. 0–16, 2016, doi: 10.1088/0953-2048/29/5/055009.

[91] J. D. Weiss *et al.*, "Introduction of the next generation of CORC® wires with engineering current density exceeding 650 A mm-2 at 12 T based on SuperPower's ReBCO tapes containing substrates of 25 μm thickness," *Supercond. Sci. Technol.*, vol. 33, no. 4, 2020, doi: 10.1088/1361-6668/ab72c6.

[92] A. Anvar, V. A., Ilin, K., Yagotintsev, K. A., Monachan, B., Ashok, B. K., Kortman, B. A., … Nijhuis, "Bending of CORC® cables and wires: finite element parametric study and experimental validation," *Biochem. J.*, 2018.

[93] M. Majoros, M. D. Sumption, E. W. Collings, and D. Van Der Laan, "Stability and normal zone propagation in YBCO CORC cables," *Supercond. Sci. Technol.*, vol. 29, no. 4, p. 0, 2016, doi: 10.1088/0953-2048/29/4/044006.

[94] D. C. Van Der Laan, X. F. Lu, and L. F. Goodrich, "Compact GdBa2Cu3O7-δ coated conductor cables for electric power transmission and magnet applications," *Supercond. Sci. Technol.*, vol. 24, no. 4, pp. 1–6, 2011, doi: 10.1088/0953-2048/24/4/042001.

[95] V. A. Anvar *et al.*, " Enhanced critical axial tensile strain limit of CORC ® wires: FEM and analytical modeling ," *Supercond. Sci. Technol.*, vol. 35, no. 5, p. 055002, 2022, doi: 10.1088/1361-6668/ac5c87.

[96] K. Katagiri, S. Sato, N. Tsuchiya, and K. Kasaba, "Bending fatigue characteristics of DyBaCuO bulk superconductor," *Phys. C Supercond. its Appl.*, vol. 468, no. 15–20, pp. 1424–1427, 2008, doi: 10.1016/j.physc.2008.05.245.

[97] A. L. Mbaruku and J. Schwartz, "Fatigue behavior of Y-Ba-Cu-O/hastelloy-C coated conductor at 77 K," *IEEE Trans. Appl. Supercond.*, vol. 18, no. 3, pp. 1743–1752, 2008, doi: 10.1109/TASC.2008.2003491.

[98] S. R. and J. Schwartz and Department, "Tensile fatigue behavior and crack growth in GdBa2Cu3O7−x /stainless-steel coated conductor grown via reactive co-evaporation," *Supercond. Sci. Technol.*, vol. 30, no. 6pp, p. 045013, 2017, doi: https://doi.org/10.1088/1361-6668/aa604e.

[99] S. Rogers, W. K. Chan, and J. Schwartz, "Effects of room-temperature tensile fatigue on critical current and n-value of IBAD-MOCVD YBa2Cu3O7-x/Hastelloy coated conductor," *Supercond. Sci. Technol.*, vol. 29, no. 8, pp. 1–7, 2016, doi: 10.1088/0953-2048/29/8/085013.

[1000] W. Chen *et al.*, "Fatigue Behavior of Critical Current Degradation for YBCO Tapes at 77 K," *IEEE Trans. Appl. Supercond.*, vol. 28, no. 3, 2018, doi: 10.1109/TASC.2018.2806912.

[101] H. Kitaguchi, K. Itoh, H. Kumakura, T. Takeuchi, K. Togano, and H. Wada, "Strain and fatigue tests of Bi-2223/Ag superconducting tapes," *Phys. C Supercond. its Appl.*, vol. 357–360, no. SUPPL. 1, pp. 1193–1196, 2001, doi: 10.1016/S0921-4534(01)00480-4.

[102] A. Salazar, J. Y. Pastor, and J. LLorca, "Fatigue behavior of multifilamentary BSCCO 2223/Ag superconducting tapes," *IEEE Trans. Appl. Supercond.*, vol. 14, no. 3, pp. 1941–1947, 2004, doi: 10.1109/TASC.2004.830606.

[103] H. S. Shin, J. R. C. Dizon, K. H. Kim, S. S. Oh, and D. W. Ha, "Fatigue behavior and its influence on the critical current of externally reinforced Bi-2223

superconducting tape," *IEEE Trans. Appl. Supercond.*, vol. 15, no. 2 PART III, pp. 3556–3559, 2005, doi: 10.1109/TASC.2005.849358.

[104] M. Sugano, Y. Yoshida, M. Hojo, K. Shikimachi, N. Hirano, and S. Nagaya, "Two different mechanisms of fatigue damage due to cyclic stress loading at 77 K for MOCVD-YBCO-coated conductors," *Supercond. Sci. Technol.*, vol. 21, no. 5, 2008, doi: 10.1088/0953-2048/21/5/054006.

[105] H. S. Shin and M. J. Dedicatoria, "Mechanical and transport properties of IBAD/EDDC-SmBCO coated conductor tapes during fatigue loading," *Cryogenics (Guildf).*, vol. 51, no. 6, pp. 237–240, 2011, doi: 10.1016/j.cryogenics.2010.05.005.

[106] H. S. Shin, M. B. De Leon, and M. A. E. Diaz, "Investigation of the electromechanical behaviors in Cu-stabilized GdBCO coated conductor tapes using high-cycle fatigue tests at 77 K and related fractographic observations," *Supercond. Sci. Technol.*, vol. 33, no. 2, p. 25012, 2020, doi: 10.1088/1361-6668/ab617b.

[107] J. W. Ekin *et al.*, "Transverse stress and fatigue effects in Y-Ba-Cu-O coated IBAD tapes," *IEEE Trans. Appl. Supercond.*, vol. 11, no. 1 III, pp. 3389–3392, 2001, doi: 10.1109/77.919790.

[108] S. Muto, S. Fujita, H. Sato, K. Akashi, Y. Iijima, and M. Daibo, "Fatigue behavior of REBCO coated conductors under through-thickness tensile stress," *Supercond. Sci. Technol.*, vol. 34, no. 7, 2021, doi: 10.1088/1361-6668/abf852.

[109] S. O. Mbam and X. F. Gou, "Interface crack growth rate and fatigue life of multilayer-coated conductor tapes," *Eng. Fract. Mech.*, vol. 228, p. 106910, 2020, doi: 10.1016/j.engfracmech.2020.106910.

[110] M. Hojo *et al.*, "Fatigue behaviour of YBCO coated conductor with Cu layer at 77K," *ICCM Int. Conf. Compos. Mater.*, 2009.

[111] M. B. De Leon, A. R. Nisay, and H. S. Shin, "Evaluation of electrical fatigue limits in REBCO coated conductor tapes through static fatigue testing at 77 K," *Supercond. Sci. Technol.*, vol. 35, no. 2, 2022, doi: 10.1088/1361-6668/ac32ac.

[112] I. R. Dixon, E. S. Bosque, K. Buchholz, R. P. Walsh, and H. Bai, "REBCO Coils With Variable Co-Wind Dimensions Under Static and Cyclic Axial Pressure Loads at 77 K," *IEEE Trans. Appl. Supercond.*, vol. 32, no. 6, pp. 6–9, 2022, doi: 10.1109/TASC.2022.3163084.

[113] N. Bykovsky, D. Uglietti, R. Wesche, and P. Bruzzone, "Cyclic load effect on round strands made by twisted stacks of HTS tapes," *Wire J. Int.*, vol. 50, no. 10, pp. 70–73, 2017, doi: 10.1016/j.fusengdes.2017.04.050.

[114] T. Takao *et al.*, "Degradation due to bending fatigue strain in YBCO coated conductors," *IEEE Trans. Appl. Supercond.*, vol. 19, no. 3, pp. 2988–2990, 2009, doi: 10.1109/TASC.2009.2018246.

[115] T. Matake, "An Explanation on Fatigue limit under combined stress," *Bull. JSME*, vol. vol.20, no.141, 1977, [Online]. Available: http://www.mendeley.com/research/geology-volcanic-history-eruptive-style-yakedake-volcano-group-central-japan/

[116] R. Hibbeler, “Mechanics of Materials, 8th ed. London,.” Pearson., U.K., p. 883, 2011.

[117] COMSOL Multiphysics and COMSOL, “Structural Mechanics Module,” *Manual*, p. 454, 2008, [Online]. Available: www.comsol.de

[118] John Ryan Cortez Dizon, Hyung-Seop Shin, Rock-Kil Ko, Sang-Soo Oh, “Estimation of Residual Stress in ReBCO Coated Conductor Tapes Using Various Methods, Progress in Superconductivity and Cryogenics (PSAC)/Journal of the Korea Institute of Applied Superconductivity and Cryogenics, January 2008, vol 10.

[119] J. R. C. Dizon, A. R. N. Nisay, M. J. A. Dedicatoria, R. C. Munoz, H. S. Shin, and S. S. Oh, “Analysis of Thermal Residual Stress/Strain in REBCO Coated Conductor Tapes,” *IEEE Trans. Appl. Supercond.*, vol. 24, no. 3, 2014, doi: 10.1109/TASC.2013.2292746.

[120] Ashok KB, Thomas RJ, Prakash MJ, Nijhuis A (2021) Performance limits in REBCO tape for variation in winding parameters of CORC cable and wire, Elsevier, Physica C: Superconductivity and its applications, vol 582, 15 March 2021:1353828. https://doi.org/10.1016/j.physc.2021.1353828.

[121] E. Celik, O. Sayman, R. Karakuzu, and Y. Ozman, “Numerical analysis of the influence of buffer layer thickness on the residual stresses in YBCO/La2Zr2O7/Ni superconducting materials,” *Mater. Des.*, vol. 28, no. 7, pp. 2184–2189, 2007, doi: 10.1016/j.matdes.2006.07.003.

[122] H. (Technische U. Conrad, T. (Fraunhofer I. of P. M. Klose, T. (Fraunhofer I. of P. M. Sandner, D. (Technische U. Jung, H. (Fraunhofer I. of P. M. Schenk, and H. (Technische U. & F. I. of P. M. Lakner, “Modeling the Thermally Induced Curvature of Multilayer Coatings with COMSOL Multiphysics,” *Proc. COMSOL Conf.*, 2008.

[123] C. Zhou, K. A. Yagotintsev, P. Gao, T. J. Haugan, D. C. Van Der Laan, and A. Nijhuis, “Critical current of various REBCO tapes under uniaxial strain,” *IEEE Trans. Appl. Supercond.*, vol. 26, no. 4, pp. 1–4, 2016, doi: 10.1109/TASC.2016.2535202.

[124] Dominique Francois, Andr´e Pineau, Andr´e Zaoui Mechanics of Materials, Volume 1: Micro- and Macroscopic Constitutive Behaviour, Springer publications, 2012. http://www.springer.com/series/6557.

[125] A. Ben Yahia, S. Kar, G. Majkic, and V. Selvamanickam, “Modeling-Driven Optimization of Mechanically Robust REBCO Tapes and Wires,” *IEEE Trans. Appl. Supercond.*, vol. 29, no. 5, page 1-5 2019, doi: 10.1109/TASC.2019.2907234.

[126] K. Wang, W. Ta, and Y. Gao, “The winding mechanical behavior of conductor on round core cables,” *Phys. C Supercond. its Appl.*, vol. 553, pp. 65–71, 2018, doi: 10.1016/j.physc.2018.08.012.

[127] D. C. Van Der Laan, J. D. Weiss, and D. M. McRae, “Status of CORC® cables and wires for use in high-field magnets and power systems a decade after their introduction,” *Supercond. Sci. Technol.*, vol. 32, no. 3, p. 33001, 2019, doi: 10.1088/1361-6668/aafc82.

[128] M. Sugano, T. Nakamura, T. Manabe, K. Shikimachi, N. Hirano, and S. Nagaya, “The intrinsic strain effect on critical current under a magnetic field parallel to the c axis for a MOCVD-YBCO-coated conductor,” *Supercond. Sci. Technol.*, vol. 21, no. 11, 2008, doi: 10.1088/0953-2048/21/11/115019.

[129] D. C. Van Der Laan, J. W. Ekin, J. F. Douglas, C. C. Clickner, T. C. Stauffer, and L. F. Goodrich, “Effect of strain, magnetic field and field angle on the critical current density of y Ba2Cu3O7-δ coated conductors,” *Supercond. Sci. Technol.*, vol. 23, no. 7, pp. 2–9, 2010, doi: 10.1088/0953-2048/23/7/072001.

[130] H. S. Shin, S. Y. Choi, H. S. Ha, D. W. Ha, and S. S. Oh, “Ic degradation behavior in Bi-2223 superconducting tapes under torsional deformation,” *Phys. C Supercond. its Appl.*, vol. 392–396, no. PART 2, pp. 1162–1166, 2003, doi: 10.1016/S0921-4534(03)00747-0.

[131] N. Cheggour *et al.*, “Reversible axial-strain effect and extended strain limits in Y-Ba-Cu-O coatings on deformation-textured substrates,” *Appl. Phys. Lett.*, vol. 83, no. 20, pp. 4223–4225, 2003, doi: 10.1063/1.1628818.

[132] N. C. Allen, L. Chiesa, and M. Takayasu, “Structural modeling of HTS tapes and cables,” *Cryogenics (Guildf).*, vol. 80, pp. 405–418, 2016, doi: 10.1016/j.cryogenics.2016.02.002.

[133] A. Gorospe, Z. Bautista, and H. S. Shin, “Critical current degradation behaviour of GdBCO CC tapes in pure torsion and combined tension- torsion modes,” Supercond. Sci. Technol., vol. 29, no. 10, pp. 1–9, 2016, doi: 10.1088/0953-2048/29/10/104003.

[134] P. M. Lin and J. A. Wickert, “Corrugation and buckling defects in wound rolls,” *J. Manuf. Sci. Eng. Trans. ASME*, vol. 128, no. 1, pp. 56–64, 2006, doi: 10.1115/1.2113068.

[135] COMSOL Multiphysics, “Fatigue Module,” *Train. Manual(Fatigue)*, pp. 1–71, 2005.

[136] A. Kojima *et al.*, “Study on optimal thickness of copper layer of REBCO-coated wire for quench protection,” *IOP Conf. Ser. Mater. Sci. Eng.*, vol. 502, no. 1, 2019, doi: 10.1088/1757-899X/502/1/012180.